

Ecosystem Transpiration from Eddy Covariance

**Dissertation
(kumulativ)**

zur Erlangung des akademischen Grades doctor rerum naturalium
(Dr. rer. nat.)

vorgelegt dem Rat der Chemisch-Geowissenschaftlichen Fakultät der
Friedrich-Schiller-Universität Jena

von Jacob A. Nelson, M. Sc. (Plant Science)

geboren am 3. October 1988 in Salt Lake City, Utah, United States of America

Gutachter:

1. _____

2. _____

3. _____

Tag der Verteidigung _____

Selbständigkeitserklärung

Ich erkläre, dass ich die vorliegende Arbeit selbständig und unter Verwendung der angegebenen Hilfsmittel, persönlichen Mitteilungen und Quellen angefertigt habe.

Ort, Datum, Unterschrift

Summary

Background: Transpiration is an integral part of the earth system, not only because plant water use is the dominant path by which water flows from the soil to the atmosphere, but also because water loss from leaves is intrinsically connected to CO_2 uptake and provides a key link between global carbon and water cycles. Transpiration, while well studied at the scale of plants and leaves, remains difficult to quantify at the ecosystem, regional, and global scales. Differentiating between water vapor which has passed through plants, and is thus biologically controlled, and water vapor which is evaporated from surfaces without active control from plants through stomatal regulation is extremely challenging at the ecosystem scale with heterogeneous landscapes containing diverse plant species accessing soil water reserves at varying depths. Furthermore, plant species and communities have very different strategies for regulating water use to respond to environmental conditions. Understanding the mechanism that determine water use across species and in time is still a crucial challenge to predict ecosystem responses to future drought and climate variability.

Current methodologies to quantify transpiration at scales greater than a single plant have key drawbacks. For example, scaling measurements from individual plants within the ecosystem to the ecosystem as a whole can be problematic because of a lack of high spatial and temporally dense sampling due in part to the high cost and effort of such field campaigns. Predictions of transpiration from modeling approaches which can be applied at large scales, such as from the large earth system models used for future climate predictions or empirical functions tied to remote sensing datasets used for forest and crop monitoring, produce very different results. The disagreement across modeling approaches illustrates a fundamental lack of understanding of how communities of plants use water.

One potential solution to characterizing transpiration on broader scales is to use eddy covariance to estimate ecosystem transpiration. Eddy covariance has been widely utilized to measure water, carbon, and energy fluxes, with synthesis initiative such as FLUXNET collating hundreds of sites around the world. However, methods for partitioning the total ecosystem water flux (evapotranspiration, ET) measured by eddy covariance systems into the individual components, i.e. transpiration (T) and abiotic evaporation (E), are needed.

Research objectives: The overarching goal of this doctoral research is to develop, evaluate, and apply an ET partitioning method which is data driven and applicable to the highest number of eddy covariance datasets as possible. To achieve this goal, three research questions (RQ) are posed:

- RQ 1:** How can information in the core eddy covariance datasets be further exploited to describe the complex plant water relationships from heterogeneous ecosystems?
- RQ 2:** Given the limited amount of independent ecosystem transpiration data concurrent with eddy covariance measurements, how can the transpiration estimates be validated?
- RQ 3:** What new insights on ecohydrological and water use strategies across major terrestrial biomes can be gained from the transpiration estimates derived from FLUXNET?

While these questions relate to the results shown in Chapters 2, 3, and 4, respectively, they gradually lead toward the main goal of the dissertation: First, understanding water and carbon flux dynamics at the ecosystem level, understanding which feeds into the transpiration estimation method. Finally, the transpiration estimation method was applied to the FLUXNET monitoring network to provide new insights on ecosystem physiology.

Data, Methods, and Models: The core datasets set used in all chapters of this thesis were the published FLUXNET synthesis datasets of eddy covariance data, which consist of sensible, latent, and ground heat energy fluxes as well as measurements of radiation and meteorology. These datasets also contain measured net ecosystem exchange of CO_2 , as well as estimates of ecosystem gross primary productivity (GPP) and respiration. The FLUXNET synthesis processing chain provides a gap-filled dataset harmonized to a half-hourly or hourly temporal resolution, providing continuous data spanning years to decades across major terrestrial biomes and covering all the climate zones. To address RQ 1, the sub-daily resolution datasets were used to develop two diurnal indicators, the diurnal water carbon index (DWCI) and the relative diurnal centroid of ET (C_{ET}^*), to characterize ecosystem responses to drought. The partitioning method described in Chapter 3 (the Transpiration Estimation Algorithm, TEA) used these diurnal indicators, along with other variables derived from the eddy covariance data, as features in a Ran-

dom Forest model able to predict water use efficiency, or the ratio of GPP to transpiration, from which an estimate of ecosystem transpiration is derived. To address RQ 2, the TEA method was tested on model output from three terrestrial biosphere models used as synthetic eddy covariance dataset to verify that the data driven approach (TEA) could replicate the known water carbon dynamics in the models. TEA was further evaluated in Chapter 4, both against two other ET partitioning methods (uWUE and Pérez-Priego) as well as against canopy transpiration estimated from sap flow measurements. To address RQ 3, TEA and the other two ET partitioning methods were applied to 251 sites globally, and analysed for expected patterns with site meteorology and remote sensing data.

Key results:

RQ 1: Diverse ecosystem responses to drought were characterized using two diurnal indicators that did not require additional measurements or data sources other than the core eddy covariance dataset. DWCI was linked to non-stomatal limitations causing a decoupling of diurnal GPP and ET, where low DWCI (indicating decoupling) was generally associated with grasses. C_{ET}^* was linked to hydraulic limitations and stomatal control where lower values represent days where the flux of ET relative to incoming radiation is shifted towards the morning, with morning shifts associated more with trees. While both morning shifts and carbon:water decoupling were linked to dry conditions, only morning shifts were associated with higher water use efficiency, indicating tree ecosystems with higher stomatal control use water more efficiently in dry conditions while grass ecosystems with less stringent stomatal control tend to run into non-stomatal limitations.

RQ 2: The uncertainties and methodological assumptions from the TEA method were well characterized by first validating transpiration estimates in the controlled terrestrial biosphere model experiments, followed by further evaluated against other eddy covariance based and validated against independent transpiration estimates. Spatial and temporal patterns of transpiration were robust and consistent, both in the ability of the TEA method to replicate model output (NashSutcliffe efficiencies generally > 0.9), as well as in the high correlation between the three eddy covariance based methods (R^2 between 0.89 and 0.94) and sap flow based estimates (R^2 between 0.76 and 0.81). However, the magnitude of transpiration remains uncertain, with a spread in the ratio of transpiration to ET (T/ET) ranging from 45% to 77%. Method assumptions on the

optimality of carbon gain to water loss were identified as the key factor controlling the magnitude of transpiration for all the eddy covariance based ET partitioning methods, where methods that assume plants optimize carbon gain to water loss tended to have T/ET ratios across FLUXNET at or below 50%, in contrast to the TEA method which does not rely on that assumption and has a T/ET ratio of 77%.

RQ 3: Broadly applicable ET partitioning methods from eddy covariance data were able to provide enough sites with continuous T and E estimates to explore not only temporal, but also spatial patterns and drivers of ecosystem transpiration. Analyzing sites with more than two complete years of transpiration and ET data showed that T/ET is 1.6 times more variable in space than in time. Furthermore, spatial variation of T/ET was shown to primarily depend on vegetation (e.g. crop/grass designation) and soil characteristics (e.g. soil silt content and coarse fragment volume), with little influence from climatic variables such as the annual mean/standard deviation of temperature and precipitation. Furthermore, the relationship between T/ET and vegetation cover, as measured from remote sensing based leaf area index, was less important than assumed in previous works, with a much greater importance of soil characteristics, grass/crop designation, and aridity, indicating that how plants access limited soil water supplies is more important than the presence or absence of vegetation in determining plant water use.

General conclusions: Overall, the work presented here demonstrates the viability and utility of ecosystem scale estimates of transpiration from eddy covariance datasets via data driven methodologies. Identifying key strengths and uncertainties in the method, such as the uncertainty in the magnitude of transpiration but strength in spatial and temporal patterns, better outlines future directions. By being broadly applicable, the TEA method can both act as a baseline for future independent transpiration estimates to compare to, as well as bridge the scale gap between plant scale studies and global process/remote sensing based models. This transfer of scale will help to both inform understanding of core plant physiology and ecology, as well as improve predictions of global water and carbon cycles in a present and future climate.

Zusammenfassung

Hintergrund: Transpiration ist ein integraler Bestandteil des Erdsystems, nicht nur, weil die Wassernutzung der Pflanzen der dominante Pfad ist, über den Wasser vom Boden in die Atmosphäre fließt, sondern auch, weil der Wasserverlust aus den Blättern untrennbar mit der CO_2 -Aufnahme verbunden ist und eine wichtige Verbindung zwischen dem globalen Kohlenstoff- und Wasserkreislauf darstellt. Die Transpiration ist zwar auf der Pflanzen- und Blattebene gut untersucht, aber auf der Skala von Ökosystemen, Regionen und der globalen Skala ist sie nach wie vor schwer zu quantifizieren. Die Unterscheidung zwischen Wasserdampf, der durch Pflanzen passiert und somit biologisch kontrolliert wird, und Wasserdampf, der von Oberflächen ohne aktive Kontrolle der Pflanzen durch stomatare Regulierung verdunstet, ist auf der Ökosystem-Skala mit heterogenen Landschaften, die verschiedene Pflanzenarten enthalten, die auf Bodenwasserreserven in unterschiedlichen Tiefen zugreifen, extrem schwierig. Darüber hinaus haben Pflanzenarten und -gemeinschaften sehr unterschiedliche Strategien zur Regulierung des Wasserverbrauchs, um auf Umweltbedingungen zu reagieren. Das Verständnis der Mechanismen, die die Wassernutzung über die Arten und die Zeit hinweg bestimmen, ist immer noch eine entscheidende Herausforderung, um die Reaktionen der Ökosysteme auf zukünftige Trockenheit und Klimavariabilität vorherzusagen.

Aktuelle Methoden zur Quantifizierung der Transpiration auf Skalen, die größer als eine einzelne Pflanze sind, haben entscheidende Nachteile. Zum Beispiel kann die Übertragung von Messungen einzelner Pflanzen innerhalb des Ökosystems auf das Ökosystem im Ganzen problematisch sein, da es an räumlich und zeitlich hochaufgelösten Stichproben mangelt, was zum Teil auf die hohen Kosten und den Aufwand solcher Feldkampagnen zurückzuführen ist. Vorhersagen der Transpiration aus Modellierungsansätzen, die auf großen Skalen angewandt werden können, wie z.B. aus Erdsystemmodellen, die für zukünftige Klimavorhersagen verwendet werden, oder empirische Funktionen, die an Fernerkundungsdatensätze gebunden sind, die für die Überwachung von Wäldern und Pflanzen verwendet werden, liefern sehr unterschiedliche Ergebnisse. Die Unstimmigkeit zwischen den Modellierungsansätzen zeigt einen grundlegenden Mangel an Verständnis darüber, wie Pflanzengemeinschaften Wasser nutzen.

Eine mögliche Lösung zur Charakterisierung der Transpiration auf breiterer Ebene ist die Verwendung der Eddy-Kovarianz zur Schätzung der Transpiration von Ökosyste-

men. Die Eddy-Kovarianz wurde bereits in großem Umfang zur Messung von Wasser-, Kohlenstoff- und Energieflüssen eingesetzt, wobei eine Syntheseinitiative wie FLUXNET hunderte Standorte auf der ganzen Welt erfasst. Allerdings werden Methoden zur Trennung des gesamten Ökosystem-Wasserflusses (Evapotranspiration, ET), der von Eddy-Kovarianz-Systemen gemessen wird, in die einzelnen Komponenten, d.h. Transpiration (T) und abiotische Evaporation (E), benötigt.

Forschungsziele: Das übergeordnete Ziel dieser Doktorarbeit ist es, eine Methode zur Aufteilung von ET zu entwickeln, zu validieren und anzuwenden, die datengetrieben und auf eine möglichst große Anzahl von Eddy-Kovarianz-Datensätzen anwendbar ist. Um dieses Ziel zu erreichen, werden drei Forschungsfragen (FF) gestellt:

- FF 1:** Wie können die Informationen in den Eddy-Kovarianz-Kerndatensätzen besser genutzt werden, um die komplexen Pflanzen-Wasser-Beziehungen von heterogenen Artengemeinschaften zu beschreiben?
- FF 2:** Wie können die Transpirationsschätzungen angesichts der begrenzten Menge an unabhängigen Ökosystem-Transpirationsdaten, die gleichzeitig mit Eddy-Kovarianz-Messungen vorliegen, validiert werden?
- FF 3:** Welche neuen Erkenntnisse über ökohydrologische und Wassernutzungsstrategien in den wichtigsten terrestrischen Biomen können aus den von FLUXNET abgeleiteten Transpirationsschätzungen gewonnen werden?

Während sich diese Fragen auf die jeweils in Kapitel 2, 3, bzw. 4 gezeigten Ergebnisse beziehen, führen sie schrittweise zum Hauptziel der Doktorarbeit hin: Zunächst wird zum Verständnis der Wasser- und Kohlenstoffflussdynamik auf Ökosystemebene beigetragen, welches in die Methode zur Transpirationsschätzung einfließt. Diese wird schließlich für das FLUXNET Messnetz angewendet und validiert, um neue über die Physiologie des Ökosystems Erkenntnisse zu gewinnen.

Daten, Methoden und Modelle: Die Kerndatensätze, die in allen Kapiteln dieser Arbeit verwendet wurden, sind die veröffentlichten FLUXNET-Synthesatensätze von Eddy-Kovarianz-Daten, die aus sensiblen, latenten und Bodenwärmeflüssen sowie Strahlungs- und meteorologischen Messungen bestehen. Diese Datensätze enthalten auch den gemessenen Netto-Ökosystemaustausch von CO_2 sowie Schätzungen der Bruttoprimärproduktivität (GPP) und der Respiration von Ökosystemen. Die FLUXNET-Syntheseverarbeitungskette liefert einen lückenhaften Datensatz, der auf eine halbstündliche oder stündliche zeitliche

Auflösung harmonisiert ist und kontinuierliche Daten über Jahre bis Jahrzehnte für die wichtigsten terrestrischen Biome und alle Klimazonen liefert. Um FF 1 zu adressieren, wurden die täglich aufgelösten Datensätze verwendet, um zwei tageszeitliche Indikatoren zu entwickeln: den Wasser-Kohlenstoff-Index (DWCI) und den relativen tageszeitlichen Schwerpunkt der ET (C_{ET}^*), um die Reaktionen von Ökosystemen auf Trockenheit zu charakterisieren. Die in Kapitel 3 beschriebene Methode zur Aufteilung von ET (der Transpirationsschätzungsalgorithmus, TEA) verwendete diese täglichen Indikatoren zusammen mit anderen Variablen, die aus den Eddy-Kovarianz-Daten abgeleitet wurden, als Merkmale in einem Random-Forest-Modell. Dieses Modell ist in der Lage, die Wassernutzungseffizienz oder das Verhältnis von GPP zu Transpiration vorherzusagen, woraus eine Schätzung der Ökosystemtranspiration abgeleitet wird. Um FF 2 zu beantworten, wurde die TEA-Methode am Modell-Output von drei terrestrischen Biosphärenmodellen getestet, die als synthetischer Eddy-Kovarianz-Datensatz verwendet wurden, um zu verifizieren, dass der datengetriebene Ansatz (TEA) die bekannte Wasser-Kohlenstoff-Dynamik in den Modellen replizieren konnte. TEA wurde in Kapitel 4 weiter evaluiert, sowohl gegenüber zwei anderen ET-Verteilungsmethoden (uWUE und Pérez-Priego) als auch gegenüber der aus Saftstrommessungen geschätzten Transpiration von Baumkronen. Zur Beantwortung von Frage 3 wurden TEA und die beiden anderen ET-Verteilungsmethoden auf 251 Standorte weltweit angewendet und hinsichtlich zu erwartender Muster mit Standortmeteorologie und Fernerkundungsdaten analysiert.

Hauptergebnisse:

FF 1: Diverse Ökosystem-Reaktionen auf Trockenheit wurden mit zwei tageszeitlichen Indikatoren charakterisiert, die keine zusätzlichen Messungen oder Datenquellen auSSer dem Eddy-Kovarianz-Kerndatensatz erforderten. Dabei wurde DWCI mit nicht-stomatären Einschränkungen in Verbindung gebracht, die eine Entkopplung von diurnaler GPP und ET verursachen, wobei ein niedriger DWCI (der auf eine Entkopplung hinweist) im Allgemeinen mit Gräsern assoziiert wurde. C_{ET}^* wurde mit hydraulischen Begrenzungen und stomatärer Kontrolle in Verbindung gebracht, wobei niedrigere Werte für Tage stehen, an denen der ET-Fluss relativ zur einfallenden Strahlung zum Morgen hin verschoben ist, was eher mit Bäumen in Verbindung gebracht werden kann. Während sowohl die morgendlichen Verschiebungen als auch die Kohlenstoff-Wasser-Entkopplung mit trockenen Bedingungen zusammenhängen, waren nur die morgendlichen Verschiebungen mit einer höheren Wassernutzungseffizienz verbunden. Das deutet darauf hin, dass Baum-Ökosysteme mit einer höheren stomatären Kontrolle das Wasser unter trockenen

Bedingungen effizienter nutzen, während Gras-Ökosysteme mit einer weniger strengen Kontrolle der Stomata dazu neigen, an nicht-stomatäre Grenzen zu stoßen.

FF 2: Die Unsicherheiten und methodischen Annahmen der TEA-Methode wurden charakterisiert, indem zunächst die Transpirationsschätzungen in den kontrollierten terrestrischen Biosphären-Modellexperimenten validiert wurden, und anschließend einer weiteren Evaluierung gegen andere Eddy-Kovarianz-basierte und gegen unabhängige Transpirationsschätzungen erfolgte. Die räumlichen und zeitlichen Muster der Transpiration waren robust und konsistent, sowohl in der Fähigkeit der TEA-Methode, den Modell-Output zu replizieren (Nash-Sutcliffe-Effizienzen im Allgemeinen $> 0,9$), als auch in der hohen Korrelation zwischen den drei Eddy-Kovarianz-basierten Methoden (R^2 zwischen 0,89 und 0,94) und den saftflussbasierten Schätzungen (R^2 zwischen 0,76 und 0,81). Die Größenordnung der Transpiration bleibt jedoch unsicher, mit einer Streuung des Verhältnisses von Transpiration zu ET (T/ET) zwischen 45% und 77%. Methodische Annahmen zur Optimalität des Kohlenstoffgewinns gegenüber dem Wasserverlust wurden als Schlüsselfaktor identifiziert, der die Größe der Transpiration für alle Eddy-Kovarianz-basierten ET-Verteilungsmethoden steuert. Methoden, die davon ausgehen, dass Pflanzen den Kohlenstoffgewinn gegenüber dem Wasserverlust optimieren, tendieren zu T/ET-Verhältnissen bei oder unter 50% für FLUXNET Standorte, während die TEA-Methode, die sich nicht auf diese Annahme stützt, ein T/ET-Verhältnis von 77% prognostiziert.

FF 3: Breit anwendbare ET-Verteilungsmethoden aus Eddy-Kovarianz-Daten waren in der Lage, genügend Standorte mit kontinuierlichen T- und E-Schätzungen zu erzeugen, um nicht nur zeitliche, sondern auch räumliche Muster und Treiber der Ökosystemtranspiration zu untersuchen. Die Analyse von Standorten mit mehr als zwei vollständigen Jahren an Transpirations- und ET-Daten zeigte, dass T/ET räumlich 1,6-mal variabler ist als zeitlich. Darüber hinaus zeigte sich, dass die räumliche Variation von T/ET in erster Linie von der Vegetation (z. B. Pflanzen-/Grasbezeichnung) und den Bodeneigenschaften (z. B. Schluffgehalt und Grobfragmentvolumen) abhängt, mit geringem Einfluss von klimatischen Variablen wie dem Jahresmittelwert/Standardabweichung von Temperatur und Niederschlag. Darüber hinaus war die Beziehung zwischen T/ET und der Vegetationsbedeckung, gemessen anhand des fernerkundungsbasierten Blattflächenindex, weniger wichtig als in früheren Arbeiten angenommen, mit einer im Vergleich viel größeren Bedeutung der Bodeneigenschaften, der Gras-/Kulturpflanzenbezeichnung und der Trockenheit. Hieraus lässt sich schließen, dass die Art und Weise, wie Pflanzen auf begrenzte Bodenwasservorräte zugreifen, bei der Bestimmung der pflanzlichen Wasser-

nutzung wichtiger ist als das Vorhandensein oder Fehlen von Vegetation.

Allgemeine Schlussfolgerungen: Insgesamt zeigt die hier vorgestellte Arbeit die Realisierbarkeit und den Nutzen von Schätzungen der Transpiration auf Ökosystemebene aus Eddy-Kovarianz-Datensätzen mittels datengesteuerter Methoden. Die Identifizierung von Schlüsselstärken und -unsicherheiten der Methode, wie z.B. die Unsicherheit in der Magnitude der Transpiration, aber die Stärke in der Herleitung räumlicher und zeitlicher Mustern, skizziert zukünftige Forschungsrichtungen. Da die TEA-Methode breit anwendbar ist, kann sie sowohl als Basis für zukünftige unabhängige Transpirationsschätzungen dienen, mit denen sie verglichen werden kann, als auch die Skalenslücke zwischen Studien auf der Pflanzenebene und globalen prozess- und fernerkundungsbasierten Modellen überbrücken. Dieser Skalentransfer wird dazu beitragen, sowohl das Verständnis der grundlegenden Pflanzenphysiologie und -ökologie, als auch die Vorhersagen des globalen Wasser- und Kohlenstoffkreislaufs in einem gegenwärtigen und zukünftigen Klima zu verbessern.

Contents

Chapter 1

Introduction

“Had they fortun'd to have fallen into this statical way of inquiry, persons of their great application and sagacity had doubtless made considerable advances in the knowledge of the nature of Plants. This is the only sure way to measure the several quantities of nourishment, which Plants imbibe and perspire, and thereby to see what influence the different states of Air have on them. This is the likeliest method to find out the Sap's velocity, and the force with which it is imbibed: As also to estimate the great power that nature exerts in extending and pushing forth her productions, by the expansion of the Sap.”

Stephen Hales, *Vegetable Staticks*, 1727

1.1 The importance of how plants use water

The flow of water from the soil through plants is the primary hydraulic conduit along the soil-plant-atmosphere continuum, providing both the turgor pressure terrestrial plants need to grow as well as a nutrient highway to the photosynthetic powerhouses in the leaves. Though photosynthesis from marine organisms had already produced an oxygen rich atmosphere 2.3 billion years ago (Lyons et al., 2014), plants only colonized land about 400 million years ago (Kenrick and Crane, 1997). The major adaptation that allowed plants to thrive outside an aquatic environment is a vascular system to transport water to leaves which control water flow via small, closable pores (stomates) in the otherwise impermeable outer surface of the leaf, an adaptation that led to a 90% decrease in atmospheric CO_2 levels (Beerling et al., 2001; Mora et al., 1996). Apart from shaping atmospheric compositions, terrestrial vascular plants are the main primary producers of food and organic material which humans depend on. As such, methods to monitor and study plants and how they use water, measured as transpiration, are key to understanding the earth system as a whole, as transpiration directly influences global carbon, nutrient, energy, and hydrological cycles.

Transpiration (T) is the evaporation of water from the above ground organs of vascular plants after passing through plant tissues and intercellular spaces. Transpiration is distinct from abiotic evaporation (E), which is the flux of water from surfaces such as

leaf exteriors, stems, litter, or soil. The combined biotic and abiotic water fluxes are termed evapotranspiration (ET), a term which is a portmanteau of the words evaporation and transpiration. From the perspective of physics, both abiotic evaporation and transpiration would be simply the total ecosystem evaporation with the key difference that transpiration is actively regulated by plants, and therefore there are recent calls to move away from using the word evapotranspiration (Miralles et al., 2020). However, the term is useful in physiology and as such will be used here for consistency with the previously published chapters.

Transpiration is the intersection of water and carbon, as no known terrestrial plants manage the needed gas exchange of CO_2 and O_2 without water loss. Furthermore, the same plant traits that promote photosynthesis; such as leaves with a high surface area to volume ratio positioned in high sunlight; are also traits that promote transpiration, meaning water loss is inherently coupled to carbon fixation. On average globally, every 100 g of CO_2 fixed corresponds to 36 kg of water transpired (based on current estimates of global annual fluxes: 120 PgC gross primary productivity (GPP) (Jung et al., 2019), $6.7 \times 10^4 km^3$ water ET (Pan et al., 2020), and 64% T/ET (Good et al., 2015)). This high loss of water per unit carbon fixed creates a situation water limitations to carbon uptake due a lack of water is relatively common, indeed water availability is likely the dominant control of global terrestrial GPP (Jung et al., 2017).

Transpiration is not a purely negative phenomenon, as the flow of water also provides a highway for nutrients to be extracted from the soil and transported to leaves. Furthermore, plants have developed a number of traits and strategies for maximizing water resources (De Kauwe et al., 2015). For example, the ability of plants to access water reserves from deep soil layers is a vital ecosystem process and allows for sustained evaporative cooling, which in turn modulates air temperature (Fischer et al., 2007). Root systems used to extract water reserves also hold soil together and increase water use between precipitation events promoting water retention time and precipitation use (Carminati et al., 2010). On broad scales, ecosystem water fluxes may push precipitation into continents, acting as rain conveyor belts (Sheil and Murdiyarso, 2009; Spracklen et al., 2012). As transpiration from vascular plants is a key control valve on the global terrestrial water cycle, a better understanding of plant water fluxes will lead to an improved understanding of the earth system in general.

Quantification of transpiration is not only just an academic endeavor, but rather has real

world implications. For example, a meta-analysis from Liu et al. (2017) estimates 3.0 to 4.3 billion people will be living in areas exposed to water scarcity in the year 2050, and further highlights plant water use as a key uncertainty that is often overlooked when estimating water scarcity. Droughts characterized by limited soil moisture compounded by high atmospheric demand are projected to increase in both intensity and frequency (Zhou et al., 2019), and have been shown to significantly impact global GPP (Stocker et al., 2019) as well as pose a significant threat to global food security (He et al., 2019). In addition to the higher strain on existing water systems caused by climate change, many negative emission technologies for removing carbon from the atmosphere are projected to have significant water requirements (Smith et al., 2016; Rosa et al., 2020) and wide spread utilization could cause further stress to already fatigued freshwater systems.

Historical interest in transpiration has come out of the forestry and agricultural sectors (Wilm et al., 1944), as water has always driven economies and indeed been a key factor shaping the spread of humanity. Indeed, the preface of *Vegetable Staticks* by Stephen Hales (Hales et al., 1727), which reported the first measurements of transpiration, states “... so doubtless a farther insight into the vegetable æconomy must needs proportionally improve our skill in Agriculture and Gardening...” Being agriculturally focused, previous work on transpiration has been predominantly based on controlled environment and agricultural field studies (Kool et al., 2014). These studies have laid the groundwork for modern physiological understanding of plant water use. However, with climate change and the increasing interest in global cycles of the past decades, broader scale studies of how ecosystems, regions, and continents use water have become more prevalent (Fisher et al., 2017; Allen et al., 2015; Bernacchi and VanLoocke, 2015). The chapters of this thesis work toward bridging the existing gap between plant scale knowledge and measurements and the global processes through ecosystem scale estimates of transpiration.

1.2 Transpiration at different scales

Transpiration is a key phenomenon which is studied by many different fields and in many different contexts. These different approaches are generally tied to different scales. For example, a physiologist measuring a leaf sees transpiration as the dominant water

flux and might use units such as $mmol H_2O \cdot m^{-2} \cdot s^{-1}$. In contrast, a hydrologist looking across catchment basins will see transpiration as just one component in an orchestra of water fluxes which are measured in the thousands of $km^3 \cdot yr^{-1}$ of water. These different perspectives of the same fundamental process yield important insights, though transferring the principles of hydrology to the scale of a single leaf and vice versa can be challenging. As noted, this dissertation focuses on ecosystem scale, which can more easily integrate both micro- and macro-scale processes. Therefore, the following sections will briefly outline the core principles from scales which are important to understanding ecosystem transpiration.

1.2.1 Leaf and stomate

Transpiration in a simplified context, such as what would describe a leaf in a cuvette, can be characterized using simple Fickian diffusion,

$$T = 1.6 \cdot g_s \cdot (e_i - e_a)$$

where T is transpiration, g_s is the stomatal conductance of CO_2 , 1.6 is the ratio of the conductance of water to the conductance of CO_2 , and e_i and e_a are the intercellular and ambient water vapor concentrations, respectively. In the simplistic view, as well as in many more complex models, g_s is the key parameter to be estimated (Berry et al., 2010). Furthermore, g_s is what is actively modulated by plants and can be seen as the primary biological control valve. This modulation is key, as it both differentiates T and E fluxes and links the carbon and water cycles. The combination of the impermeable plant outer layers with well regulated openings for gas exchange (i.e. stomates) are a major advantage for terrestrial plants, allowing plants to mitigate CO_2 uptake to water loss, or water use efficiency (WUE). Versions of WUE and stomatal conductance are used in applications across scales, from basic physiology (Damour et al., 2010) to land surface models (Knauer et al., 2015), and therefore much work has been done to characterize the key factors influencing stomatal conductance. Stomates have been shown to respond to conditions that effect both photosynthesis and water loss such as light, temperature, ambient CO_2 concentrations, and atmospheric demand for water:

Stomatal response to light: Stomates open in response to light. The light response is

a clear example of the optimization of stomates to increase carbon gain to water loss, as opening stomates in the absence of light would result in no photosynthetic uptake while still allowing for water loss (Deans et al., 2019). The exception is in plants who utilize Crassulacean acid metabolism (CAM) photosynthesis, where stomates show a reversed response to light because CO_2 is stored in plant tissues during the night to be used for photosynthesis during the day as a water conservation adaptation (Osmond, 1978).

Stomatal response to VPD: Increasing atmospheric demand for water is typically measured as vapor pressure deficit (VPD), i.e. the difference between inter-cellular and ambient water vapor concentration. In general, exposing leaves to high VPD causes stomates to close (Buckley, 2005), which limits water losses when evaporative demand is high. This stomatal closure is seen as an evolutionary advantage because of the high cost of water per unit carbon gained under high VPD conditions which can result in very low WUE.

Stomatal response to temperature: The stomatal response to temperature can be difficult to differentiate from the effect of VPD, as stomates respond strongly to VPD, and VPD is directly related to temperature. However, there is evidence that high temperatures cause stomates to open to promote leaf cooling, even when photosynthesis is reduced due to very high temperatures (Urban et al., 2017b), potentially reducing WUE.

Stomatal response to ambient CO_2 : The stomatal response to CO_2 has been of high interest in recent years due to rising atmospheric CO_2 levels (Ainsworth and Rogers, 2007). The CO_2 effect has been well documented, showing that plants exposed to higher ambient CO_2 decrease stomatal aperture and therefore conductance (Morison, 1985). The decrease in conductance causes a reduction to transpiration, while at the same time the increase in CO_2 gradient between air inside and outside leaf increases the carbon uptake relative to stomatal conductance, ultimately causing an increase in WUE.

The fundamental understanding of stomates from individual leaves is currently the basis for modeling carbon assimilation and transpiration at all scales. The semi-empirical Ball-Berry model (Ball et al., 1987), or a derivative thereof, is the most common model of stomatal conductance used today (Berry et al., 2010). The Ball-Berry family of models calculates stomatal conductance as a function of net photosynthetic assimilation rate (which encapsulates the light and temperature responses), relative humidity (or

VPD depending on the model variant), and atmospheric CO_2 concentration, with two parameters: g_0 the minimum stomatal conductance in the absence of light and g_1 the sensitivity of photosynthetic assimilation to g_s , which relates to WUE. While the original Ball-Berry model was developed based on leaf experiments in a controlled environment, Cowan and Farquhar (1977) postulated that stomates should act in a way that maximizes carbon gain to water loss (stomatal optimality theory), generally characterized as stomates closing in response to high VPD to reduce water losses. Medlyn et al. (2011) has since shown that the empirical formulations of g_s match well with those derived from stomatal optimality principles, thus providing a unified framework for understanding and estimating stomatal function. However, studies have suggested that the stomatal response to VPD is not optimal (Lin et al., 2018), possibly due to non-stomatal limitations which disproportionately effect carbon uptake relative to water loss such (e.g. decreases in mesophyll conductance of CO_2 or limitation in carbon fixation pathways) (Reichstein et al., 2002; Novick et al., 2016b). Uncertainty and biases in stomatal conductance models have broad implications for estimates of carbon and water fluxes at other scales because entire ecosystems are often modeled as a “big leaf”, with leaf level processes upscaled to canopy and ecosystem level via an integration over the leaf area index (LAI). The implications of the uncertainty of this transfer of scale are explored further in Section 1.2.4.

1.2.2 Regional and global hydrology

Transpiration fits directly into the water balance equation, which is a fundamental equation in hydrology,

$$P = R + (E + T) + \delta S$$

where P is precipitation, R is runoff, $(E + T)$ is abiotic evaporation and transpiration, and δS is the change in water storage. While transpiration is known to be one of the largest terrestrial water fluxes (Oki and Kanae, 2006), plants are sometimes overlooked in the field of regional and global scale hydrology where ET can be considered the “background water footprint” (Bogardi et al., 2013). For example, in examining trends in terrestrial water storage and attributing those trends to underlying causes, Felfelani et al. (2017) did not explicitly reference plants. While Felfelani et al. (2017) did men-

tion crop irrigation and deforestation as drivers of terrestrial water storage, direct plant responses to climate change, such as changes in stomatal sensitivity with rising CO_2 (Gedney et al., 2006), were overlooked. On the one hand, removing plants from the large scale hydrological equation is understandable, as plants can be difficult to model across large and heterogeneous areas. However, there have been recent calls to integrate the fractured sub-disciplines of hydrology, including ecohydrology (Brooks et al., 2015; Clark et al., 2017). Of course, much research is being done with regards to regional plant-hydrology interactions, such as recent papers showing that groundwater can influence ET partitioning (Maxwell and Condon, 2016), and that plant activity can be affecting groundwater reserves (Koirala et al., 2017). Direct observations of transpiration at regional scales would likely improve understanding of regional and global hydrology.

1.2.3 Global

In general, global estimates of ET agree (Pan et al., 2020), but the individual components; transpiration, soil evaporation, and canopy interception evaporation; often have large disagreements (Wei et al., 2017; Talsma et al., 2018). One method to constrain the individual components of the global water budget is by using the ratio of heavy to light isotopes of water as a tracer, because while water vapor from soil evaporation is depleted of heavy isotopes, water vapor from transpiration is often assumed to be the same as the source root zone water, thus giving a unique isotopic signature to each process. Using models constrained by the isotopic signatures from oceans, run-off, evapotranspiration, and precipitation, Good et al. (2015) estimated a global T/ET of $64 \pm 13\%$ (mean ± 1 standard deviation) where ET includes transpiration, soil evaporation, interception, and evaporation from surface waters. An estimate of 64% is similar to other estimates based on up-scaling site level estimates of T/ET, both by ecozone ($61 \pm 15\%$, Schlesinger and Jasechko (2014)) and via an empirical function of T/ET with LAI ($57.2 \pm 6.8\%$, Wei et al. (2017)).

Currently, the isotopic and site-level data to estimate global T/ET are too sparse to accurately resolve T/ET in time. As discussed in Section 4.4.2, efforts to upscale site level T/ET data to global estimates rely on fewer than 100 studies with some studies dating back to 1941. Similarly, global isotopic estimates rely on even fewer surface measurements to constrain global estimates, e.g. six evapotranspiration isotope mea-

measurements in Good et al. (2015) and isotope measurements from only 56 lake catchments in Jasechko et al. (2013). Therefore, transpiration estimates must rely on model assumptions to constrain the problem. However, based on the spread in T/ET estimates, the assumptions used in different modeling approaches do not agree (Figure 1.1). Typical strategies for modeling transpiration on a global level range from process based models, e.g. the components of earth system models such as those used in the Coupled Model Intercomparison Project (CMIP), or can be based on relatively simple and/or empirical relationships paired with external data sources, such as estimates based on remote sensing data (Stoy et al., 2019). However, both process models and remote sensing based methods can show high variability among T/ET estimates. For example CMIP5 models ranged from 15 to 60% T/ET (Berg and Sheffield, 2019), while T/ET from 3 different remote sensing products ranged from 24 to 75% T/ET (Miralles et al., 2016). This large spread in the magnitude of T/ET, with many estimates not agreeing that transpiration is the dominant component of ET as is generally agreed upon from the data derived estimates of T/ET (e.g. site up-scaled and isotope based estimates), demonstrates a fundamental deficiency in how transpiration is modeled and understood on a global scale. More data driven estimates of transpiration, both in space and in time, could help diagnose the issues with global models by providing a better understanding on the key driver of T/ET.

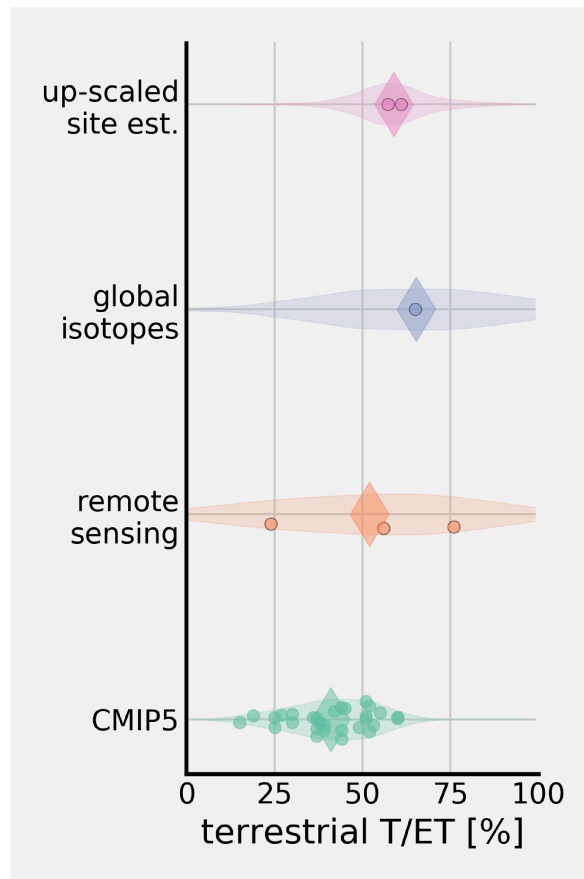


Figure 1.1 Global transpiration as a fraction of terrestrial ET. Shading represents the probability density functions based on either model variability (CMIP5 and remote sensing) or reported uncertainty (global isotopes and up-scaled site estimates). CMIP5 data from Berg and Sheffield (2019), remote sensing data from Miralles et al. (2016), global isotopes from Good et al. (2015) and up-scaled site estimates from Wei et al. (2017) and Schlesinger and Jasechko (2014).

1.2.4 Scale mismatch and source of error

While the generalized stomatal conductance model formulations derived from leaf level experiments and optimality theory (e.g. the Ball-Berry and Medelyn models, see Section 1.2.1) have come a long way in describing water and carbon fluxes from plants, ecosystems which are composed of diverse individuals are much harder to generalize and do not always behave as a leaf in a cuvette. Here we revisit the leaf level responses of stomates from Section 1.2.1, but in the context of ecosystems:

Ecosystem response to light: While the incidence angle of how light hits a single leaf

is less important than the total amount of light, diffuse light caused by clouds and aerosols has the effect of spreading incoming light energy over more leaves which increases overall plant photosynthetic efficiency. In essence, rather than leaves at the top of the canopy receiving the majority of the light and overloading photochemical pathways (Müller et al., 2001), diffuse light allows for more of the canopy to contribute to carbon uptake resulting in a more efficient use of light overall (Li et al., 2014). Diffuse light not only improves carbon uptake per unit light, but also increases water use efficiency (Pedruzo-Bagazgoitia et al., 2017; Gao et al., 2018) and the fraction of energy used for evaporating water relative to total available energy (evaporative fraction) (Wang et al., 2008). Including the effect of diffuse light in land surface models has been shown to have large impacts on the estimated global carbon sinks (Mercado et al., 2009), but the implications on global water fluxes is less well characterized.

Ecosystem response to VPD: While the stomatal response to VPD has been relatively well characterized, high values of VPD typically correspond to periods of overall water limitations where whole plant survival strategies may alter the carbon cost of water calculus and thus stomatal responses. For example, the long hydraulic pathways in trees are more susceptible to damage under water stress and therefore many plant adaptations, such as increased stomatal closure or dropping leaves, have evolved to prevent mortality (Choat et al., 2018). Furthermore, high VPD is often associated with soil water depletion and water stress (Zhou et al., 2019). While the effect of VPD has been shown to be stronger than that of soil moisture supply (Novick et al., 2016a), many stomatal models still fail to capture the effects of drought (Damour et al., 2010), which is further compounded by the diverse responses to water limitation found in different ecosystems (De Kauwe et al., 2015).

Ecosystem response to temperature: While mean temperatures can be a key predictor of vegetation activity, extreme temperatures can cause direct damage to plant tissues, which can have long term effects on carbon and water fluxes. Cold weather events have been shown to impact ecosystem water and carbon fluxes by causing vegetation damage leading to decreases in vegetation and photosynthetic activity long after the initial event (Gu et al., 2008). Furthermore, plants can also change stomatal function to increase evaporative cooling from transpiration, at a cost to photosynthesis, in order to prevent high temperature damage. Drake et al. (2018) showed a complete decoupling of water and carbon fluxes in Eucalyptus trees by exposing them to extreme heat over four consecutive days, with severe limitations to photosynthesis but continued transpiration,

an effect which could not be explained by stomatal optimality. In a further study, De Kauwe et al. (2019) did not find widespread evidence of decoupling due to extreme heat across 14 sites, however the authors note that ET was used as a proxy of transpiration which could obscure the physiological decoupling effect due to influences of abiotic evaporation.

Ecosystem response to ambient CO_2 : While the effect of increased CO_2 causing stomates to close, thus reducing transpiration while increasing WUE, is well established at the leaf scale, the ecosystem scale response has been much more uncertain. Keenan et al. (2013) reported that the increasing trend in WUE over time (associated with the increase in CO_2 from anthropogenic sources) in 14 forested sites was much larger than predicted by terrestrial biosphere models. However, Knauer et al. (2017) determined that such a large trend was not plausible, finding that transpiration at the ecosystem scale was less sensitive to increases in CO_2 than at the leaf scale due to a decoupling between the conditions experienced by individual leaves compared to the general ecosystem atmosphere. For example, in a free-air CO_2 enrichment experiment, Wullschlegel et al. (2002) showed that while seasonal stomatal conductance was reduced by 22% in the elevated CO_2 treatments, the reduction was primarily found in upper canopy leaves, with mid and lower canopy leaves showing little reduction in stomatal conductance, and only a 14% reduction in integrated canopy conductance and a 10% reduction in transpiration.

The above examples demonstrate that while models are able to generalize stomatal conductance, and thus water and carbon fluxes, under typical experimental conditions, the whole plant and community responses can be much harder to generalize. The normal carbon cost of water calculous to optimize carbon uptake to water loss might change due to longer term strategies of survival, and non-stomatal effects can also alter the carbon to water relationship independent of stomatal conductance (Novick et al., 2016b; De Kauwe et al., 2019). All of these potential sources of error have major implications for predicting not only carbon and water fluxes, but also how the earth system will respond to a changing climate, and as such, recent reviews have highlighted the water to carbon relationship is a major point of improvement in understanding both terrestrial carbon (Rogers et al., 2017; Dietze et al., 2014), and water cycles (Fisher et al., 2017; Allen et al., 2015; Bernacchi and VanLoocke, 2015).

1.3 Eddy covariance: a measure at ecosystem scale

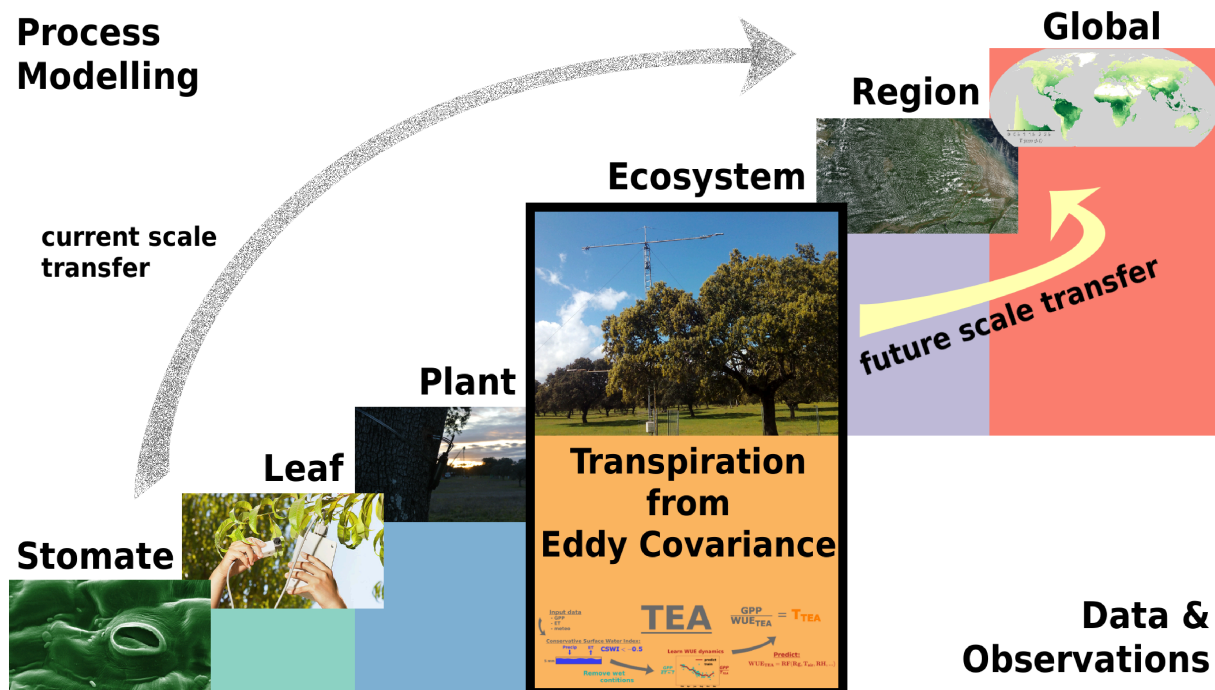


Figure 1.2 Transpiration from eddy covariance data provides the missing step between physiological measurements at the leaf/plant scale and global to regional modeling. The data driven approach presented in Chapter 3 (the Transpiration Estimation Algorithm, TEA) provides an alternate view of ecohydrological function compared to the process based approaches which rely on scaling stomatal conductance processes to global scales. Leaf photo from Peggy Greb (CC BY 2.0), Plant and Ecosystem photos from Mirco Miglivacca.

The eddy covariance technique is one of the most successfully utilized methods for estimating ecosystem water, carbon, and energy fluxes. Eddy covariance measures energy and gas fluxes from within a tower footprint, with radii typically on the order of a few hundred meters to one or two kilometers. While eddy covariance is suitable to measure many gases and tracers, systems typically measure fluxes of latent and sensible energy, CO_2 , as well as radiation and meteorological variables. Such systems run nearly continuously, with some systems now having run for over 20 years, e.g. the Harvard Forest site has been running since 1991 (Munger, 2016). Around 1995, the eddy covariance community formed plans to aggregate data from sites around the world (Baldocchi et al., 1996), producing a homogenized flux network or FLUXNET (Baldocchi, 2020) (Fig-

ure 1.3). Synthesis of the flux data has shown to be powerful for studies of ecosystem function around the world, as well as for model evaluations, parameterizations, and links to global data such as remote sensing (Baldocchi, 2020).

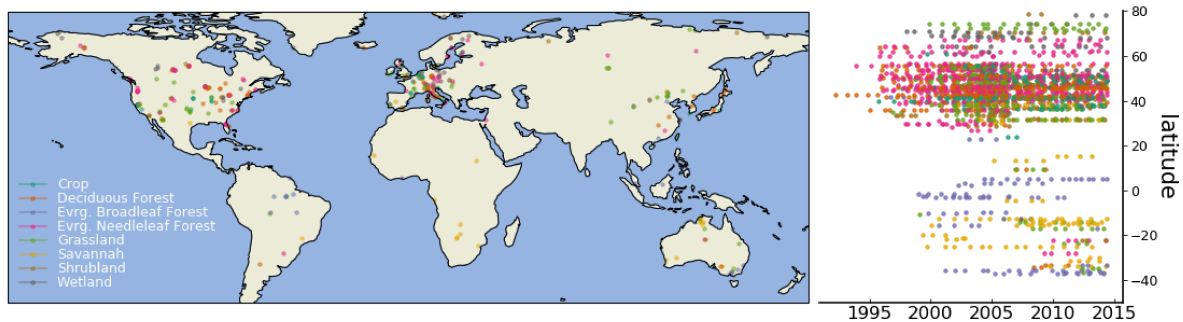


Figure 1.3 Locations and time-spans of eddy covariance data used in this dissertation, colored by plant functional type (PFT).

Analysis of CO_2 fluxes from eddy covariance have proven particularly useful, due to methods for estimating gross primary productivity (GPP) and ecosystem respiration (RECO) (Reichstein et al., 2005a; Lasslop et al., 2010). GPP estimates have given insights into ecosystem functioning from a data driven perspective (Musavi et al., 2017; Baldocchi, 2020), and have been used to inform and evaluate the global models which drive global policy decisions concerning climate change (Baldocchi and Penuelas, 2019; Bonan et al., 2011). The success of the partitioning of the net CO_2 flux has in part motivated the search for ET partitioning methods based on eddy covariance data, with the hope that a better understanding of ecosystem scale transpiration will similarly influence the water components of global models. However, partitioning ET is a more challenging problem, in part because both E and T are primarily driven by VPD and water availability, in contrast to the carbon fluxes where GPP is driven primarily by light and RECO primarily by temperature. To overcome these difficulties, many approaches to estimate ecosystem transpiration have utilized additional physiological measurements, such as sap flow or leaf estimates of stomatal conductance, rather than relying solely on the core eddy covariance data which integrates the entire ecosystem signal. However, plant and ecosystem scale estimates are not always consistent (Medlyn et al., 2017; Medrano et al., 2015), and there are significant uncertainties in up-scaling plant measurements such as sap flow (Oren et al. (1998), ermák et al. (2004), and see Section 4.4.2). Furthermore, dependence on measurements additional to the core eddy covariance datasets greatly limits the amount of historical data where transpiration could be

estimated.

The approaches of estimating ecosystem scale transpiration are reviewed briefly in Section 3.1, and in depth in Stoy et al. (2019) (co-authored during the work of this thesis). The advantages and disadvantages of common methods are briefly summarized in Table 1.1. While these approaches are important and have their advantages, the limited number of measurements are likely not enough to characterize global variability, so a method that uses the existing eddy covariance datasets would be much more powerful in constraining global uncertainty. Therefore, the core objective of this thesis is to develop and evaluate a data driven method for estimating transpiration from eddy covariance data.

Table 1.1 A brief overview of methods for estimating ecosystem scale transpiration. Methods are reviewed in detail in Stoy et al. (2019) and Section 3.1.

| Advantages | Limitations | Citation |
|---|--|-----------------------|
| Flux-variance similarity | | |
| Requires few additional measurements and has a firm theoretical foundation. | Sensitive to WUE assumptions and data processing limitations. | Scanlon et al. (2019) |
| Sap flow | | |
| Widely available datasets (SAPFLUXNET) directly connected to physiology. | Methodological uncertainties (see Section 4.4.2), only for trees | Poyatos et al. (2019) |
| Carbonyl sulfide | | |
| Provides an independent method to estimate canopy conductance. | Unknown sinks/sources of OCS and lack of measurements. | Whelan et al. (2018) |
| Isotopes | | |
| Gives an ecosystem integrated estimate. | High uncertainties and lack of measurements. | Beyer et al. (2020) |

| Advantages | Limitations | Citation |
|---|--|----------------------------|
| Above and below canopy EC | | |
| Same temporal resolution and integrated ecosystem estimates as normal EC. | Combines understory T and soil E and lack of measurements. | Paul-Limoges et al. (2020) |

1.4 Technical approach and use of machine learning

While an ET partitioning method should be built off of sound physical and physiological principles, the limitations of current ecosystem stomatal models necessitates a method which does not make too many physiological assumptions. Utilizing machine learning gives a data driven perspective, allowing the resulting transpiration estimates to be more independent from processed based models. Machine learning approaches, guided by expert knowledge, provide the opportunity to exploit statistical relationships in the data in a robust and powerful way (Jordan and Mitchell, 2015; Reichstein et al., 2019).

Previous works have shown the potential benefits of using machine learning techniques on eddy covariance data and have the advantage of being able to extract complex relationships in the data. For example, machine learning based methods for partitioning NEE have been developed and generally agree with widely accepted methods (Desai et al., 2008; Tramontana et al., 2020). Furthermore, the data driven approaches may have advantages over traditional methods which impose hard theoretical constraints, such as NEE partitioning methods which dictate the shape of the photosynthetic light response curve (Tramontana et al., 2020).

While other machine learning methods exist, Random Forests (Breiman, 2001) are used in every chapter of this dissertation, due to the robust nature of the algorithm and its proven ability to perform well in many situations. Random Forest have previously been used as a bench mark when comparing methods due to the fact its robust ability to produce results with minimal configuration (Besnard et al., 2019). The key use of Random Forest in this work is embedded in the TEA algorithm (Chapter 3), where the ability to predict quantiles (Meinshausen, 2006) is key to the functionality of the algorithm.

1.5 Aims, outline, and objectives

The practical objective of this thesis was to produce a method for estimating transpiration from existing eddy covariance datasets that is generally applicable and data driven. Given that the method is data driven, much of the work involved comes not only from the technical building of the methodology, but first evaluating the data as well as patterns within the data which the method can exploit (Chapter 2), then technical evaluation of the method and uncertainties (Chapter 3), and finally application of the method and evaluation of the resulting global patterns (Chapter 4). Chapter 2 looks at diurnal patterns of water and carbon fluxes, introducing two indices which were shown to hold information on drought response and are used in the subsequent chapters. Chapter 3 introduces the Transpiration Estimation Algorithm (TEA) and evaluates the method using model output in controlled experiments where all ecosystem fluxes are known. Chapter 4 then uses TEA, as well as other transpiration estimation methods, to estimate transpiration across FLUXNET and evaluate global patterns. While much of the work of the thesis is synthesized in Chapter 4, Chapter 5 summarizes the findings as well as gives an overview of work which has since utilized TEA and an outlook of future work.

1.5.1 Research questions

RQ 1: How can information in the core eddy covariance datasets be further exploited to describe the complex plant water relationships from heterogeneous communities?

As outlined in this introduction, there are known limitations to current stomatal and transpiration models. Furthermore, supplementary input data, such as leaf measurements, sap flow, and plant available soil moisture are hard to quantify on broad scales. A key question that emerges is whether one can capture the dynamic ecosystem responses in WUE and transpiration with the core EC measurements, therefore giving the biggest impact of broad-scale transpiration estimates across a large variety of ecosystems from the existing eddy covariance datasets. Can complex ecosystem processes such as drought be identified through the ecosystem responses alone, such as via indicators from diurnal cycles?

RQ 2: Given the limited amount of independent ecosystem transpiration data concurrent with eddy covariance measurements, how can the transpiration estimates be validated?

The lack of ecosystem scale transpiration estimates both necessitates an ET partitioning method, but also makes validation of the transpiration estimates from the partitioning methods difficult. Furthermore, many partitioning methods, including the TEA method described in Chapter 3, assume that transpiration dominates ET in a way that allows for a model to be built using the ET measurement directly. As reviewed in Stoy et al. (2019), this assumption is often debated and is a major critique of these methods. Can the assumption transpiration dominates ET during some periods be made and how will the violation of this assumption impact the resulting WUE and transpiration estimates?

RQ 3: What new insights on ecohydrological and water use strategies across major terrestrial biomes can be gained from the transpiration estimates derived from FLUXNET?

Current global predictions of T/ET are highly uncertain, uncertainties which will likely propagate into carbon and hydrological cycles for future climate predictions. The data driven approach from TEA applied to the FLUXNET dataset may give insight as to how to better model transpiration dynamics from diverse ecosystems. How can the potentially broad spatio-temporal coverage of transpiration estimates from FLUXNET inform the current understanding of transpiration?

Chapter 2

Water stress induced breakdown of carbon-water relations: indicators from diurnal FLUXNET patterns

Biogeosciences, 15, 2433–2447, 2018
<https://doi.org/10.5194/bg-15-2433-2018>
© Author(s) 2018. This work is distributed under the Creative Commons Attribution 3.0 License.



Water-stress-induced breakdown of carbon–water relations: indicators from diurnal FLUXNET patterns

Jacob A. Nelson¹, Nuno Carvalhais^{1,2}, Mirco Migliavacca¹, Markus Reichstein^{1,3}, and Martin Jung¹

¹Department of Biogeochemical Integration, Max Planck Institute for Biogeochemistry, Jena, Germany

²Faculdade de Ciências e Tecnologia, FCT, Universidade Nova de Lisboa, Lisbon, Portugal

³Michael Stifel Center Jena for Data-Driven and Simulation Science, Jena, Germany

Correspondence: Jacob A. Nelson (jnelson@bgc-jena.mpg.de)

Received: 20 April 2017 – Discussion started: 16 October 2017

Revised: 8 February 2018 – Accepted: 27 February 2018 – Published: 20 April 2018

Abstract. Understanding of terrestrial carbon and water cycles is currently hampered by an uncertainty in how to capture the large variety of plant responses to drought. In FLUXNET, the global network of CO₂ and H₂O flux observations, many sites do not uniformly report the ancillary variables needed to study drought response physiology. To this end, we outline two data-driven indicators based on diurnal energy, water, and carbon flux patterns derived directly from the eddy covariance data and based on theorized physiological responses to hydraulic and non-stomatal limitations. Hydraulic limitations (i.e. intra-plant limitations on water movement) are proxied using the relative diurnal centroid (C_{ET}^*), which measures the degree to which the

water use efficiency (WUE) models, we found the mean differences between expected and observed WUE to be -0.09 to $0.44 \mu\text{mol mmol}^{-1}$ and -0.29 to $-0.40 \mu\text{mol mmol}^{-1}$ for decoupled and morning-shifted days, respectively, compared to mean differences -1.41 to $-1.42 \mu\text{mol mmol}^{-1}$ in dry conditions, suggesting that morning shifts/hydraulic responses are associated with an increase in WUE, whereas decoupling/non-stomatal limitations are not.

1 Introduction

Water stress induced breakdown of carbon-water relations: indicators from diurnal FLUXNET patterns

Jacob A. Nelson¹, Nuno Carvalhais^{1,2}, Mirco Migliavacca¹, Markus Reichstein^{1,3},
Martin Jung¹

¹Department of Biogeochemical Integration, Max Planck Institute for Biogeochemistry, Jena, Germany

²Faculdade de Ciências e Tecnologia, FCT, Universidade Nova de Lisboa

³Michael-Stifel-Center Jena for Data-Driven and Simulation Science, Jena, Germany

Understanding of terrestrial carbon and water cycles is currently hampered by an uncertainty in how to capture the large variety of plant responses to drought. In FLUXNET, the global network of CO₂ and H₂O flux observations, many sites do not uniformly report the ancillary variables needed to study drought response physiology. To this end, we outline two data-driven indicators based on diurnal energy, water, and carbon flux patterns derived directly from the eddy covariance data and based on theorized physiological responses to hydraulic and non-stomatal limitations. Hydraulic limitations (i.e. intra-plant limitations to water movement) are proxied using the relative diurnal centroid (C_{ET}^*), which measures the degree to which the flux of evapotranspiration (ET) is shifted toward the morning. Non-stomatal limitations (e.g. inhibitions of biochemical reactions, RuBisCO activity, and/or mesophyll conductance) are characterized by the Diurnal Water:Carbon Index (DWCI), which measures the degree of coupling between ET and gross primary productivity (GPP) within each day. As a proof of concept we show the response of the metrics at 6 European sites during the 2003 heatwave event, showing varied response of morning shifts and decoupling. Globally, we found indications of hydraulic limitations in the form of significantly high frequencies of morning shifted days in dry/Mediterranean climates and savanna/evergreen plant functional types (PFT), whereas high frequencies of decoupling were dominated by dry climates and grassland/savanna PFTs indicating a prevalence of non-stomatal limitations in these ecosystems. Overall, both the diurnal centroid and DWCI were associated with high net radiation and low latent energy typical of drought. Using three water use efficiency (WUE) models, we found the mean differences between expected and observed WUE to be -0.09 to 0.44 umol/mmol and -0.29 to -0.40 umol/mmol for decoupled and morning shifted days respectively compared to mean differences -1.41 to -1.42 umol/mmol in dry conditions, suggesting that morning shifts/hydraulic responses are associated with an increase in WUE whereas decoupling/non-stomatal limitations are not.

2.1 Introduction

Processes such as photosynthesis and transpiration are so intimately linked that knowledge and assumptions about one process are needed to accurately understand the other. Unfortunately, the relationship between carbon and water cycles is not fully understood (Tang et al., 2014), passing the biases and uncertainties caused by an incomplete carbon:water framework back onto flux estimates specifically and global water and carbon cycle interactions and dynamics in general (Keenan et al., 2013; Schlesinger and Jasechko, 2014; Ito and Inatomi, 2012). One source of uncertainty that is increasingly being identified is the diverse responses of plants to water limitation (Zhou et al., 2013; Dietze et al., 2014; Rogers et al., 2017), which hampers the understanding and predictability of water and carbon cycles during drought. Here we outline potential causes of uncertainty in carbon:water dynamics in an effort to outline data-derived inductors based on current theory.

Classically, vegetation water and carbon fluxes are linked by stomates, where an open stomate allows CO₂ to enter the leaf and, consequentially, water is lost. Most theoretical frameworks make some form of assumption that carbon assimilation (*A*) and water losses (*T*) are both contingent primarily on leaf stomatal conductance (*g_s*). This assumed relationship allows us to pass between the realms of carbon and water, based on the assumption that at any given time both *A* and *T* are proportional to the stomatal conductance multiplied by the difference in internal and external CO₂ and water vapor concentrations. More specifically,

$$A = g_s \cdot \Delta c \quad \text{and} \quad T = 1.6 \cdot g_s \cdot \Delta v \quad (2.1)$$

where *c* and *v* are the differences in inner and outer stomatal cavity concentrations of CO₂ and water vapor, respectively. These diffusion equations lead to the relatively consistent carbon:water ratio, generally expressed as a water use efficiency ($WUE = A/T$). At the ecosystem level where direct measurements of *A* and *T* are not available, *WUE* is simply calculated as the ratio of gross primary productivity (*GPP*) to total evapotranspiration (*ET*) (Kuglitsch et al., 2008). These carbon:water links are fundamental to understanding how stomata are regulated and underly key functioning in mechanistic plant and ecosystem models. One such set of models are those based on optimality the-

ory which posit that plants tend to optimize carbon gains to water losses, such as those described by Katul et al. (2010) and Katul et al. (2009). These concepts from Katul, which carry the assumptions of RuBisCO (light) limitation, were built upon by Zhou et al. (2014) and Zhou et al. (2015) to give the equation,

$$uWUE = \frac{GPP \cdot \sqrt{VPD}}{ET} \quad (2.2)$$

where the \sqrt{VPD} accounts for the stomatal response to vapor pressure deficit (VPD) assuming stomatal response optimizes carbon gain to water losses. Accounting for the VPD response allows for a more stable metric of WUE that is temporally more stable and physiologically more meaningful, such as when comparing the diurnal cycles of carbon and water. As ET is the sum of both T and non-biological evaporation (e.g. soil and intercepted evaporation), often periods during and shortly after rain events are excluded from WUE estimates to minimize the influence of non-plant evaporation. Ultimately, calculations of WUE provide a simple summary of the cost in water per carbon gain and becomes an indicator for how plants have and will adapt to the physical limitations of their changing environments (Keenan et al., 2013; Tang et al., 2014).

Though assuming a rigid carbon:water relationship works well in conditions when ecosystems are moderately wet, conditions associated with the majority of carbon and water fluxes, an inflexible carbon:water assumption is unsatisfactory in that these assumptions may breakdown as plants shift from light to water limitations. Indeed, in a review of leaf level stomatal conductance models, Damour et al. (2010) concluded that the majority of stomatal models fail to adequately capture the effects of drought. This failure to capture the effects of drought is not only disconcerting as water limited conditions are when ecosystems are most at risk, but an incomplete framework tends to propagate errors and uncertainties from models into estimates of the water and carbon cycles. For instance, in outlining a road map for improved modeling of photosynthesis, Rogers et al. (2017) noted as key recommendations both improving information about water:carbon relations (in the form of the stomatal slope parameter g_1) as well as improving understanding of the response of carbon assimilation to drought. Similarly, in an analysis of parameter uncertainties for a terrestrial biosphere model, Dietze et al. (2014) found that two of the top five parameters contributing to the predictive uncertainty of net primary productivity were associated with plant water regulation. This uncertainty is reflected in the stomatal conductance parameterization

exercise from Knauer et al. (2015), where the authors were able to improve model performance in predicting EC measured GPP and ET by including atmospheric effects (in the form of VPD) on stomatal conductance, but concluded that further improvement required global understanding of water limitation response variation across plant functional traits and growing conditions, which is currently unavailable.

Two ideas to account for the errors in carbon:water assumptions under dry conditions have begun to emerge: that hydraulic limitations in transporting water from root to leaf change stomatal responses and thus limit transpiration under high demand, or that changes in the intra-leaf processes of carbon transport and fixation under drought conditions result in non-stomatal limitations that impact carbon assimilation independently of water fluxes (Novick et al., 2016b).

As soil water potentials in the root zone become increasingly negative, the long-term plant strategy may turn from optimizing carbon fixation to preventing damage to hydraulic architecture (Tyree and Sperry, 1988). As such, stomata and transpiration are likely to increasingly respond not just to atmospheric conditions, but also soil moisture. Under this hydraulic limitation framework, a plant will be reacting to the inability to transport water, even though the key control mechanism for a plant is via the stomata, possibly expressed as an increase in sensitivity. Such assumptions are consistent with the mechanisms encoded in some land surface and ecosystem models, which account for water limitations by scaling the water to carbon ratio in relation to available soil moisture. Though this method should link the leaf physiology to the soil and thus capture some hydraulic limitation, it has been criticized for not capturing the variety of drought responses found in different plant species and ecosystems (De Kauwe et al., 2015). This diversity in plant responses has been pointed to as a key point of uncertainty in earth system models (Dietze et al., 2014).

Though ecosystem water and carbon fluxes are predominantly controlled by stomates, non-stomatal or bio/photo-chemical inhibitions to carbon assimilation are worth considering as they have the capacity to decouple the water-carbon exchange. This decoupling could include conditions where the stomates are transpiring water but intra-leaf factors are slowing carbon fixation, changing the intrinsic water use efficiency directly. Intra-leaf factors could include effects such as production of reactive oxygen species (Lawlor and Tezara, 2008); environmental limitations to the photosynthetic pathways, such as leaf temperature (Medlyn et al., 2002); or declines in mesophyll conductance (Flexas

et al., 2012). Non-stomatal limitations have been observed at ecosystem scale (Reichstein et al., 2002; Migliavacca et al., 2009), though the exact mechanism is difficult to elucidate (Reichstein, 2003). These effects likely vary between species, as well as with the rate of onset of drought, access to water, and other environmental conditions.

2.1.1 Objectives

There seems to be a collective conclusion that the breakdown of carbon:water assumptions needs to be better characterized in general, and specifically for implementation in modeling frameworks (De Kauwe et al., 2015; Manzoni, 2014; Zhou et al., 2013; Flexas et al., 2012; Egea et al., 2011). Though the problem is becoming clear, the way forward is hampered by an uncertainty in how to capture the large variety in the response to drought across climates, strategies, and species. In this sense, the use of EC measured diurnal patterns of carbon, water, and energy fluxes to derive clues on ecosystem drought responses at a daily resolution could prove valuable both as a means to identify potential periods of ecosystem stress, inform machine learning algorithms on ecophysiological conditions not found in environmental variables, as well as benchmarking a models ability to capture sub-daily dynamics. To this end, we propose two data-driven indicators of water stress, the diurnal water:carbon index (DWCI) and the relative diurnal centroid in LE (C_{ET}^*). Both metrics are derived directly from the EC data and based on expected physiological responses to hydraulic and non-stomatal limitations. Using these data-driven indicators we then characterize the distribution of these limitations across a global spread of climate and vegetation types. Finally, we explore the ability of these indicators to detect the disagreements between modeled and observed water use efficiency, and explore how these biases may be attributed to hydraulic and non-stomatal limitations.

2.2 Methods and Materials

2.2.1 Data

Carbon, water, and every fluxes measured with EC, as well as meteorological data, were obtained from the 2007 FLUXNET La Thuile Synthesis Dataset (*FLUXNET Data*

Download 2007). Half-hourly latent heat and net ecosystem exchange (NEE) fluxes were collected and processed using standard QA/QC procedures (Papale et al., 2006), gap-filling and partitioning algorithms (Reichstein et al., 2005b). From the database, half-hourly gross primary productivity (GPP) and ET data (derived from latent heat flux measurements) were downloaded and used for the following analysis. An interactive map of sites used can be found in File S1.

In order to provide a consistent measure of ecosystem dryness that can be utilized across sites, the ratio of water evaporated to potential water evaporated was calculated as evaporative fraction (EF), or the fraction of actual ET to Potential ET (PET). PET was calculated as the daily fraction between the measured ET and estimated ET via a Priestly-Taylor model (Priestley and Taylor, 1972) using site measured net radiation (R_n) and air temperature (T_{air}). The slope (alpha parameter) was fit for each site-year using 95th quantile regression (Koenker and Bassett Jr, 1978) instead of using the original 1.26 value derived for a “well watered crop” (Priestley and Taylor, 1972).

In order to get high quality data and minimize the influence of abiotic evaporation (hereafter just evaporation), all data was filtered with the aim to include only non-gap filled data in the growing season with dry surface conditions. Growing season was defined as all days where $GPP > 1 \text{ gC} \cdot \text{m}^{-2} \cdot \text{d}^{-1}$ and daily mean air temperature > 5 °C. These threshold were shown to give good response in the proposed metrics while minimizing variability due to low diurnal signals, a sensitivity analysis of which can be found in supplementary Figure S2. In an effort to minimize contributions of evaporation, the conservative soil wetness index (CSWI) was employed which was designed to estimate whether the ecosystem is likely to have “dry” surfaces and therefore ET is likely to be dominated by transpiration. This approach requires a certain amount of evaporation to occur after a rain event before the surface is considered to be “dry” and can be contrasted to the method of removing a set time period after rain employed in previous studies (Medlyn et al., 2017; Beer et al., 2009; Keenan et al., 2013). CSWI is calculating by first quantifying the storage at time t (S_t) as,

$$S_t = \min(S_{t-1} + P_t - ET_t, S_o) \quad (2.3)$$

where ET_t and P_t are the ET and precipitation at time-step t respectively, S_t is effectively capped at a maximum storage value of S_o , which was set to 5 mm. Furthermore, to make

the metric conservative in regards to assumed water inputs, any precipitation event will refill the storage from 0 mm,

$$CSWI = \max(S_t, \min(P_t, S_o)) \quad (2.4)$$

which has the effect of requiring all precipitation up to 5 mm to be evaporated from the system before negative storage can occur. Any gaps in the precipitation data were assumed to be a precipitation event of 5 mm in order to prevent any unmeasured precipitation from biasing the results by inadvertently including rainy days. Code and further outline of the algorithm can be found in File S3 as well as at Nelson (2017). Evaporation was assumed to be negligible when $CSWI < 0$. This method was used over the more standard method of removing 1-5 days after a rain event, as it does not make the assumption that the surface will dry in a fixed amount of time, instead relying on a minimum amount of ET. As a comparison, the median time period for the CSWI to go from fully wet ($CSWI=5$) to “dry” ($CSWI \leq 0$) was 3.5 days across all sites in summer, where summer was defined as the period when daily potential radiation above median daily potential radiation for each site.

The data filtering as outlined in this section was designed to isolate periods firmly in the growing season when plants are active and the signal of ET is most likely to be dominated by plant controls.

2.2.2 Relative diurnal centroid (C_{ET}^*)

As soils dry, it becomes more difficult to transport stem and root zone moisture to the leaf, potentially causing hydraulic limitations for the plant to transport water. This shift was seen in eddy covariance data in a study by Wilson et al. (2003), who examined the shift of latent compared to sensible heat, which suggested that a shift in water fluxes towards dawn can be indicative of afternoon stomatal closure. Shifts were further explored in a modeling study by Matheny et al. (2014) which found that the morning shift was not well captured by models and attributed the errors to inadequate hydraulic limitations in the models. The daily cycle of wetting and drying acts as a capacitor in the hydraulic circuit, allowing water stores to be more easily transported in the morning and depleting in the afternoon. As bulk soil moisture declines, this effect may be strong

enough to shift the diurnal cycle of ET significantly toward the morning. Quantifying diurnal shifts in EC data using the diurnal centroid was first explored by Wilson et al. (2003): defined as the flux weighted mean hour, or

$$C_{flux} = \frac{\sum flux_t \cdot t}{\sum flux_t} \quad (2.5)$$

where t is a regular, sub-daily time interval (here t measures as decimal hour at half-hourly time-step). The resulting C_{flux} is the weighted mean hour of the diurnal cycle of that particular flux for that particular day. For example, if a calculated C_{ET} for a given day (using measurements of decimal hour) equals 12.25, this would entail that the weighted mean for that day is 15 minutes past noon. Figure 1 shows an example of the shifts in the monthly average cycle from a wet month to a dry month. In order to isolate a shift, we then had to control for variations in global radiation (Rg), both fluctuations due to clouds and differences in the timing of solar noon. Therefore, the difference between the diurnal centroids of ET (C_{ET}) and Rg (C_{Rg}) was calculated as

$$C_{ET}^* = C_{Rg} - C_{ET} \quad (2.6)$$

giving C_{ET}^* as the diurnal centroid of ET relative to Rg. The resulting values of C_{ET}^* are not tied to the carbon cycle, which can be affected by non-stomatal limitations and generally shows a more prominent midday depression. Annotated code for the CSWI calculation can be found in File S4 as well as at Nelson (2017). Though a diurnal centroid can be calculated for any diurnal cycle, basing a metric on the morning shift of ET relative to Rg has the advantage of targeting the non-atmospheric drivers of the water flux, of which there are few ancillary variables.

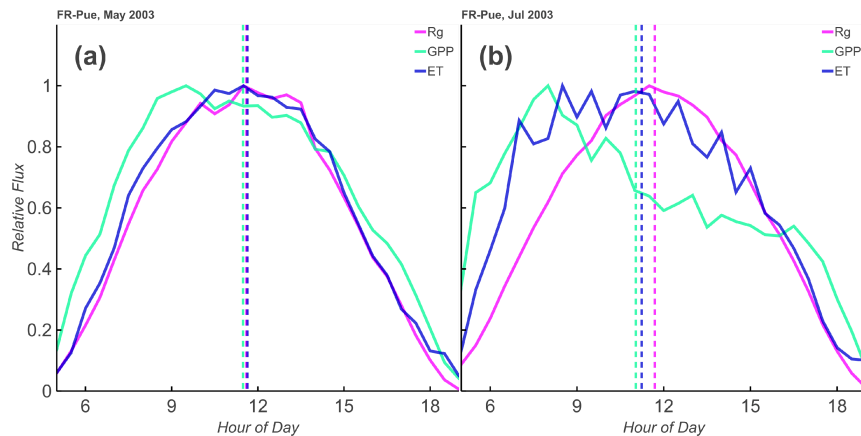


Figure 2.1 One month average cycle (solid lines) and accompanying diurnal centroid (vertical dashed lines) of incoming shortwave radiation (Rg), evapotranspiration (ET), and gross primary productivity (GPP) at the Peuchabon, France ('FR-Pue') site during 2003. May is relatively wet (32 mm rainfall, left) and July is relatively dry (0 mm rainfall, right). While ET and Rg correspond well in the wet month, the dry month shows a distinct phase shift in both GPP and ET fluxes towards the morning, as well as a midday depression in GPP.

2.2.3 Diurnal water carbon index (DWCI)

If transpiration and carbon assimilation are predominantly controlled by stomatal conductance, it follows that their diurnal cycles should be largely in sync. In other words, regardless of a plant's maximum T or A, if the stomata start to close, both rates should decrease by a similar percentage. On the other hand, non-stomatal limitations that inhibit carbon assimilation independent of water have the capability to alter the diurnal cycle on just one flux, causing them to decouple. In an effort to quantify the degree of carbon:water coupling for an individual day, we examined the relationship of GPP and ET, where,

$$ET \propto GPP \cdot \sqrt{VPD} \quad (2.7)$$

or,

$$ET = i \cdot GPP \cdot \sqrt{VPD} \quad (2.8)$$

This relationship incorporates the assumption that, at least over short time scales, the amount of carbon that enters the leaf is proportional to the amount of water that leaves, and also incorporates the non-linear response of stomates to VPD (Katul et al., 2010; Katul et al., 2009; Zhou et al., 2014). This model, though simple, has been shown to work well across a variety of EC sites (Zhou et al., 2015). Figure 2 (upper panels a,b) shows a comparison between the daily cycles in a wet and dry month. By calculating a daily correlation between the normalized daily cycles of ET and $GPP \cdot \sqrt{VPD}$, we come to a correlation coefficient for each day (see Figure 2, lower panels c,d). For well watered days in the growing season the two signals tend to be well correlated (>0.9), but tends to be less correlated in periods of stress, a comparison of which can be seen in Figure 2 (lower).

As it is, this daily correlation coefficient is dependent on the signal strength, or magnitude, of the flux. Low correlation values could just as easily be from carbon:water decoupling as to a low signal to noise ratio. Therefore, to produce a more robust metric and account for these statistical decreases in correlation, we turned the daily correlation coefficient into an index based on its rank in a distribution of correlation coefficients from artificial datasets. These artificial datasets are constructed using the diurnal signal from potential radiation, with Gaussian noise ($\mathcal{N}(0, \sigma)$) added according to the standard deviation random uncertainty of the ET and NEE fluxes, or

$$LE_{artificial} = \frac{Rg_{pot}}{Rg_{pot}} \cdot \overline{LE} + \mathcal{N}(0, \sigma_{LE|NEE}^2) \quad (2.9)$$

and

$$NEE_{artificial} = \frac{Rg_{pot}}{Rg_{pot}} \cdot \overline{NEE} + \mathcal{N}(0, \sigma_{NEE|LE}^2) \quad (2.10)$$

Uncertainties of the NEE and ET fluxes were estimated from the gap filling procedure of Reichstein et al. (2005b), with the uncertainty equal to the standard deviation of flux measurements within a time window and similar meteorological conditions. As GPP is calculated from gap-filled values of NEE, the uncertainty from NEE was used for GPP. Furthermore, the correlation structure between the noises in LE and NEE was preserved in the artificial dataset.

In essence, by using the underlying signal from potential radiation, both the artificial ET and $GPP \cdot \sqrt{VPD}$ are perfectly correlated when no noise is added. Adding noise then isolates the decoupling effect of signal to noise ratio. An artificial correlation coefficient can then be calculated from the two artificial datasets in the same manner as from the real dataset, and this experiment is repeated 100 times for each day, giving a daily distribution of artificial correlation coefficients. The rank of the real correlation coefficient in the distribution from the artificial set gives a probability that the carbon and water signals are actually coupled. The resulting index has a range of 0-100, with 100 indicating that the real correlation coefficient was greater than the entire artificial set, and therefore it is very likely that carbon and water are coupled. From this index we can now quantify if the water and carbon signals are coupled for any given day, and therefore shed light onto whether the two fluxes are only controlled by the opening and closing of stomates. Annotated code for this calculation can be found in File S5 as well as at Nelson (2017).

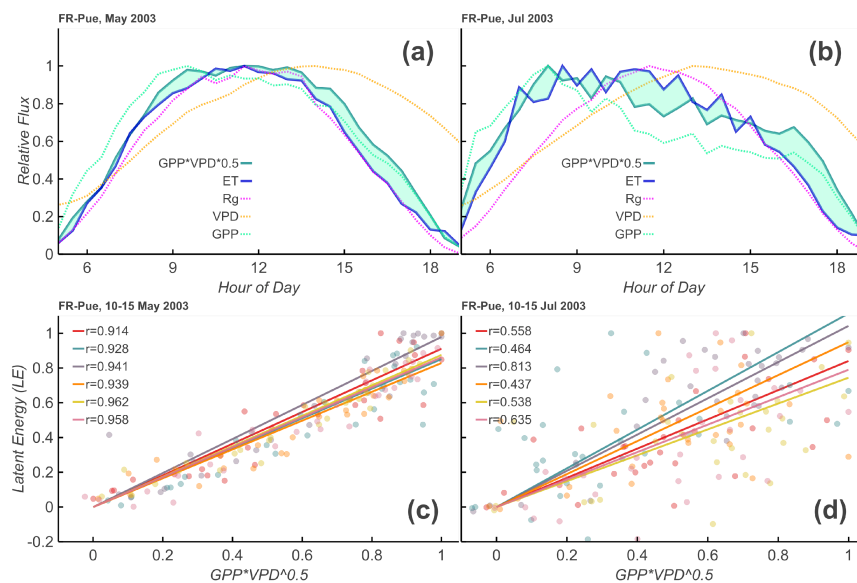


Figure 2.2 Theoretical overview of diurnal water carbon index upper panels: One month average diurnal cycle of incoming shortwave radiation (Rg), evapotranspiration (ET), vapor pressure deficit (VPD), gross primary productivity (GPP), and $GPP * VPD^{-0.5}$ at the Peuchabon Forest, France (‘FR-Pue’) site during 2003. Discrepancies between $GPP * VPD^{-0.5}$ and ET increase from the relatively wet May (32 mm rainfall, left) to the relatively dry July (0 mm rainfall, right). lower panels: These discrepancies are reflected in the daily correlation values between $GPP * VPD^{-0.5}$ and ET, giving an indication of the appropriateness of the uWUE model for each day, as well as the degree of coupling between water and carbon signals.

2.2.4 Models and parameter estimation

In order to benchmark whether these metrics are capturing information that is possibly not being captured in modern model frameworks, three simple models were used to estimate WUE (GPP/ET) for each day at each site and compared to actual flux data. The purpose of the exercise was to evaluate if bias in the model predictions were associated with decoupled or morning shifted days, thus indicating that the metrics are corresponding to information that the models are unable to capture. Here we utilize three models to provide a spectrum of theoretical to empirical basis. The “Katul-Zhou” model, as defined and used in calculation of the DWCI, is based in stomatal optimization theory (Katul et al., 2010; Katul et al., 2009; Zhou et al., 2015), which makes the assumption that the WUE is constant if corrected by the effect of VPD, using an inverse square root as the assumed relationship. Though the constant nature of uWUE may not be correct, with the optimal carbon cost of water changing over day or weeks (Manzoni et al., 2013; Palmroth et al., 2013), a yearly parameter of uWUE was estimated which is consistent with other modeling exercises (Zhou et al., 2016a). One step away from a theoretical basis is a revision of this model by Boese et al. (2017), the “Boese” model, where an additional radiation term was added such that,

$$ET = i \cdot GPP \cdot \sqrt{VPD} + r \cdot Rg \quad (2.11)$$

where i and r are parameters fit to each site-year. This relationship with Rg was shown to have a better predictive performance for EC data from 115 sites (Boese et al., 2017). The interpretation of this extra radiation term is not clear and is difficult to reconcile with the current understanding of physiology. It is possible the term could be related to biophysical effects, e.g. VPD at leaf surface vs the measured ambient VPD. Nevertheless, the Boese model is an empirical and ecosystem scale model that complements the theoretical and originally leaf-level model from Katul-Zhou.

Parameters of these models were estimated for each site-year. The Boese model parameters were fit using trimmed least squares regression (TLS) which minimizes the 90th percentile of SSE to prevent influence of large outliers (Rousseeuw, 1983; Reth et al., 2005). As the error in both ET and GPP are assumed to be of similar magnitude, the i parameter in the Katul-Zhou model was calculated using geometric mean regression, where the final slope was calculated as the geometric mean of the parameters from

$$ET = i_{GPP} \cdot GPP \cdot \sqrt{VPD} \text{ and } GPP \cdot \sqrt{VPD} = \frac{ET}{i_{ET}} \quad (2.12)$$

Both the Katul-Zhou and Boese models are theoretically based and here implemented have the underlying assumptions of RuBisCO-limited conditions and constant carbon cost of water throughout the season which may not reflect reality. Therefore a fully empirical and highly non-linear model can give insight into how much information is actually stored in the data while minimizing any assumptions. As a fully empirical model, a random forest regression (RandomForestRegressor from Pedregosa et al. (2011) based on Breiman (2001)) was fit to half-hourly ET data for each site using R_g , VPD, T_{air} , GPP and year as input parameters. Values were estimated using 50 trees with predictions made using out-of-bag estimates to prevent over-fitted model predictions.

2.3 Results

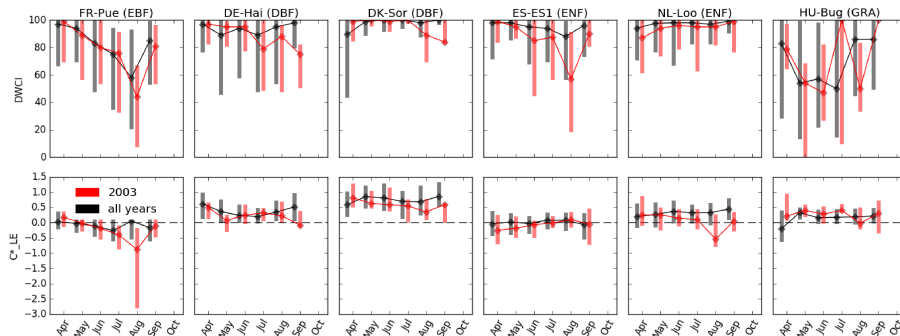


Figure 2.3 Monthly median diurnal water carbon index (DWCI, lower panels) and diurnal centroids (C_{ET}^* , upper panels) for 6 sites in Europe. Data from all years available (black) is compared to 2003 (red) during which a drought event resulted in high temperatures and low precipitation throughout the summer. Note DWCI of 0-100 indicate lowest-highest probability of diurnal carbon:water coupling and C_{ET}^* of -1 to 1 indicate one hour morning shifted to one hour afternoon shifted ET. Vertical bars represent interquartile range. Sites from 4 plant functional types: evergreen broadleaf (EBF), deciduous broadleaf (DBF) and evergreen needleleaf (ENF) forests, as well as grasslands (GRA). Ecosystems show tendencies of morning shifts (e.g. DK-Sor and NL-Loo) and carbon:water decoupling (e.g. ES-ES1 and HU-Bug) during the drought year.

As a case study, C_{ET}^* and DWCI time-courses for six sites from Europe are shown in Figure 3, with an emphasis on 2003 when the continent was struck by a heatwave that was shown to effect both the carbon and water cycles (Ciais et al., 2005; Reichstein et al., 2007; Granier et al., 2007). For DWCI, forest sites showed high water:carbon coupling throughout the growing season, with the exception of Puechabon (FR-Pue) which showed a regular seasonal cycle of decoupling. The grassland site (HU-Bg) showed a higher variability in DWCI compared to the forest sites (all others). All sites showed either a decrease in median DWCI or an increase in variability during 2003, generally in July or August, particularly at Hainich (DE-Hai), Bugacpuszta (HU-Bug), and El Saler (ES-ES1). This increase in decoupling during 2003 is consistent with the hypothesis of non-stomatal limitations being expressed in hot, dry conditions which can affect carbon fixing mechanisms. Median diurnal centroid values across all years varied in absolute magnitude, but were generally near or above zero, i.e. the water cycle showed no shift or an afternoon shift. One exception would be the Mediterranean oak forest of Puechabon, which shows a slight seasonal cycle of morning shifts going from a slight afternoon shift to a slight morning shift during June, July, and August. During drought years, sites that showed distinctive morning shifts were Puechabon (FR-Pue), Soroe (DK-Sor), and Loobos (NL-Loo). The framework that morning shifts are associated with water stress from soil moisture depletion would be supported by the increase in morning shifts during 2003, though factors such as species composition and access to soil water would play a significant role and could account for the differences among sites. All sites had significantly different ($p < 0.05$, Wilcoxon rank-sum test) DWCI values between 2003 and all other years except Puechabon, whereas with C_{ET}^* only Puechabon, Soroe, and Loobos showed significant differences.

2.3.1 Distribution of data driven indicators by vegetation type and climate

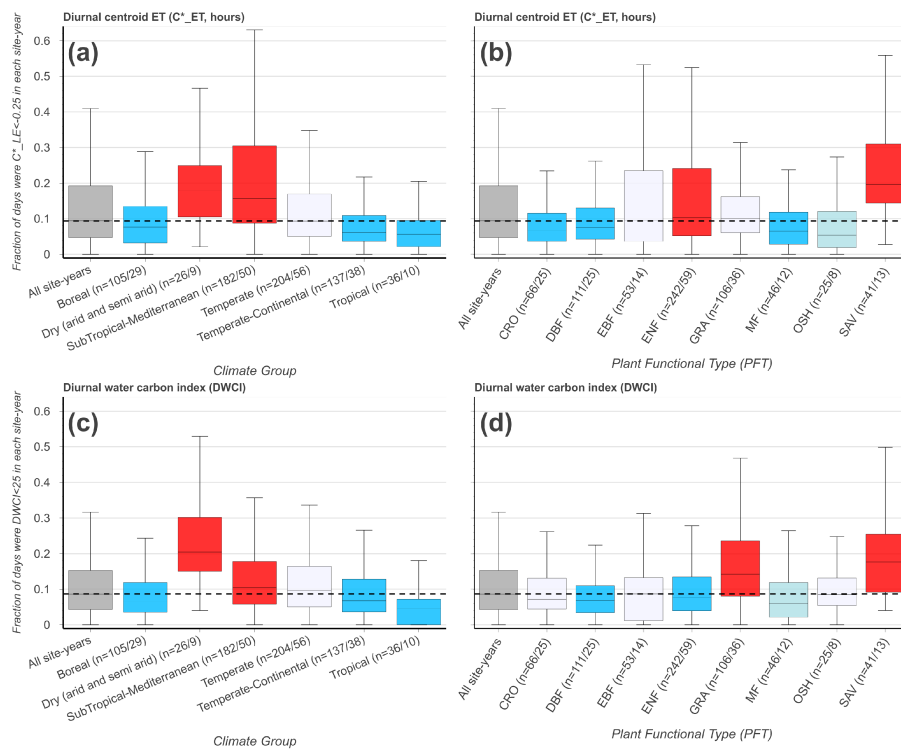


Figure 2.4 The frequency of morning-shifted Diurnal Centroids ($C^*_{ET} < -0.25$ hours, upper panels a,b) and low diurnal water carbon index ($DWCI < 25$, lower panels c,d) for 690 fluxnet site-years/192 sites, grouped by climate group (left panels a,c) and plant functional type (right panels b,d). Group labels on x-axis indicate the number of site-years/sites ($n = \text{site-years/sites}$) for each category. Dashed line is the median for all site-years. Color shade indicates level of significance, with light colors and dark colors having p-values < 0.10 and < 0.05 respectively (Wilcoxon–Mann–Whitney two-sample rank-sum test), red and blue colors indicate distributions higher and lower respectively compared to data from all sites excluding the group. Only sites-years with at least 20 data points and groups with more than 5 site-years were included.

The frequency of low values of diurnal centroid and DWCI across climate groups and plant functional types is shown in Figure 4. The thresholds designating decoupling and morning shifts were 25 and -0.25 for DWCI and C^*_{ET} respectively. These thresholds were chosen to highlight frequency differences between sites and were shown to have large metric responses under dry conditions while having low frequencies under wetter conditions (see sensitivity analysis in supplementary Figure S2). Furthermore, these thresh-

olds results in a similar median frequency of uncoupled and morning shifted days between all site-years being 8.7% and 9.4% of days respectively. The similarity in median frequencies across site-years allowed for easier inter-comparison between the two metrics. The frequency of decoupling and morning shifts using these thresholds for each site can be found in the map found in File S1. Though there is a fairly large variance across climate groups and plant functional types, low values of both DWCI and C_{ET}^* occur at higher frequencies in savanna ecosystems and dry or Mediterranean climates. Conversely, lower frequencies of both metrics are seen in tropical, boreal, and temperate-continental climates. Strikingly, the arid and semi-arid climate group seems to be associated with the majority of low DWCI occurrences, with a median frequency of about 20% of days being uncoupled between site-years. Overall, frequencies were highly variable within plant functional types. Interestingly, C_{ET}^* seems to be more variable in moderately dry ecosystems with potentially deep roots, favoring woodier savannas and evergreen needle-leaf forests over grasslands and open shrub lands. In contrast, DWCI shows similarly high frequencies from savannas and grasslands. The differing responses between tree and grass dominated ecosystems can be further seen in Figure 5, where savanna and grassland ecosystems show a distinct decrease in DWCI under conditions of low EF, in contrast to the forested sites which show a higher degree of carbon:water coupling, though still a slight decrease. Forested ecosystems show a higher degree of morning shift under low EF conditions when compared to grasslands, with savannas being somewhere between the two.

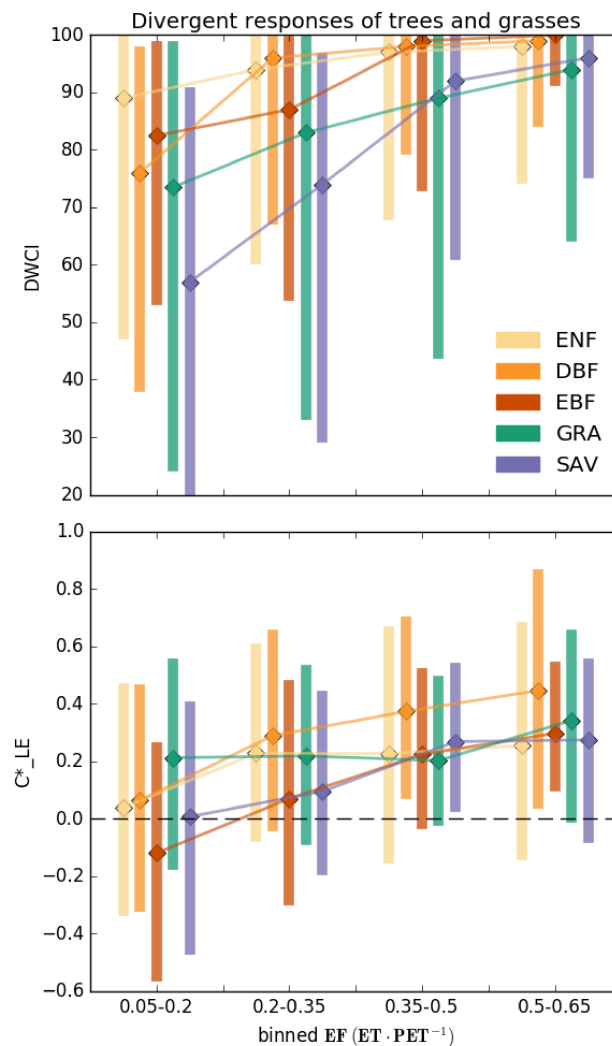


Figure 2.5 Median diurnal water carbon index (DWCI, upper panel) and diurnal centroid (C_{ET}^* , lower panel) of plant functional types binned by evaporative Fraction (EF, low values indicate dry conditions). Note DWCI of 0-100 indicate lowest-highest probability of diurnal carbon:water coupling and C_{ET}^* of -1 to 1 indicate one hour morning shifted to one hour afternoon shifted ET. Evergreen needleleaf (ENF), deciduous broadleaf (DBF), and evergreen broadleaf (EBF) forests show increased morning shifts (low C_{ET}^*) with decreasing EF when compared to grassland (GRA) sites which tended to have decreased carbon:water decoupling (low DWCI) with decreasing EF. Savanna ecosystems (SAV) show a high degree of decoupling and intermediate levels of morning shifts. Vertical bars represent interquartile range.

The response of both variables to drought stress is further observed in Figure 6, where low mean values of both DWCI and C_{ET}^* are associated with conditions of high net radiation and low latent energy, indicative of drought. As this figure includes all days from

all sites which meet the filtering outlined in the Data subsection of the Methods, i.e. dry periods in the growing season, these figures exhibit the universality of the metrics across climates, ecosystems, and time periods. This pattern is much cleaner with the diurnal centroid than with DWCI, though mean values are generally above 50 for most bins, indicating that most days are well coupled. Low values of both indicators are also seen under conditions with low R_n and high latent energy (as seen by the dark streak at the top edged in Figures 6c,e), which is generally not associated with drought stress. Further analysis showed that these points are also associated with energy balance over closure, where the sum of latent and sensible heat is greater than net radiation ($ET+H>R_n$, see Figure S2) and therefore likely represent a data problem rather than a physiological response. Removing all days where the energy balance is over closed did not alter the patterns associated with drought. Apart from the response to periods of high LE and low R_n , the metrics showed diverging response when looking at EF (ET/PET which is similar to LE/R_n) and VPD, with DWCI showing a much stronger response to VPD and C_{ET}^* showing a much stronger response to EF (Figure 6a,d). This difference in response would indicate that DWCI is more responsive to atmospheric demand (estimated via VPD) and C_{ET}^* is more responsive to water limitations. Both DWCI and C_{ET}^* also show a trend with low GPP, although in the case of the diurnal centroid the effect is limited to both low GPP and ET (Figure 6c,g).

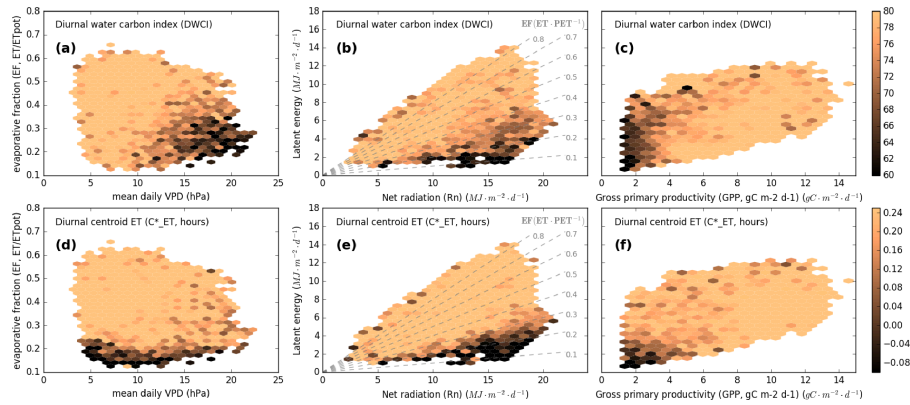


Figure 2.6 Mean DWCI (upper panels) and C_{ET}^* (lower panels) with respect to evaporative fraction (EF) by vapor pressure deficit VPD (a,d), latent energy (LE) by Rn (b,e) and LE by GPP (c,g). Note DWCI of 0-100 indicate lowest-highest probability of diurnal carbon:water coupling and C_{ET}^* of -1 to 1 indicate one hour morning shifted to one hour afternoon shifted ET. Points with high Rn and low LE are associated with both low DWCI and C_{ET}^* , indicating that both metrics are related to water limitations. Though both metrics are associated with low EF, DWCI shows a much higher response to atmospheric demand as measured by VPD, with C_{ET}^* showing very limited response. Both metrics, and DWCI in particular, show low values with high ET and low Rn, though these points are also associated with over closed energy balances ($LE+H>Rn$). Both metrics are associated with low GPP, but the C_{ET}^* is restricted to both low GPP and ET, indicating water and carbon can decouple over a wider range of water stress. This also holds when points with energy balance over-closer are excluded (data not shown).

2.3.2 Difference between modeled and actual WUE

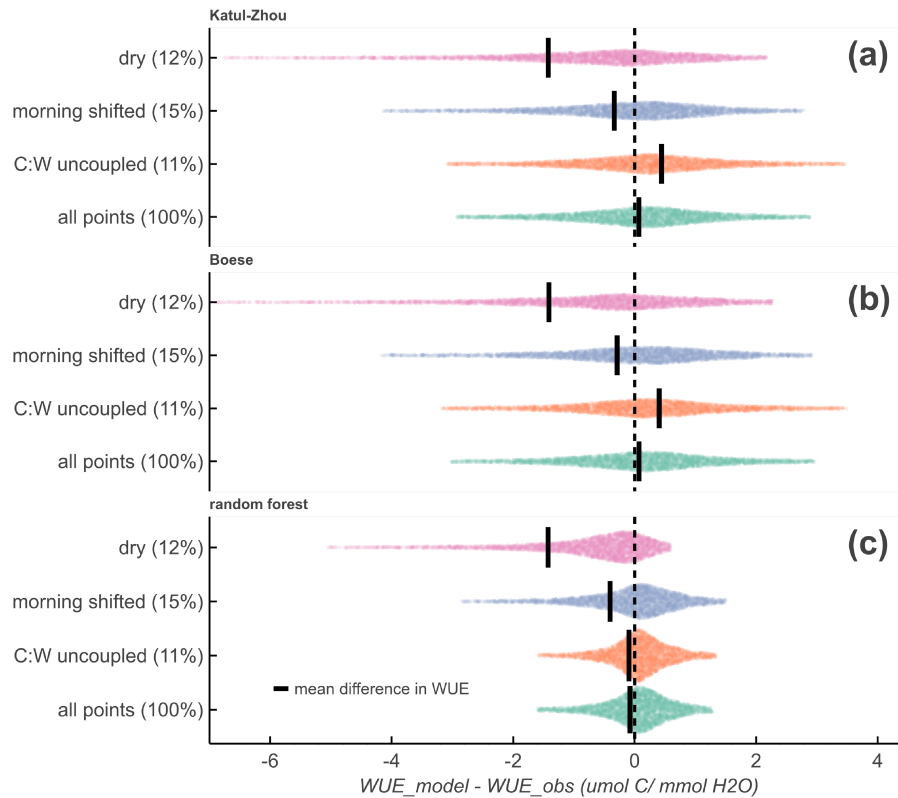


Figure 2.7 Difference in modeled and measured WUE for Katul-Zhou (a), Boese (b), and random forest (c) models. The random forest model was fit using R_g , VPD, T_{air} , GPP, and year. Thresholds designating dry, morning shifted, and C:W uncoupled days were $EF < 0.2$, $C_{ET}^* < -0.25$, and $DWCI < 25$ respectively for each day. The distributions span from the 5th to 95th percentiles, and the width of each gives an indication of the variance, which is larger in the sub groups compared to all points. Furthermore, the mean difference in WUE (black lines) tends to be shifted in dry and morning shifted days indicating a mean underestimation of WUE by the models mostly due to the long tails. Decoupled days show higher variance, but no clear pattern in under- or over-estimation. The percentage of days in each category are designated next to y-axis label in parenthesis.

Figure 7 shows the difference between expected and observed WUE from the Katul-Zhou, Boese, and random forest (RF) models, with respect to conditions of drought as characterized by low evaporative fraction ($EF < 0.2$), C:W decoupling ($DWCI < 25$), and morning shifts ($C_{ET}^* < -0.25$). This exercise was designed to test whether the metrics were associated with bias in the models, indicating that the metrics are able to cap-

ture information that the models are not (as further outlined in Methods and Materials subsection “models and parameter estimation”). For all models, the dry days show the largest average shift between expected and observed WUE, followed by morning shifted days. Uncoupled days show the smallest shifts for all models, with an overestimation of WUE for the Katul-Zhou and Boese models and no significant shift of WUE with the random forest model. As all models were calibrated within a site-year, the over or under estimation of WUE indicate an inability of the model to capture a change in the system. Cases of mean mis-estimation tended to be influenced by long tails in the distribution with median differences being less exaggerated. However, these long tails are indicative of major model error in periods where the ecosystem is likely under stress conditions.

2.4 Discussion

2.4.1 Looking beyond sums and means

The proposed metrics, DWCI and C_{ET}^* , depart from more traditional methods to summarize from sub-daily to daily timescales such as sums and means. This departure is advantageous in that it extracts added information that may have been otherwise ignored by turning the focus from signal amplitude to the signal shape. However, these new metrics also come with their own set of caveats, most notably issues with data quality confounding interpretability. Both metrics are susceptible to noise, as one or two errant points within a day can be reflected as a decrease in correlation or a shift in diurnal centroid. This is evident from the existence of very afternoon shifted C_{ET}^* , sometimes by more than an hour, which the authors have no proposed explanation for other than noise in the data. However, attributing highly afternoon shifted points as poor data requires further investigation. Note here that the “resting” C_{ET}^* seems to be slightly afternoon shifted, which could be caused by real physiological factors such as differences in the incoming SW radiation (R_g) used in the calculation and net radiation (R_n), higher atmospheric demand (VPD) in the afternoon driving higher ET, or increased convection throughout the day resulting in higher transport of water away from the canopy, and is likely a combination of all three. Differences in resting C_{ET}^* between sites could also be from instrumental causes such as radiometric sensors which are not adequately leveled or dirty, though the consistent, slight afternoon shifts would

suggest this is a real response. Despite the possible shortcomings, both metrics show a definite response to drought conditions across the broad array of sites, climates, and ecosystems contained in FLUXNET (see Figure 6), and give valuable insight into the underlying physiology. Given the broad nature of the analysis here, the metrics and hypothesis presented would benefit from site specific validations such as looking to see if the morning shifts and decoupling are indeed associated with lower soil moisture levels, leaf water potentials, and/or decreases in sap flux. Sap flux in particular could give some interesting insights, as the diurnal patterns in sap flux velocity will also have an offset to incoming radiation related to tree capacitance, therefore relating sap flow diurnal centroids to the ET diurnal centroid could give some information on changes in plant water recharge. Furthermore, the diurnal centroid base metrics complement the hysteresis quantification methods such as those employed by Zhou et al. (2014) and Matheny et al. (2014), with the advantage of C_{ET}^* being compensated for cloudy conditions and possibly comparatively less influence of noise, though an intercomparison would be useful to explore the strengths and weaknesses of the different approaches. By providing both the equations and related code of the metrics, we the authors hope the metrics will be used by the community for both validation and to further ecophysiological understanding.

2.4.2 Trees, grass, and drought stress

By comparing climate groups and PFTs with the frequent occurrence of low DWCI and C_{ET}^* from Figure 4, we can note two striking differences: evergreen broad- and needle-leaf forests show high variability of morning shifted days but not uncoupled days, whereas grasslands show significantly high uncoupled but not morning shifted days. The pattern is further seen in Figure 5, where the distinct divergent responses of decoupling and morning shifts between tree and grass dominated systems. This disparity may indicate an interaction of C_{ET}^* not only with drought, but hydraulic sensitivity. The association of morning shifts to hydraulic sensitivity is further strengthened by Figure 6a,d where C_{ET}^* shows a much stronger response to EF rather than VPD, indicating that morning shifts of ET are not simply due to stomatal closure due to VPD but in fact a response to drought conditions. The shorter hydraulic system of grasses may not necessitate stomatal closure under high demands (Holloway-Phillips and Brodrigg, 2011), thus causing less frequent phase shifts even under drought conditions. In contrast, tree

ecosystems may only exhibit higher hydraulic stresses, associated with both dryness and a more sensitive hydraulic strategy. Temperate-continental and tropical climates all showed a low frequency of morning shifted days, even though they are occupied by large trees with cavitation susceptible vascular systems (Konings and Gentine, 2016), suggesting that these ecosystems show limited drought stress even with the hydraulic susceptibility. Similarly, the high degree of variability of morning shifted frequency between site-years in sub-tropical/Mediterranean and evergreen broad- and needle-leaf forests could either indicate variation in the response in hydraulic stress between sites, or that hydraulic stress is only expressed some years, leading to high and low frequencies within the same site.

In this way, it seems that though C_{ET}^* is less noisy as a drought indicator (see Figure 6), it may only be of use in tree systems that are more prone to hydraulic stress. However, this does put the metric in a rather unique position in that it could be used as a global scale hydraulic indicator, having potential application in exploring ecosystem level isohydricity (Martínez-Vilalta and Garcia-Forner, 2016), or the degree to which risks vascular system damage to continue to extract water. Isohydricity is intrinsically a concept that relates to an individual plant, as dynamics of rooting depth, hydraulic conductances, and sensitivities to VPD can vary within individuals of the same species at the same location. However, these factors are all interrelated, as hydraulic and stomatal conductances drive transpiration dynamics which control the rate of depletion of root zone water which can then feed back to stomatal sensitivity, such as via ABA signaling (Wilkinson and Davies, 2002). As such, current estimates of isohydricity require plant level measurements, which are currently restrained to the individual scale, i.e. from actual leaf measurements (Martínez-Vilalta et al., 2014) or to global scale, but only 0.5 degree resolution estimates from radar (Konings and Gentine, 2016). This limitation of large and small scales leaves a knowledge gap at the size of an eddy covariance footprint, hindering the study of ecosystem response to drought. However, under the assumption that the morning shifts seen under low evaporative fraction are related to increased stomatal sensitivity in response to root zone moisture depletion, it may be possible to compare the onset and speed with which the diurnal centroid shifts toward the mornings as ecosystems dry. In this way, one could infer the ecosystem response to soil moisture, without explicitly knowing the soil moisture. The resulting relationship could prove useful as a data derived ecosystem functional property, giving direct information on variations in water limitation response.

2.4.3 C:W decoupling and energy balance closure

In addition to error from single data points, both metrics, but especially the DWCI, show some relationship with energy balance over closure. Energy balance mismatch is a common phenomenon in EC measurements, with under closure ($ET+H < R_n$) being a more common concern (Leuning et al., 2012; Wilson et al., 2002). Issues with energy balance closure can be, among other causes, attributed to advection, where energy, water, and carbon are transported in and out of the tower footprint, complicating an absolute accounting of these quantities (Barr et al., 2006; Brötz et al., 2014; Wilson et al., 2003). The apparent association of DWCI and over closure could be due to transfer of moist air from the surrounding landscape, causing the DWCI to be more contingent on the mixing of source air and less from plant controls. In this scheme, the over closure seen in Figure 6 could be caused by the mixing of outside moist air into the drier air from the EC site, causing an increase in latent energy. However, the infiltrating air sources could also have similar or drier moisture levels which would not necessarily be seen as over closure. In this scenario, this infiltrating air could contain varying carbon and water concentrations, again causing a carbon:water decoupling, but one that would not be associated with over closure. If this effect has no diurnal pattern, and thus does not generally influence the mean diurnal centroid in ET, it could explain why the patterns with dryness are much clearer with C_{ET}^* compared to DWCI. This would have the implication that DWCI is then a mixture of advection and non-stomatal signals, complicating the biological interpretability. However, the association with dryness in both metrics gives credence that they do indeed reflect some physiology, if we assume EBC should not be influenced by dryness level. Furthermore, if potential stress conditions are removed, the DWCI could be useful as a metric of advection in the system, even when the energy balance is relatively well closed.

2.4.4 WUE shifts associated with metrics and not captured by models

Figure 7 demonstrates the strong tendency of the models to underestimation WUE in dry conditions. This is true even for the fully non-linear and empirical random forest model, indicating that the model under-performance is not necessarily due to an incomplete model framework, but due to a lack of information to constrain the problem.

Given the association of both metrics with drought (Figure 6), one could expect that the models would underestimate WUE in uncoupled and morning shifted days. Though this is the case with morning shifted days, decoupling shows no underestimations of WUE, with even a mean overestimation in the case of the Katul-Zhou and Boese models. Given the limitations outlined in the previous sections, one could blame noise for the lack of WUE shift, but this does not reconcile with the higher frequency of decoupling during dry days which should bias the WUE estimates. Furthermore, as the more empirical random forest model reduces the prediction variability, leaving a slight WUE underestimation, indicating that some of the overestimation from the Katul-Zhou and Boese models may be tied to limitations of the underlying assumptions, yet the distribution from the RF model still lacks the long tails of underestimation characteristic of the dry points. Extending these findings to the underlying hypotheses of the metrics, namely hydraulic and non-stomatal limitations, we could conclude that the hydraulic controls do impose a greater water use advantage than non-stomatal limitations. In other words, the findings suggest that days with water:carbon decoupling, and possibly non-stomatal limitations, do not improve WUE, whereas hydraulic responses can improve WUE. As WUE is a ratio, this does not shed any light onto the change in productivity, as low values of WUE may indicate that a plant is still productive, but at a higher water cost. However, solid conclusions would require further analysis with some site specific measurements of actual plant function.

Though the models used here are relatively simple and lack the complexities and feedbacks found in more vigorous ecosystem models, Matheny et al. (2014) also demonstrated the fundamental inability of 9 different land-surface models with 4 different stomatal conductance schemes to capture diurnal variability which the authors attributed to inadequate representation of how water gets from the soil to the leaf. Given the demonstrated phenomenon of morning shifts and decoupling across sites under dry conditions, the metrics here provide a benchmarking tool for mechanistic models to test their ability to replicate these patterns, suggesting that the models are capable of expressing hydraulic and non-stomatal limitations. Furthermore, in the case of machine learning approaches, the metrics may provide a useful input parameter which summarizes these diurnal effects, as is evidence by the difference in response the bias in RF modeled WUE, i.e. while both metrics are associated with low EF, RF WUE was underestimated with morning shifted days but not decoupled days implying that two different strategies are being captured by the metrics. As such, by demonstrating the utility of

the metrics, and providing code and explanations for calculation, we hope they become useful to the community at large.

2.5 Conclusions

Both the DWCI and the C_{ET}^* demonstrate an ability to show consistent patterns with drought across a broad array of sites, climates, and ecosystems, with the added advantage of being tied to theoretical underpinnings. Particularly, the demonstrated patterns give novel information about carbon water relations and hydrological dynamics that are not currently present at ecosystem scale across a database as large as FLUXNET. These metrics and their underlying theory provide a data derived example differentiating the hydrological response of tree and grass plant functional types, as well as give evidence for the presence and absence of a WUE advantage from hydraulic and stomatal limitations respectively. Going forward, these metrics can be used as a tool to further understand the diversity of ecosystem drought responses.

2.6 codedataavailability

Code used to calculate the metrics described here can be found both in the supplementary materials as well as at Nelson (2017). Data used in this analysis can be found at <http://fluxnet.fluxdata.org/>

2.7 acknowledgements

This work used eddy covariance data acquired by the FLUXNET community and in particular by the following networks: AmeriFlux (U.S. Department of Energy, Biological and Environmental Research, Terrestrial Carbon Program (DE-FG02-04ER63917 and DE-FG02-04ER63911)), AfriFlux, AsiaFlux, CarboAfrica, CarboEuropeIP, CarboItaly, CarboMont, ChinaFlux, Fluxnet -Canada (supported by CFCAS, NSERC, BIOCAP, Environment Canada, and NRCan), GreenGrass, KoFlux, LBA, NECC, OzFlux, TCOSSiberia, USCCC. We acknowledge the financial support to the eddy covariance data harmonization provided by CarboEuropeIP, FAOGTOSTCO, iLEAPS, Max Planck Institute for Bio-

geochemistry, National Science Foundation, University of Tuscia, Université Laval and Environment Canada and US Department of Energy and the database development and technical support from Berkeley Water Center, Lawrence Berkeley National Laboratory, Microsoft Research eScience, Oak Ridge National Laboratory, University of California-Berkeley, University of Virginia.

Chapter 3

Coupling water and carbon fluxes to constrain estimates of transpiration: the TEA algorithm

AGU100 ADVANCING
EARTH AND
SPACE SCIENCE



Journal of Geophysical Research: Biogeosciences

RESEARCH ARTICLE

10.1029/2018JG004727

Key Points:

- TEA is a method for extracting water use efficiency (WUE) dynamics from flux data with minimal assumptions
- Validation shows that TEA is able to derive patterns of WUE and transpiration from three different models
- Method is applicable to eddy covariance data sets, opening the door to wide-scale transpiration estimates

Supporting Information:

- Supporting Information S1

Correspondence to:

J. A. Nelson,
jnelson@bgc-jena.mpg.de

Citation:

Nelson, J. A., Carvalhais, N., Cuntz, M., Delpierre, N., Knauer, J., Ogée, J., et al. (2018). Coupling water and carbon fluxes to constrain estimates of transpiration: The TEA algorithm. *Journal of Geophysical Research: Biogeosciences*, 123, 3617–3632. <https://doi.org/10.1029/2018JG004727>










Received 7 AUG 2018

Accepted 15 NOV 2018

Accepted article online 23 NOV 2018

Published online 21 DEC 2018

Coupling Water and Carbon Fluxes to Constrain Estimates of Transpiration: The TEA Algorithm

Jacob A. Nelson¹ , Nuno Carvalhais^{1,2} , Matthias Cuntz³ , Nicolas Delpierre⁴ , Jürgen Knauer¹ , Jérôme Ogée⁵ , Mirco Migliavacca¹ , Markus Reichstein^{1,6} , and Martin Jung¹ 

¹Department of Biogeochemical Integration, Max Planck Institute for Biogeochemistry, Jena, Germany, ²Faculdade de Ciências e Tecnologia, Universidade Nova de Lisboa, Lisbon, Portugal, ³INRA, Université de Lorraine, UMR1137 Ecology et Ecophysiologie Forestières, Champenoux, France, ⁴Ecologie Systématique Evolution, Université Paris-Sud, CNRS, AgroParisTech, Université Paris-Saclay, Orsay, France, ⁵INRA, UMR 1391 ISPA, Villenave d'Ornon, France, ⁶Michael-Stifel-Center Jena for Data-Driven and Simulation Science, Jena, Germany

Abstract Plant transpiration (T), biologically controlled movement of water from soil to atmosphere, currently lacks sufficient estimates in space and time to characterize global ecohydrology. Here we describe the Transpiration Estimation Algorithm (TEA), which uses both the signals of gross primary productivity and evapotranspiration (ET) to estimate temporal patterns of water use efficiency (WUE, i.e., the ratio between gross primary productivity and T) from which T is calculated. The method first isolates periods when T is most likely to dominate ET. Then, a Random Forest Regressor is trained on WUE within the filtered periods and can thus estimate WUE and T at every time step. Performance of the method is validated using terrestrial biosphere model output as synthetic flux data sets, that is, flux data where WUE dynamics are encoded in the model structure and T is known. TEA reproduced temporal patterns of T with modeling efficiencies above 0.8 for all three models: JSBACH, MuSICA, and CASTANEA. Algorithm output is robust to data set noise but shows some sensitivity to sites and model structures with relatively constant evaporation levels, overestimating values of T while still capturing temporal patterns. The ability to capture between-site variability in the fraction of T to total ET varied by model, with root-mean-square error values between algorithm predicted and modeled T/ET ranging from 3% to 15% depending on the model. TEA provides a widely applicable method for estimating WUE while requiring minimal data and/or knowledge on physiology which can complement and inform the current understanding of underlying processes.

Plain Language Summary While it is widely known that plants need water to survive, exactly

Coupling water and carbon fluxes to constrain estimates of transpiration: the TEA algorithm

Jacob A. Nelson¹, Nuno Carvalhais^{1,2}, Matthias Cuntz³, Nicolas Delpierre⁴, Jürgen Knauer¹, Jérôme Ogée⁵, Mirco Migliavacca¹, Markus Reichstein^{1,6}, Martin Jung¹

¹Department of Biogeochemical Integration, Max Planck Institute for Biogeochemistry, Jena, Germany

²Faculdade de Ciências e Tecnologia, FCT, Universidade Nova de Lisboa

³INRA, Université de Lorraine, UMR1137 Ecology et Ecophysiologie Forestières, Route d'Amance, 54280 Champenoux, France

⁴Ecologie Systématique Evolution, Univ. Paris-Sud, CNRS, AgroParisTech, Université Paris-Saclay, 91400 Orsay, France

⁵INRA, UMR 1391 ISPA, 33140 Villenave d'Ornon, France

⁶Michael-Stifel-Center Jena for Data-Driven and Simulation Science, Jena, Germany

Keypoints

- *TEA, a method for extraction of water use efficiency (WUE) dynamics from flux data with minimal assumptions*
- *Validation shows TEA is able to derive patterns of WUE and transpiration from 3 different models*
- *Method is applicable to eddy covariance datasets, opening the door to wide-scale transpiration estimates*

Plant transpiration (T), biologically controlled movement of water from soil to atmosphere, currently lacks sufficient estimates in space and time to characterize global ecohydrology. Here we describe the Transpiration Estimation Algorithm (TEA), which uses both the signals of gross primary productivity (GPP) and evapotranspiration (ET) to estimate temporal patterns of water use efficiency (WUE, i.e. the ratio between GPP and T) from which T is calculated. The method first isolates periods when T is most likely to dominate ET. Then, a Random Forest Regressor is trained on WUE within the filtered periods, and can thus estimate WUE and T at every time-step. Performance of the method is validated using terrestrial biosphere model output as synthetic flux datasets, i.e. flux data where WUE dynamics are encoded in the model structure and T is known. TEA reproduced temporal patterns of T with modeling efficiencies above 0.8 for all 3 models: JSBACH, MuSICA, and CASTANEA. Algorithm output is robust to dataset noise, but shows some sensitivity to sites and model structures with relatively constant evaporation levels, overestimating values of T while still capturing temporal patterns. Ability to capture between site variability in the fraction of T to total ET varied by model, with RMSE values between algorithm predicted and modeled T/ET ranging from 3 to 15 % depending on model. TEA provides a widely applicable method for estimating WUE while requiring minimal data and/or knowledge on physiology which can complement and inform the current understanding of underlying processes.

While it is widely known that plants need water to survive, exactly how much water plants in an ecosystem use is harder to quantify. However, many places have been measuring how much total water leaves an ecosystem, both the water plants use directly and the water that simply evaporates from the soil or the surfaces of leaves, using eddy covariance towers. These eddy covariance towers also measure the coming and going of carbon, such as the total amount of carbon taken up by photosynthesis. Here, we present the idea that by using the signals from both photosynthesis and total water losses together, we can capture the water signal related to plants, namely transpiration, using an algorithm called TEA. To verify that TEA is working how we expect, we test it out using artificial ecosystem simulations where transpiration and photosynthesis come from mathematical models. By thoroughly testing TEA, we have a better idea of how it will work in a real world situation, hopefully opening the door for a better understanding on how much water ecosystems are using and how it might affect our changing planet.

3.1 Introduction

At current state, transpiration (T) is a key ecosystem process that lacks the widespread and consistent estimates necessary to study ecohydrological processes globally. For example, a recent meta-analysis by Wei et al. (2017) analyzed an aggregation of ecosystem level T estimates resulting in a dataset of only 64 studies conducted between 1941 and 2014, a relatively sparse dataset when attempting to capture global variability. As such, demand for T datasets that can encompass the variety of ecosystem responses to water availability has been highlighted as a key need, both from the perspectives of the water (Fisher et al., 2017) and carbon (Rogers et al., 2017) cycle communities. Though transpiration and evaporation (E) processes are built into most ecosystem and land surface models, resulting estimates are poorly constrained, as can be seen in the spread of global T/ET estimates from CMIP5 which ranged from 22-58% (Wei et al., 2017). Here we present an approach for estimating T which is applicable to eddy covariance (EC) networks, and is data driven providing an alternative perspective to current process based approaches.

The difficulty in partitioning evapotranspiration (ET) into the biotic component (transpiration, T) and the abiotic component (here evaporation, E) is partially due to equifinality, as E and T share the same primary environmental drivers making the problem difficult to constrain. From the view point of physics, transpiration is an evaporation which is then modulated by stomatal resistance, making the task of distinguishing the two fluxes particularly challenging. However, a key distinction of T lies in that it is regulated by an active process via stomatal control, which is linked to plant photosynthesis. To this end, the method we propose aims to utilize this link between water and carbon cycles as the key differentiating process between E and T in an effort to distinguish the two.

As reviewed in Kool et al. (2014), many approaches to partition ET attempt to pair a separate E and/or T distinguishing estimate, such as measurements of sap flux, isotope fractionation, or carbonyl sulfide (OCS) flux, in tandem with an ET estimate. Sap flux measurements, which estimate the flow of water through a stem (Granier, 1987), is currently the most widespread method. Though sap flux measurements have proven to be effective at measuring tree water fluxes, estimating ecosystem T relies on upscaling point source sap flow estimates based on an approximation of sapwood area, which can

be problematic in ecosystems with high plant diversity, hampering suitability for universal application (Oishi et al., 2008; Poyatos et al., 2016). Isotopic methods take advantage of the isotopic fractionation of water oxygen ($^{18}\text{O}/^{16}\text{O}$) and hydrogen ($^2\text{H}/^1\text{H}$) which occurs from evaporation but not root uptake, producing isotopic signatures related to the T:E ratio. Isotopic methods have been used both at global scales (Jasechko et al., 2013; Good et al., 2015) and at high temporal resolutions (Good et al., 2014), yet are limited in the number of sites and length of time-series. In general, global isotopic estimates of T/ET tend to be higher than site estimates (Wei et al., 2017), some even controversially so (Coenders-Gerrits et al., 2014). The OCS method attempts to use the flux of OCS uptake by leaves to estimate ecosystem canopy conductance directly, as the pathways of CO_2 and OCS are similar (Sandoval-Soto et al., 2005; Whelan et al., 2017). The calculation of conductance is simplified when using OCS, as it does not have the complication of having a large source component such as is the case with respiration and CO_2 (Wehr et al., 2017). While the OCS method is promising, the novelty and potential complications due to alternate sources/sinks of OCS (Wohlfahrt, 2017; Gimeno et al., 2017) have resulted in limited applications in practice.

Due to the limits of current T estimates, and shortfalls in understanding ecosystem water dynamics, data driven approaches can provide an alternate perspective. Widespread monitoring of both water and CO_2 fluxes provide rich datasets which can inform T estimates by utilizing concepts of water use efficiency (WUE), here defined as the ratio of gross primary productivity (GPP) to T. At present, data driven approaches to estimate ecosystem WUE and T do exist, such as the method proposed by Zhou et al. (2016a) (hereafter referred to as the SZhou method") which is based on estimates of annual underlying water use efficiency from gross primary productivity (GPP) and vapor pressure deficit (VPD), calculated as

$$uWUE_t = \frac{GPP_t \cdot \sqrt{VPD_t}}{ET_t} \quad (3.1)$$

where the \sqrt{VPD} term represents an approximate stomatal response which is broadly applied to many ecosystems. $uWUE$ is related to the carbon cost of water which is assumed to be constant in light limited leaves over timescales of days to weeks. By incorporating the \sqrt{VPD} term, the carbon:water relationship becomes linear and $uWUE$ values can be estimated using linear regression where $uWUE$ is the slope parameter. The Zhou method makes a T/ET estimate by taking the ratio of a normal linear regression of

uWUE estimated within one day (which would include the E component), and the 95th percentile regression of annual uWUE which is assumed to contain only transpiration. The key assumptions are then that uWUE is constant within a year and that the 95th percentile of uWUE corresponds to conditions where $E \approx 0$. E is most likely to be zero at high percentiles because these points correspond to periods with the highest ratio of GPP/ET, whereas points with a high E component would increase ET with no added T causing the uWUE to decrease. Points over the 95th percentile are assumed not to be representative of uWUE, possibly due to noise.

While Zhou et al. (2016a) and other data driven WUE estimates (Beer et al., 2009; Scott and Biederman, 2017) have laid the foundation for globally useful WUE and T estimates, they have yet to be rigorously validated, likely in part due to the limited availability of verification datasets as described in the previous section. Notably, assumptions on ecosystem WUE dynamics which are not fully understood must be taken into consideration. In particular, non-linearities in the GPP to T relationship must be addressed such as the known effects from stomatal response (VPD) (Beer et al., 2009; Katul et al., 2009; Zhou et al., 2014). Though the Zhou method does attempt to account for VPD effects, the resulting uWUE estimate is tied to annual time periods and does not allow for seasonal or diurnal variations in plant and ecosystem responses, only accounting for the VPD response. Boese et al. (2017) concluded that the uWUE framework could be outperformed by empirical models that included incoming radiation, suggesting that only incorporating VPD may not be sufficient to characterize the carbon:water relationships at ecosystem level. As such, the method proposed here attempts to derive WUE dynamics from a data-driven perspective, using a non-linear, machine learning method to characterize the carbon:water relationship and thus make few assumptions on the ecosystem WUE dynamics.

3.1.1 Method outline and objectives

We identify two key limitations of the current methods outlined: 1) Restricted applicability or spatiotemporal scope, particularly with direct T measurements; 2) Strong assumptions of carbon:water relationship, particularly with EC dependent methods, which have the potential to bias WUE and T estimates.

We aim to overcome the first limitation by basing the method only on water, energy, and

carbon EC fluxes with associated meteorological data to make predictions at half-hourly to hourly scale with minimal data requirements.

To address the second limitation, we validated the presented ET partitioning method against model output in an effort to assess sensitivities and limitations. The use of artificial datasets has proven useful both in the field of biogeochemistry (Jung et al., 2009), as well as adjacent fields (Jasechko et al., 2014; Ishizaki et al., 2014). We used three separate models in an effort to reduce the influence of any one set of model assumptions.

Here we introduce the Transpiration Estimation Algorithm (TEA), which uses ecosystem WUE ($eWUE = GPP/ET$) to predict transpiration in two steps (see Figure 1): (1) a data-filtration step to isolate the signal of ET for periods where E is minimized and ET is likely dominated by the signal of T, i.e. during periods of the growing season with dry surfaces; and (2) a step which predicts the WUE using meteorological variables, as well as information derived from the carbon and energy fluxes. This prediction of WUE translates to a novel transpiration estimate which aims to be capable of capturing seasonal and diurnal dynamics with wide application potential.

The key hypothesis to be tested here is: does the TEA algorithm capture the dynamics of WUE and T encoded in the models? If the method cannot capture WUE dynamics from the three different models, we can assume it will not capture real world WUE dynamics, thus the exercise is a sanity check on whether TEA is capable of extracting physiological patterns of ecosystem WUE. Furthermore, we explore scenarios when a key assumption is broken, i.e. evaporation is persistent at every point in time, as well as how evaporation can bias the results, and how to mitigate this bias using percentile regression.

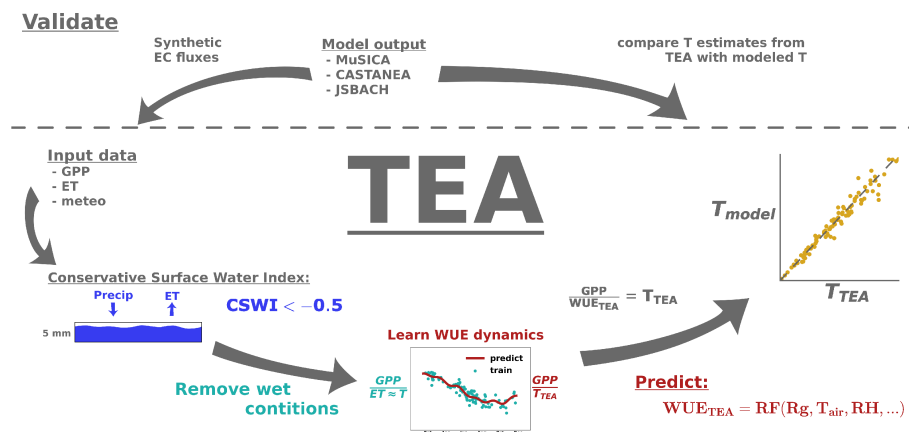


Figure 3.1 Theoretical outline of both the TEA algorithm (lower section) and validation steps (upper section). TEA consists of a filtration step to isolate dry periods when vegetation is active using the conservative surface water index (CSWI), then a Random Forest Regressor is trained on the filtered dataset to characterize WUE dynamics, which are then predicted for the entire time-series. The validation scheme involves using model output as a synthetic flux dataset, to evaluate if TEA is able to replicate the WUE dynamics encoded in the models.

3.2 Methods

3.2.1 Isolating training periods

To accomplish the characterization of T in time, we used the assumption that the signal of $T/ET \approx 1$ under conditions where the ecosystem has minimal surface moisture and the plants are photosynthetically active, as manifest via the set of filters outlined in Table 1. Filters were constructed from half hourly flux and meteorological data which excluded periods that did not meet filter criteria (individual half hours were removed). Periods likely to have no or low photosynthetic activity were removed, such as night time values or periods with low temperatures, as well as full days that did not reach a minimum threshold of total daily GPP. Periods expected to have high surface moisture were removed using the conservative surface wetness index (CSWI), a shallow bucket model where the bucket represents the surface water storage (S) for each half-hourly time-step t (S_t) relative to the last precipitation event, or,

$$S_t = \min(S_{t-1} + P_t - ET_t, S_{max}) \quad (3.2)$$

where P_t is the precipitation at time t and S_{max} is the maximum allowable storage (size of bucket). S_{max} was set to 5 mm, and values from 3-9 mm showed no difference in filter utility (data not shown, further discussed in section 4.2). The CSWI is then calculated as

$$CSWI = \max(S_t, \min(P_t, S_{max})). \quad (3.3)$$

Periods were considered sufficiently dry based on a CSWI limit, i.e. periods where $CSWI < limit$ are assumed to have dry surfaces. As opposed to other methods of identifying wet and dry conditions, such as removing periods after rain events, the CSWI accounts for the amount of rain evaporated and therefore compensates for small rain events which may evaporate relatively quickly as well as for periods of low ET after rain events such as persistent clouds reducing radiation inputs where surfaces may stay wet longer. As the appropriate limit for CSWI was unknown, this limit then becomes an input parameter to the algorithm which is not optimized, or hyperparameter, hence a sensitivity analysis was conducted across a range of limits from 2 to -3 mm (see section 3.2 in Results). The CSWI limits were not extended past -3 mm, as lower limits resulted in fewer than 500 half-hours remaining in the training dataset at some sites, which was considered too few to properly characterize site variability. Note that the limit of 500 half-hours is arbitrary and possibly conservative, however results indicate stricter limits (i.e. $CSWI < -3$ mm) may cause the training dataset to only include periods of water stress and decrease prediction performance (see Figure 7). Similarly for CSWI, periods when daily GPP was too low were also filtered in an effort to remove periods when the plants are relatively inactive, such as transition periods from winter to spring. A minimum daily threshold of $0.5 \text{ gCm}^{-2}\text{d}^{-1}$ was found to give a good performance, and a sensitivity analysis to daily GPP filter can be found in supplementary Figure S1.

Each individual filter was combined (logical AND), resulting in a filtered time-series that was then used to calculate half-hourly values of eWUE to be used as a training dataset in the next section, hereafter referred to as the training dataset.

Table 3.1 Overview of filters used to isolate conditions where the signal of ET is dominated by T. *GPP* and T_{air} filters were designed to ensure plants are active, while *Rg* filters remove nighttime values. The *CSWI* filter attempts to remove periods where the surface is likely to be wet, a sensitivity analysis of which can be found in section 3.2.

| variable | long name | half-hourly limit | daily limit |
|-------------|---------------------------------------|--|--|
| <i>GPP</i> | gross primary productivity | > 0.05 $\mu\text{molC} \cdot \text{m}^{-2} \cdot \text{s}^{-1}$ | > 0.5 $\text{gC} \cdot \text{m}^{-2} \cdot \text{d}^{-1}$ |
| T_{air} | air temperature | $> 5 \text{ }^\circ\text{C}$ | - |
| <i>Rg</i> | incoming radiation | $> 0 \text{ W} \cdot \text{m}^{-2}$ | - |
| <i>CSWI</i> | conservative surface wetness index | < -3 to 2 mm | - |

3.2.2 Modeling WUE and predicting T

Using a set of features \mathbf{X} , we trained a random forest regressor (RF) (RandomForestRegressor from Pedregosa et al. (2011) based on Breiman (2001)) on eWUE within the training dataset (for each site) made with the filters outlined in Table 1. Features consisted of four meteorological variables: incoming radiation (*Rg*), air temperature (T_{air}), relative humidity (RH), wind speed (*u*); four derived variables: the derivative of a Gaussian filtered *GPP* (GPP'), the *Rg* normalized diurnal centroid of ET (C_{ET}^*), the diurnal water:carbon index (DWCI), conservative surface wetness index (*CSWI*); as well as daily potential radiation ($Rg_{pot,daily}$), the derivative of daily potential radiation ($Rg'_{pot,daily}$), and year. The resulting feature vector \mathbf{X} is,

$$\mathbf{X} = [Rg, T_{air}, RH, u, Rg_{pot,daily}, Rg'_{pot,daily}, CSWI, GPP', C_{ET}^*, DWCI, year]. \quad (3.4)$$

Note that C_{ET}^* measures the morning shift of diurnal ET, and DWCI measures the degree of correlation in one day between *GPP* and ET; a detailed explanation of C_{ET}^* , DWCI, and *CSWI* can be found in Nelson et al. (2018b), code for which can be found at Nelson (2017). The set of features \mathbf{X} was designed to give the RF regressor information on processes that may impact WUE.

The full time-series of WUE was then predicted for all half-hours (unfiltered data) using

the resulting model as,

$$WUE_{t,pred} = RF_P(\mathbf{X}_t, P) \quad (3.5)$$

where P is the percentile used from each resulting predictive leaf, or prediction percentile (Meinshausen, 2006). Quantile random forest regression is analogous to the linear quantile regression use by the Zhou method, but makes no assumptions on linearity.

The RF utilized 100 trees which were fully grown, and each splitting node consisted of a maximum number of features equal to one third the total number of features, rounded up. A sensitivity analysis of the number of trees and max number of feature parameters can be found in supplementary Figure S2.

As ET in the training dataset is assumed to be only a proxy of T, there is likely E still present even after filtering. For example, when making a prediction for a particular half hour the process would work as follows: features of the half hour would be fed to the RF (R_g , T_{air} , RH, etc...); in turn the RF will return a number of WUE values which it has identified as associated with the particular features of that half hour; this set of returned values can then be summarized, which is typically via the mean, but can also be a median or any other quantile such as the percentiles used here. If one assumes that all these WUE values from the RF for a half hour represents a single "true WUE" (GPP/T) that is contaminated by some residual evaporation ($GPP/(T+E)$), the best summary statistic to use would be the maximum, as that would be the point most likely to have minimal residual evaporation. However, because the assumption that the WUE values returned from the RF likely do not represent a single "true WUE", and instead variability comes both from residual evaporation and variability in WUE, the most appropriate percentile is not known. Therefore, the magnitude of predicted WUE can be adjusted using the percentile of prediction from the random forest and the optimum percentile, another hyperparameter which is not known a priori. A sensitivity analysis of prediction percentiles can be found in results section 3.2. Note that extraction of percentiles from 50-100 are the result of a single prediction step with a single trained RF regressor, i.e. the RF was not retrained for each percentile.

Given an estimate of WUE, the prediction of transpiration at time t was calculated as,

$$T_t = \frac{GPP_t}{WUE_{t,pred}} \quad (3.6)$$

for each half hour, where nighttime values of T are considered zero. The evaporation component at time t was then estimated as,

$$E_t = ET_t - T_t. \quad (3.7)$$

All code for processing and partitioning, as well as interactive examples, can be found in Nelson (2018).

3.2.3 Model output used for method evaluation

To test the predictive performance of the method, WUE and T estimates were compared to output from three separate models with different underlying carbon:water coupling mechanisms: CASTANEA (Delpierre et al., 2012; Dufrêne et al., 2005), JSBACH (Reick et al., 2013; Knauer et al., 2015), and MuSICA (Ogée et al., 2003; Potier et al., 2015; Wilkinson et al., 2015). Each model comes from a slightly different perspective, characterized by different model structures and ways of dealing with carbon-water relationships. JSBACH differs from the other two models in that it is a land surface model designed to be integrated into a global climate model, which was run off-line for this study. MuSICA separates the canopy into multiple layers, with each layer containing various plant components each with their own water status, light regime, and age. CASTANEA focuses on the growth, carbon allocation, and water budget of a monospecific forest stand.

Models were run using meteorological forcing data from 73 different sites, with 85 model runs in total (see full list in File S6). Meteorological forcing data for the models came directly from the flux towers. This exercise was designed to test whether the method is capable of extracting a known carbon:water relationship even when the underlying assumptions are different. The ability of the algorithm to infer the complex formulations from these process based models gives credence to the capability of the method to estimate these processes in real data. Therefore, the method was applied to the modeled GPP and ET fluxes paired with the respective forcing meteorological data,

with the resulting TEA algorithm transpiration estimates compared to the modeled T. An intercomparison of the three models which used the same meteorological forcing dataset can be seen for three sites in Figure 2. Key distinctions between the models can be seen in the LAI and T/ET, with highest values of leaf area index (LAI) from CASTANEA and MuSICA, and highest T/ET values being from JSBACH. An overview of key model features can be found in Table 2.

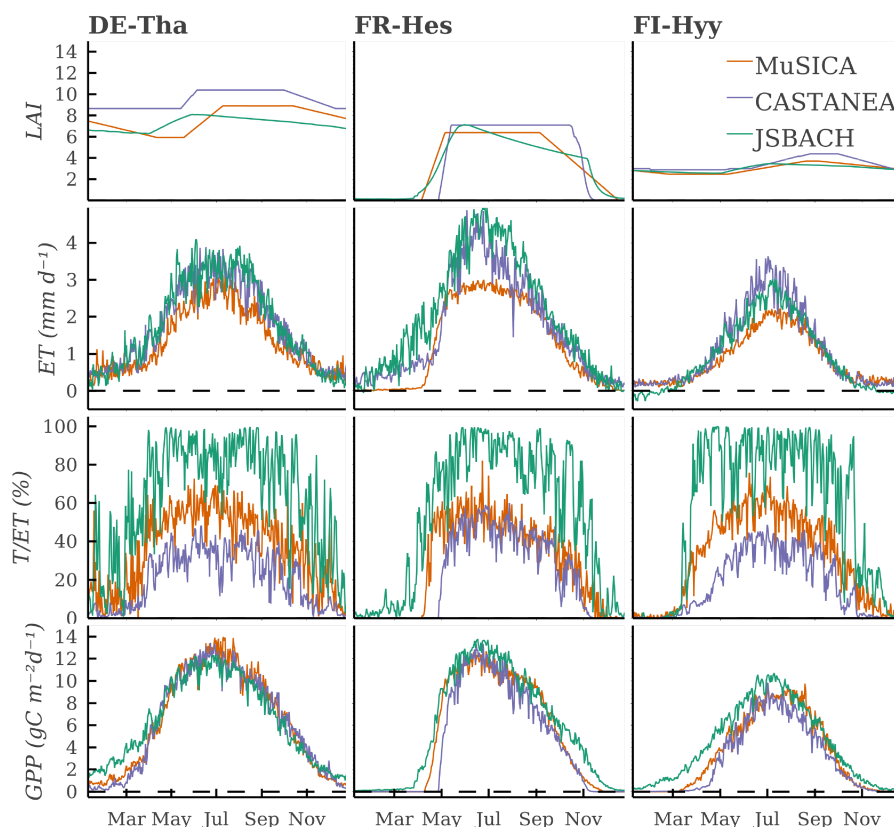


Figure 3.2 Average seasonal cycle of 4 output variables from JSBACH, CASTANEA, and MuSICA, all driven with the same meteorological forcing from three forest sites. Modeled years were 1997-2011 for FI-Hyy and FR-Hes, and 1997-2010 for DE-Tha. Data presented corresponds to daily data averaged across all years, and are intended to show seasonal trends.

Comparisons between model output and TEA estimations were focused on two key aspects: replication of patterns and minimizing bias. The ability to capture patterns was assessed using the modeling efficiency (MEF, Nash and Sutcliffe (1970)), calculated as:

$$MEF = 1 - \frac{\sum (T_{t,model} - T_{t,TEA})^2}{\sum (T_{t,model} - \overline{T_{model}})^2}, \quad (3.8)$$

As this metric is meant to identify only patterns so as to differentiate bias due to consistent over/under estimations and inability to capture temporal patterns, the mean values of T_{TEA} and T_{model} are removed prior to calculating the MEF. Quantification of bias was calculated as a relative bias,

$$bias = \frac{\sum T_{t,TEA} - \sum T_{t,model}}{\sum T_{t,model}}. \quad (3.9)$$

Table 3.2 Overview of key processes in the 3 models used for validation.

| MuSICA | |
|-------------------|--|
| interception | canopy rain interception and water storage on leaf surfaces are computed in each vegetation layer using a water balance equation and the concept of maximum storage capacity, scaled by the leaf area of each layer (Rutter et al., 1971). Evaporation from the interception storage is taken at the potential rate in each layer. More details are provided in Potier et al. (2015) |
| water stress | stomatal conductance, leaf photosynthetic capacity, and/or root hydraulic conductivity downregulated based on instantaneous (Tuzet) or predawn (Ball, Leuning) leaf water potential |
| stomatal conduct. | Ball et al. (1987), Leuning (1995), or Tuzet et al. (2003) depending on parameterisations available for individual sites |
| soil evap. | litter acts as a separate, insulating layer |
| phenology | dates of phenology events (bud burst, senescence) and minimum/maximum leaf area are constant throughout the simulation and supplied by the user |
| JSBACH | |
| interception | water storage for the whole canopy, scaled by LAI, with evaporation from interception storage at the potential rate |

| | |
|-------------------|---|
| water stress | non-linear reduction of g_1 (stomatal slope parameter) and photosynthetic capacity (V_{cmax} and J_{max}) based on available soil moisture |
| stomatal conduct. | Medlyn et al. (2011) |
| soil evap. | soil evaporation coming from top soil layer (of 5) |
| phenology | Logistic Growth Phenology model (LoGro-P); calculation depends on the phenotype, dependent on temperature, soil moisture, and NPP; for evergreen and deciduous forests (described in Böttcher et al. (2016)): heat sum approach in combination with a critical number of chill days |
| CASTANEA | |
| interception | water storage for the whole canopy, function of WAI (wood area index) and LAI |
| water stress | linear reduction of g_1 based on extractable soil water content |
| stomatal conduct. | Ball et al. (1987) |
| soil evap. | evaporation coming from both litter and top soil layer, soil moisture levels updated daily |
| phenology | LAI dynamics based on degree-days (Delpierre et al., 2009); for coniferous trees, winter regulation of photosynthetic-transpiration activity further modulated by thermal acclimation (Delpierre et al., 2012) |

3.2.4 Noise and evaporation sensitivity experiments

To isolate the effects of noise and training set E, two artificial experiments were conducted where the data from each model run were used to create a series of new experimental datasets. The first case attempted to assess the sensitivity of the TEA algorithm hyperparameters to the presence of noise, which is likely to be present in real EC data and is not present in the model output. The second experiment aimed to isolate the effect of E on prediction bias, with the aim of understanding how a persistent fraction of E may potentially bias T estimates.

To test the effects of noise, Random Gaussian noise was added to the original modeled GPP and ET values with a standard deviation corresponding to a scaling factor (s) according to percentages of the original value: 5, 10, 15, 20, and 25%. The experimental

GPP and ET fluxes were then calculated as,

$$flux_{t,noise} = N \left(flux_{t,original}, (flux_{t,original} \cdot s)^2 \right) \quad (3.10)$$

with the resulting eWUE containing noise in both the GPP and ET components. Noise levels were designed to encompass the range expected in real EC data (Hollinger and Richardson, 2005).

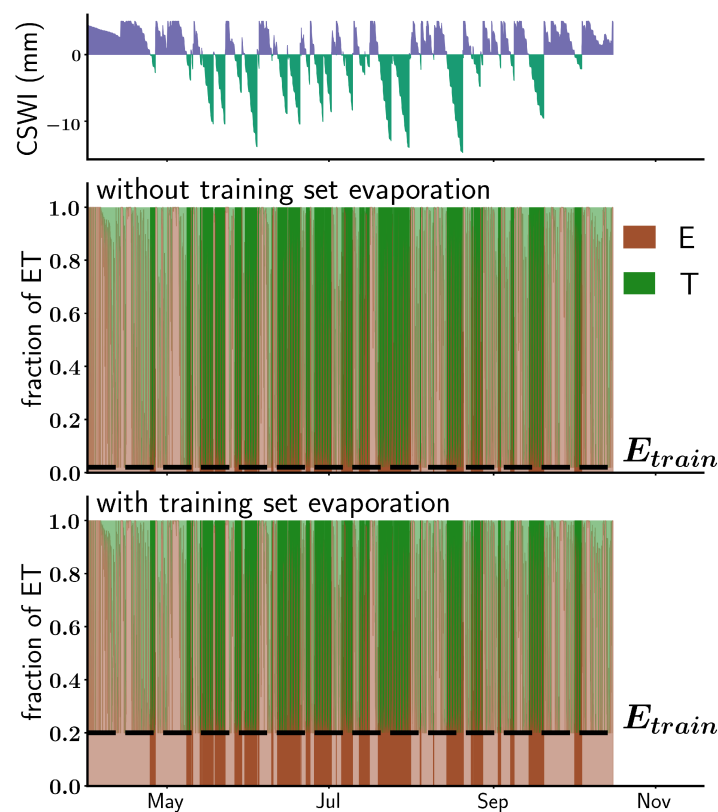


Figure 3.3 Conceptual diagram showing persistent evaporation in the training dataset (E_{train}). In the case without persistent evaporation, many periods of the training dataset contain little E_{train} , meaning the algorithm can likely find periods where $eWUE=WUE$, $(GPP/ET)=(GPP/T)$, and $ET=T$. In the case with high E_{train} , every period contains significant E, which is likely to cause a bias in WUE estimates and ultimately an over-estimation of T.

To isolate the effect of E on prediction bias, it is important to distinguish between total E and E which is persistent within the training dataset (E_{train} , see Figure 3 for a conceptual overview). As the RF is trained on GPP/ET within the filtered periods, only E which is present in the training dataset can bias WUE predictions. To quantify how sensitive

the method is to E_{train} , experimental ET data were calculated from simulated model T data to give a consistent E_{train} for the entire time-series which could not be filtered via CSWI. E_{train} levels ranged from 0 to 50% of ET, with some added noise to give some uncharacterizable variability. Calculations utilized a multiplier (e_{factor}) which was centered on the desired E_{train} , with standard deviation equal to 25% of E_{train} :

$$e_{t,factor} = N(E_{train}, (E_{train} \cdot 0.25)^2) \quad (3.11)$$

from which ET was calculated as,

$$ET_t = \frac{T_t}{1 - e_{t,factor}}. \quad (3.12)$$

The resulting ET dataset had a consistent fraction of E_{train} in ET which was independent to the magnitude of ET and which the random forest was unable to characterize. The range of E in the experiments encompassed the E levels in the original model training datasets, which reached values up to 37%.

These two experimental datasets were then partitioned using the exact same procedure as the original dataset.

3.2.5 Application to real EC data

The TEA algorithm was used as described above to partition the real eddy covariance data from three sites: Hesse beech forest in France (FR-Hes, Granier et al. (2008)); a Scots pine forest in Hyytiala, Finland (FI-Hyy, Mammarella et al. (2009)); and a spruce forest at Anchor Station Tharandt, Germany (DE-Tha, Grünwald and Bernhofer (2007)). Flux data were flagged as good or bad quality as per Papale et al. (2006), and gap filling and net ecosystem exchange partitioning were performed as per Reichstein et al. (2005b). TEA estimates from real flux data can be found as part of the discussion.

3.3 Results

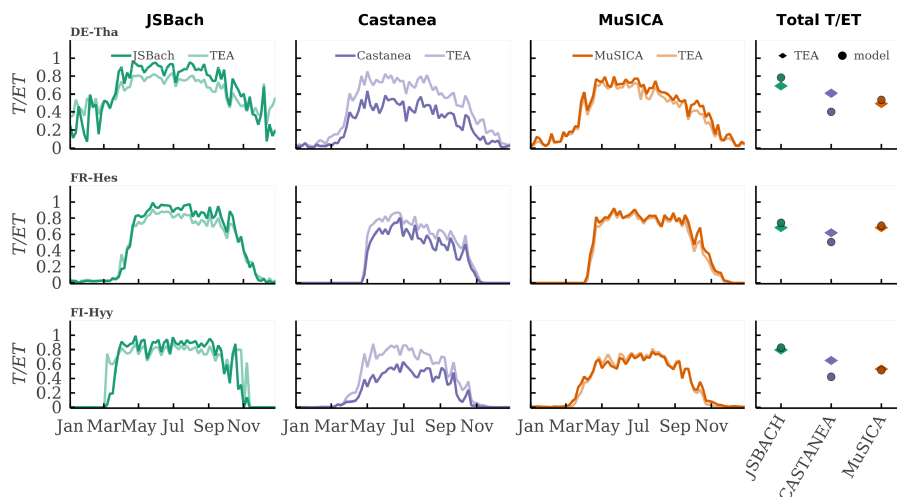


Figure 3.4 Average seasonal cycle of T/ET both from model output and the TEA estimate from model output, as well as total T/ET from the entire time-series. TEA algorithm was run on each individual site and model independently. Modeled years were 1997-2011 for FI-Hyy and FR-Hes, and 1997-2010 for DE-Tha. Data presented corresponds to daily data averaged across all years, and are intended to show seasonal trends.

Figure 4 shows the average annual cycle of T/ET for the three sites run by each model with the same forcing dataset, as well as the total T/ET values. For clarity, TEA estimated values are reported here using hyperparameter values of: CSWI limit of -0.5 mm and the 75th prediction percentile. The 75th prediction percentile corresponds to the median of the percentiles 50-100 and offers a value useful to quantify spatial and temporal patterns (see section 3.2 for sensitivity analysis of hyperparameters and section 4.2 for a discussion on their use). It can seem surprising that the TEA algorithm, which is trained on periods when E is assumed to be zero, performs so well given that the mean daily evaporation across years is often over 40% (Fig. 2). This is because this mean daily evaporation includes night-time periods (when all ET is likely from evaporation) and rainy or post-rain periods, while the TEA algorithm training dataset excludes all those periods (via the radiation and CSWI filters). Thus, the amount of evaporation in the training data-set is much lower than seen in these two plots. The ability of TEA to extract the WUE dynamics can be seen in Figure 5, with seasonal and diurnal WUE patterns of T_{TEA}/ET matching those of T_{model}/ET , including during periods where ET/GPP shows

the obvious effects of E during the wet winter periods.

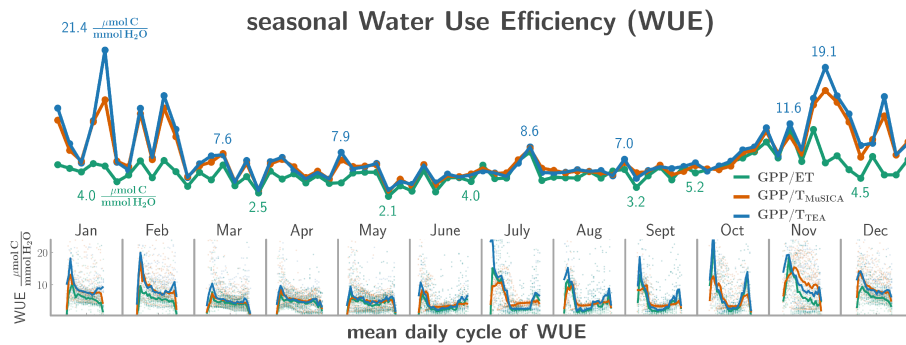


Figure 3.5 The TEA algorithm captures mean seasonal and daily cycles of WUE from MuSICA output forced with data from Yatir Forest from 2001. Mean daily cycles are based on half hourly data for each month, whereas the seasonal cycles are an average from 5 days.

3.3.1 Resulting partitioning performance

The predictive performance of the TEA algorithm applied to the model outputs across both aggregated time scales, as well as across all sites, is shown in Figure 6. The median MEF values between T_{TEA} and T_{model} are greater than 0.9 for all models across all time aggregations up to quarterly, with a slight decrease at annual aggregation. This decrease in performance at annual scale may be due to the limited variability at these timescales, as well as the limited number of years at some sites. Model bias varies between sites and particularly between models, indicating that the optimal prediction percentile for minimizing bias may vary for each model (see section 3.2 for analysis of prediction percentiles). The method performed well spatially, i.e. across sites, with slopes between predicted and modeled T/ET varying between 1.02 and 1.12.

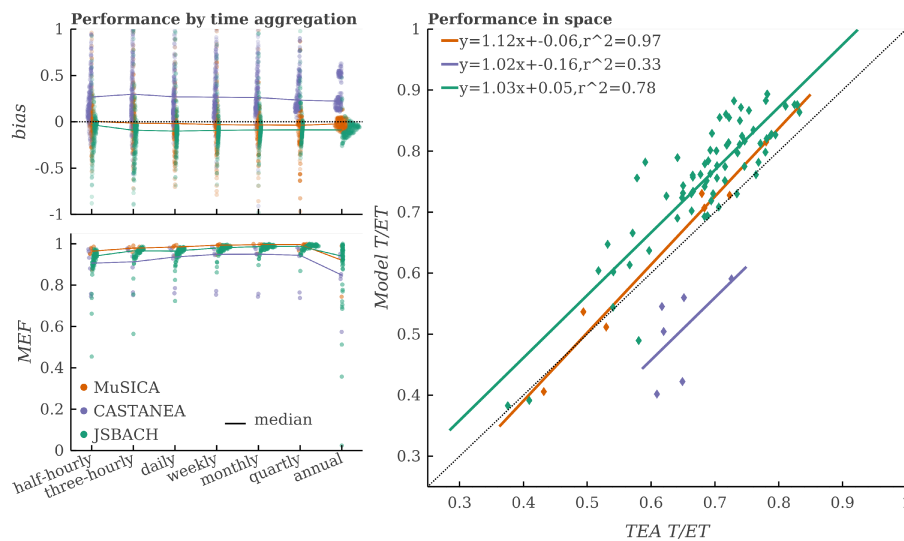


Figure 3.6 Overall model performance in space (right) and time (left). All models show high correlation across timescales, with some degradation at annual scale. In space (i.e. across sites), the TEA algorithm shows the highest agreement with the MuSICA model runs ($r^2 \approx 0.97$), and RMSE for JSBACH, CASTANEA, and MuSICA were 8.4%, 15.3%, and 3.2% respectively.

Using the wider range of sites afforded by JSBACH, site characteristics such as aridity index, mean annual temperature, max LAI, and PFT were shown to have no significant effect on MEF or bias (see supplementary Figure S3).

3.3.2 Sensitivity to hyperparameters: CSWI limit and prediction percentile

The TEA algorithm provides two key hyperparameters to tune the resulting WUE and transpiration estimates: the CSWI limit which controls the amount of required accumulated ET after a rain event before data is included in the training dataset, and the prediction percentile which adjusts the predictions higher or lower, i.e. closer to the limits of the training dataset eWUE values. As the CSWI limit attempts to remove E contaminated data, the limit should be optimized to maximize the MEF between T_{TEA} and T_{model} while maintaining the a high number of points in the training dataset. As seen in Figure 7a, MEF values improve with limits below 0 mm and stabilize below a limit of -0.5 mm. Furthermore, spatial correlations (Figure 7b) show a similar improvement at a limit of -0.5 mm, followed with a sharp decline from the JSBACH runs below a limit

of -2.0 mm. A CSWI limit of -0.5 mm was used for all further analysis (see section 4.2 for further discussion).

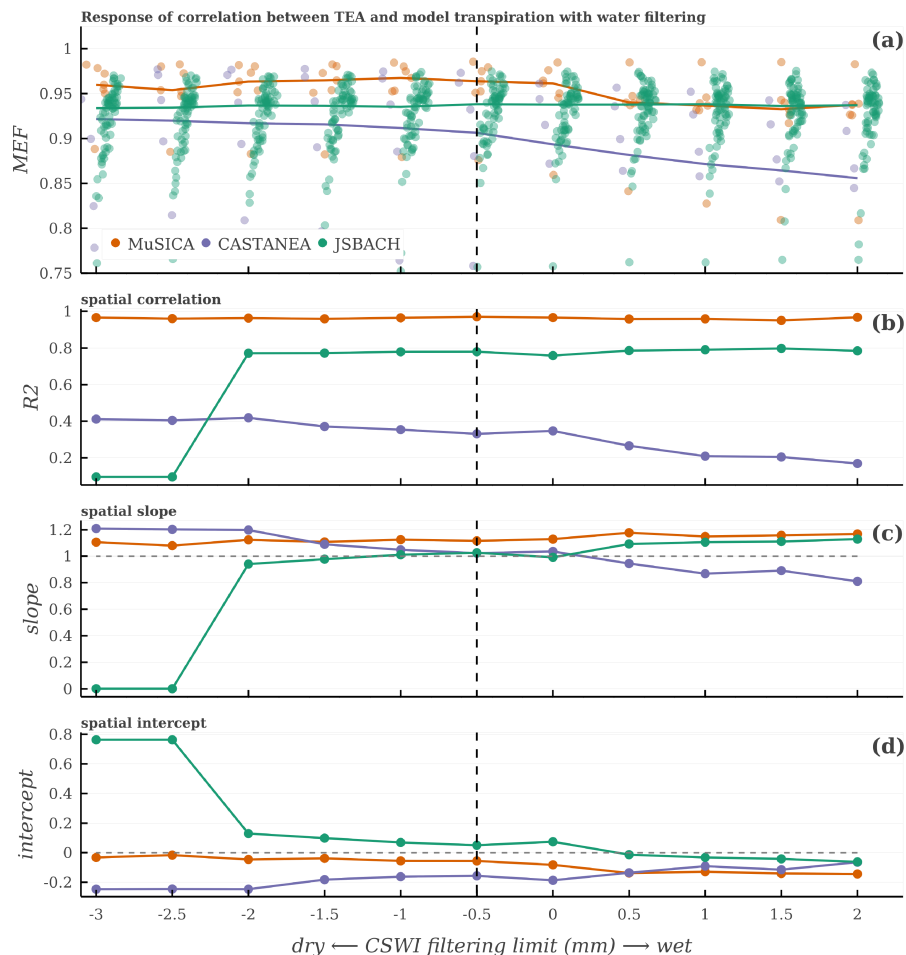


Figure 3.7 Sensitivity of TEA performance to CSWI limit hyperparameter. Though low CSWI limits help reduce the impact of E_{train} , strict filters also decrease the number of points available in the training dataset, which can exclude some wet sites entirely. A filter of -0.5 shows good MEF between T_{TEA} and T_{model} across sites (a), with little improvement using stricter filtering. The negative effect of strict filtering can be seen in the spatial correlation (b) of the JSBACH models, which significantly decreases at limits less than -2.

Figure 8 shows sensitivity and model performance with respect to prediction percentile. MEF for each prediction percentile was generally above 0.7 for all models and sites, with some MEF values less than 0.7 at the highest (P_{100}) and lowest (P_{50}) prediction percentiles (Figure 8a). In accordance with the hypothesis laid out in Zhou et al. (2016a), prediction percentiles closer to the limit which maximizes the GPP:ET ratio

should be associated with periods where E contamination is minimized. In contrast, looking at the relative bias between T_{TEA} and T_{model} (Figure 8b), we found that the prediction percentile which minimizes bias varied depending on model, with optimal prediction percentiles to minimize bias for CASTANEA being around P_{95} , compared to P_{70} for MuSICA, and P_{60} for JSBACH. This difference in optimal prediction percentiles may be due to the differences in the inherent residual E predicted by the models (see Figure 2), with CASTANEA having the highest level of E throughout the growing season (and highest bias minimized prediction percentile) and JSBACH having the lowest. The supplementary Figure S4, which shows the relationship of E/ET in prediction points at various prediction percentiles, further indicates that indeed the E component from TEA predictions is minimized at different percentiles for the three models.

Sensitivity to training set evaporation and noise

As seen in Figure 8d, the TEA algorithm shows a response in bias to E_{train} (see section 2.4 for experimental outline), with the slope between bias and E_{train} being between 1 to 2 for the 50 – 90th prediction percentiles. These slopes correspond to a worst-case scenario, representing a situation where a site would have a constant E component, e.g. a site where E never goes below 15% of ET at any time. So if a site is estimated to have at least 15% E_{train} at every half-hour, the transpiration rates may be 22% overestimated using the 75th prediction percentile. An overestimation of 150% of E_{train} is consistent with the CASTANEA model runs, which across sites has a mean E_{train} of 20% and a mean total bias of 32%, which translates to a mean overestimation of total T/ET of 14%. For context the percentage of training dataset half hours with less than 15% E/ET was on average 67%, 33%, and 95% for MuSICA, JSBACH, and CASTANEA respectively, with the lowest percentage, 6%, for the Hyytiälä Forest simulation from CASTANEA.

Though the highest prediction percentiles show the lowest sensitivity to E_{train} and could thus mitigate this bias, high prediction percentiles also show large sensitivity to noise (Figure 8c, see section 2.4 for experimental outline), indicating that directly using prediction percentiles above P_{95} is not suitable. Prediction percentiles below P_{90} show less sensitivity to noise, with slopes between MEF and the noise to signal ratio (inverse of signal to noise ratio use to simplify sign convention) generally being between -0.1 and 0 for the majority of sites. To put a slope of -0.1 into context, if a site had an MEF of 0.9 and a noise to signal ratio of 1:10, the same site would have an MEF of 0.83 if

noise was then added making the noise to signal ratio 1:2 (see Section 4.2 for further discussion).

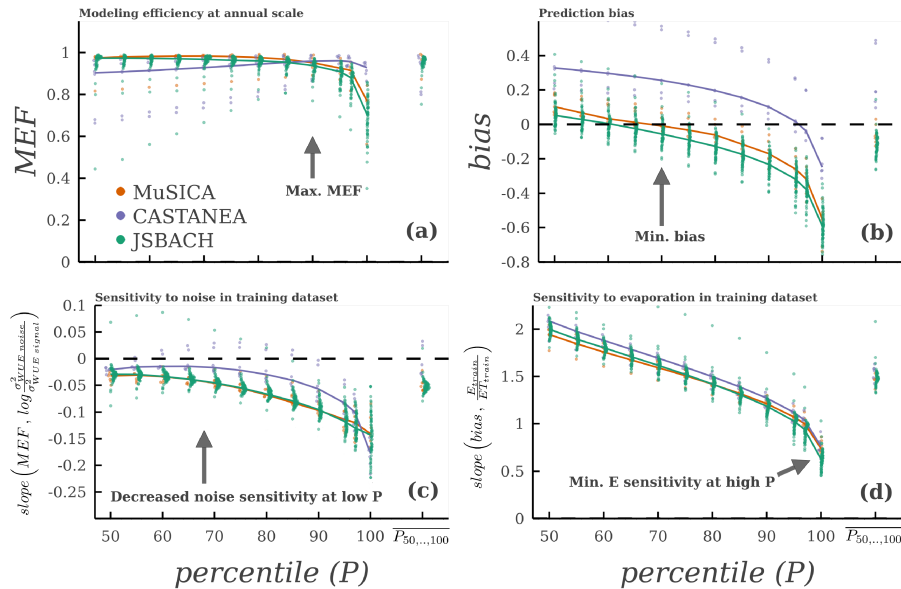


Figure 3.8 Sensitivity analysis of prediction percentile (P) used in TEA. Modeling efficiency (a), while generally stable, shows the highest values at relatively high percentiles ($P \approx 80 - 90$), whereas bias (b) is minimized at around P_{70} for MuSICA and JSBACH. Similarly, percentiles near the maximum (P_{100}) shows the lowest sensitivity to evaporation content in the training dataset (d), yet these high percentiles are also very sensitive to noise in the training dataset (c). Given that residual evaporation will likely be present in the training dataset, causing predictions to be overestimated, percentiles below the median (P_{50}) can be discounted. As such, by treating each percentile above the median ($P \geq 50$) as an equally likely estimate we can calculate the mean of $T_{P_{50}}, \dots, T_{P_{100}}$, the results of which are seen as the far right points in each plot, or the median which corresponds to P_{75} .

3.4 Discussion

3.4.1 Broadly applicable WUE and T estimates

The validation experiment presented here indicates that while ET is composed of two signals (E and T) by pairing the ET signal with GPP, TEA is able to extract the WUE dynamics and thus the biologically controlled T signal. Figures 5 and 6 demonstrate that TEA estimated WUE captures variability in transpiration from sub-daily to inter-annual

scales and between sites, particularly when comparing only simulations from an individual model. The relatively fine temporal resolution of TEA provides the possibility of exploring the dynamics of carbon:water interactions such as seasonal and diurnal cycles. In general, the method as outlined here can be directly applied to real EC data with minimal alteration, allowing for potential global application, with the limitations and cautionary remarks described in the following sections. As a demonstration of TEA using real data, Figure 9 shows a comparison of modeled T/ET at three sites compared to the TEA algorithm estimated T/ET using actual EC data. T estimates from TEA using real EC data fall between the process model T estimates, all while requiring no parameterizations nor having any assumptions on the underlying biological processes. Importantly, TEA does not rely on the model data in any way, as model runs were only used as a validation experiment, thus TEA is purely data driven and represents the statistical prediction of WUE and T based on input data of GPP, ET, and meteorological data. To see the value that these widely applicable methods provide, one needs to look no further than the partitioning of carbon EC fluxes, which have provided a wealth of information despite having known limitations (Reichstein et al., 2012). Combining such widely applicable methods, such as TEA, with the unconstrained processed based models and the sparse independent T measurements provides a multifaceted and complementary view of ecosystem T.

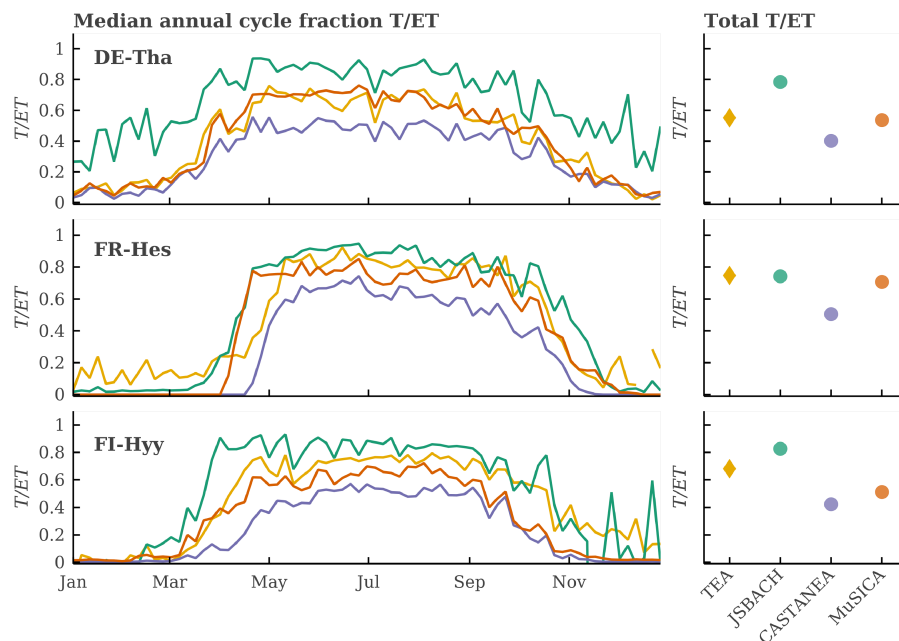


Figure 3.9 Comparison of mean seasonal cycle of T/ET (5 day aggregation) results from model simulations (JSBACH, CASTANEA, and MuSCIA) and TEA algorithm partitioning of original EC data (ET, GPP, and meteorological variables). Modeled years were 2001-2006 for FI-Hyy and FR-Hes, and 1998-2003 for DE-Tha. Seasonal cycles are an average of 5 days.

Though methods for estimating T from independent measurements such as upscaled sap flux methods have existed for decades, there are still relatively few published values that coincide with eddy covariance sites. One set of estimates at Hesse forest gives a seasonal T/ET (2 May to 27 Oct) from sap flux upscaling of 0.72, 0.82, and 0.86 for 1997, 1998, and 1999 respectively (Vainshtein, 2010), which is in relative agreement with the TEA estimates from eddy covariance data at Hesse forest being 0.75, 0.82, and 0.73. Though an in-depth comparison to independent T measurements is beyond the scope of this analysis, initiatives such as SAPFLUXNET, which aims to aggregate sap flux datasets from around the world (Poyatos et al., 2016), as well as aggregations of isotope based measurements and the continued aggregation of eddy covariance dataset will help constrain ecosystem transpiration estimates within the next few years.

3.4.2 Sensitivities and limitations

As seen in Figure 7, the CSWI limit hyperparameter should always be less than zero. However, prediction performance did not improve at increasingly negative values and may actually deteriorate performance due to declines in sample size. This lack of improvement indicates that CSWI, though likely an improvement to time based methods, does not do well at indicating degrees of moisture levels past simple wet and dry. Therefore, a CSWI value of around -0.5 or -1.0 mm is warranted, as it creates the largest sample size while still being below zero. It is possible that the TEA algorithm could be improved with a filter that better minimizes the amount of evaporation left in the training dataset, E_{train} , such as using surface soil moisture data. As such, the TEA algorithm would likely benefit from site specific information on water status, both as a means to filter the training dataset and as a predictor variable. Additionally, it should be noted that as the filtering step removes all periods during and immediately after rain, these periods will not be represented in the training dataset and therefore any response of WUE during these rainy periods will not be captured. However, as none of the filters was based on humidity levels, periods of high relative humidity are included in the training dataset, so both stressed and unstressed conditions will be included in the training dataset. As rain specifically should not have a dramatic influence on WUE. Indeed, we did not observe any error increase in the validation dataset during wet periods.

Overall, the method tends to be more precise than accurate, i.e. it robustly produces precise patterns but with a propensity for systematic over- or underestimation. In particular, the method is sensitive to E_{train} such as is the case with the CASTANEA model runs, producing an overestimation of transpiration while still capturing the temporal patterns across timescales. The CASTANEA simulations here provide an important test as to how E can impact the TEA estimates, as the simulations have not only relatively high E/ET throughout the year, but, due to the fact that soil moisture levels are updated daily, E/ET is also relatively consistent throughout the day. Therefore, the training dataset from CASTANEA simulations is always contaminated by E, in contrast to MuSICA which can have daily E but still have periods when T dominates within that day, and JSBACH which has very low E throughout the growing season (see Figure S4). That being said, it is possible to predict an accurate average T/ET using a higher prediction percentile even when E is always present as long as there is variability in WUE (see Figure S5), though the highest WUE values will be underestimated.

Given that the optimal prediction percentile for minimizing bias differed among the three models, all prediction percentiles above the 50th can be considered equally likely predictors, with P_{50} representing the case with no E_{train} and a constant WUE, and P_{100} representing the maximum eWUE. The result is a distribution of estimates for WUE and T, which can be translated into an average and uncertainty. As this distribution tends to be rather skewed, the median of this distribution (or P_{75}) is likely a more robust estimator. While the lower bound of the distribution is well bounded, the maximum (P_{100}) case could still systematically underestimate WUE if E_{train} is significantly higher than zero. In contrast, P_{100} could also grossly overestimate WUE as it can correspond to conditions which are not at all representative, e.g. conditions of high humidity when WUE tends to infinity, which can be further complicated with the added effects of noise.

Ecosystems with sparse vegetation coverage are likely most at risk of having high E_{train} levels, and therefore overestimation, as the canopy is potentially not the key control on ET. The risk of overestimation is especially high at wetland sites with exposed open water. Therefore, site specific estimations are warranted to determine if TEA estimations would benefit from hyperparameter adjustments such as using a higher prediction percentile, improved training set filtering, or other improvements based on site knowledge (e.g. filtering periods during irrigation). Another important consideration when applying the method to actual data is the existence of noise which is not present in the synthetic validation datasets. This is particularly pertinent due to very large or small values of WUE (a ratio) during mornings and evenings when the fluxes are low. In this case, a filter for small values of either ET, GPP, or Rg will likely be warranted, even though the method was shown to be relatively insensitive to noise for most prediction percentiles (Figure 7c). Given the considerations outlined above, a general framework for implementing TEA for eddy covariance data would be to use a CSWI limit of -0.5 mm and the 75th percentile for prediction, which corresponds to the median of predictions from the 50th to 100th percentiles.

3.5 Conclusion

In its current state, ecosystem transpiration is far a more concrete physiological concept than it is actually quantifiable, as one can isolate transpiration in relatively controlled leaf or plant scale experiments in contrast to the difficulties of isolating soil and in-

terception evaporation components from the transpiration of each needle and leaf at a field site. However, by utilizing the carbon cycle, transpiration dynamics can be extracted from the overall evapotranspiration signal. As such, the TEA algorithm is a novel evapotranspiration partitioning method designed for eddy covariance datasets which is able to capture dynamics in water use efficiency and transpiration across spatial and temporal scales. The method is the first such evapotranspiration partitioning approach to attempt such an extensive validation exercise, utilizing a synthetic experiment of process model output, which demonstrates the ability of the method to replicate the carbon:water relationship across three model frameworks. Furthermore, we outline the biases and uncertainties of the approach with particular respect to effect of persistent evaporation fluxes, with the prospect that by thoroughly scrutinizing and testing the limits of TEA we can open the door to wide scale application.

Acknowledgments

The authors would like to thank those who gave thoughtful input and feedback on the manuscript such as Sven Boese, Sujan Koirala, and Gustau Camps-Valls. Jacob Nelson would like to thank Bernhard Ahrens for initial editing work, and Tiana Hammer for personal and scientific support. The authors would like to thank the broader eddy covariance community, who's work and expertise are fundamental for this analysis. This work used eddy covariance data acquired and shared by the FLUXNET community, including these networks: AmeriFlux, AfriFlux, AsiaFlux, CarboAfrica, CarboEuropeIP, CarboItaly, CarboMont, ChinaFlux, Fluxnet-Canada, GreenGrass, ICOS, KoFlux, LBA, NECC, OzFlux-TERN, TCOS-Siberia, and USCCC. The ERA-Interim reanalysis data are provided by ECMWF and processed by LSCE. The FLUXNET eddy covariance data processing and harmonization was carried out by the European Fluxes Database Cluster, AmeriFlux Management Project, and Fluxdata project of FLUXNET, with the support of CDIAC and ICOS Ecosystem Thematic Center, and the OzFlux, ChinaFlux and AsiaFlux offices. FLUXNET data can be found at <http://fluxnet.fluxdata.org/>

Data and code used in this analysis can be found in the associated repository: Nelson (2018)

Chapter 4

Ecosystem transpiration and evaporation: insights from three water flux partitioning methods across FLUXNET sites

Received: 14 January 2020 | Accepted: 24 June 2020

DOI: 10.1111/gcb.15314

PRIMARY RESEARCH ARTICLE

Global Change Biology | WILEY

Ecosystem transpiration and evaporation: Insights from three water flux partitioning methods across FLUXNET sites

Jacob A. Nelson¹  | Oscar Pérez-Priego² | Sha Zhou^{3,4,5} | Rafael Poyatos^{6,7}  | Yao Zhang³  | Peter D. Blanken⁸ | Teresa E. Gimeno^{9,10} | Georg Wohlfahrt¹¹ | Ankur R. Desai¹² | Beniamino Gioli¹³  | Jean-Marc Limousin¹⁴ | Damien Bonal¹⁵ | Eugénie Paul-Limoges¹⁶ | Russell L. Scott¹⁷ | Andrej Varlagin¹⁸ | Kathrin Fuchs¹⁹  | Leonardo Montagnani²⁰  | Sebastian Wolf²¹ | Nicolas Delpierre²²  | Daniel Berveiller²² | Mana Gharun²¹ | Luca Beletti Marchesini^{23,24}  | Damiano Gianelle²³  | Ladislav Šigut²⁵  | Ivan Mammarella²⁶ | Lukas Siebicke²⁷ | T. Andrew Black²⁸ | Alexander Knohl^{27,29} | Lukas Hörtnagl³⁰ | Vincenzo Magliulo³¹ | Simon Besnard^{1,32}  | Ulrich Weber¹ | Nuno Carvalhais^{1,33} | Mirco Migliavacca¹ | Markus Reichstein^{1,34} | Martin Jung¹

¹Department of Biogeochemical Integration, Max Planck Institute for Biogeochemistry, Jena, Germany

²Department of Biological Sciences, Macquarie University, Sydney, NSW, Australia

³Lamont-Doherty Earth Observatory of Columbia University, Palisades, NY, USA

⁴Earth Institute, Columbia University, New York, NY, USA

⁵Department of Earth and Environmental Engineering, Columbia University, New York, NY, USA

⁶CREAF, Cerdanyola del Vallès, Spain

⁷Universitat Autònoma de Barcelona, Cerdanyola del Vallès, Spain

⁸Department of Geography, University of Colorado, Boulder, CO, USA

⁹Basque Centre for Climate Change, Scientific Campus of the University of the Basque Country, Leioa, Spain

¹⁰IKERBASQUE, Basque Foundation for Science, Bilbao, Spain

..

Ecosystem transpiration and evaporation: insights from three water flux partitioning methods across FLUXNET sites

Jacob A. Nelson¹, Oscar Pérez-Priego³, Sha Zhou^{4,5,6}, Rafael Poyatos^{7,33}, Yao Zhang⁴, Peter D. Blanken⁹, Teresa E. Gimeno^{10,11}, Georg Wohlfahrt¹², Ankur R. Desai¹³, Beniamino Gioli¹⁴, Jean-Marc Limousin¹⁵, Damien Bonal¹⁶, Eugénie Paul-Limoges¹⁷, Russell L. Scott¹⁸, Andrej Varlagin¹⁹, Kathrin Fuchs²⁰, Leonardo Montagnani²¹, Sebastian Wolf²², Nicolas Delapierre²³, Daniel Berveiller²³, Mana Gharun²², Luca Beletti Marchesini^{24,25}, Damiano Gianelle²⁴, Ladislav Iqut²⁶, Ivan Mammarella²⁷, Lukas Siebicke²⁸, T. Andrew Black²⁹, Alexander Knohl^{28,30}, Lukas Hörtnagl³¹, Vincenzo Magliulo³², Simon Besnard^{1,34}, Ulrich Weber¹, Nuno Carvalhais^{1,2}, Mirco Migliavacca¹, Markus Reichstein^{1,8}, Martin Jung¹

¹Department of Biogeochemical Integration, Max Planck Institute for Biogeochemistry, Jena, Germany

²Faculdade de Ciências e Tecnologia, FCT, Universidade Nova de Lisboa

³Department of Biological Sciences, Macquarie University, Sydney, NSW, Australia

⁴Lamont-Doherty Earth Observatory of Columbia University, Palisades, New York, USA

⁵Earth Institute, Columbia University, New York, New York, USA

⁶Department of Earth and Environmental Engineering, Columbia University, New York, New York, USA

⁷CREAF, Cerdanyola del Vallès, Spain

⁸Michael-Stifel-Center Jena for Data-Driven and Simulation Science, Jena, Germany

⁹Department of Geography, University of Colorado, Boulder, Colorado

¹⁰Basque Centre for Climate Change, Scientific Campus of the University of the Basque Country, Leioa, Spain

¹¹IKERBASQUE, Basque Foundation for Science, Bilbao, Spain

¹²Department of Ecology, University of Innsbruck, Innsbruck, Austria

¹³University of Wisconsin-Madison, Department of Atmospheric and Oceanic Sciences, Madison, WI, USA

¹⁴Institute of Bioeconomy (IBE), National Research Council of Italy (CNR), Firenze, Italy

¹⁵CEFE UMR 5175, CNRS, Univ Montpellier, Univ Paul Valéry Montpellier 3, EPHE, IRD, F- 34293 Montpellier, France

¹⁶Université de Lorraine, AgroParisTech, INRA, UMR Silva, Nancy, France

¹⁷Department of Geography, University of Zurich, Zurich, Switzerland

¹⁸Southwest Watershed Research Center, USDA-ARS, Tucson, AZ, United States

¹⁹A.N. Severtsov Institute of Ecology and Evolution, Russian Academy of Sciences, Moscow, Russia

²⁰Karlsruhe Institute of Technology (KIT) Institute of Meteorology and Climate Research - Atmospheric Environmental Research, Garmisch-Partenkirchen, Germany

²¹Forest Service, Autonomous Province of Bolzano-Bozen, Bolzano-Bozen, Italy

²²Department of Environmental Systems Science, ETH Zurich, Zurich, Switzerland

²³Ecologie Systématique Evolution, Univ. ParisSud, CNRS, AgroParisTech, Université ParisSaclay, Orsay, France

²⁴Department of Sustainable AgroEcosystems and Bioresources, Research and Innovation Centre, Fondazione Edmund Mach, San Michele all'Adige, Italy

²⁵Department of Landscape Design and Sustainable Ecosystems, Agrarian Technological Institute, RUDN University, Moscow, Russia

²⁶Department of Matter and Energy Fluxes, Global Change Research Institute of the Czech Academy of Sciences, Brno, Czech Republic

²⁷Institute for Atmospheric and Earth System Research INAR / Physics, Faculty of Science, University of Helsinki, Finland

²⁸Bioclimatology, University of Goettingen, Göttingen, Germany

²⁹Faculty of Land and Food Systems, University of British Columbia, Vancouver, Canada

³⁰Centre of Biodiversity and Sustainable Land Use, University of Goettingen, Germany

³¹Institute of Agricultural Sciences, ETH Zurich, Zurich, Switzerland

³²Institute for Agricultural and Forest Systems in the Mediterranean (ISAFoM), National Research Council of Italy (CNR), Ercolano, Italy

³³Universitat Autònoma de Barcelona, Cerdanyola del Vallès, Spain

³⁴Laboratory of Geo-Information Science and Remote Sensing, Wageningen University and Research Center, Wageningen, Netherlands

We apply and compare three widely applicable methods for estimating ecosystem transpiration (T) from eddy covariance (EC) data across 251 FLUXNET sites globally. All three methods are based on the coupled water and carbon relationship, but they differ in assumptions and parameterizations. Intercomparison of the three daily T estimates shows high correlation among methods (R between 0.80 and 0.87), but a spread in magnitudes of T/ET (evapotranspiration) from 45% to 77%. When compared at six sites with concurrent EC and sap flow measurements, all three EC based T estimates show higher correlation to sap flow based T than EC based ET. The partitioning methods show expected tendencies of T/ET increasing with dryness (vapor pressure deficit and days since rain) and with leaf area index. Analysis of 140 sites with high quality estimates for at least two continuous years shows that T/ET variability was 1.6 times higher across sites than across years. Spatial variability of T/ET was primarily driven by vegetation and soil characteristics (e.g. crop or grass designation, minimum annual leaf area index, soil coarse fragment volume) rather than climatic variables such as mean/standard deviation of temperature or precipitation. Overall, T and T/ET patterns are plausible and qualitatively consistent among the different water flux partitioning methods implying a significant advance made for estimating and understanding transpiration globally, while the magnitudes remain uncertain. Our results represent the first extensive EC-data based estimates of ecosystem T permitting a data driven perspective on the role of plants' water use for global water and carbon cycling in a changing climate.

4.1 Introduction

Transpiration (T) is the flux of water vapor and latent energy returned to the atmosphere by vascular plants, mainly through the stomatal pores on their foliage and concurrent with photosynthesis. T is thus the nexus of the terrestrial water, carbon, and energy cycles, making T a key process in the Earth System. Better understanding of T could have practical implications through better understanding of plant water use and water limitations (Allen et al., 2015; Bernacchi and VanLoocke, 2015), understanding which can then improve water resource management and prevent economic losses (Fisher et al., 2017). However, estimating ecosystem scale T is challenging, so T is generally studied extensively in laboratories, plant growth chambers, and greenhouses. The difficulty of estimating ecosystem T is due to heterogeneities in the physical and physiological properties and processes underlying plant water uptake and ecosystem water use (Kool et al., 2014). These challenges cause limited availability and large uncertainties in ecosystem T estimates, and this propagates to uncertainties in biosphere-atmosphere feedbacks relevant for projections of climate change by Earth System models (Fisher et al., 2017).

The eddy covariance (EC) technique has been proven to be a useful tool for measuring ecosystem water, carbon, and energy fluxes worldwide (Baldocchi, 2019). A key advantage of the EC technique is the near continuous, sub-daily sampling and the intermediate spatial scale of measurements which integrates over the ecosystem and can be linked to remote sensing products (Jung et al., 2011; Kumar et al., 2016; Chu et al., 2017). EC measures aggregate fluxes, and therefore fluxes related to individual processes must be estimated using modeling and post-processing. In the case of carbon dioxide (CO_2), net ecosystem exchange of CO_2 fluxes (NEE) can be partitioned into gross primary productivity (GPP) and ecosystem respiration (R_{eco}) (Reichstein et al., 2005a; Lasslop et al., 2010). Applying the CO_2 partitioning methods across many sites from communities willing to collaborate (e.g. FLUXNET) has proven valuable in a wide range of contexts (Baldocchi, 2008), from model evaluation (Friend et al., 2007) to empirical upscaling of global products (Jung et al., 2011). The opportunity to replicate the success of CO_2 flux partitioning with water flux partitioning has resulted in a number of methods that attempt to distinguish the physiologically regulated T flux from the measured evapotranspiration (ET) flux, which also contains abiotic evaporation (E) from soil and canopy intercepted water. Partitioning the existing ET from FLUXNET would

improve cross site comparisons of GPP to T dynamics, which have previously relied on filtering each site for periods after rain events to minimize the effect of E.

Here we applied three recent methods for estimating T from EC datasets: the underlying water use efficiency (uWUE) method (Zhou et al., 2016a), the Pérez-Priego method (Perez-Priego et al., 2018), and the Transpiration Estimation Algorithm (TEA) method (Nelson et al., 2018a). We focused on methods which utilize current EC datasets, such as FLUXNET and the associated regional networks, which include continuous measurements of CO_2 , sensible, and latent heat fluxes, as well as meteorological variables at half-hourly or hourly time-steps. All three methods utilize GPP estimates to partition E and T from ET, as CO_2 uptake and water vapor losses from T are both regulated via stomata in higher plants and are thus inherently linked (Cowan and Farquhar, 1977). Note that other ET partitioning methods exist, including methods that only use EC datasets, which are not highlighted here. Such methods include Scott and Biederman (2017), which may not be applicable at non-water-limited sites, and Li et al. (2019) which requires ancillary data such as canopy height and soil moisture. As reviewed in Anderson et al. (2017), other methods for estimating transpiration are being developed, such as flux variance partitioning of high frequency data using water use efficiency measured at the leaf scale (Scanlon and Kustas, 2010; Scanlon et al., 2019), measurement of isotopes (Wang et al., 2012; Berkelhammer et al., 2016), carbonyl sulfide (Whelan et al., 2018), or concurrent below and above canopy eddy covariance measurements (Paul-Limoges et al., 2020). For a more detailed analysis of various water flux partitioning approaches, see Stoy et al. (2019).

4.1.1 Drivers of T and knowledge gaps

A key difficulty in distinguishing T from E is the fact that both fluxes are inherently the same physical process, evaporation, with the core difference being that T is actively regulated by vegetation, e.g. through changes in stomatal conductance and/or root water uptake. One example is the effect of vapor pressure deficit (VPD), which on the one hand drives T and E but on the other causes stomatal closure in plants thus inhibiting T. Stomatal closing due to high VPD prevents excess plant water loss relative to carbon gain. As VPD increases, T losses would increase with no corresponding effect on GPP (assuming no other change in the environment, stomatal conductance, or non-stomatal limitations), resulting in a decrease in water use efficiency ($WUE = GPP/T$). This de-

crease in WUE has been shown to be a power function of VPD both from in situ chamber experiments (Pérez-Priego et al., 2010; Villalobos et al., 2012) and derived from theory (Medlyn et al., 2011). While this relationship has been demonstrated from GPP/ET ratios derived from EC data in rain free periods (Zhou et al., 2014; Zhou et al., 2015), it should be clearly evident in a GPP/T product, and thus can be used as a first order check on the T estimates.

Another expected pattern is the relationship between LAI and T/ET. Studies using site level estimates of T/ET show a strong coupling to LAI (Wang et al., 2014; Wei et al., 2017). This link between T/ET and LAI is in some respects intuitive: an LAI of zero would mean no vegetation and no T; and increasing vegetation coverage would mean more transpiring surfaces and more shading of soil thus increasing T/ET. However, seasonal covariation may not correspond to a causal relationship, as part of the co-variation could be attributed to other seasonal patterns such as cycles in soil water availability or phenology. By modeling T/ET as a function of LAI, Wei et al. (2017) were able to capture between 43 and 87% of the variance depending on vegetation type. However, Wang et al. (2014) showed high variability of T/ET at low values of LAI, which was in part explained by plant growing stage (particularly in crops). Based on a temperate needle leaf forest site, Berkelhammer et al. (2016) reported that while LAI did match seasonal T/ET dynamics, no significant relationship was found at diel, daily, or annual timescales, indicating the LAI relationship is tied to seasonality. If LAI is a key driver of T/ET, one would expect a relationship between the two at other scales, in particular LAI should correlate with T/ET in space. Using a mechanistic ecohydrological model, Fatichi and Pappas (2017) found no relationship between mean site T/ET and LAI, rather the major driver of uncertainty was the parameterization of the hydraulic properties of the topsoil in the model. Pairing T estimates from EC and remote sensing estimates of LAI would allow for a consistent and broad scale examination of the relationship of LAI and T/ET, and test whether the seasonal relationship observed translates to a spatial relationship indicating that LAI is a key driver of T/ET.

Apart from LAI, T/ET could be related to water availability, as plants have access to deeper soil moisture and can thus sustain a high transpiration rate for longer periods after rain pulses. However, many studies show no relationship between T/ET and precipitation (Schlesinger and Jasechko, 2014; Fatichi and Pappas, 2017), and little relationship with water stress indicators such as soil water potential (Wang et al., 2014) or wetness index (ratio of mean precipitation to potential ET, Fatichi and Pappas (2017)

). Vegetation type could also play a key role in how ET is partitioned, and indeed most previous meta-analyses of site level T/ET data have used some form of segregation by plant functional type (Wang et al., 2014; Schlesinger and Jasechko, 2014; Wei et al., 2017). However, these groupings tend to be imposed for data interpretation, with limited exploration into what ecosystem properties actually drive differences in ecosystem T/ET, and therefore a more in depth analysis is warranted.

4.1.2 Objectives

Here we present estimates of ET partitioning from three different methods across FLUXNET, providing a dataset of transpiration estimates at ecosystem level from sub-daily to annual values and covering many climate zones and biomes. These three methods are first compared against each other to identify how well they agree. The partitioning methods are then compared to an independent data source (scaled-up sap flow measurements), both to demonstrate absolute performance and to ensure that T estimates are adding information compared to the original ET estimates. After initial assessment, we examine the T estimates for expected patterns, such as the seasonal covariation of LAI and T/ET as well as responses to dry conditions such as the expected decrease of WUE to high VPD and the increase of T/ET during dry down events. We also demonstrate the potential inadequacies of calculating WUE as GPP/ET due to E, even when filtering for rain free days. Finally, we use full year estimates of T and ET to explore the drivers of variability in T/ET across sites.

4.2 Methods

4.2.1 EC data

Flux data from the FLUXNET2015 dataset (Pastorello et al., 2017) were used. In some cases, sites were included from the previous La Thuile dataset when not available in the FLUXNET2015 release. An overview of the variables used in this study can be found in Supplementary Table S1. In all cases, GPP was estimated from the EC-measured NEE using the night-time flux partitioning method (Reichstein et al., 2005a).

The sites used in this study are distributed widely across the globe and they represent diverse ecosystems from a variety of climatological conditions. However, the global distribution of observations is largely biased toward Western countries in the Northern Hemisphere, with most of the sites located in USA, Western Europe and East Asia. All sites, as well as the plant function type (PFT) designation are listed in both table and map form in Supplementary File S1.

4.2.2 ET partitioning methods

Descriptive overview of the T partitioning methods

The uWUE method relies on estimates of the underlying water use efficiency (uWUE), defined as,

$$uWUE = \frac{GPP \cdot \sqrt{VPD}}{ET}, \quad (4.1)$$

where VPD is the vapor pressure deficit. Two uWUE variants are calculated from half-hourly data: 1) the potential uWUE ($uWUE_p$) is calculated at an annual scale using a 95th percentile regression between $GPP \cdot \sqrt{VPD}$ and ET , representing conditions with the highest carbon gain to water loss and thus where $T \approx ET$; 2) the apparent uWUE ($uWUE_a$) is estimated as the linear regression slope from a daily or 8 daily window, or directly from eq. 4.1 when estimating at half-hourly resolution. $uWUE_p$ is assumed to be constant throughout a year, corresponding to the maximum carbon gain to water loss given that \sqrt{VPD} linearizes the ET to GPP relationship, as has been shown across a large variety of sites and has been linked to stomatal optimality (Zhou et al., 2014). T/ET is then estimated as,

$$\frac{T}{ET} = \frac{uWUE_a}{uWUE_p} \quad (4.2)$$

As the method utilizes comparatively simple computations, $uWUE_p$ and $uWUE_a$ calculated as slopes or ratios, the uWUE method is the simplest of the three methods to calculate.

The Pérez-Priego method on the other hand utilizes a more complete “big leaf” model,

where four different parameters are fit in a five day moving window. The fit parameters relate to the response of canopy conductance to VPD, photosynthetically active radiation, and temperature, as well as to the response of the maximum photosynthetic rate to VPD and ambient CO_2 . The method also incorporates the leaf optimality concept, i.e. carbon gain to water loss is maximized, by integrating a penalty in the cost function for parameters that result in poor leaf carbon:water optimality. One distinctive feature of the Pérez-Priego method is that it never makes the assumption that $T \approx ET$.

Finally, the TEA method utilizes a non-parametric model, a version of Random Forest (Breiman, 2001), to predict WUE (GPP/T). The model is trained on the ecosystem water use efficiency ($WUE_{eco} = GPP/ET$) during periods in the growing season and when surfaces are likely to be dry, i.e where E/ET should be minimal. Periods likely to have wet surfaces are filtered based on precipitation input and ET in a shallow bucket, water balance scheme (see Nelson et al. (2018a) for a full description). The RF, trained on WUE_{eco} from the filtered periods, then predicts WUE (now GPP/T) for the full time series. To further compensate for the existence of evaporation in the training dataset, a higher prediction percentile of WUE is output from the RF (Meinshausen, 2006). Nelson et al. (2018a) determined that the 75th percentile was the most appropriate prediction percentile based on the best performance when assessed against synthetic data from three terrestrial biosphere models. In contrast to the uWUE or Pérez-Priego methods, the TEA method utilizes a machine learning approach that allows for the predicted WUE to be dynamic in time and not strictly driven by assumed physiological responses—for example, the response of WUE to VPD comes from the data itself rather than an assumption of leaf carbon:water optimality.

In summary, the three methods are characterized by key differences in their assumptions, structure, and conceptualization: number of parameters (one or two in uWUE depending on temporal scale vs four in Pérez-Priego), parametric vs non-parametric (uWUE and Pérez-Priego vs TEA), the assumption that $T \approx ET$ for some portion of the data (uWUE and TEA vs Pérez-Priego), and the inclusion of physiological parameters describing the leaf carbon:water optimality (Pérez-Priego and uWUE vs TEA).

Application of T methods to EC data

The uWUE method was implemented based on the published description (Zhou et al., 2016a), with $uWUE_p$ estimates made for each year and $uWUE_a$ estimates derived using

the 8-day moving window. The resulting Python code can be found in the associated code repository (Nelson, 2020b). The uWUE method was also estimated at half-hourly scale by directly calculating $uWUE_a = GPP \cdot \sqrt{VPD} \cdot ET^{-1}$ (Zhou et al., 2018).

The Pérez-Priego method was implemented using an open source R package (Perez-Priego and Wutzler, 2019). Parameter optimization was performed on a daily basis using a 5-day moving window containing high-quality data: (i) quality flags of the CO_2 fluxes = 0 (directly measured, non-gap-filled according to Reichstein et al. (2005a)); and (ii) half hours with measured precipitation removed.

The TEA algorithm used code version v1.06 (Nelson, 2019), which was updated from the original published version with minor modifications to improve data filtering and include additional checks to ensure night-time T fluxes were set to zero.

Though each method has been previously described in the respective publications, an in depth tutorial for each method can be found as both an interactive and static form in the associated code repository (Nelson, 2020b). Furthermore, the data can be accessed from Nelson (2020a).

Comparison and evaluation of the methods was complicated due to differences in how the methods were applied. In particular, the estimation procedure from Pérez-Priego did not always find adequate solutions for the parameters, resulting in some erratic values of T and thus preventing continuous estimates of T, affecting on average 29% of the data across sites. Missing Pérez-Priego values due to inadequate parameters were not gap-filled, which limited the daily and monthly aggregate values of T to periods without missing data, leaving very few complete months. Due to the differences in applicability, comparisons of all three EC based partitioning methods was limited to intercomparisons between the methods and with the sap flow data, while broader comparisons (e.g. across years or sites) were done only with the TEA and uWUE methods.

4.2.3 Sap flow estimates

Stand transpiration was obtained by upscaling sap flow measurements (T_{SF}) from six forest sites in the SAPFLUXNET database (Poyatos et al., 2016) which overlapped in time with the FLUXNET2015 dataset (Supplementary Table S2). SAPFLUXNET datasets contain sub-daily sap flow rates, scaled to the tree level according to site-specific pro-

cedures, which are documented within the dataset metadata (Poyatos et al., 2019). In order to obtain stand-level T, we first temporally aggregated the data to daily sap flow values per tree ($kg\ day^{-1}$) and retained only those days with sufficient coverage (80% of the sub-daily time-steps). We then normalized sap flow per unit basal area of each tree and averaged the values for each species present in the datasets. In all datasets, the species in which sap flow was measured represented >90% of the stand basal area (Supplementary Table S2). The value of species-specific sap flow per basal area was multiplied by the basal area of each species in the stand and then data from all species were summed to obtain stand-level transpiration ($mm\ day^{-1}$). All the tree and stand-level variables needed for the upscaling were extracted from the metadata corresponding to each dataset (Poyatos et al., 2019).

4.2.4 Gridded and remote sensing data

This study utilized three different sources of remote sensing data to explore the spatial and temporal relationships between vegetation indices and T/ET. First, leaf area index (LAI) and fraction of photosynthetically active radiation (fPAR) estimates for each FLUXNET site were derived from the Joint Research Centre Two-stream Inversion Package (TIP) product (Pinty et al., 2011) and summarized for each site using the mean, minimum, maximum, standard deviation, and the 95th and 99th percentiles. Furthermore, the entire multi-temporal Collection 1 from the Landsat 4, 5, 7 and 8 archives (<https://www.usgs.gov/>) was collected. The blue, red, near-infrared (NIR), and short-wave infrared (SWIR) spectral bands (<https://landsat.usgs.gov/what-are-band-designations-landsat-satellites>) were retrieved to compute normalized difference vegetation index (NDVI) (Tucker, 1979), enhanced vegetation index (EVI) (Huete et al., 2002), and normalized difference water index (NDWI) (Jin and Sader, 2005) vegetation indices. Low-quality Landsat pixels due to clouds, cloud shadows, snow, and ice were masked out (Zhu and Woodcock, 2012; Zhu et al., 2015). Finally, 4-day values (as the best pixel from a four day window) of LAI from the MCD15A3H version 6 MODIS product (Myneni and Knyazikhin, 2015) were used to analyze the relationship of LAI to T/ET (i.e. Figure 4.3). The quality layer for LAI (i.e. FparLai_QC) of the MCD15A3H version 6 product was used for filtering out low-quality observations (i.e. cloudy pixels and pixels covered with snow/ice were discarded). For both Landsat and MODIS products, the data extraction and the preprocessing chains (i.e. cloud, cloud shadow masking, and

downloading) were implemented in the Google Earth Engine (GEE) platform (Gorelick et al., 2017) (<https://earthengine.google.com/>). Landsat (i.e. NDVI, EVI, and NDWI) and MODIS (i.e. MCD15A3H LAI) data were summarized for each site using the mean and 95th percentiles.

Additionally as spatial covariates of T/ET, five soil properties for each site were estimated using the SOILGRIDS dataset (Hengl et al., 2017): coarse fragment volume, soil pH, and percent of clay, sand, and silt. Soil properties were summarized for each site using a weighted mean for the full depth available. In all cases, spatial data were aggregated from an area within ≈ 1 km of the tower location by taking the mean for all good quality pixels in the selected area.

4.2.5 Spatial modeling of T/ET and variable importance

To infer potential drivers of the spatial variability of T/ET, 44 different variables composed of estimated soil properties, vegetation indices from remote sensing, plant functional type classifications, and climate variables measured on site were used to predict site average annual T/ET (one value per site) using a Random Forest model (Breiman, 2001). Variables were pre-selected using the approach of Jung and Zscheischler (2013), which attempts to maximize the model performance while minimizing the required number of variables. Variable selection was repeated ten times and all resulting models were compared to select the top performing feature set. Furthermore, feature importance was estimated by examining the selection frequency of each variable, with the assumption that important features will be selected often in top performing models, while less important features will be selected infrequently. The selection frequencies of the ten independent feature selection runs was then summarized as a mean and standard deviation.

4.3 Results

4.3.1 Inter-comparison of the ET partitioning methods

In general, all three methods agreed with respect to overall patterns, with the lowest correlation (Spearman, R_{sp}) of daily T found between uWUE and Pérez-Priego ($R_{sp} = \}$)

and the highest between uWUE and TEA ($R_{sp} = \}$). For context, the correlations between T from the three methods and ET ranged from R_{sp} of 0.71 to 0.82. The magnitude (daily sum) of T_{TEA} was much higher than those of the other two methods, with T_{uWUE} and $T_{Prez-Priego}$ being 68% and 58% of T_{TEA} , respectively, across all sites. Figure 4.1 shows an inter-comparison of the three methods at daily resolution. Note that the results presented here used the night-time partitioning method to estimate GPP (Reichstein et al., 2005a), which is highly consistent with T estimates from the day-time partitioned GPP (Lasslop et al., 2010) (Supplementary Figure S1).

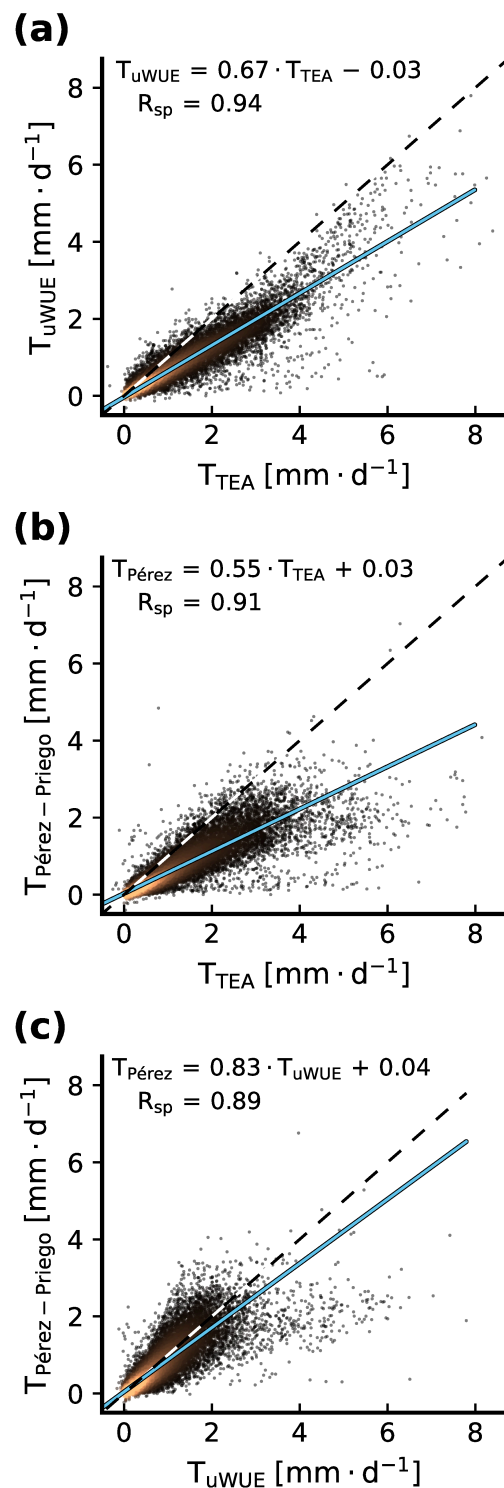


Figure 4.1 Inter-comparison of the three T estimation methods presented here at daily resolution. Points ($n = 53390$ from 127 sites) come from the intersection of all methods where T could be estimated. R_{sp} values correspond to Spearman rank correlations to reduce the influence of outliers. Linear equation was estimated using orthogonal-least-squares regression which assumes observational errors exist in both x and y. Dark to light point coloration corresponds to low to high relative point density, respectively.

4.3.2 Evaluation with sap flow T estimates

As an independent evaluation, all three EC based T estimates were compared to estimates of stand T computed from sap flow sensors (T_{SF}) at 6 different forest sites at daily resolution. Overall, the EC based T estimates had a higher correlation with T_{SF} compared to total ET from EC, with correlations averaging 0.81, 0.78, and 0.76 for T_{TEA} , $T_{Perez-Priego}$, and T_{uWUE} , respectively, compared to 0.70 for ET (Figure 4.2). The bias between T from the EC partitioning methods and T_{SF} ($T_{EC} - T_{SF}$) was smaller compared to the bias between ET and T_{SF} , with site root mean square error (RMSE) between 0.33-1.36, 0.28-0.67, and 0.36-0.96 $mm\ day^{-1}$ for the TEA, uWUE and Pérez-Priego methods, respectively, compared to 0.53-1.95 $mm\ day^{-1}$ for ET.

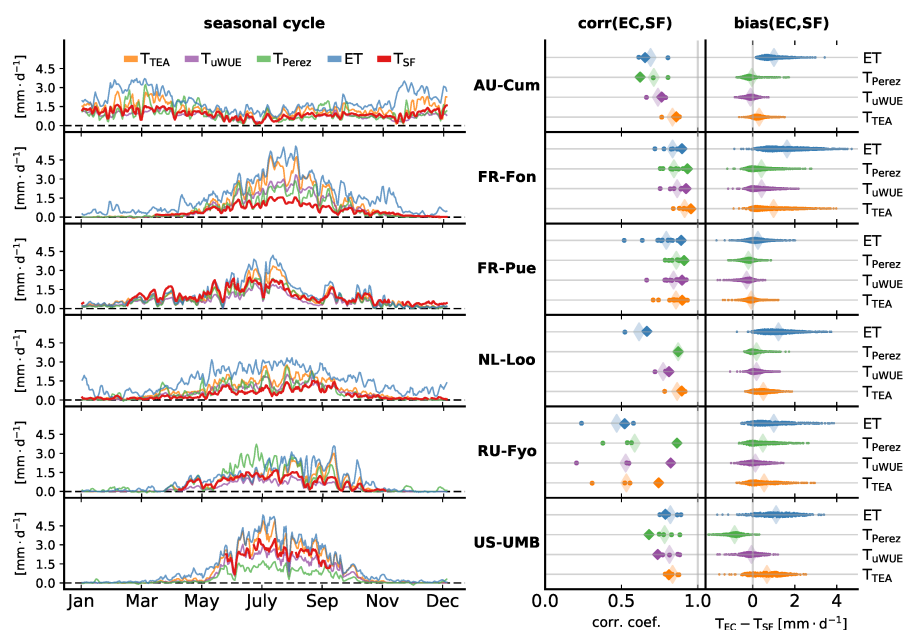


Figure 4.2 Comparison of sap flow based estimates of transpiration (T_{SF}) against estimated transpiration (T) and measured evapotranspiration (ET) from eddy covariance (EC). Note the three different sizes of markers in the correlation plots ($corr(EC,SF)$, Pearson correlation), where the largest markers represents the mean correlation, the smallest markers represent the correlations from each available year, and the medium sized markers represent the selected year shown (time series in the left column of sub-figures).

4.3.3 T/ET patterns with LAI and seasonality

Figure 4.3 shows the relationship of T/ET across the FLUXNET dataset for each method compared to LAI derived from MODIS, grouped into eight plant functional types (PFTs). Additionally, a line is shown describing the relationship between T/ET and LAI derived from Wei et al. (2017), where non-EC based T/ET estimates were used to derive parameters a and b in the model,

$$\frac{T}{ET} = a \cdot e^{b \cdot LAI}. \quad (4.3)$$

The estimates of a and b per PFT were taken from Wei et al. (2017) to calculate the T/ET response to LAI shown (Wei method). Compared to the Wei method, the EC based methods showed a more gradual decline in T/ET as LAI approaches zero, with the exception of ecosystems dominated by deciduous vegetation, i.e. crops and temperate broad-leaved forests. At LAI values above $1 \text{ m}^2 \cdot \text{m}^{-2}$, the higher T/ET values from the TEA method were more consistent with the Wei method, with the uWUE and Pérez-Priego estimated T/ET being significantly lower. Note that the curves from the Wei method are based on site LAI estimates whereas the data in Figure 4.3 were derived from remote sensing based LAI which may not reflect what was seen by the EC systems.

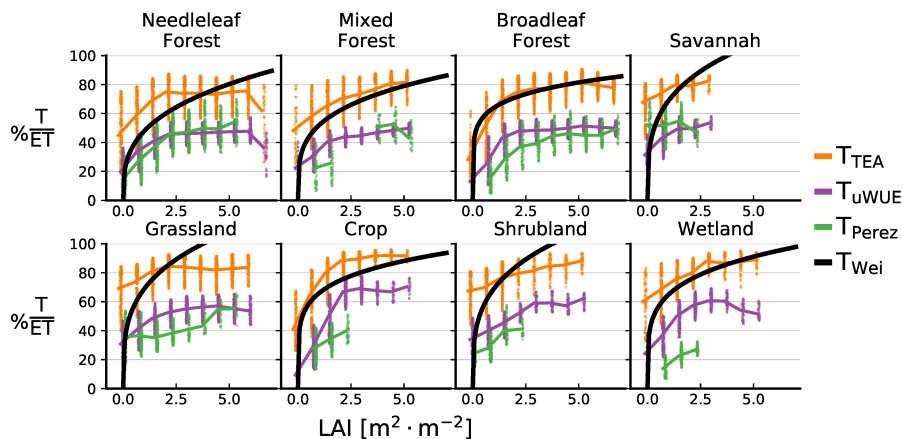


Figure 4.3 Daily T/ET from each EC based method as a function of MODIS LAI. For each PFT, the associated relationship derived from Wei et al. (2017) is shown in black, which was derived from site level T/ET estimates. Points show the distribution within the given LAI bin, truncated to the 25th and 75th percentiles. PFTs were grouped to match those found in Wei et al. (2017) and are slightly different compared to subsequent figures.

Utilizing the fact that the TEA and uWUE methods could be successfully applied at most FLUXNET sites, Figure 4.4 gives an overview of the mean seasonal cycle of T/ET for eight PFTs. Overall, the seasonal patterns of T/ET are largely consistent between the two methods, showing larger T/ET during the growing season as expected. The differences in magnitude are immediately clear for the TEA and uWUE methods, with peak seasonal T/ET being on average 83% and 58%, respectively. Interestingly, both methods showed a relatively consistent peak season T/ET value across all PFTs, even between PFTs dominated by different climates, e.g. similar max T/ET between evergreen broadleaf forests which are primarily in tropical and sub-tropical regions and evergreen needleleaf forests which are primarily located in temperate regions. Note that the PFT groupings in Figure 4.4 were selected to better capture both differences in plant function and biomes, such as separating deciduous forests from evergreen broadleaf forests, and are slightly different from those in Figure 4.3 which correspond to the groupings from Wei et al. (2017).

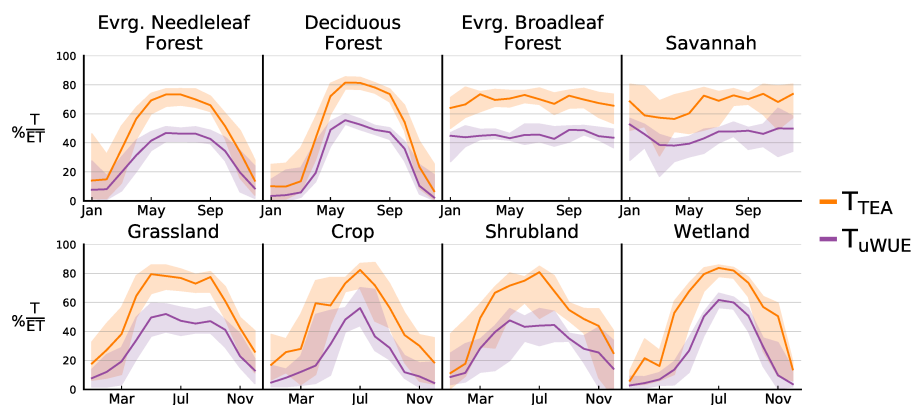


Figure 4.4 Mean monthly seasonal cycles of T/ET grouped by PFT from the TEA and uWUE methods. Mean seasonal cycles for each site are grouped by PFT, with lines indicating the median across sites and shading indicating the interquartile range. Note that data from sites in the Southern Hemisphere have been shifted by six months, e.g. January in the figure would correspond to July in a Southern Hemisphere site.

4.3.4 WUE and T/ET patterns with VPD

Figure 4.5 shows the exponential type relationship of WUE (GPP/T) to VPD for the TEA, uWUE, and Pérez-Priego methods across all sites where T could be estimated by all methods. In contrast, a similar decay was not evident for WUE computed as GPP/ET , lacking the distinctive rise as VPD approaches zero. The reason why the GPP/ET rela-

tionship does not exponentially rise as VPD approaches zero is due to a sharp decrease in T/ET at low VPD (Figure 4.5). In other words, as VPD decreases, T/ET also decreases, likely due to the fact that periods of low VPD correspond to periods after rain or dewfall when surfaces are wet and the evaporation component of ET is relatively high. Consequently, the higher E/ET proportion masked the physiological effect of enhanced WUE at low VPD conditions, highlighting the conceptual bias of ET based water use efficiency estimates and the added value of ET partitioning.

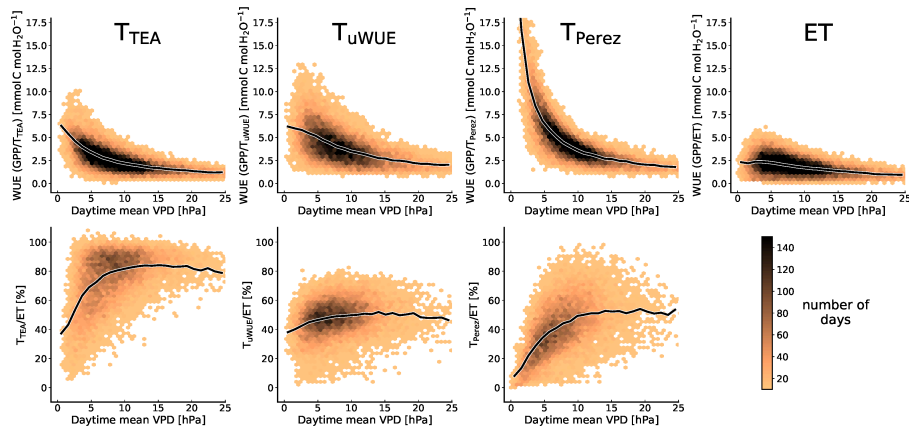


Figure 4.5 Relationship of both WUE (top row) and T/ET (bottom row) to day-time mean VPD at daily scale across 124 sites. Lines indicate the median value from one hPa wide bins. Only days with a mean temperature above 5°C, at least 1 mm day⁻¹ of ET, and where all three partitioning methods could be applied were included.

4.3.5 Remaining evaporation in consecutive rain-free days

Previous studies used ET as a proxy for T by filtering for periods after rain events with the assumption that T will dominate ET; for example, assuming that E will become negligible after three days with no significant rain (e.g. Knauer et al. (2018)). To test this hypothesis, we estimated E/ET (where $E = ET - T$) across all possible sites and grouped into periods of zero to five or more consecutive days after rain, both at the daily and sub-daily scales. In the case of daily resolution, E estimates from all three methods show declining E/ET over the first three consecutive rain free days. However, no method showed zero evaporation, instead falling to 50%, 44% and 16% average E/ET after 5 or more days after rain for Pérez-Priego, uWUE, and TEA, respectively. Though daily E/ET did not fall to zero, the diurnal cycles from all methods indicated periods during the day when E/ET is zero. These diurnal cycles showed contrasting patterns. Both the TEA and

Pérez-Priego methods showed a tendency for higher E/ET in the morning compared to afternoon, with the pattern being much more prominent for the Pérez-Priego method where it persists even after five days without rain, whereas the pattern almost disappears for TEA under drier conditions. The uWUE method consistently showed a peak in E/ET during the afternoon, with the lowest E/ET in the morning hours.

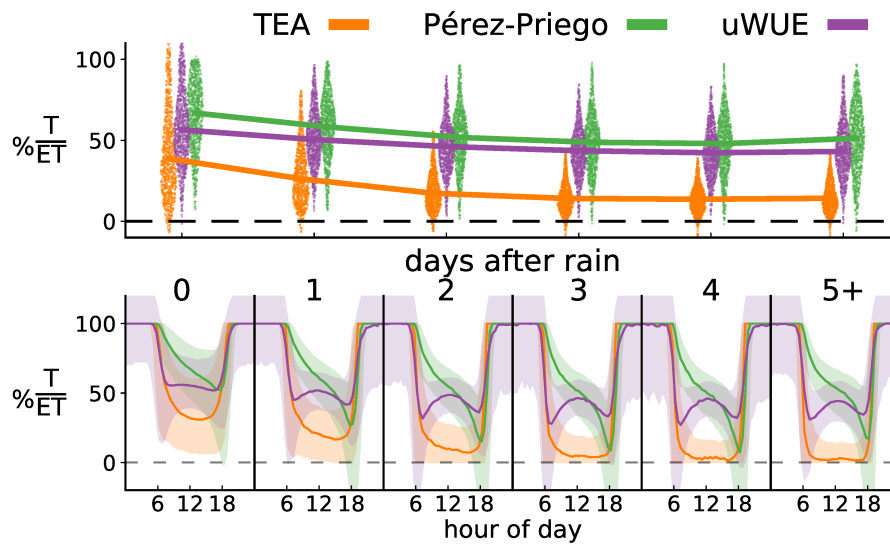


Figure 4.6 Percentage of evaporation (E/ET) estimated using the TEA, uWUE, and Pérez-Priego methods for progressive days after rain (rainy days defined as receiving > 0.1 mm in one day). Upper and lower panels show daily aggregated and diurnal cycles of E/ET , respectively. Diurnal cycles are estimated as the median for each half hour, with the interquartile range shown as shading. Only days with a mean temperature above 5°C , at least 1 mm day^{-1} of ET, and where all partitioning methods could be applied for all half hours in a day were included.

4.3.6 Patterns of between-site T/ET variability

Perhaps the most significant advantage of the widely applicable T estimations is the possibility to make complete annual estimates of T , as they permit the comparison of inter-annual and across site T and T/ET variability. As seen in Figure 4.7, T_{TEA}/ET and T_{uWUE}/ET both showed 60% higher variability (standard deviation) between sites than between years (mean of TEA and uWUE). In other words, T/ET was much more different from one site to another compared to from different years of the same site. This higher spatial variability would suggest that annual T/ET was more related to site characteristics than to the year-to-year changes in environmental conditions.

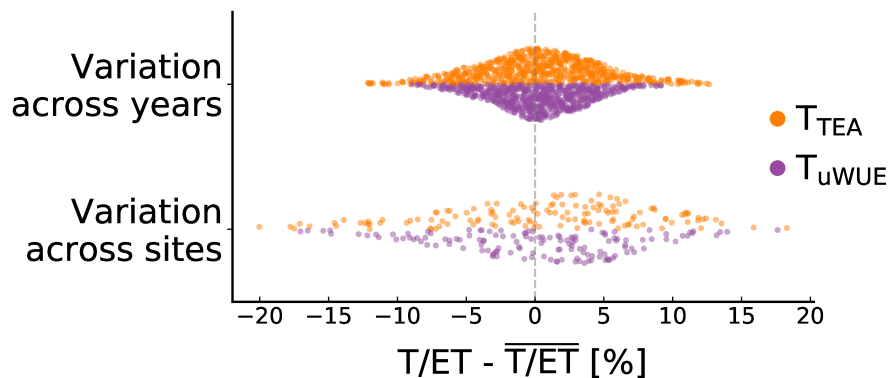


Figure 4.7 Comparison of variability of T/ET across years and across sites. Variability across years was calculated as the T/ET for each year of one site minus the mean across years from that site (only sites with at least 2 years of data). Each point refers to a site and the vertical spread indicates the distribution of points (the uWUE method is mirrored for better comparability). Variability across sites was calculated as the mean T/ET for each site minus the mean across all 140 sites. Overall, the standard deviations across sites was 1.6 and 1.5 times the standard deviations across years (for the uWUE and TEA methods, respectively).

Figure 4.8 shows the model performance of a random forest model for predicting site T/ET for both TEA and uWUE based estimates. The models had Nash-Sutcliffe efficiencies (NSE, Nash and Sutcliffe (1970)) of 0.44 and 0.43 for TEA and uWUE respectively. Overall, the model tended to deflate the variance in site T/ET , indicating an incomplete variable set. Figure 4.9 shows an estimate of variable importance based on how often each variable was selected in the best models (all models with $NSE > NSE_{max} - 0.05$). The five most frequently chosen variables were cropland designation, minimum LAI, soil coarse fragment volume, grassland designation, and soil percent silt content, followed by a number of vegetation indices. Interestingly, most meteorological variables, which were the only variables actually measured at site level, were rarely selected, with mean and standard deviation of annual precipitation never being selected in the best models.

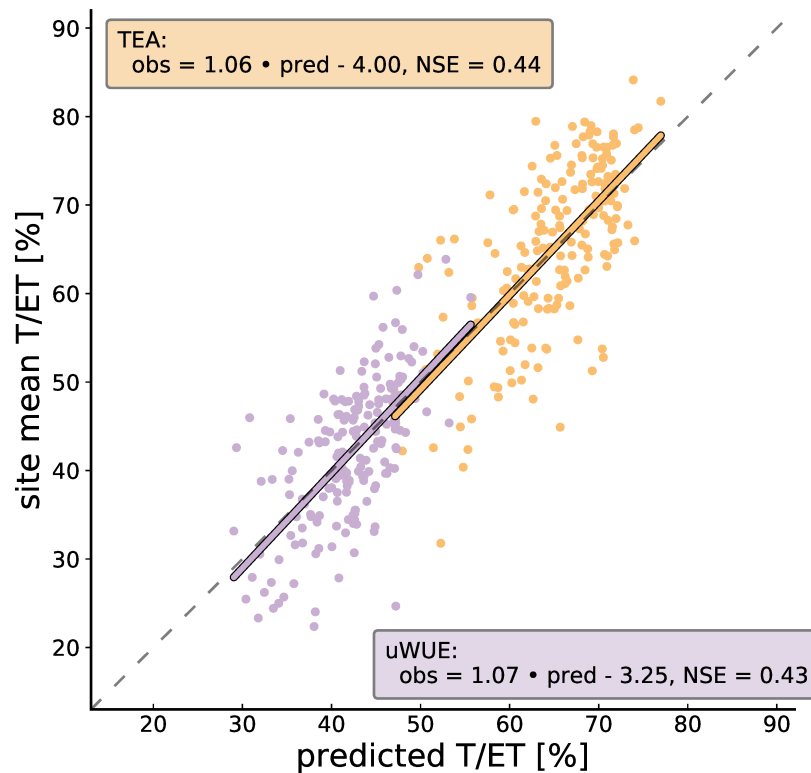


Figure 4.8 Evaluation of the performance of the Random Forest model according to the amount of spatial variability explained across sites. Predicted values are from the out of bag estimates of T/ET, i.e. estimates from the Random Forest model that do not use the corresponding point being predicted. Features used in this model were: mean LANDSAT NDMI, crop designation, grassland designation, min. MODIS LAI, mean MODIS EVI, coarse fragment vol., soil pH, % sand.

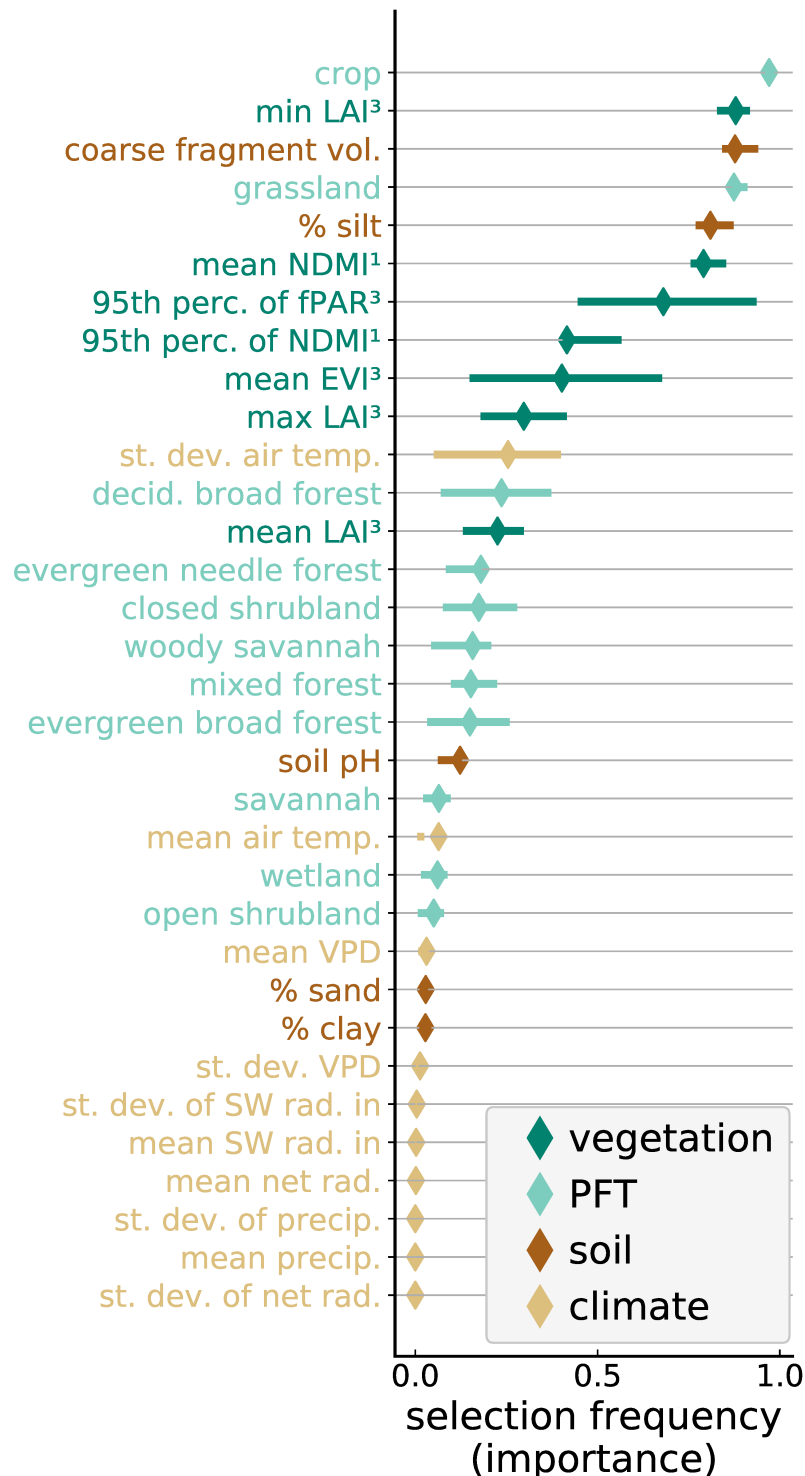


Figure 4.9 Selection frequency, or how often each variable was selected during feature selection, gives an indication of variable importance. Points represent the median selection frequency from ten iterations of feature selection, with the interquartile range shown as error bars. Remote sensing derived variables come from either \acute{z} LANDSAT, \acute{s} TIP, or \acute{s} MODIS (see Methods for a full description). PFT designations are site reported. Climate data comes from site measurements. Soil data was derived from the SOILGRIDS dataset (Hengl et al., 2017).

4.4 Discussion

4.4.1 Assessment of EC based T estimates and their added value over ET

T/ET estimates from the TEA, uWUE, and Pérez-Priego methods across FLUXNET showed overall consistent patterns; for example, with respect to LAI, VPD, and seasonality. Furthermore, T from the partitioning methods, when compared to ET, showed higher correlation with the measured and upscaled sap flow data (Figure 4.2) and a more physiologically plausible WUE response to VPD (Figure 4.5), indicating that T from the partitioning methods better represents the true plant physiology driven T than the bulk flux (ET). Indeed, ET may not be an adequate approximation of T even five days after rain (Figure 4.6). This may have implications in the larger than theoretically expected increases in WUE as a result of increasing atmospheric CO_2 concentration (Keenan et al., 2013) or the discrepancy between leaf and ecosystem WUE (Medlyn et al., 2017), both of which were previously estimated using ET from periods two or more days after rain.

Though the patterns of T seemed to agree well between the methods, it is obvious that there still persists a large spread in the magnitude of the estimated T/ET (Figure 4.3). T/ET estimates from the uWUE and Pérez-Priego methods were smaller and more similar in magnitude ($T/ET = 0.45$) and 45% respectively, calculated as a slope of daily T and ET) compared to values from the TEA method ($T/ET = 0.70$). Though the magnitude of T/ET is difficult to estimate over broad scales, Schlesinger and Jasechko (2014) estimated 67%, 57%, and 55% mean T/ET for temperate deciduous forests, temperate grasslands, and temperate coniferous forests, respectively, which was closer to the TEA method (70%, 67%, and 62%.) compared to the uWUE method (45%, 43%, and 40%).

One potential limitation of all three methods is that they use a GPP estimate, and are thus tied to the biases and uncertainties of the NEE partitioning methods. However, supplementary Figure S1 shows that, when comparing T estimated from both night-time (Reichstein et al., 2005a) and day-time (Lasslop et al., 2010) based GPP, the resulting two T estimates have a higher correlation than the two GPP products do to each other. In other words, T estimates are consistent even when the underlying GPP estimate has changed. This is likely due both to averaging aspects of the methods (e.g. parameters

estimated in moving windows in the uWUE and Pérez-Priego methods) and that GPP is not directly used (e.g. Pérez-Priego calculates T from stomatal conductance and VPD) or canceled out in the final step of T estimation (e.g. TEA estimates T as GPP divided by predicted WUE thus canceling out GPP, i.e. $T = GPP \cdot (GPP/T)^{-1}$, similar for uWUE). However, systematic biases in GPP and ET can affect the ET partitioning methods in different ways. For example, Supplementary Figure S3 shows the response of the estimated T after applying each method to a dataset with manipulations to either GPP or ET fluxes. In short, the Pérez-Priego method is directly affected by major changes or errors in GPP, but is independent of ET. In contrast, both the uWUE and TEA methods are robust to systematic errors in GPP, e.g. a unit conversion error which doubled GPP would have no effect on the estimated T from either method. Short term errors, such as if either GPP or ET were erroneously doubled for only one or two weeks, can significantly affect TEA and uWUE. In general, uWUE is more sensitive to short term errors in GPP, and TEA is more sensitive to short term errors in ET. Errors in the peak growing season have the highest impact on estimated T. Apart from GPP and ET, all three T estimation methods integrate many measurements and therefore require not only high eddy covariance measurements, but also high quality radiation, temperature, humidity, wind, and precipitation data.

4.4.2 Differences between the methods

The TEA and uWUE methods are the more conceptually similar of the three methods, yet they differ in two key ways. First, the TEA method estimates WUE using a non-parametric model allowing WUE to change seasonally and diurnally, whereas the uWUE method models WUE as only varying with \sqrt{VPD} within a single year. This distinction in how the two methods model WUE likely explains the differences seen in mean seasonal (Figure 4.4) and diurnal (Figure 4.6) patterns. Second, while both methods use a form of quantile prediction, the uWUE method predicts the potential WUE ($uWUE_p$) using the 95th percentile where $GPP \cdot \sqrt{VPD}$ is maximum relative to ET. In contrast, the TEA method uses the 75th percentile based on previous modeling experiments (Nelson et al., 2018a) and assumes that while higher values of the predicted distribution more accurately reflect the true WUE, the highest prediction percentiles may overestimate WUE and thus underestimate T. This second difference is the primary cause for large difference in magnitudes, and when the 90th or 95th prediction percentiles from TEA are

used, the resulting T estimates are of similar magnitude to the uWUE based T estimates with minimal change in temporal correlation between the two (Supplementary Figure S2). Therefore, the magnitude of T from both the TEA and uWUE methods is still uncertain to some degree, with TEA being more consistent with the Wei method (Figure 4.3) and uWUE more consistent with the sap flow based T (Figure 4.2). As demonstrated for the TEA and uWUE methods, uncertainty of the magnitudes of T is determined by the design and implementation of partitioning algorithms.

Until independent estimates of T become more abundant and the models can be better constrained, the remaining uncertainty in magnitude should be acknowledged when using these methods. While many new methods for independently estimating T at ecosystem scale are being developed, sap flow based methods will likely be one of the key tools in the near future. However, validation studies have raised concerns about the potential biases incurred by most sap flow methods (Flo et al., 2019; Steppe et al., 2010) and additional uncertainty remains from upscaling from sap flow sensors to trees and to stands (Oren et al., 1998; Ermák et al., 2004). Sap flow upscaled to the ecosystem also only includes canopy T rather than both canopy and understory T, which is captured with an EC system (Blanken et al., 1997). All of these issues could contribute to the differences in magnitude between SF and EC, suggesting that neither measurement technique should be considered the best reference in all cases when it comes to the magnitude of ecosystem T. Nevertheless, sap flow measurements offers reasonable temporal patterns of canopy transpiration and sap flow-derived transpiration has often compared well with independent measurements (Flo et al., 2019; McCulloh et al., 2007) and with evapotranspiration at larger scales (Wilson et al., 2001).

Another key difference between the three methods is in assumptions on the optimality response of stomata to maximize carbon gain to water loss. The Pérez-Priego method explicitly incorporates optimality via an additional term in the cost function which penalizes sub-optimal parameter sets. The uWUE method also incorporates the concept of optimality, both in the \sqrt{VPD} relationship of GPP to T which mirrors theoretical frameworks based on the optimality concept (Medlyn et al., 2011) and implicitly by the use of the 95th percentile when calculating $uWUE_p$, which was intended to find periods where $T \approx ET$ but also has the consequence of maximizing carbon gain to water loss. However, the resulting low values of T/ET from both methods (mean site $T_{uWUE}/ET = 42\%$, with the Pérez-Priego method presumably lower, compared to 65% for the TEA method) runs counter to the current consensus from site level and isotope estimates that T is the dom-

inant terrestrial water flux (Wei et al., 2017; Schlesinger and Jasechko, 2014). Though global estimates still contain uncertainties, such as the limited number of ground studies (64 in Wei et al. (2017) and 81 in Schlesinger and Jasechko (2014)) and uncertainties in T/ET ratios estimated by global isotope studies (Coenders-Gerrits et al., 2014), the low T/ET estimated by the uWUE and Pérez-Priego methods indicates that how optimality is understood and implemented in these methods may need to be refined, such as including hydraulic (Sperry et al., 2017; Eller et al., 2018) and/or non-stomatal limitations (De Kauwe et al., 2019).

4.4.3 Emergent spatial patterns of ecosystem T/ET

A large portion of the variability in T and ET are both driven by climatic drivers, particularly the available energy and atmospheric capacity to drive the evaporative process. Therefore, because much of these climatic effects cancel out when looking at T/ET, it makes sense that climate shows little control over across site variation (Figure 4.9). This lack of control of T/ET from climate, particularly the limited role of annual precipitation, is consistent with previous findings (Fatichi and Pappas, 2017; Schlesinger and Jasechko, 2014; Paschalis et al., 2018). Apart from the limited control from climate, the relative stability of T/ET across sites can be explained by two hypotheses: (1) the effects of interception and soil evaporation largely cancel each other out with regards to increasing vegetation cover (Good et al., 2017), and (2) ecosystems tend to adapt to utilize the water resources available. In the case of the first hypothesis, energy limited ecosystems with higher LAI would also have an increased interception pool, whereas water limited ecosystems may have smaller interception pools but more evaporation coming from the soil. So both dense and sparse canopies will lead to lower T/ET with a maximum somewhere in between. The second hypothesis would suggest that plants adapted to dry ecosystems would incorporate water saving strategies leading to improved utilization of the limited precipitation, thus increasing T/ET. The combination of these two hypotheses possibly accounts for the T/ET ratio being relatively conserved across very different ecosystems. However, both the mean and 95th percentile of NDMI did show high importance in predicting site T/ET, indicating that water stress may influence T/ET, which is consistent with previous findings (Fatichi and Pappas, 2017).

The high values of T/ET at low LAI seen in Figure 4.3 and consistent with Wang et al. (2014), along with the limited importance of mean or maximum LAI in predicting site

T/ET (Figure 4.9), would indicate that T/ET may be less sensitive to LAI than previously assumed, particularly in space. However, many land surface and remote sensing based models formulate ET partitioning in part as a function of vegetation structure such as fraction of vegetation or LAI (Talsma et al., 2018; Lian et al., 2018). Care should be taken not to equate the presence of vegetation to high T/ET. However, as seen in Figure 4.8, much of the variance in T/ET remains unexplained, meaning that the current set of covariates was either not representative of the EC data (i.e. spatial mismatch between satellite data and eddy covariance footprint climatology; Cescatti et al. (2012)) and/or some important drivers of ecosystem T/ET may not have been included, such as temporal dynamics, crop type, forest age, or disturbance history.

4.4.4 Outlook

We demonstrated the progress made in estimating transpiration from eddy covariance measured bulk evapotranspiration by three complementary partitioning methods. Both tests against independent sap flow based estimates and the overall consistency of T and T/ET patterns among methods suggests an important step forward in estimating plant water use at ecosystem scale. The added value of transpiration estimates compared to bulk ET is clearly evident, particularly for assessing ecophysiological more meaningful water use efficiency patterns along atmospheric (VPD) and soil dryness gradients. Previous studies assessing water use efficiency based on flux tower data assumed negligible daily evaporation after a few consecutive rain-free days. Our results suggest that this assumption may be inadequate, implying that those studies may be revisited with ecosystem T estimates which may help in reconciling apparent contradictions with leaf-level estimates and theory.

Of course, the key limitation of the methods is that the magnitude of T is still left unconstrained, with the magnitude of T being tied to assumptions on how water loss to carbon gain is optimized. While the uWUE and Pérez-Priego methods tend to increase WUE giving a higher carbon gain to water loss, the resulting T/ET tends to be lower than the global consensus. However, care should be taken not to assume a method which results in a T/ET value close to the current estimates of $\approx 60\%$ constitutes an accurate method, as current global T data are still uncertain.

In addition to the unconstrained magnitudes, discrepancies of diurnal T/ET patterns

from the different flux partitioning methods further indicate a lack of theoretical and data constraints for diurnal water-carbon coupling, emphasizing the need for further studies and a better understanding of this aspect. Increased abundance and higher availability of concurrent sap flow and EC measurements allowing comparisons will help to improve flux partitioning methods. This is contingent on continued efforts to evaluate and reduce uncertainties connected with upscaling of tree sap flow measurements to ecosystem transpiration e.g. due to the omission of the understory. To facilitate corroborations with independent large scale transpiration constraints from isotopes, a next step is to upscale the ecosystem transpiration estimates from flux towers to the globe as was previously done with carbon and energy fluxes. This further opens doors of assessing cross-consistencies with process-based land surface model simulations and remote sensing based approaches, particularly with respect to the unexpectedly low sensitivity of T/ET spatial variation with climate and leaf area index across FLUXNET sites found here.

4.5 Data Sharing and Accessibility

Data that support the findings of this study are openly available from Zenodo <http://doi.org/10.5281/zenodo.1123456>. Furthermore, a tutorial of how to produce the transpiration estimates can be found in the associated repository at <https://github.com/jnelson18/ecosystem-transpiration>.

Acknowledgments

We acknowledge insightful discussions with Dario Papale and apologize for having a cappuccino after lunch. We further acknowledge Ulrich Weber for preparing the cappuccino. MG acknowledges funding by Swiss National Science Foundation project ICOS-CH Phase 2 20FI20_173691. L was supported by the Ministry of Education, Youth and Sports of the Czech Republic within the CzeCOS program, grant number LM2015061, and by SustES-Adaptation strategies for sustainable ecosystem services and food security under adverse environmental conditions (CZ.02.1.01/0.0/0.0/16_019/0000797). GW acknowledges support by the Austrian National Science Fund (FWF, project I03859) and the Province of South Tyrol (“Cycling of carbon and water in mountain ecosystems under changing climate and land use”). RP was supported by grants CGL2014-55883-JIN, RTI2018-095297-J-I00 (Spain) and by a Humboldt Research Fellowship for Experienced Researchers (Germany). This work used eddy covariance data acquired and shared by the FLUXNET community, including these networks: AmeriFlux, AfriFlux, AsiaFlux, CarboAfrica, CarboEuropeIP, CarboItaly, CarboMont, ChinaFlux, Fluxnet-Canada, GreenGrass, ICOS, KoFlux, LBA, NECC, OzFlux-TERN, TCOS-Siberia, and USCCC. The ERA-Interim reanalysis data are provided

by ECMWF and processed by LSCE. The FLUXNET eddy covariance data processing and harmonization was carried out by the European Fluxes Database Cluster, AmeriFlux Management Project, and Fluxdata project of FLUXNET, with the support of CDIAC and ICOS Ecosystem Thematic Center, and the OzFlux, ChinaFlux and AsiaFlux offices.

Chapter 5

Synthesis

This chapter first summarizes the key concepts from the preceding chapters which are referenced in this synthesis via an overview of how the research developed over time. Key results are then discussed in the context of the broader research and literature by answering the three research questions. Finally, the concluding summary outlines key conclusions as well as gives an outlook on future research directions.

5.1 Summary of key concepts and research development

While the overarching objective of the thesis was to produce an ET partitioning method for eddy covariance data, the lack of consistent measurements related to ecosystem water status, such as soil moisture or leaf water potential, necessitated an initial study to develop indicators which characterize diverse ecosystem responses to drought without requiring supplemental data not in the core eddy covariance datasets. Two data driven indicators were developed in Chapter 2 which were designed to capture information directly from the diurnal patterns of ecosystem fluxes which could be used to directly indicate ecosystem water limitations. The diurnal centroid of ET relative to incoming radiation (C_{LE}^* , see Section 2.2.2) measures the phase shift of ET, which shifts towards the morning under dry conditions possibly due to higher stomatal control, intra-plant limitations to water movement, and daily cycles of water redistribution. The diurnal water carbon index (DWCI, see Section 2.2.3) measures the coupling of diurnal water and carbon fluxes, which can decouple under dry conditions due to non-stomatal limitations of carbon assimilation which affect GPP but not ET (e.g. via inhibitions of biochemical reactions, RuBisCO activity, and/or mesophyll conductance). Another indicator of ecosystem dryness was introduced in Chapter 3, the conservative surface wetness index (CSWI, see Section 3.2.1), which indicates the amount of ET relative to the last rain event, and was designed to isolate periods when surfaces are likely to be dry.

These three indicators laid the ground work for development of the Transpiration Estimation Algorithm (TEA) described in Chapter 3, which trains a machine learning model from data filtered for dry periods (defined by the CSWI) to predict WUE and transpiration using DWCI, C_{LE}^* , and meteorological variables as predictors. Initial assessment of the key assumptions in TEA, such as the assumption that $T \approx ET$ during some periods, was done using model output from three terrestrial biosphere models (TBM) used

as synthetic eddy covariance datasets in a controlled study where the underlying WUE and transpiration were known. The synthetic data study demonstrated that TEA could accurately reproduce spatial and temporal patterns of WUE and transpiration, but the magnitude of transpiration was sensitive to a key hyperparameter, i.e. the prediction percentile, and a prediction percentile of 75 was chosen based on the best overall performance across the synthetic datasets.

The TEA method, along with two other eddy covariance based ET partitioning methods (uWUE and Pérez-Priego), were then applied to the entire FLUXNET dataset. The three partitioning methods were shown to be highly correlated at the daily scale, and all three showed high correlation to independent sap flow based estimates of canopy transpiration. Furthermore, the transpiration estimates from eddy covariance showed expected responses of T/ET and seasonality, increases of transpiration during dry-down periods, and a decrease in WUE with increasing VPD. Finally, site estimates of transpiration from over 200 FLUXNET sites were paired with climate and remote sensing data to explore the spatial variability of transpiration and T/ET.

How can information in the core eddy covariance datasets be further exploited to describe the complex plant water relationships from heterogeneous communities?

Complex ecophysiological responses to water stress which are difficult to describe with generalized models can be captured using diurnal indicators of hydraulic and non-stomatal limitations (e.g. C_{LE}^* and DWCI). These indicators can inform data driven methods to estimate WUE and transpiration (such as TEA), as well as help diagnose the occurrence of water stress and diagnose shortcomings in stomatal conductance models.

Given the limited amount of independent ecosystem transpiration data concurrent with eddy covariance measurements, how can the transpiration estimates be validated?

Evaluation strategies which characterize uncertainties related to theoretical assumptions, such as the model studies in Chapter 3, not only improve the accuracy of transpiration estimates from TEA, but also identified that the key source of uncertainty in the magnitude from eddy covariance based transpiration estimates were those on carbon gain to water loss optimality, which is in contrast to previous suppositions.

What new insights on ecohydrological and water use strategies across major terrestrial biomes can be gained from the transpiration estimates derived from FLUXNET?

The greater spatial context afforded by the transpiration estimates from TEA applied over FLUXNET indicated that the key spatial drivers of T/ET are properties related to water access and use, such as soil properties and drought responses, rather than the simple presence or absence of vegetation (e.g. mean site leaf area index) as is currently seen in land surface models.

5.2 Key results and discussion

5.2.1 How can information in the core eddy covariance datasets be further exploited to describe the complex plant water relationships from heterogeneous communities?

The complex ecosystem responses to stress are difficult to capture with generalized models (Matheny et al., 2014; Renner et al., 2021; De Kauwe et al., 2015), which highlights the need for alternative methods to capture plant water stress information. The aim of developing and using the metrics introduced in Chapter 2 was to use them in TEA to capture diverse drought responses in a data driven way, with the metrics used as features to predict WUE within TEA (Section 3.2.2). However, the utility of the metrics has been shown to extend beyond just being predictors in TEA, as they can also help identify and understand integrated physiological responses to drought, such as hydraulic and non-stomatal limitations. A core advantage of the diurnal indicators is that they summarize high frequency patterns in the data, patterns which are lost in a simple daily mean or sum. This section identifies some examples of how using these metrics, as well as the information from transpiration estimates from TEA, can inform and improve our understanding of ecosystem functioning.

The relationship between plant water use and the the need to avoid hydraulic failure of vascular tissues is complex, however C_{LE}^* may help identify the effects of hydraulic limitation. As ecosystems dry out and demand for water starts to outpace supply, smaller water pools such as in the root zone or plant stems show pronounced effects of daily filling and emptying (Goldstein et al., 1998; Couvreur et al., 2014). Differing plant strate-

gies start to emerge under these drought conditions such as the isohydricity spectrum (Martínez-Vilalta et al., 2014), i.e. the strategic trade-off during drought between higher stomatal control to reduce the risk of xylem embolism or risking high water potential gradients to maintain high GPP. Konings and Gentine (2016) used satellite data as an estimate of isohydricity to show a clear response with plant height, with tall trees being more isohydric, likely due to the long hydraulic pathways being prone to embolism and cavitation. C_{LE}^* was also associated with forested ecosystems, and showed clear patterns of morning shifts in tree ecosystems which experience dry conditions, possibly due to a more isohydric behavior. For example, Puéchabon forest showed intense morning shifts during the 2003 drought compared to a normal year (Figure 2.3). Trees also utilize stem water, measured as hydraulic capacitance, to maintain transpiration and possibly prevent cavitation. Salomón et al. (2017) found stem hydraulic capacitance at Puéchabon decreased 60% over the dry season, while the contribution of stored water to transpiration was estimated to increase from 2 to 5%, demonstrating the dynamic adaptation the ecosystem has developed to cope with drought. Puéchabon also has extensive sap flow measurements making it an excellent test site to validate transpiration estimates, and though all the partitioning methods analysed in Chapter 4 performed well at Puéchabon, TEA showed the highest correlation and lowest RMSE when compared to canopy sap flow (R^2 ranged between 0.860-0.874 and RMSE between 0.32-0.42 for all the methods). The high correlation demonstrates the advantages of a data driven estimate which integrates a metric of hydraulic limitations, as process based models are often unable to reproduce these morning shifts associated with physiological responses to moisture limitations (Renner et al., 2019).

Detection of non-stomatal limitations via DWCI, as well as the differences seen in the eddy covariance based partitioning methods which relates to assumptions on maximizing carbon gain to water loss, underline the limitations of stomatal optimality theory. The experiments in Drake et al. (2018) showed non-optimal stomatal response in the extreme, where tree photosynthesis nearly completely halted during extremely high temperatures ($> 43^\circ\text{C}$) while transpiration persisted. Other experimental studies have reported similar behaviors, with sustained transpiration reducing leaf temperatures during heat events at the expense of carbon uptake (Slot et al., 2016; Urban et al., 2017a; Urban et al., 2017b). While De Kauwe et al. (2019) did not find significant evidence of decoupling across 14 eddy covariance sites, the analysis looked at correlations of day-time integrated GPP and LE, while the effect reported in Drake et al. (2018) showed no

decrease in morning, rather only in afternoon, hours. Figure 5.1 shows that DWCI does indeed decrease at high temperatures indicating heat related carbon-water decoupling, particularly when transpiration (as estimated by TEA) is reduced. Apart from just high heat, drought interactions have been implicated in causing non-stomatal limitations, possibly from reduction in carboxylation capacity and thus CO_2 fixation rates (Zhou et al., 2013), generation of reactive oxygen species (Lawlor and Tezara, 2008), or declines in mesophyll conductance which inhibits CO_2 movement within the leaf (Flexas et al., 2012). DWCI was also associated with dry conditions, and less associated with an increase in WUE over theoretical expectations than C_{LE}^* (Figure 2.7), highlighting that non-stomatal limitations are likely to be less photosynthetically efficient. These non-stomatal effects from drought have been shown to lead to poor performance of stomatal conductance models (Novick et al., 2016b; Zhou et al., 2013; Reichstein et al., 2002), further highlighting the need for data driven indicators and estimates of transpiration which do not make the assumption that stomatal conductance and carbon assimilation are coupled.

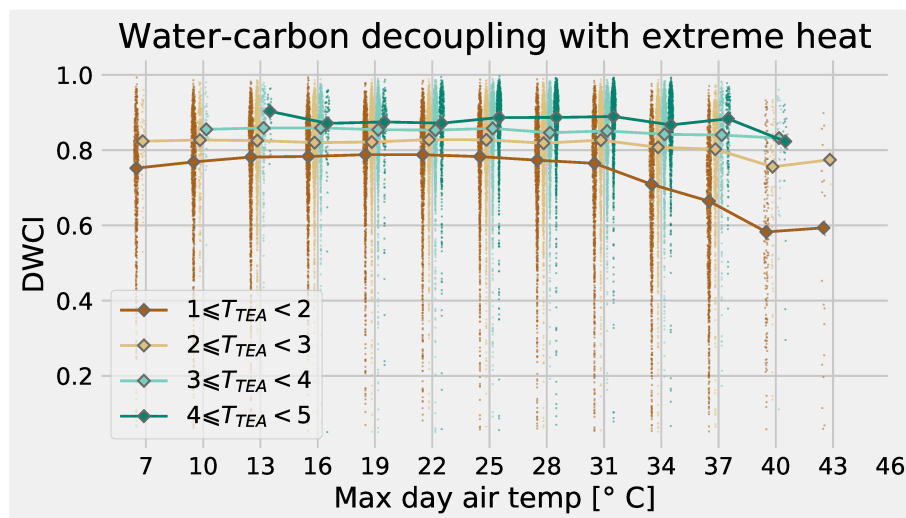


Figure 5.1 Relationship with Diurnal Water Carbon Index (DWCI) and max daily temperature. Diamond markers indicate median DWCI within the temperature bin. Reduction in DWCI is seen at high temperatures when transpiration as estimated by TEA (T_{TEA} , $mm\ d^{-1}$) is low, indicating water limitations. Data was filtered for high quality and a minimum daily mean GPP of $1\ \mu mol\ CO_2\ m^{-2}\ s^{-1}$.

Whole ecosystem responses are very different compared to individuals due to divergent plant strategies, such as the different responses of forest and grasslands, which further complicates generalized attempts to characterize them. As seen in Figure 2.6,

both C_{LE}^* and DWCI are related to periods of high net radiation and low latent energy, periods indicative of water limitation, however, the two indicators showed divergent drought responses between tree and grass dominated systems (Figure 2.5). A similar result was found in an analysis of forest and grassland sites during the 2018 drought in Switzerland, where Gharun et al. (2020) showed a decoupling of water and carbon in grass sites not seen in forested sites. Divergent responses can even be seen from plants within the same genus, as Zhou et al. (2016b) showed differences in acclimation to drought between *Eucalyptus* species, with species native to dry habitats showing less stomatal and biochemical limitations than species from wet habitats. These effects need to be accounted for in land surface models, as De Kauwe et al. (2015) showed that ignoring the higher ability of ecosystems adapted to dry conditions leads to an over estimation of drought effects on carbon and water fluxes. Because TEA uses a data driven approach, and learns from each ecosystem individually, the resulting transpiration estimates should be able to capture a wider variety of drought responses. While TEA was able to capture the WUE responses (Figure 3.5) from the model output used in the initial validation of Chapter 3, the models are not likely to have the same types of phase lags or decoupling seen in real EC data, and therefore the exact importance of these indicators in predicting WUE can be difficult to assess. However, in contrast to the data driven approach of TEA, the two other transpiration estimating methods used in Chapter 4 (uWUE and Perez-Priego) predominantly use time and VPD to control diurnal variability, and indeed the resulting diurnal behaviors of partitioned fluxes are quite different (Figure 4.6). Alternatively, TEA feeds sub-daily information directly into the algorithm via the indicators, and lets the data speak for itself, giving a distinct view over process based approaches which have been shown to not capture sub-daily patterns (Matheny et al., 2014; Renner et al., 2021). This strategy might be useful in other fields, with the diurnal metrics being used to inform and evaluate other empirical models, as demonstrated in the Research Perspective below, where the accuracy of transpiration estimates from SIF data (Shan et al., 2019) was associated with carbon-water decoupling as indicated by lower DWCI.

Research Perspective: sub-daily indicators of water stress and transpiration estimates from SIF

Sun-induced fluorescence is seen as a promising near-surface and remote sensing tool to monitor ecosystem processes related to photosynthesis (Porcar-Castell et al., 2014), and in recent years attempts have been made to also use SIF as a link to estimate transpiration. A method to predict transpiration from SIF would provide not only an independent data source for quantifying ecosystem transpiration, but also lead to potential global transpiration monitoring via remote sensing estimates of SIF (Pagán et al., 2019). Here we summarize two studies that tested a SIF based method for estimating transpiration at three different eddy covariance sites which demonstrated good agreement between T_{SIF} and T_{TEA} , as well as explore how using DWCI could help diagnose methodological issues in empirical SIF based models.

Experimental method: Shan et al. (2019) developed an empirical relationship between SIF and canopy conductance calculated from eddy covariance data, and the SIF estimated canopy conductance was then used with the Penman-Montieth equation to estimate transpiration (T_{SIF}). T_{SIF} was then compared to eddy covariance data during the growing season at a mixed temperate forest (Harvard Forest) and a seasonally dry savanna (Majadas de Tiétar). In a follow up study, Shan et al. (2021) again compared the results of an improved version of T_{SIF} to eddy covariance based ET both at Harvard Forest and an irrigated maize site (Shangqiu), and also compared T_{SIF} to transpiration estimates from both TEA and the Pérez-Priego methods.

High agreement with TEA: The improved version of T_{SIF} from Shan et al. (2021) showed a high correlation with ET from eddy covariance at Harvard Forest ($R^2 = 0.70$) and an even higher correlation at Shangqiu ($R^2 = 0.78$). Comparing T_{SIF} to T_{TEA} directly showed an improved correlation for Harvard Forest ($R^2 = 0.76$) with no improvement at Shangqiu ($R^2 = 0.78$) (Figure S12 in Shan et al. (2021)), and found a similar magnitude between T_{SIF} and T_{TEA} (T_{TEA}/T_{SIF} was 0.897 and 1.035 for Harvard Forest and Shangqiu respectively). A similar comparison between T_{SIF} and $T_{Perez-Priego}$ showed a slight improvement ($R^2 = 0.73$) and reduced performance ($R^2 = 0.39$) compared to ET for Harvard Forest and Shangqiu respectively, with much lower transpira-

tion estimates ($T_{Perez-Priego}/T_{SIF}$ was 0.638 and 0.419 for Harvard Forest and Shangqui respectively).

Decoupling associated with poor SIF model performance: While the earlier Shan et al. (2019) study did not compare directly to T_{TEA} , the inclusion of the seasonally dry Majadas site did offer an opportunity look at the impact of water stress on the the SIF-transpiration relationship. The correlation between T_{SIF} and ET from eddy covariance in the old model was lower than the improve model for Harvard Forest ($R^2 = 0.57$), and lower still at Majadas ($R^2 = 0.13$). The authors suggested that the poor performance could be the result of dry conditions at the savanna site during the summer season causing transpiration and carbon uptake to decouple. Figure 5.2 shows a significantly different flux weighted mean DWCI (Mann-Whitney p-value < 0.01) between Harvard Forest and Majadas, being 0.78 and 0.69 respectively, and also a significantly higher DWCI at Shangqui (0.85) from the later study, which as an irrigated crop, likely had the least amount of water stress. Thought only three sites, the results suggest that the performance of T_{SIF} is related to diurnal decoupling of water and carbon fluxes, possibly due to non-stomatal limitations from water limitation, demonstrating the ability the sub-daily indicators to diagnose physiological responses which are not captured by models relying on assumptions of coupling between stomatal conductance and photosynthesis.

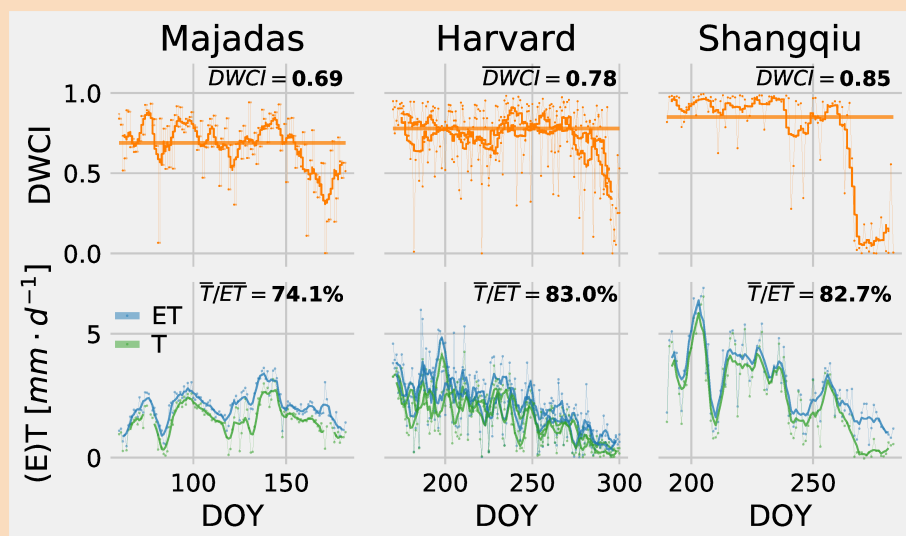


Figure 5.2 Diurnal Water Carbon Index (DWCI), transpiration (from TEA) and ET during the growing season at a seasonally dry savanna (Majadas de Tiétar), a mixed temperate forest (Harvard), and an irrigated maize field (Shangqui).

5.2.2 Given the limited amount of independent ecosystem transpiration data concurrent with eddy covariance measurements, how can the transpiration estimates be validated?

Assessment of the sensitivity of core methodological assumptions from the model studies in Chapter 3 was key in evaluating the strengths and weaknesses TEA, and furthermore identified that the degree to which GPP should be maximized relative to transpiration causes most of the uncertainty in the magnitude of transpiration rather than the assumption that $T \approx ET$ as was commonly thought. Previous methods have primarily used the high correlation between T/ET and vegetation indexes such as EVI (Zhou et al., 2016a) or LAI (Li et al., 2019; Scott and Biederman, 2017) as a verification of accurate transpiration estimates. Other validation exercises rely on comparisons with independent estimates from one or two sites (Perez-Priego et al., 2018; Scanlon et al., 2019; Zhou et al., 2018). While these exercises are necessary to provide independent validation, they lack the spatial and temporal scope to properly characterize methodological assumptions and sensitivities across many different ecosystems. In contrast, the controlled experiments from Chapter 3 using model output to evaluate TEA allowed for implicit assumptions to be tested and is in contrast to how other methods approached validation. While TEA was shown to over estimate models with more abiotic evaporation, and thus are more likely to violate the $T \approx ET$ assumption in TEA, the model results show that within a single model “reality,” TEA was able to accurately differentiate T/ET across sites, and biases caused by higher model “reality” abiotic evaporation could be compensated by the prediction percentile which is a key hyperparameter in TEA that controls the resulting magnitude of transpiration. The ability of the prediction percentile to compensate for increased abiotic evaporation, which at first glance should violate the $T \approx ET$ assumption in TEA, without deteriorating the ability to capture temporal patterns is due to the fact that evaporation is likely not constant in time, therefore some periods where $T \approx ET$ are likely to exist in the high frequency data which TEA is able to exploit. In other words, the amount of abiotic evaporation is not so much the issue, rather the frequency that abiotic evaporation occurs in the training dataset (i.e. after filtering for wet periods), which seems to be much more consistent across sites. While discussion of hyperparameters may seem rather technical for a synthesis, the selection of a lower prediction percentile based on how TEA performed in the mod-

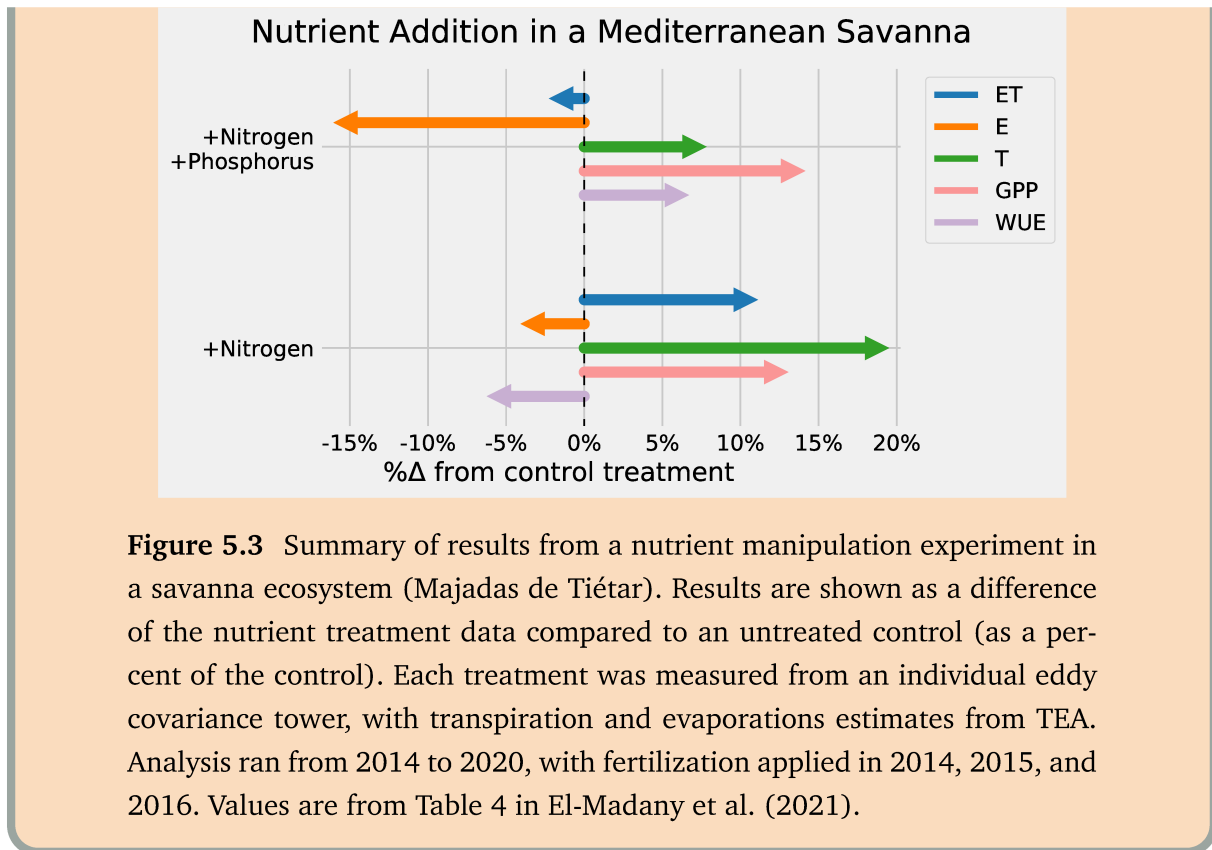
eling study, rather than selecting a high prediction percentile which would correspond to maximizing carbon gain to water loss, directly resulted in relatively higher T/ET ratios from TEA, being around 77% across FLUXNET compared to 45 and 52% for the Pérez-Priego and uWUE methods respectively, of which both methods tried to limit the impacts of the $T \approx ET$ assumption by instead assuming plants maximize carbon gain to water loss. However, the low T/ET values seen across FLUXNET sites from the Pérez-Priego and uWUE methods, which is a result of the optimality assumptions, would be in contrast to the general consensus that transpiration is the dominant component of ET, especially given that FLUXNET sites tend to be highly vegetated and undisturbed and may have higher T/ET than the global average. Subsequent work has also corroborated the higher transpiration estimates from TEA. Scott et al. (2020) did a comparison of the uWUE, TEA, and Li (Li et al., 2019) methods at two dry sites and showed that the seasonal pattern of T/ET from the TEA and Li methods were consistent with previous measurements, both in magnitude and seasonal cycle, with estimates from the uWUE method being too low. Ma et al. (2020) also found that adjusting the hyperparameters from the uWUE method to relax the optimality assumption was more accurate in an oak savanna, with the resulting hyperparameter being similar to what was found to be most consistent with TEA across all FLUXNET sites (Appendix C Figure S2). Shan et al. (2021) also found a more similar magnitude between T_{SIF} and T_{TEA} , while the Pérez-Priego method was much lower. These results indicate that the optimality assumption tends to overestimate WUE, resulting in an underestimation of transpiration, further highlighting the importance of data driven and adaptive methodologies such as TEA which make few assumptions on physiological functioning.

Going forward, the broad applicability of TEA will allow the eddy covariance based transpiration estimates to act as a baseline for future methodological intercomparisons. Because TEA, which has already been well characterized as far as strengths and limitations, can be applied the same way at forest, wetland, or boreal sites, future independent methods for estimating ecosystem transpiration at eddy covariance sites can then be compared to the TEA estimates thus immediately giving a broader context to single site studies. Furthermore, continued efforts to aggregate independent estimates of transpiration such as SAPFLUXNET (Poyatos et al., 2019), as well as calls for similar efforts to aggregate methods such as above and below canopy EC (Paul-Limoges et al., 2020), and isotopic (Penna et al., 2018) methods, along with further processing of eddy covariance data (Papale, 2020), will allow for broad, multi-site, multi-method

meta analyses of ecosystem transpiration within the next few years. Such an analysis will hopefully greatly narrow the uncertainty of the magnitude of transpiration. In line with this effort, the code for the TEA algorithm is not only published (Nelson, 2020c), but also in depth installation instructions and tutorials on how to apply all the methods used in Chapter 4 are freely available to facilitate utilization by the broader eddy covariance community (Nelson, 2020b). In the meantime, transpiration estimates from TEA are already shedding light on ecosystem responses to climate and environmental drivers (including nutrient availability), as seen in the Research Highlight below.

Research Highlight: transpiration and WUE dependence on N:P stoichiometry

El-Madany et al. (2021), via a nutrient manipulation experiment in a Mediterranean savanna ecosystem (Majadas de Tiétar, FLUXNET codes ES-LMa, ES-LM1, and ES-LM2), showed that both nitrogen and nitrogen+phosphorus addition treatments increased GPP compared to the untreated control plot. However, the nitrogen treatment showed a comparatively higher increase in transpiration (estimated using TEA) resulting in an overall decrease in WUE (compared to the control treatment). In contrast, the nitrogen+phosphorus treatment showed a marginal increase in transpiration and a significant decrease in abiotic E, resulting in both an increase of WUE and a slight decrease in overall ET. El-Madany et al. (2021) concluded that while both treatments increased biomass, the nitrogen treatment, which resulted in an increase in the N:P ratio and potential phosphorus limitations, resulted in an increase in transpiration to extract more phosphorus from the soil. Furthermore, phosphorus has been shown to cause a decrease in stomatal conductance and increase WUE (Maire et al., 2015), an effect that was seen both in surface conductance estimates derived from T_{TEA} and from $\delta^{13}C$. The increases in WUE were accompanied by decreases in abiotic evaporation possibly due to increased LAI, thus shading more soil surfaces, leading to opposing responses in the biotic and abiotic water fluxes and highlighting the importance of ET partitioning for ecohydrological understanding. These results are summarized in Figure 5.3.



5.2.3 What new insights on ecohydrological and water use strategies across major terrestrial biomes can be gained from the transpiration estimates derived from FLUXNET?

Eddy covariance base ET partitioning can provide spatially explicit intermediary ecosystem scale estimates of transpiration with higher measurement densities than currently available. These transpiration estimates are able to connect not only to physiological data, such as leaf measurements or sap flow, but also to remote sensing and earth system models with spatial context. TEA was able to accurately capture the between site variability in T/ET from the model experiments in Chapter 3 for three model structures despite very different abiotic evaporation magnitudes between the validation models (see Figure 3.6). The site level estimates of transpiration from TEA applied across FLUXNET used in section 4.3.6 (Figures 4.7 and 4.8) consisted of 204 sites after quality control (across site mean of $T/ET = 65 \pm 11$), more than double the historical literature data gathered by Schlesinger and Jasechko (2014) (81 studies, global $T/ET = 61 \pm 15\%$), triple those used to derive an LAI based T/ET estimate in Wei et al. (2017) (global 64

studies, $T/ET = 57 \pm 7\%$), and six-fold more than the those used to constrain land surface model output in Lian et al. (2018) (global 33 studies, $T/ET = 62 \pm 6\%$). Furthermore, underlying the 204 sites are 818 complete site-years of data, whereas many literature site estimates correspond to one year or less. More than 900 active and historical EC sites are estimated to exist, providing the potential for high representativeness of global ecosystem transpiration (Chu et al., 2017).

Models of transpiration need to take into account the impacts of soil available water and responses to drought, rather than relying on vegetation to describe T/ET . Because of the sparsity of current field estimates, previous work on spatial variability of T/ET has relied on modeled relationships. LAI is often assumed to be a primary driver of T/ET , where the presence of vegetation results in more shading of soil surfaces and utilization of deeper soil moisture via roots. For example, both Lian et al. (2018) and Berg and Sheffield (2019) identified LAI as the primary driver of T/ET in land surface model output. An exploration of the key spatial drivers of T/ET (i.e. driver of the variability of the mean T/ET across sites) based on both the TEA and uWUE methods suggests that mean vegetation indexes were not the sole drivers of T/ET , rather crop or grassland designation, soil properties, and a remote sensing based dryness index (Figures 4.9 and 5.3), suggesting that a more holistic approach is needed to estimate T/ET which incorporates processes affecting plant access to soil water reserves (e.g. soil texture and rooting depth) and adaptations to drought (see Section 5.2.1). An alternate paradigm put forward by Good et al. (2017), suggests that ecosystems with a maximum T/ET should be where evaporative demand is near or slightly exceeds precipitation input because dry ecosystems result in patchy vegetation and more soil evaporation whereas wet ecosystems with large canopy surfaces will have high evaporation of intercepted water. The “mesic maximum” theory from Good et al. (2017) goes on to suggest that global transpiration and rooting depth are optimized to use available precipitation inputs. In this way, the idea that LAI causes high T/ET may need to be reversed, rather that plants will utilize water resources where they are available. Scott et al. (2020) provides a nice case study, where two dryland ecosystems (an upland grass site and a riparian woodland) with nearly identical climate and with relatively low LAI ($1 \text{ m}^2 \cdot \text{m}^{-2}$ and $2 \text{ m}^2 \cdot \text{m}^{-2}$, respectively) show not only very different T/ET ratios (46% and 74% for the grassland and woodland respectively), but the woodland also has an annual ET more than twice that of the annual precipitation. So in effect, much of the water transpired at the woodland comes from the surrounding area via lateral flow, a process which has

been implicated as lacking in land surface models (Maxwell and Condon, 2016). Effects such as these are likely to play an even larger role as increases in irrigation and irrigation efficiency produce more and more green areas with minimal evaporation loss (Wada et al., 2017), indeed crop designation was the most important variable predicting spatial T/ET across FLUXNET (Figure 4.9). Overall, future work on transpiration and T/ET variability should focus less on the presence of absence of vegetation, but rather factors controlling plant available water such as rooting depth, soil properties, lateral flow, and ecosystem drought response. Potential effects of these controlling factors on constraining global T/ET estimates is explored in the Research Outlook below.

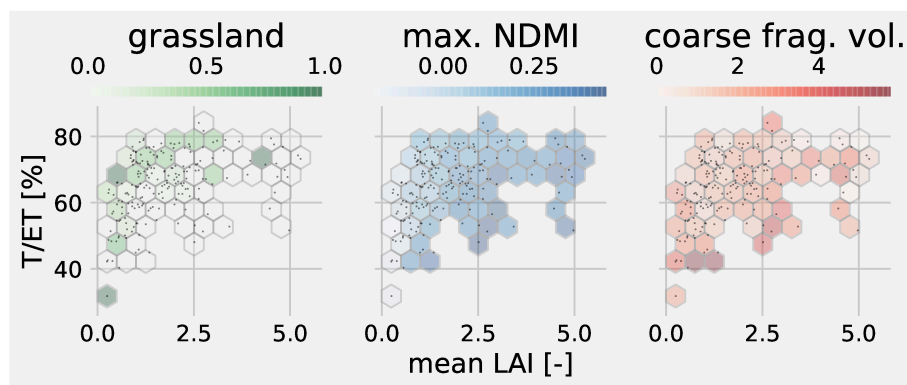


Figure 5.4 The relationship between T/ET from FLUXNET (via TEA) and mean LAI derived from MODIS. Colors indicate the patterns of grassland (fractions of sites within a bin designated as grassland), normalized difference moisture index (NDMI, from LANDSAT), and soil coarse fragment volume (from SOILGRIDS). See Section 4.2.5 for complete data description.

Research Outlook: constraining land surface models with site estimates of T/ET

It is generally established that the model experiments from land surface models show an under estimation of T/ET, and the dominant driver controlling T/ET for all models is LAI (Lian et al., 2018; Berg and Sheffield, 2019). Though the bias in T/ET could be the result of biases in LAI, most models are also over estimating LAI compared to remote sensing based estimates, which if corrected would result in an even lower T/ET ratio. Here we explore how higher density site estimates of T/ET from TEA can shed new light on constraining T/ET in land surface models.

Experimental method: Lian et al. (2018) used site estimates from 33 sites as an emergent constraint on global estimated T/ET from CMIP5 model simulations to produce a global T/ET estimate of $62 \pm 6\%$, which is more in line with previously published estimates. The emergent constraint used the high correlation between model global T/ET and the mean T/ET from the $1^\circ \times 1^\circ$ grid cell containing the site estimates.

TEA shows good consistency with site estimates: Using 204 FLUXNET sites with transpiration estimates from TEA shows a relatively consistent distribution of site T/ET compared to the site measurements from Lian et al. (2018), with nearly identical mean values (65 ± 11 and 64 ± 12 for TEA and Lian respectively) and similar magnitudes at spatially coincident sites (Figure 5.4a and 5.4b).

Representativeness of site samples: Figure 5.4c shows that the variability between FLUXNET sites less than 0.5° away from each other (i.e. those that could be in the same $1^\circ \times 1^\circ$ grid cell) is just as high as the variability across all sites, indicating that T/ET changes drastically over relatively short distances. One critique of matching site estimates with global data is that research sites tend to be more highly vegetated and productive, potentially resulting in an over estimated global T/ET due to selection bias (Schimel et al., 2015). However, as discussed in Section 5.2.3, vegetation is likely not the dominant factor controlling T/ET, and key variables such as lateral flow and rooting depth should

be taken into account when assessing site representativeness. These key variables may also be more heterogeneous than climate and vegetation properties and therefore more difficult to characterize across coarse spatial scales. Indeed, taking the mean T/ET from all countries with at least five sites ($n=10$ countries) resulted in a range of mean T/ET values between 61-69%, with countries ranging from Australia to Finland (both with mean T/ET values of $\sim 62\%$). The implication of these results, as well as those discussed in the previous sections, suggests that a more fundamental examination of the controls on transpiration is warranted.

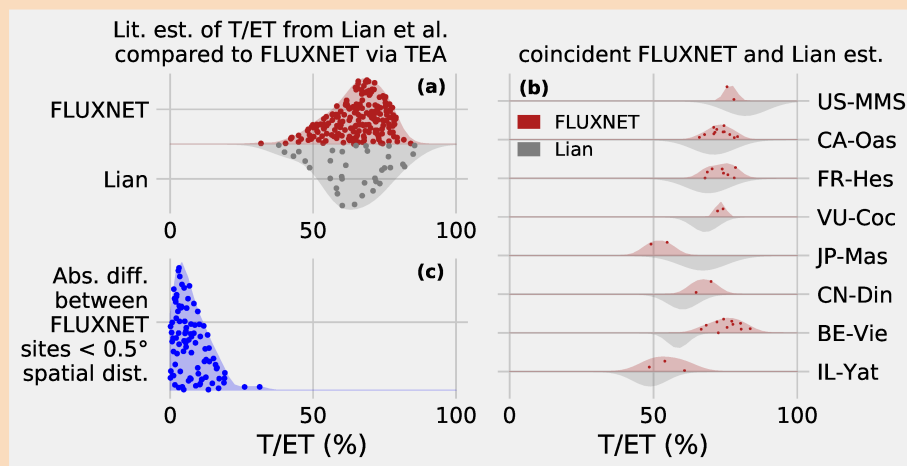


Figure 5.5 Comparison between T/ET estimates from literature used in Lian et al. (2018) and T/ET from FLUXNET using transpiration estimates from TEA. FLUXNET values were estimated as the mean of T/ET across available years. **(a)** Compares the distribution of T/ET from 33 Lian values compared to 204 values from FLUXNET. **(b)** Comparison of spatially coincident points. As values are not always coincident in time, all available FLUXNET years are shown as points, with distributions showing temporal variability. Distributions from Lian values represent reported measurement uncertainty. **(c)** As Lian et al. (2018) used site estimates to constrain models run on $1^\circ \times 1^\circ$ spatial resolution, FLUXNET estimates are dense enough to compare the variability among sites less than 0.5° away, demonstrating that within grid cell variability is as large as global variability.

5.2.4 Outlook

Here we show that data driven estimates of transpiration provide the much needed spatio-temporally density needed to gain a better understanding of ecohydrological function and to bridge the current gap between leaf level understanding of water and carbon fluxes and global processes. Going forward, transpiration from eddy covariance can be paired with gridded remote sensing and meteorological data and up-scaled, such as the FLUXCOM methodology (Jung et al., 2020), providing globally available partitioned water fluxes from eddy covariance. These new products will allow for a more in depth analysis of both hydrology and global carbon cycles. Figure 5.6 shows an initial attempt at up-scaling transpiration, which while having a global T/ET consistent with the current consensus, has not yet been rigorously verified. However, an analysis ready product should be available in the near future. TEA, as well as other ET partitioning methods, should continue to be developed, improved, and validated. Improvements such as diagnosing better predictors of WUE to be used within TEA, as well as corrections for known biases in eddy covariance data (Mammarella et al., 2009), will provide high quality estimates of ecosystem scale transpiration, which can then be validated against new and existing independent measurements (Poyatos et al., 2019). These broad scale ecosystem transpiration methods can then inform both understanding of ecohydrology and plant physiology as well as improve the next generation of remote sensing and process based global estimates of transpiration.

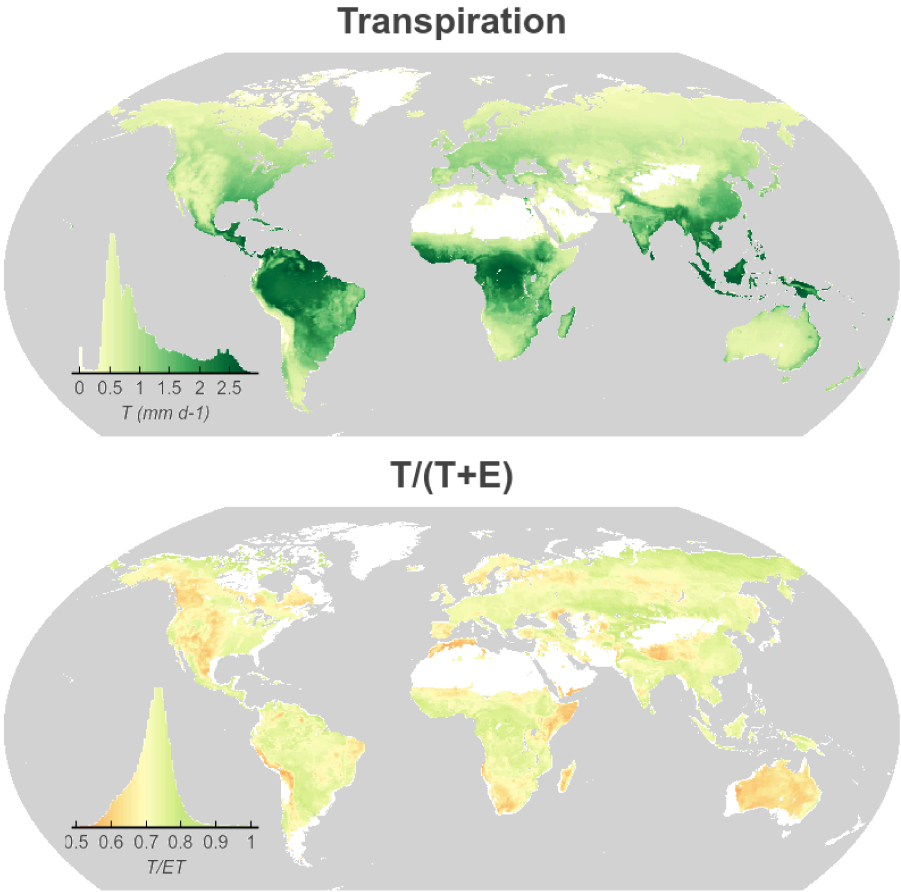


Figure 5.6 Initial attempts at transpiration upscaling using the FLUXCOM methodology.

References

- Ainsworth E. A. and Rogers A. (Mar. 2007). The Response of Photosynthesis and Stomatal Conductance to Rising [CO₂]: Mechanisms and Environmental Interactions: Photosynthesis and Stomatal Conductance Responses to Rising [CO₂]. en. *Plant, Cell & Environment*, 30, 258–270.
- Allen C. D., Breshears D. D., and McDowell N. G. (Aug. 2015). On Underestimation of Global Vulnerability to Tree Mortality and Forest Die-off from Hotter Drought in the Anthropocene. en. *Ecosphere*, 6, art129.
- Anderson R. G., Zhang X., and Skaggs T. H. (2017). Measurement and Partitioning of Evapotranspiration for Application to Vadose Zone Studies. en. *Vadose Zone Journal*, 16.
- Baldocchi D. (2008). 'Breathing' of the Terrestrial Biosphere: Lessons Learned from a Global Network of Carbon Dioxide Flux Measurement Systems. en. *Australian Journal of Botany*, 56, 1.
- Baldocchi D. D. (Sept. 2019). How Eddy Covariance Flux Measurements Have Contributed to Our Understanding of *Global Change Biology*. en. *Global Change Biology*,
- Baldocchi D. D. (Jan. 2020). How Eddy Covariance Flux Measurements Have Contributed to Our Understanding of *Global Change Biology*. en. *Global Change Biology*, 26, 242–260.
- Baldocchi D. and Penuelas J. (Apr. 2019). The Physics and Ecology of Mining Carbon Dioxide from the Atmosphere by Ecosystems. en. *Global Change Biology*, 25, 1191–1197.
- Baldocchi D., Valentini R., Running S., Oechel W., and Dahlman R. (June 1996). Strategies for Measuring and Modelling Carbon Dioxide and Water Vapour Fluxes over Terrestrial Ecosystems. en. *Global Change Biology*, 2, 159–168.

- Ball J. T., Woodrow I. E., and Berry J. A. (1987). A Model Predicting Stomatal Conductance and Its Contribution to the Control of Photosynthesis under Different Environmental Conditions. en. In: *Progress in Photosynthesis Research*. Biggins J. (ed.). Dordrecht: Springer Netherlands, pp. 221–224.
- Barr A., Morgenstern K., Black T., McCaughey J., and Nesic Z. (Nov. 2006). Surface Energy Balance Closure by the Eddy-Covariance Method above Three Boreal Forest Stands and Implications for the Measurement of the CO₂ Flux. en. *Agricultural and Forest Meteorology*, 140, 322–337.
- Beer C., Ciais P., Reichstein M., Baldocchi D., Law B. E., Papale D., Soussana J.-F., Ammann C., Buchmann N., Frank D., Gianelle D., Janssens I. A., Knohl A., Köstner B., Moors E., Rouspard O., Verbeeck H., Vesala T., Williams C. A., and Wohlfahrt G. (June 2009). Temporal and Among-Site Variability of Inherent Water Use Efficiency at the Ecosystem Level: VARIABILITY OF INHERENT WUE. en. *Global Biogeochemical Cycles*, 23, n/a–n/a.
- Berling D. J., Osborne C. P., and Chaloner W. G. (Mar. 2001). Evolution of Leaf-Form in Land Plants Linked to Atmospheric CO₂ Decline in the Late Palaeozoic Era. en. *Nature*, 410, 352–354.
- Berg A. and Sheffield J. (May 2019). Evapotranspiration Partitioning in CMIP5 Models: Uncertainties and Future Projections. en. *Journal of Climate*, 32, 2653–2671.
- Berkelhammer M., Noone D. C., Wong T. E., Burns S. P., Knowles J. F., Kaushik A., Blanken P. D., and Williams M. W. (June 2016). Convergent Approaches to Determine an Ecosystem's Transpiration Fraction: TRANSPIRATION FRACTION OF TWO FORESTS. en. *Global Biogeochemical Cycles*, 30, 933–951.
- Bernacchi C. J. and VanLoocke A. (Apr. 2015). Terrestrial Ecosystems in a Changing Environment: A Dominant Role for Water. en. *Annual Review of Plant Biology*, 66, 599–622.
- Berry J. A., Beerling D. J., and Franks P. J. (June 2010). Stomata: Key Players in the Earth System, Past and Present. en. *Current Opinion in Plant Biology*, 13, 232–239.
- Besnard S., Carvalhais N., Arain M. A., Black A., Brede B., Buchmann N., Chen J., Clevers J. G. P. W., Dutrieux L. P., Gans F., Herold M., Jung M., Kosugi Y., Knohl A., Law B. E., Paul-Limoges E., Lohila A., Merbold L., Rouspard O., Valentini R., Wolf S., Zhang X., and Reichstein M. (Feb. 2019). Memory Effects of Climate and Vegetation Affecting Net Ecosystem CO₂ Fluxes in Global Forests. en. *PLoS ONE*, 14. Hui D. (ed.), e0211510.

- Beyer M., Kühnhammer K., and Dubbert M. (Sept. 2020). In Situ Measurements of Soil and Plant Water Isotopes: A Review of Approaches, Practical Considerations and a Vision for the Future. en. *Hydrology and Earth System Sciences*, 24, 4413–4440.
- Blanken P. D., Black T. A., Yang P. C., Neumann H. H., Nesic Z., Staebler R., den Hartog G., Novak M. D., and Lee X. (Dec. 1997). Energy Balance and Canopy Conductance of a Boreal Aspen Forest: Partitioning Overstory and Understory Components. en. *Journal of Geophysical Research: Atmospheres*, 102, 28915–28927.
- Boese S., Jung M., Carvalhais N., and Reichstein M. (Jan. 2017). The Importance of Radiation for Semi-Empirical Water-Use Efficiency Models. en. *Biogeosciences Discussions*, 1–22.
- Bogardi J. J., Fekete B. M., and Vörösmarty C. J. (Dec. 2013). Planetary Boundaries Revisited: A View through the ‘Water Lens’. en. *Current Opinion in Environmental Sustainability*, 5, 581–589.
- Bonan G. B., Lawrence P. J., Oleson K. W., Levis S., Jung M., Reichstein M., Lawrence D. M., and Swenson S. C. (May 2011). Improving Canopy Processes in the Community Land Model Version 4 (CLM4) Using Global Flux Fields Empirically Inferred from FLUXNET Data. en. *Journal of Geophysical Research*, 116.
- Böttcher K., Markkanen T., Thum T., Aalto T., Aurela M., Reick C., Kolari P., Arslan A., and Pulliainen J. (July 2016). Evaluating Biosphere Model Estimates of the Start of the Vegetation Active Season in Boreal Forests by Satellite Observations. en. *Remote Sensing*, 8, 580.
- Breiman L. (Oct. 2001). Random Forests. *Machine Learning*, 45, 5–32.
- Brooks P. D., Chorover J., Fan Y., Godsey S. E., Maxwell R. M., McNamara J. P., and Tague C. (Sept. 2015). Hydrological Partitioning in the Critical Zone: Recent Advances and Opportunities for Developing Transferable Understanding of Water Cycle Dynamics: CRITICAL ZONE HYDROLOGY. en. *Water Resources Research*, 51, 6973–6987.
- Brötz B., Eigenmann R., Dörnbrack A., Foken T., and Wirth V. (July 2014). Early-Morning Flow Transition in a Valley in Low-Mountain Terrain Under Clear-Sky Conditions. en. *Boundary-Layer Meteorology*, 152, 45–63.
- Buckley T. N. (Aug. 2005). The Control of Stomata by Water Balance: Tansley Review. en. *New Phytologist*, 168, 275–292.
- Carminati A., Moradi A. B., Vetterlein D., Vontobel P., Lehmann E., Weller U., Vogel H.-J., and Oswald S. E. (July 2010). Dynamics of Soil Water Content in the Rhizosphere. en. *Plant and Soil*, 332, 163–176.

- ermák J., Kuera J., and Nadezhdina N. (Sept. 2004). Sap Flow Measurements with Some Thermodynamic Methods, Flow Integration within Trees and Scaling up from Sample Trees to Entire Forest Stands. en. *Trees*, 18, 529–546.
- Cescatti A., Marcolla B., Santhana Vannan S. K., Pan J. Y., Román M. O., Yang X., Ciais P., Cook R. B., Law B. E., Matteucci G., Migliavacca M., Moors E., Richardson A. D., Seufert G., and Schaaf C. B. (June 2012). Intercomparison of MODIS Albedo Retrievals and in Situ Measurements across the Global FLUXNET Network. en. *Remote Sensing of Environment*, 121, 323–334.
- Choat B., Brodribb T. J., Brodersen C. R., Duursma R. A., López R., and Medlyn B. E. (June 2018). Triggers of Tree Mortality under Drought. en. *Nature*, 558, 531–539.
- Chu H., Baldocchi D. D., John R., Wolf S., and Reichstein M. (Feb. 2017). Fluxes All of the Time? A Primer on the Temporal Representativeness of FLUXNET: FLUXES ALL OF THE TIME? en. *Journal of Geophysical Research: Biogeosciences*, 122, 289–307.
- Ciais P., Reichstein M., Viovy N., Granier A., Ogée J., Allard V., Aubinet M., Buchmann N., Bernhofer C., Carrara A., Chevallier F., De Noblet N., Friend A. D., Friedlingstein P., Grünwald T., Heinesch B., Keronen P., Knohl A., Krinner G., Loustau D., Manca G., Matteucci G., Miglietta F., Ourcival J. M., Papale D., Pilegaard K., Rambal S., Seufert G., Soussana J. F., Sanz M. J., Schulze E. D., Vesala T., and Valentini R. (Sept. 2005). Europe-Wide Reduction in Primary Productivity Caused by the Heat and Drought in 2003. en. *Nature*, 437, 529–533.
- Clark M. P., Bierkens M. F. P., Samaniego L., Woods R. A., Uijlenhoet R., Bennett K. E., Pauwels V. R. N., Cai X., Wood A. W., and Peters-Lidard C. D. (July 2017). The Evolution of Process-Based Hydrologic Models: Historical Challenges and the Collective Quest for Physical Realism. en. *Hydrology and Earth System Sciences*, 21, 3427–3440.
- Coenders-Gerrits A. M. J., van der Ent R. J., Bogaard T. A., Wang-Erlandsson L., Hrachowitz M., and Savenije H. H. G. (Feb. 2014). Uncertainties in Transpiration Estimates. *Nature*, 506, E1–E2.
- Couvreur V., Vanderborght J., Draye X., and Javaux M. (Nov. 2014). Dynamic Aspects of Soil Water Availability for Isohydric Plants: Focus on Root Hydraulic Resistances. en. *Water Resour. Res.*, 50, 8891–8906.
- Cowan I. R. and Farquhar G. D. (1977). Stomatal Function in Relation to Leaf Metabolism and Environment. In: *Symposia of the Society for Experimental Biology*. Vol. 31, pp. 471.

- Damour G., Simonneau T., Cochard H., and Urban L. (July 2010). An Overview of Models of Stomatal Conductance at the Leaf Level: Models of Stomatal Conductance. en. *Plant, Cell & Environment*, no–no.
- De Kauwe M. G., Zhou S.-X., Medlyn B. E., Pitman A. J., Wang Y.-P., Duursma R. A., and Prentice I. C. (Dec. 2015). Do Land Surface Models Need to Include Differential Plant Species Responses to Drought? Examining Model Predictions across a Mesic-Xeric Gradient in Europe. en. *Biogeosciences*, 12, 7503–7518.
- De Kauwe M. G., Medlyn B. E., Pitman A. J., Drake J. E., Ukkola A., Griebel A., Pendall E., Prober S., and Roderick M. (Feb. 2019). Examining the Evidence for Decoupling between Photosynthesis and Transpiration during Heat Extremes. en. *Biogeosciences*, 16, 903–916.
- Deans R. M., Brodribb T. J., Busch F. A., and Farquhar G. D. (Apr. 2019). Plant Water-use Strategy Mediates Stomatal Effects on the Light Induction of Photosynthesis. en. *New Phytologist*, 222, 382–395.
- Delpierre N., Dufrêne E., Soudani K., Ulrich E., Cecchini S., Boé J., and François C. (June 2009). Modelling Interannual and Spatial Variability of Leaf Senescence for Three Deciduous Tree Species in France. en. *Agricultural and Forest Meteorology*, 149, 938–948.
- Delpierre N., Soudani K., François C., Le Maire G., Bernhofer C., Kutsch W., Misson L., Rambal S., Vesala T., and Dufrêne E. (Mar. 2012). Quantifying the Influence of Climate and Biological Drivers on the Interannual Variability of Carbon Exchanges in European Forests through Process-Based Modelling. en. *Agricultural and Forest Meteorology*, 154-155, 99–112.
- Desai A. R., Richardson A. D., Moffat A. M., Kattge J., Hollinger D. Y., Barr A., Falge E., Noormets A., Papale D., Reichstein M., and Stauch V. J. (June 2008). Cross-Site Evaluation of Eddy Covariance GPP and RE Decomposition Techniques. en. *Agricultural and Forest Meteorology*, 148, 821–838.
- Dietze M. C., Serbin S. P., Davidson C., Desai A. R., Feng X., Kelly R., Kooper R., LeBauer D., Mantooh J., McHenry K., and Wang D. (Mar. 2014). A Quantitative Assessment of a Terrestrial Biosphere Model's Data Needs across North American Biomes: PEcAn/ED Model-Data Uncertainty Analysis. en. *Journal of Geophysical Research: Biogeosciences*, 119, 286–300.
- Drake J. E., Tjoelker M. G., Vårhammar A., Medlyn B. E., Reich P. B., Leigh A., Pfautsch S., Blackman C. J., López R., Aspinwall M. J., Crous K. Y., Duursma R. A., Kumarathunge D., De Kauwe M. G., Jiang M., Nicotra A. B., Tissue D. T., Choat B.,

- Atkin O. K., and Barton C. V. M. (June 2018). Trees Tolerate an Extreme Heatwave via Sustained Transpirational Cooling and Increased Leaf Thermal Tolerance. en. *Glob Change Biol*, 24, 2390–2402.
- Dufrêne E., Davi H., François C., Le Maire G., Le Dantec V., and Granier A. (2005). Modelling Carbon and Water Cycles in a Beech Forest: Part I: Model Description and Uncertainty Analysis on Modelled NEE. *Ecological Modelling*, 185, 407–436.
- Egea G., Verhoef A., and Vidale P. L. (Oct. 2011). Towards an Improved and More Flexible Representation of Water Stress in Coupled PhotosynthesisStomatal Conductance Models. en. *Agricultural and Forest Meteorology*, 151, 1370–1384.
- Eller C. B., Rowland L., Oliveira R. S., Bittencourt P. R. L., Barros F. V., da Costa A. C. L., Meir P., Friend A. D., Mencuccini M., Sitch S., and Cox P. (Nov. 2018). Modelling Tropical Forest Responses to Drought and El Niño with a Stomatal Optimization Model Based on Xylem Hydraulics. en. *Philosophical Transactions of the Royal Society B: Biological Sciences*, 373, 20170315.
- Fatichi S. and Pappas C. (July 2017). Constrained Variability of Modeled $T : ET$ Ratio across Biomes: Transpiration:Evapotranspiration Ratio. en. *Geophysical Research Letters*, 44, 6795–6803.
- Felfelani F., Wada Y., Longuevergne L., and Pokhrel Y. N. (Oct. 2017). Natural and Human-Induced Terrestrial Water Storage Change: A Global Analysis Using Hydrological Models and GRACE. en. *Journal of Hydrology*, 553, 105–118.
- Fischer E. M., Seneviratne S. I., Vidale P. L., Lüthi D., and Schär C. (Oct. 2007). Soil MoistureAtmosphere Interactions during the 2003 European Summer Heat Wave. en. *Journal of Climate*, 20, 5081–5099.
- Fisher J. B., Melton F., Middleton E., Hain C., Anderson M., Allen R., McCabe M. F., Hook S., Baldocchi D., Townsend P. A., Kilic A., Tu K., Miralles D. D., Perret J., Lagouarde J.-P., Waliser D., Purdy A. J., French A., Schimel D., Famiglietti J. S., Stephens G., and Wood E. F. (Apr. 2017). The Future of Evapotranspiration: Global Requirements for Ecosystem Functioning, Carbon and Climate Feedbacks, Agricultural Management, and Water Resources: THE FUTURE OF EVAPOTRANSPIRATION. en. *Water Resources Research*, 53, 2618–2626.
- Flexas J., Barbour M. M., Brendel O., Cabrera H. M., Carriquí M., Díaz-Espejo A., Douthe C., Dreyer E., Ferrio J. P., Gago J., Gallé A., Galmés J., Kodama N., Medrano H., Niinemets Ü., Peguero-Pina J. J., Pou A., Ribas-Carbó M., Tomás M., Tosens T., and Warren C. R. (Sept. 2012). Mesophyll Diffusion Conductance to

- CO₂: An Unappreciated Central Player in Photosynthesis. en. *Plant Science*, 193-194, 70–84.
- Flo V., Martinez-Vilalta J., Steppe K., Schuldt B., and Poyatos R. (June 2019). A Synthesis of Bias and Uncertainty in Sap Flow Methods. en. *Agricultural and Forest Meteorology*, 271, 362–374.
- FLUXNET Data Download (2007).
- Friend A. D., Arneth A., Kiang N. Y., Lomas M., Ogée J., Rödenbeck C., Running S. W., Santaren J.-D., Sitch S., Viovy N., Ian Woodward F., and Zaehle S. (Mar. 2007). FLUXNET and Modelling the Global Carbon Cycle. en. *Global Change Biology*, 13, 610–633.
- Gao X., Gu F., Mei X., Hao W., Li H., Gong D., and Li X. (Mar. 2018). Light and Water Use Efficiency as Influenced by Clouds and/or Aerosols in a Rainfed Spring Maize Cropland on the Loess Plateau. en. *Crop Sci.*, 58, 853–862.
- Gedney N., Cox P. M., Betts R. A., Boucher O., Huntingford C., and Stott P. A. (Feb. 2006). Detection of a Direct Carbon Dioxide Effect in Continental River Runoff Records. en. *Nature*, 439, 835–838.
- Gharun M., Hörtnagl L., Paul-Limoges E., Ghiasi S., Feigenwinter I., Burri S., Marquardt K., Etzold S., Zweifel R., Eugster W., and Buchmann N. (Oct. 2020). Physiological Response of Swiss Ecosystems to 2018 Drought across Plant Types and Elevation. en. *Phil. Trans. R. Soc. B*, 375, 20190521.
- Gimeno T. E., Ogée J., Royles J., Gibon Y., West J. B., Burlett R., Jones S. P., Sauze J., Wohl S., Benard C., Genty B., and Wingate L. (Aug. 2017). Bryophyte Gas-Exchange Dynamics along Varying Hydration Status Reveal a Significant Carbonyl Sulphide (COS) Sink in the Dark and COS Source in the Light. en. *New Phytologist*, 215, 965–976.
- Goldstein G., Andrade J. L., Meinzer F. C., Holbrook N. M., Cavelier J., Jackson P., and Celis A. (Apr. 1998). Stem Water Storage and Diurnal Patterns of Water Use in Tropical Forest Canopy Trees. en. *Plant Cell Environ*, 21, 397–406.
- Good S. P., Moore G. W., and Miralles D. G. (Dec. 2017). A Mesic Maximum in Biological Water Use Demarcates Biome Sensitivity to Aridity Shifts. en. *Nature Ecology & Evolution*, 1, 1883–1888.
- Good S. P., Noone D., and Bowen G. (2015). Hydrologic Connectivity Constrains Partitioning of Global Terrestrial Water Fluxes. *Science*, 349, 175–177.
- Good S. P., Soderberg K., Guan K., King E. G., Scanlon T. M., and Caylor K. K. (Feb. 2014). $\delta^2\text{H}$ Isotopic Flux Partitioning of Evapotranspiration over a Grass Field

- Following a Water Pulse and Subsequent Dry Down. en. *Water Resources Research*, 50, 1410–1432.
- Gorelick N., Hancher M., Dixon M., Ilyushchenko S., Thau D., and Moore R. (2017). Google Earth Engine: Planetary-Scale Geospatial Analysis for Everyone. *Remote Sensing of Environment*, 202, 18–27.
- Granier A. (Dec. 1987). Evaluation of Transpiration in a Douglas-Fir Stand by Means of Sap Flow Measurements. en. *Tree Physiology*, 3, 309–320.
- Granier A., Reichstein M., Bréda N., Janssens I., Falge E., Ciais P., Grünwald T., Aubinet M., Berbigier P., Bernhofer C., Buchmann N., Facini O., Grassi G., Heinesch B., Ilvesniemi H., Keronen P., Knohl A., Köstner B., Lagergren F., Lindroth A., Longdoz B., Loustau D., Mateus J., Montagnani L., Nys C., Moors E., Papale D., Peiffer M., Pilegaard K., Pita G., Pumpanen J., Rambal S., Rebmann C., Rodrigues A., Seufert G., Tenhunen J., Vesala T., and Wang Q. (Mar. 2007). Evidence for Soil Water Control on Carbon and Water Dynamics in European Forests during the Extremely Dry Year: 2003. en. *Agricultural and Forest Meteorology*, 143, 123–145.
- Granier A., Bréda N., Longdoz B., Gross P., and Ngao J. (Jan. 2008). Ten Years of Fluxes and Stand Growth in a Young Beech Forest at Hesse, North-Eastern France. en. *Annals of Forest Science*, 65, 704–704.
- Grünwald T. and Bernhofer C. (May 2007). A Decade of Carbon, Water and Energy Flux Measurements of an Old Spruce Forest at the Anchor Station Tharandt. en. *Tellus B*, 59, 387–396.
- Gu L., Hanson P. J., Post W. M., Kaiser D. P., Yang B., Nemani R., Pallardy S. G., and Meyers T. (Mar. 2008). The 2007 Eastern US Spring Freeze: Increased Cold Damage in a Warming World? en. *BioScience*, 58, 253–262.
- Hales, Stephen, Gribelin S., Innys J., Innys W., Woodward T., W., Innys. J., and Woodward T. (1727). *Vegetable Staticks, or, An Account of Some Statical Experiments on the Sap in Vegetables : Being an Essay towards a Natural History of Vegetation : Also, a Specimen of an Attempt to Analyse the Air, by a Great Variety of Chymio-Statical Experiments; Which Were Read at Several Meetings before the Royal Society* /. London :Printed for W. and J. Innys ... :|and T. Woodward,
- He X., Estes L., Konar M., Tian D., Anghileri D., Baylis K., Evans T. P., and Sheffield J. (Oct. 2019). Integrated Approaches to Understanding and Reducing Drought Impact on Food Security across Scales. en. *Current Opinion in Environmental Sustainability*, 40, 43–54.

- Hengl T., Mendes de Jesus J., Heuvelink G. B. M., Ruiperez Gonzalez M., Kilibarda M., Blagoti A., Shangguan W., Wright M. N., Geng X., Bauer-Marschallinger B., Guevara M. A., Vargas R., MacMillan R. A., Batjes N. H., Leenaars J. G. B., Ribeiro E., Wheeler I., Mantel S., and Kempen B. (Feb. 2017). SoilGrids250m: Global Gridded Soil Information Based on Machine Learning. en. *PLOS ONE*, 12. Bond-Lamberty B. (ed.), e0169748.
- Hollinger D. Y. and Richardson A. D. (2005). Uncertainty in Eddy Covariance Measurements and Its Application to Physiological Models. *Tree physiology*, 25, 873–885.
- Holloway-Phillips M.-M. and Brodribb T. J. (Feb. 2011). Minimum Hydraulic Safety Leads to Maximum Water-Use Efficiency in a Forage Grass: Minimum Hydraulic Safety, Maximum Water-Use Efficiency. en. *Plant, Cell & Environment*, 34, 302–313.
- Huete A., Didan K., Miura T., Rodriguez E., Gao X., and Ferreira L. (Nov. 2002). Overview of the Radiometric and Biophysical Performance of the MODIS Vegetation Indices. en. *Remote Sensing of Environment*, 83, 195–213.
- Ishizaki Y., Yokohata T., Emori S., Shiogama H., Takahashi K., Hanasaki N., Nozawa T., Ogura T., Nakaegawa T., Yoshimori M., Yoshida A., and Watanabe S. (Feb. 2014). Validation of a Pattern Scaling Approach for Determining the Maximum Available Renewable Freshwater Resource. en. *Journal of Hydrometeorology*, 15, 505–516.
- Ito A. and Inatomi M. (Apr. 2012). Water-Use Efficiency of the Terrestrial Biosphere: A Model Analysis Focusing on Interactions between the Global Carbon and Water Cycles. en. *Journal of Hydrometeorology*, 13, 681–694.
- Jasechko S., Birks S. J., Gleeson T., Wada Y., Fawcett P. J., Sharp Z. D., McDonnell J. J., and Welker J. M. (Nov. 2014). The Pronounced Seasonality of Global Groundwater Recharge. en. *Water Resources Research*, 50, 8845–8867.
- Jasechko S., Sharp Z. D., Gibson J. J., Birks S. J., Yi Y., and Fawcett P. J. (Apr. 2013). Terrestrial Water Fluxes Dominated by Transpiration. en. *Nature*, 496, 347–350.
- Jin S. and Sader S. A. (Feb. 2005). Comparison of Time Series Tasseled Cap Wetness and the Normalized Difference Moisture Index in Detecting Forest Disturbances. en. *Remote Sensing of Environment*, 94, 364–372.
- Jordan M. I. and Mitchell T. M. (July 2015). Machine Learning: Trends, Perspectives, and Prospects. en. *Science*, 349, 255–260.
- Jung M., Reichstein M., and Bondeau A. (2009). Towards Global Empirical Upscaling of FLUXNET Eddy Covariance Observations: Validation of a Model Tree Ensemble Approach Using a Biosphere Model. *Biogeosciences*, 6, 2001–2013.

- Jung M., Reichstein M., Margolis H. A., Cescatti A., Richardson A. D., Arain M. A., Arneth A., Bernhofer C., Bonal D., Chen J., Gianelle D., Gobron N., Kiely G., Kutsch W., Lasslop G., Law B. E., Lindroth A., Merbold L., Montagnani L., Moors E. J., Papale D., Sottocornola M., Vaccari F., and Williams C. (Sept. 2011). Global Patterns of Land-Atmosphere Fluxes of Carbon Dioxide, Latent Heat, and Sensible Heat Derived from Eddy Covariance, Satellite, and Meteorological Observations. en. *Journal of Geophysical Research*, 116.
- Jung M., Reichstein M., Schwalm C. R., Huntingford C., Sitch S., Ahlström A., Arneth A., Camps-Valls G., Ciais P., Friedlingstein P., Gans F., Ichii K., Jain A. K., Kato E., Papale D., Poulter B., Raduly B., Rödenbeck C., Tramontana G., Viovy N., Wang Y.-P., Weber U., Zaehle S., and Zeng N. (Jan. 2017). Compensatory Water Effects Link Yearly Global Land CO₂ Sink Changes to Temperature. en. *Nature*, 541, 516–520.
- Jung M., Schwalm C., Migliavacca M., Walther S., Camps-Valls G., Koirala S., Anthoni P., Besnard S., Bodesheim P., and Carvalhais N. (2019). Scaling Carbon Fluxes from Eddy Covariance Sites to Globe: Synthesis and Evaluation of the FLUXCOM Approach. *Biogeosciences Discussions*,
- Jung M., Schwalm C., Migliavacca M., Walther S., Camps-Valls G., Koirala S., Anthoni P., Besnard S., Bodesheim P., Carvalhais N., Chevallier F., Gans F., Goll D. S., Haverd V., Köhler P., Ichii K., Jain A. K., Liu J., Lombardozzi D., Nabel J. E. M. S., Nelson J. A., O'Sullivan M., Pallandt M., Papale D., Peters W., Pongratz J., Rödenbeck C., Sitch S., Tramontana G., Walker A., Weber U., and Reichstein M. (Mar. 2020). Scaling Carbon Fluxes from Eddy Covariance Sites to Globe: Synthesis and Evaluation of the FLUXCOM Approach. en. *Biogeosciences*, 17, 1343–1365.
- Jung M. and Zscheischler J. (2013). A Guided Hybrid Genetic Algorithm for Feature Selection with Expensive Cost Functions. en. *Procedia Computer Science*, 18, 2337–2346.
- Katul G. G., Palmroth S., and Oren R. (Aug. 2009). Leaf Stomatal Responses to Vapour Pressure Deficit under Current and CO₂ -Enriched Atmosphere Explained by the Economics of Gas Exchange. en. *Plant, Cell & Environment*, 32, 968–979.
- Katul G., Manzoni S., Palmroth S., and Oren R. (Mar. 2010). A Stomatal Optimization Theory to Describe the Effects of Atmospheric CO₂ on Leaf Photosynthesis and Transpiration. en. *Annals of Botany*, 105, 431–442.

- Keenan T. F., Hollinger D. Y., Bohrer G., Dragoni D., Munger J. W., Schmid H. P., and Richardson A. D. (July 2013). Increase in Forest Water-Use Efficiency as Atmospheric Carbon Dioxide Concentrations Rise. *Nature*, 499, 324–327.
- Kenrick P. and Crane P. R. (Sept. 1997). The Origin and Early Evolution of Plants on Land. en. *Nature*, 389, 33–39.
- Knauer J., Werner C., and Zaehle S. (Oct. 2015). Evaluating Stomatal Models and Their Atmospheric Drought Response in a Land Surface Scheme: A Multibiome Analysis: MULTIBIOME STOMATAL MODEL EVALUATION. en. *Journal of Geophysical Research: Biogeosciences*, 120, 1894–1911.
- Knauer J., Zaehle S., Medlyn B. E., Reichstein M., Williams C. A., Migliavacca M., De Kauwe M. G., Werner C., Keitel C., Kolari P., Limousin J.-M., and Linderson M.-L. (Feb. 2018). Towards Physiologically Meaningful Water-Use Efficiency Estimates from Eddy Covariance Data. en. *Global Change Biology*, 24, 694–710.
- Knauer J., Zaehle S., Reichstein M., Medlyn B. E., Forkel M., Hagemann S., and Werner C. (Mar. 2017). The Response of Ecosystem Water-Use Efficiency to Rising Atmospheric CO₂ Concentrations: Sensitivity and Large-Scale Biogeochemical Implications. en. *New Phytologist*, 213, 1654–1666.
- Koenker R. and Bassett Jr G. (1978). Regression Quantiles. *Econometrica: journal of the Econometric Society*, 33–50.
- Koirala S., Jung M., Reichstein M., de Graaf I. E. M., Camps-Valls G., Ichii K., Papale D., Ráduly B., Schwalm C. R., Tramontana G., and Carvalhais N. (May 2017). Global Distribution of Groundwater-Vegetation Spatial Covariation: Global Groundwater-Vegetation Relations. en. *Geophysical Research Letters*, 44, 4134–4142.
- Konings A. G. and Gentine P. (July 2016). Global Variations in Ecosystem-Scale Isohydrlicity. en. *Global Change Biology*,
- Kool D., Agam N., Lazarovitch N., Heitman J., Sauer T., and Ben-Gal A. (Jan. 2014). A Review of Approaches for Evapotranspiration Partitioning. en. *Agricultural and Forest Meteorology*, 184, 56–70.
- Kuglitsch F. G., Reichstein M., Beer C., Carrara A., Ceulemans R., Granier A., Janssens I. A., Koestner B., Lindroth A., and Loustau D. (2008). Characterisation of Ecosystem Water-Use Efficiency of European Forests from Eddy Covariance Measurements. *Biogeosciences Discussions*, 5, 4481–4519.

- Kumar J., Hoffman F. M., Hargrove W. W., and Collier N. (Aug. 2016). Understanding the Representativeness of FLUXNET for Upscaling Carbon Flux from Eddy Covariance Measurements. en. *Earth System Science Data Discussions*, 1–25.
- Lasslop G., Reichstein M., Papale D., Richardson A. D., Arneth A., Barr A., Stoy P., and Wohlfahrt G. (Jan. 2010). Separation of Net Ecosystem Exchange into Assimilation and Respiration Using a Light Response Curve Approach: Critical Issues and Global Evaluation: SEPARATION OF NEE INTO GPP AND RECO. en. *Global Change Biology*, 16, 187–208.
- Lawlor D. W. and Tezara W. (May 2008). Causes of Decreased Photosynthetic Rate and Metabolic Capacity in Water-Deficient Leaf Cells: A Critical Evaluation of Mechanisms and Integration of Processes. en. *Annals of Botany*, 103, 561–579.
- Leuning R. (Apr. 1995). A Critical Appraisal of a Combined Stomatal-Photosynthesis Model for C3 Plants. en. *Plant, Cell and Environment*, 18, 339–355.
- Leuning R., van Gorsel E., Massman W. J., and Isaac P. R. (Apr. 2012). Reflections on the Surface Energy Imbalance Problem. en. *Agricultural and Forest Meteorology*, 156, 65–74.
- Li T., Heuvelink E., Dueck T. A., Janse J., Gort G., and Marcelis L. F. M. (July 2014). Enhancement of Crop Photosynthesis by Diffuse Light: Quantifying the Contributing Factors. en. *Annals of Botany*, 114, 145–156.
- Li X., Gentine P., Lin C., Zhou S., Sun Z., Zheng Y., Liu J., and Zheng C. (Feb. 2019). A Simple and Objective Method to Partition Evapotranspiration into Transpiration and Evaporation at Eddy-Covariance Sites. en. *Agricultural and Forest Meteorology*, 265, 171–182.
- Lian X., Piao S., Huntingford C., Li Y., Zeng Z., Wang X., Ciais P., McVicar T. R., Peng S., Ottlé C., Yang H., Yang Y., Zhang Y., and Wang T. (July 2018). Partitioning Global Land Evapotranspiration Using CMIP5 Models Constrained by Observations. en. *Nature Climate Change*, 8, 640–646.
- Lin C., Gentine P., Huang Y., Guan K., Kimm H., and Zhou S. (Mar. 2018). Diel Ecosystem Conductance Response to Vapor Pressure Deficit Is Suboptimal and Independent of Soil Moisture. en. *Agricultural and Forest Meteorology*, 250-251, 24–34.
- Liu J., Yang H., Gosling S. N., Kumm M., Flörke M., Pfister S., Hanasaki N., Wada Y., Zhang X., Zheng C., Alcamo J., and Oki T. (June 2017). Water Scarcity Assessments in the Past, Present, and Future: REVIEW ON WATER SCARCITY ASSESSMENT. en. *Earth's Future*, 5, 545–559.

- Lyons T. W., Reinhard C. T., and Planavsky N. J. (Feb. 2014). The Rise of Oxygen in Earth's Early Ocean and Atmosphere. en. *Nature*, 506, 307–315.
- Ma S., Eichelmann E., Wolf S., Rey-Sanchez C., and Baldocchi D. D. (Dec. 2020). Transpiration and Evaporation in a Californian Oak-Grass Savanna: Field Measurements and Partitioning Model Results. en. *Agricultural and Forest Meteorology*, 295, 108204.
- El-Madany T. S., Reichstein M., Carrara A., Martín M. P., Moreno G., Gonzalez-Cascon R., Peñuelas J., Ellsworth D. S., Burchard-Levine V., Hammer T. W., Knauer J., Kolle O., Luo Y., Pacheco-Labrador J., Nelson J. A., Perez-Priego O., Rolo V., Wutzler T., and Migliavacca M. (Apr. 2021). How Nitrogen and Phosphorus Availability Change Water Use Efficiency in a Mediterranean Savanna Ecosystem. en. *J Geophys Res Biogeosci*,
- Maire V., Wright I. J., Prentice I. C., Batjes N. H., Bhaskar R., van Bodegom P. M., Cornwell W. K., Ellsworth D., Niinemets Ü., Ordonez A., Reich P. B., and Santiago L. S. (June 2015). Global Effects of Soil and Climate on Leaf Photosynthetic Traits and Rates: Effects of Soil and Climate on Photosynthetic Traits. en. *Global Ecology and Biogeography*, 24, 706–717.
- Mammarella I., Launiainen S., Gronholm T., Keronen P., Pumpanen J., Rannik Ü., and Vesala T. (Sept. 2009). Relative Humidity Effect on the High-Frequency Attenuation of Water Vapor Flux Measured by a Closed-Path Eddy Covariance System. en. *Journal of Atmospheric and Oceanic Technology*, 26, 1856–1866.
- Manzoni S. (Oct. 2014). Integrating Plant Hydraulics and Gas Exchange along the Drought-Response Trait Spectrum. en. *Tree Physiology*, 34, 1031–1034.
- Manzoni S., Vico G., Palmroth S., Porporato A., and Katul G. (Dec. 2013). Optimization of Stomatal Conductance for Maximum Carbon Gain under Dynamic Soil Moisture. en. *Advances in Water Resources*, 62, 90–105.
- Martínez-Vilalta J. and Garcia-Forner N. (2016). Water Potential Regulation, Stomatal Behaviour and Hydraulic Transport under Drought: Deconstructing the Iso/Anisohydric Concept: Deconstructing the Iso/Anisohydric Concept. en. *Plant, Cell & Environment*,
- Martínez-Vilalta J., Poyatos R., Aguadé D., Retana J., and Mencuccini M. (Oct. 2014). A New Look at Water Transport Regulation in Plants. en. *New Phytologist*, 204, 105–115.
- Matheny A. M., Bohrer G., Stoy P. C., Baker I. T., Black A. T., Desai A. R., Dietze M. C., Gough C. M., Ivanov V. Y., Jassal R. S., Novick K. A., Schäfer K. V. R., and

- Verbeeck H. (July 2014). Characterizing the Diurnal Patterns of Errors in the Prediction of Evapotranspiration by Several Land-Surface Models: An NACP Analysis: Error Patterns in Modeled Transpiration. en. *Journal of Geophysical Research: Biogeosciences*, 119, 1458–1473.
- Maxwell R. M. and Condon L. E. (July 2016). Connections between Groundwater Flow and Transpiration Partitioning. en. *Science*, 353, 377–380.
- McCulloh K. A., Winter K., Meinzer F. C., Garcia M., Aranda J., and Lachenbruch B. (Sept. 2007). A Comparison of Daily Water Use Estimates Derived from Constant-Heat Sap-Flow Probe Values and Gravimetric Measurements in Pot-Grown Saplings. en. *Tree Physiology*, 27, 1355–1360.
- Medlyn B. E., De Kauwe M. G., Lin Y.-S., Knauer J., Duursma R. A., Williams C. A., Arneth A., Clement R., Isaac P., Limousin J.-M., Linderson M.-L., Meir P., Martin-StPaul N., and Wingate L. (Nov. 2017). How Do Leaf and Ecosystem Measures of Water-Use Efficiency Compare? en. *New Phytologist*, 216, 758–770.
- Medlyn B. E., Dreyer E., Ellsworth D., Forstreuter M., Harley P. C., Kirschbaum M. U. F., Le Roux X., Montpied P., Strassmeyer J., and Walcroft A. (2002). Temperature Response of Parameters of a Biochemically Based Model of Photosynthesis. II. A Review of Experimental Data. *Plant, Cell & Environment*, 25, 1167–1179.
- Medlyn B. E., Duursma R. A., Eamus D., Ellsworth D. S., Prentice I. C., Barton C. V. M., Crous K. Y., De Angelis P., Freeman M., and Wingate L. (June 2011). Reconciling the Optimal and Empirical Approaches to Modelling Stomatal Conductance: RECONCILING OPTIMAL AND EMPIRICAL STOMATAL MODELS. en. *Global Change Biology*, 17, 2134–2144.
- Medrano H., Tomás M., Martorell S., Flexas J., Hernández E., Rosselló J., Pou A., Escalona J.-M., and Bota J. (June 2015). From Leaf to Whole-Plant Water Use Efficiency (WUE) in Complex Canopies: Limitations of Leaf WUE as a Selection Target. en. *The Crop Journal*, 3, 220–228.
- Meinshausen N. (2006). Quantile Regression Forests. *Journal of Machine Learning Research*, 7, 983–999.
- Mercado L. M., Bellouin N., Sitch S., Boucher O., Huntingford C., Wild M., and Cox P. M. (Apr. 2009). Impact of Changes in Diffuse Radiation on the Global Land Carbon Sink. en. *Nature*, 458, 1014–1017.
- Migliavacca M., Meroni M., Manca G., Matteucci G., Montagnani L., Grassi G., Zenone T., Teobaldelli M., Godeed I., Colombo R., and Seufert G. (Sept. 2009). Seasonal and Interannual Patterns of Carbon and Water Fluxes of a Poplar

- Plantation under Peculiar Eco-Climatic Conditions. en. *Agricultural and Forest Meteorology*, 149, 1460–1476.
- Miralles D. G., Jiménez C., Jung M., Michel D., Ershadi A., McCabe M. F., Hirschi M., Martens B., Dolman A. J., Fisher J. B., Mu Q., Seneviratne S. I., Wood E. F., and Fernández-Prieto D. (Feb. 2016). The WACMOS-ET Project &Ndash; Part 2: Evaluation of Global Terrestrial Evaporation Data Sets. en. *Hydrology and Earth System Sciences*, 20, 823–842.
- Miralles D. G., Brutsaert W., Dolman A. J., and Gash J. H. (June 2020). *On the Use of the Term 'Evapotranspiration'*. en. Preprint. Hydrology.
- Mora C. I., Driese S. G., and Colarusso L. A. (Feb. 1996). Middle to Late Paleozoic Atmospheric CO₂ Levels from Soil Carbonate and Organic Matter. en. *Science*, 271, 1105–1107.
- Morison J. I. L. (Aug. 1985). Sensitivity of Stomata and Water Use Efficiency to High CO₂. en. *Plant Cell Environ*, 8, 467–474.
- Müller P., Li X.-P., and Niyogi K. K. (Apr. 2001). Non-Photochemical Quenching. A Response to Excess Light Energy. en. *Plant Physiol.*, 125, 1558–1566.
- Munger J. (2016). *AmeriFlux US-Ha1 Harvard Forest EMS Tower (HFR1)*. en.
- Musavi T., Migliavacca M., Reichstein M., Kattge J., Wirth C., Black T. A., Janssens I., Knohl A., Loustau D., Roupsard O., Varlagin A., Rambal S., Cescatti A., Gianelle D., Kondo H., Tamrakar R., and Mahecha M. D. (Feb. 2017). Stand Age and Species Richness Dampen Interannual Variation of Ecosystem-Level Photosynthetic Capacity. en. *Nature Ecology & Evolution*, 1.
- Myneni R. and Knyazikhin Y. (2015). MCD15A3H MODIS/Terra+Aqua Leaf Area Index/FPAR 4-Day L4 Global 500m SIN Grid V006.
- Nash J. and Sutcliffe J. (Apr. 1970). River Flow Forecasting through Conceptual Models Part I A Discussion of Principles. *Journal of Hydrology*, 10, 282–290.
- Nelson J. A. (Oct. 2017). *Jnelson18/Fluxnettools: Initial Release*.
- Nelson J. A. (Feb. 2018). *Jnelson18/TranspirationEstimationAlgorithm: Release for Publication Review*.
- Nelson J. A. (Feb. 2019). *Jnelson18/TranspirationEstimationAlgorithm: Force T to 0 at Night*. Zenodo.
- Nelson J. A. (Aug. 2020a). *Ecosystem Transpiration from FLUXNET*. Zenodo.
- Nelson J. A. (June 2020b). *Jnelson18/Ecosystem-Transpiration: Additional Installation Instructions*. Zenodo.

- Nelson J. A. (June 2020c). *Jnelson18/TranspirationEstimationAlgorithm: Addition of DOI Tag*. Zenodo.
- Nelson J. A., Carvalhais N., Cuntz M., Delpierre N., Knauer J., Ogée J., Migliavacca M., Reichstein M., and Jung M. (Dec. 2018a). Coupling Water and Carbon Fluxes to Constrain Estimates of Transpiration: The TEA Algorithm. en. *Journal of Geophysical Research: Biogeosciences*,
- Nelson J. A., Carvalhais N., Migliavacca M., Reichstein M., and Jung M. (Apr. 2018b). Water-Stress-Induced Breakdown of Carbon Water Relations: Indicators from Diurnal FLUXNET Patterns. en. *Biogeosciences*, 15, 2433–2447.
- Novick K. A., Ficklin D. L., Stoy P. C., Williams C. A., Bohrer G., Oishi A. C., Papuga S. A., Blanken P. D., Noormets A., Sulman B. N., Scott R. L., Wang L., and Phillips R. P. (Nov. 2016a). The Increasing Importance of Atmospheric Demand for Ecosystem Water and Carbon Fluxes. en. *Nature Clim Change*, 6, 1023–1027.
- Novick K. A., Miniati C. F., and Vose J. M. (Mar. 2016b). Drought Limitations to Leaf-Level Gas Exchange: Results from a Model Linking Stomatal Optimization and Cohesion-Tension Theory: Drought Limitations to Gas Exchange. en. *Plant, Cell & Environment*, 39, 583–596.
- Ogée J., Brunet Y., Loustau D., Berbigier P., and Delzon S. (2003). MuSICA, a CO₂, Water and Energy Multilayer, Multileaf Pine Forest Model: Evaluation from Hourly to Yearly Time Scales and Sensitivity Analysis. *Global Change Biology*, 9, 697–717.
- Oishi A. C., Oren R., and Stoy P. C. (Oct. 2008). Estimating Components of Forest Evapotranspiration: A Footprint Approach for Scaling Sap Flux Measurements. en. *Agricultural and Forest Meteorology*, 148, 1719–1732.
- Oki T. and Kanae S. (2006). Global Hydrological Cycles and World Water Resources. en. 313, 6.
- Oren R., Phillips N., Katul G., Ewers B. E., and Pataki D. E. (1998). Scaling Xylem Sap Flux and Soil Water Balance and Calculating Variance: A Method for Partitioning Water Flux in Forests. en. *Annales des Sciences Forestières*, 55, 191–216.
- Osmond C. B. (June 1978). Crassulacean Acid Metabolism: A Curiosity in Context. en. *Annual Review of Plant Physiology*, 29, 379–414.
- Pagán B., Maes W., Gentile P., Martens B., and Miralles D. (Feb. 2019). Exploring the Potential of Satellite Solar-Induced Fluorescence to Constrain Global Transpiration Estimates. en. *Remote Sensing*, 11, 413.
- Palmroth S., Katul G. G., Maier C. A., Ward E., Manzoni S., and Vico G. (Mar. 2013). On the Complementary Relationship between Marginal Nitrogen and Water-Use

- Efficiencies among Pinus Taeda Leaves Grown under Ambient and CO₂-Enriched Environments. en. *Annals of Botany*, 111, 467–477.
- Pan S., Pan N., Tian H., Friedlingstein P., Sitch S., Shi H., Arora V. K., Haverd V., Jain A. K., Kato E., Lienert S., Lombardozzi D., Nabel J. E. M. S., Ottlé C., Poulter B., Zaehle S., and Running S. W. (Mar. 2020). Evaluation of Global Terrestrial Evapotranspiration Using State-of-the-Art Approaches in Remote Sensing, Machine Learning and Land Surface Modeling. en. *Hydrology and Earth System Sciences*, 24, 1485–1509.
- Papale D. (June 2020). *Ideas and Perspectives: Enhancing the Impact of the FLUXNET Network of Eddy Covariance Sites*. en. Preprint. Biogeochemistry: Air - Land Exchange.
- Papale D., Reichstein M., Aubinet M., Canfora E., Bernhofer C., Kutsch W., Longdoz B., Rambal S., Valentini R., Vesala T., et al. (2006). Towards a Standardized Processing of Net Ecosystem Exchange Measured with Eddy Covariance Technique: Algorithms and Uncertainty Estimation. *Biogeosciences*, 3, 571–583.
- Paschalis A., Fatichi S., Pappas C., and Or D. (Oct. 2018). Covariation of Vegetation and Climate Constrains Present and Future T/ET Variability. en. *Environmental Research Letters*, 13, 104012.
- Pastorello G., Papale D., Chu H., Trotta C., Agarwal D., Canfora E., Baldocchi D., and Torn M. (2017). The FLUXNET2015 Dataset: The Longest Record of Global Carbon, Water, and Energy Fluxes Is Updated. *Eos*, 98.
- Paul-Limoges E., Wolf S., Schneider F. D., Longo M., Moorcroft P., Gharun M., and Damm A. (Jan. 2020). Partitioning Evapotranspiration with Concurrent Eddy Covariance Measurements in a Mixed Forest. en. *Agricultural and Forest Meteorology*, 280, 107786.
- Pedregosa F., Varoquaux G., Gramfort A., Michel V., Thirion B., Grisel O., Blondel M., Prettenhofer P., Weiss R., Dubourg V., et al. (2011). Scikit-Learn: Machine Learning in Python. *Journal of Machine Learning Research*, 12, 2825–2830.
- Pedruzo-Bagazgoitia X., Ouwersloot H. G., Sikma M., van Heerwaarden C. C., Jacobs C. M. J., and Vilà-Guerau de Arellano J. (June 2017). Direct and Diffuse Radiation in the Shallow Cumulus Vegetation System: Enhanced and Decreased Evapotranspiration Regimes. en. *Journal of Hydrometeorology*, 18, 1731–1748.
- Penna D., Hopp L., Scandellari F., Allen S. T., Benettin P., Beyer M., Geris J., Klaus J., Marshall J. D., Schwendenmann L., Volkmann T. H. M., von Freyberg J., Amin A., Ceperley N., Engel M., Frentress J., Giambastiani Y., McDonnell J. J., Zuecco G.,

- Llorens P., Siegwolf R. T. W., Dawson T. E., and Kirchner J. W. (Oct. 2018). Ideas and Perspectives: Tracing Terrestrial Ecosystem Water Fluxes Using Hydrogen and Oxygen Stable Isotopes Challenges and Opportunities from an Interdisciplinary Perspective. en. *Biogeosciences*, 15, 6399–6415.
- Perez-Priego O., Katul G., Reichstein M., El-Madany T. S., Ahrens B., Carrara A., Scanlon T. M., and Migliavacca M. (Oct. 2018). Partitioning Eddy Covariance Water Flux Components Using Physiological and Micrometeorological Approaches. en. *Journal of Geophysical Research: Biogeosciences*,
- Pérez-Priego O., Testi L., Orgaz F., and Villalobos F. J. (Apr. 2010). A Large Closed Canopy Chamber for Measuring CO₂ and Water Vapour Exchange of Whole Trees. en. *Environmental and Experimental Botany*, 68, 131–138.
- Perez-Priego O. and Wutzler T. (May 2019). *ETpartitioning: Partitioning of Eddy Covariance ET into Flux Components*.
- Pinty B., Andredakis I., Clerici M., Kaminski T., Taberner M., Verstraete M. M., Gobron N., Plummer S., and Widlowski J.-L. (May 2011). Exploiting the MODIS Albedos with the Two-Stream Inversion Package (JRC-TIP): 1. Effective Leaf Area Index, Vegetation, and Soil Properties. en. *Journal of Geophysical Research*, 116.
- Porcar-Castell A., Tyystjärvi E., Atherton J., van der Tol C., Flexas J., Pfündel E. E., Moreno J., Frankenberg C., and Berry J. A. (Aug. 2014). Linking Chlorophyll a Fluorescence to Photosynthesis for Remote Sensing Applications: Mechanisms and Challenges. en. *Journal of Experimental Botany*, 65, 4065–4095.
- Potier E., Ogée J., Jouanguy J., Lamaud E., Stella P., Personne E., Durand B., Mascher N., and Loubet B. (Oct. 2015). Multilayer Modelling of Ozone Fluxes on Winter Wheat Reveals Large Deposition on Wet Senescing Leaves. en. *Agricultural and Forest Meteorology*, 211-212, 58–71.
- Poyatos R., Granda V., Flo V., Molowny-Horas R., Steppe K., Mencuccini M., and Martínez-Vilalta J. (Mar. 2019). *SAPFLUXNET: A Global Database of Sap Flow Measurements*.
- Poyatos R., Granda V., Molowny-Horas R., Mencuccini M., Steppe K., and Martínez-Vilalta J. (Dec. 2016). SAPFLUXNET: Towards a Global Database of Sap Flow Measurements. en. *Tree Physiology*, 36. Oren R. (ed.), 1449–1455.
- Priestley C. H. B. and Taylor R. J. (1972). On the Assessment of Surface Heat Flux and Evaporation Using Large-Scale Parameters. *Monthly weather review*, 100, 81–92.
- Reichstein M., Giais P., Papale D., Valentini R., Running S., Viovy N., Cramer W., Granier A., Ogée J., Allard V., Aubinet M., Bernhofer C., Buchmann N., Carrara A.,

- Grünwald T., Heimann M., Heinesch B., Knohl A., Kutsch W., Loustau D., Manca G., Matteucci G., Miglietta F., Ourcival J., Pilegaard K., Pumpanen J., Rambal S., Schaphoff S., Seufert G., Soussana J.-F., Sanz M.-J., Vesala T., and Zhao M. (Mar. 2007). Reduction of Ecosystem Productivity and Respiration during the European Summer 2003 Climate Anomaly: A Joint Flux Tower, Remote Sensing and Modelling Analysis. en. *Global Change Biology*, 13, 634–651.
- Reichstein M. (2003). Inverse Modeling of Seasonal Drought Effects on Canopy CO₂/H₂O Exchange in Three Mediterranean Ecosystems. en. *Journal of Geophysical Research*, 108.
- Reichstein M., Camps-Valls G., Stevens B., Jung M., Denzler J., Carvalhais N., and Prabhat (Feb. 2019). Deep Learning and Process Understanding for Data-Driven Earth System Science. en. *Nature*, 566, 195–204.
- Reichstein M., Falge E., Baldocchi D., Papale D., Aubinet M., Berbigier P., Bernhofer C., Buchmann N., Gilmanov T., Granier A., Grunwald T., Havrankova K., Ilvesniemi H., Janous D., Knohl A., Laurila T., Lohila A., Loustau D., Matteucci G., Meyers T., Miglietta F., Ourcival J.-M., Pumpanen J., Rambal S., Rotenberg E., Sanz M., Tenhunen J., Seufert G., Vaccari F., Vesala T., Yakir D., and Valentini R. (Sept. 2005a). On the Separation of Net Ecosystem Exchange into Assimilation and Ecosystem Respiration: Review and Improved Algorithm. en. *Global Change Biology*, 11, 1424–1439.
- Reichstein M., Falge E., Baldocchi D., Papale D., Aubinet M., Berbigier P., Bernhofer C., Buchmann N., Gilmanov T., Granier A., Grunwald T., Havrankova K., Ilvesniemi H., Janous D., Knohl A., Laurila T., Lohila A., Loustau D., Matteucci G., Meyers T., Miglietta F., Ourcival J.-M., Pumpanen J., Rambal S., Rotenberg E., Sanz M., Tenhunen J., Seufert G., Vaccari F., Vesala T., Yakir D., and Valentini R. (Sept. 2005b). On the Separation of Net Ecosystem Exchange into Assimilation and Ecosystem Respiration: Review and Improved Algorithm. en. *Global Change Biology*, 11, 1424–1439.
- Reichstein M., Stoy P. C., Desai A. R., Lasslop G., and Richardson A. D. (2012). Partitioning of Net Fluxes. en. In: *Eddy Covariance*. Aubinet M., Vesala T., and Papale D. (eds.). Dordrecht: Springer Netherlands, pp. 263–289.
- Reichstein M., Tenhunen J. D., Rouspard O., Ourcival J.-m., Rambal S., Miglietta F., Peressotti A., Pecchiari M., Tirone G., and Valentini R. (Oct. 2002). Severe Drought Effects on Ecosystem CO₂ and H₂O Fluxes at Three Mediterranean Evergreen

- Sites: Revision of Current Hypotheses?: DROUGHT EFFECTS ON ECOSYSTEM CO₂/H₂O EXCHANGE. en. *Global Change Biology*, 8, 999–1017.
- Reick C. H., Raddatz T., Brovkin V., and Gayler V. (July 2013). Representation of Natural and Anthropogenic Land Cover Change in MPI-ESM: Land Cover in MPI-ESM. en. *Journal of Advances in Modeling Earth Systems*, 5, 459–482.
- Renner M., Brenner C., Mallick K., Wizemann H.-D., Conte L., Trebs I., Wei J., Wulfmeyer V., Schulz K., and Kleidon A. (Jan. 2019). Using Phase Lags to Evaluate Model Biases in Simulating the Diurnal Cycle of Evapotranspiration: A Case Study in Luxembourg. en. *Hydrol. Earth Syst. Sci.*, 23, 515–535.
- Renner M., Kleidon A., Clark M., Nijssen B., Heidkamp M., Best M., and Abramowitz G. (Jan. 2021). How Well Can Land-Surface Models Represent the Diurnal Cycle of Turbulent Heat Fluxes? en. *Journal of Hydrometeorology*, 22, 77–94.
- Reth S., Reichstein M., and Falge E. (Jan. 2005). The Effect of Soil Water Content, Soil Temperature, Soil pH-Value and the Root Mass on Soil CO₂ Efflux A Modified Model. en. *Plant and Soil*, 268, 21–33.
- Rogers A., Medlyn B. E., Dukes J. S., Bonan G., Caemmerer S., Dietze M. C., Kattge J., Leakey A. D., Mercado L. M., Niinemets Ü., et al. (2017). A Roadmap for Improving the Representation of Photosynthesis in Earth System Models. *New Phytologist*, 213, 22–42.
- Rosa L., Sanchez D. L., Realmonte G., Baldocchi D., and D’Odorico P. (Oct. 2020). The Water Footprint of Carbon Capture and Storage Technologies. en. *Renewable and Sustainable Energy Reviews*, 110511.
- Rousseeuw P. J. (1983). Regression Techniques with High Breakdown Point. *The Institute of Mathematical Statistics Bulletin*, 12, 155.
- Rutter A., Kershaw K., Robins P., and Morton A. (Jan. 1971). A Predictive Model of Rainfall Interception in Forests, 1. Derivation of the Model from Observations in a Plantation of Corsican Pine. en. *Agricultural Meteorology*, 9, 367–384.
- Salomón R. L., Limousin J.-M., Ourcival J.-M., Rodríguez-Calcerrada J., and Steppe K. (Aug. 2017). Stem Hydraulic Capacitance Decreases with Drought Stress: Implications for Modelling Tree Hydraulics in the Mediterranean Oak *Quercus Ilex*: Seasonality in Stem Hydraulic Capacitance. en. *Plant, Cell & Environment*, 40, 1379–1391.
- Sandoval-Soto L., Stanimirov M., von Hobe M., Schmitt V., Valdes J., Wild A., and Kesselmeier J. (June 2005). Global Uptake of Carbonyl Sulfide (COS) by Terrestrial

- Vegetation: Estimates Corrected by Deposition Velocities Normalized to the Uptake of Carbon Dioxide (CO₂). *Biogeosciences*, 2, 125–132.
- Scanlon T. M. and Kustas W. P. (Jan. 2010). Partitioning Carbon Dioxide and Water Vapor Fluxes Using Correlation Analysis. en. *Agricultural and Forest Meteorology*, 150, 89–99.
- Scanlon T. M., Schmidt D. F., and Skaggs T. H. (2019). Correlation-Based Flux Partitioning of Water Vapor and Carbon Dioxide Fluxes: Method Simplification and Estimation of Canopy Water Use Efficiency. *Agricultural and Forest Meteorology*, 279, 107732.
- Schimel D., Pavlick R., Fisher J. B., Asner G. P., Saatchi S., Townsend P., Miller C., Frankenberg C., Hibbard K., and Cox P. (May 2015). Observing Terrestrial Ecosystems and the Carbon Cycle from Space. en. *Glob Change Biol*, 21, 1762–1776.
- Schlesinger W. H. and Jasechko S. (June 2014). Transpiration in the Global Water Cycle. en. *Agricultural and Forest Meteorology*, 189-190, 115–117.
- Scott R. L. and Biederman J. A. (July 2017). Partitioning Evapotranspiration Using Long-Term Carbon Dioxide and Water Vapor Fluxes: New Approach to ET Partitioning. en. *Geophysical Research Letters*,
- Scott R. L., Knowles J. F., Nelson J. A., Gentine P., Li X., Barron-Gafford G., Bryant R., and Biederman J. A. (Nov. 2020). Water Availability Impacts on Evapotranspiration Partitioning. en. *Agricultural and Forest Meteorology*, 108251.
- Shan N., Ju W., Migliavacca M., Martini D., Guanter L., Chen J., Goulas Y., and Zhang Y. (Apr. 2019). Modeling Canopy Conductance and Transpiration from Solar-Induced Chlorophyll Fluorescence. en. *Agricultural and Forest Meteorology*, 268, 189–201.
- Shan N., Zhang Y., Chen J. M., Ju W., Migliavacca M., Peñuelas J., Yang X., Zhang Z., Nelson J. A., and Goulas Y. (Jan. 2021). A Model for Estimating Transpiration from Remotely Sensed Solar-Induced Chlorophyll Fluorescence. en. *Remote Sensing of Environment*, 252, 112134.
- Sheil D. and Murdiyarso D. (Apr. 2009). How Forests Attract Rain: An Examination of a New Hypothesis. en. *BioScience*, 59, 341–347.
- Slot M., Garcia M. N., and Winter K. (2016). Temperature Response of CO₂ Exchange in Three Tropical Tree Species. en. *Functional Plant Biol.*, 43, 468.
- Smith P., Davis S. J., Creutzig F., Fuss S., Minx J., Gabrielle B., Kato E., Jackson R. B., Cowie A., Kriegler E., van Vuuren D. P., Rogelj J., Ciais P., Milne J., Canadell J. G.,

- McCollum D., Peters G., Andrew R., Krey V., Shrestha G., Friedlingstein P., Gasser T., Grüber A., Heidug W. K., Jonas M., Jones C. D., Kraxner F., Littleton E., Lowe J., Moreira J. R., Nakicenovic N., Obersteiner M., Patwardhan A., Rogner M., Rubin E., Sharifi A., Torvanger A., Yamagata Y., Edmonds J., and Yongsung C. (Jan. 2016). Biophysical and Economic Limits to Negative CO₂ Emissions. en. *Nature Climate Change*, 6, 42–50.
- Sperry J. S., Venturas M. D., Anderegg W. R. L., Mencuccini M., Mackay D. S., Wang Y., and Love D. M. (June 2017). Predicting Stomatal Responses to the Environment from the Optimization of Photosynthetic Gain and Hydraulic Cost: A Stomatal Optimization Model. en. *Plant, Cell & Environment*, 40, 816–830.
- Spracklen D. V., Arnold S. R., and Taylor C. M. (Sept. 2012). Observations of Increased Tropical Rainfall Preceded by Air Passage over Forests. en. *Nature*, 489, 282–285.
- Steppe K., De Pauw D. J., Doody T. M., and Teskey R. O. (July 2010). A Comparison of Sap Flux Density Using Thermal Dissipation, Heat Pulse Velocity and Heat Field Deformation Methods. en. *Agricultural and Forest Meteorology*, 150, 1046–1056.
- Stocker B. D., Zscheischler J., Keenan T. F., Prentice I. C., Seneviratne S. I., and Peñuelas J. (Apr. 2019). Drought Impacts on Terrestrial Primary Production Underestimated by Satellite Monitoring. en. *Nature Geoscience*, 12, 264–270.
- Stoy P. C., El-Madany T. S., Fisher J. B., Gentine P., Gerken T., Good S. P., Klosterhalfen A., Liu S., Miralles D. G., Perez-Priego O., Rigden A. J., Skaggs T. H., Wohlfahrt G., Anderson R. G., Coenders-Gerrits A. M. J., Jung M., Maes W. H., Mammarella I., Mauder M., Migliavacca M., Nelson J. A., Poyatos R., Reichstein M., Scott R. L., and Wolf S. (Oct. 2019). Reviews and Syntheses: Turning the Challenges of Partitioning Ecosystem Evaporation and Transpiration into Opportunities. en. *Biogeosciences*, 16, 3747–3775.
- Talsma C. J., Good S. P., Jimenez C., Martens B., Fisher J. B., Miralles D. G., McCabe M. F., and Purdy A. J. (Oct. 2018). Partitioning of Evapotranspiration in Remote Sensing-Based Models. en. *Agricultural and Forest Meteorology*, 260-261, 131–143.
- Tang X., Li H., Desai A. R., Nagy Z., Luo J., Kolb T. E., Oliosio A., Xu X., Yao L., Kutsch W., Pilegaard K., Köstner B., and Ammann C. (Dec. 2014). How Is Water-Use Efficiency of Terrestrial Ecosystems Distributed and Changing on Earth? *Scientific Reports*, 4, 7483.
- Tramontana G., Migliavacca M., Jung M., Reichstein M., Keenan T. F., Camps-Valls G., Ogee J., Verrelst J., and Papale D. (July 2020). Partitioning Net Carbon Dioxide

- Fluxes into Photosynthesis and Respiration Using Neural Networks. en. *Global Change Biology*,
- Tucker C. J. (May 1979). Red and Photographic Infrared Linear Combinations for Monitoring Vegetation. en. *Remote Sensing of Environment*, 8, 127–150.
- Tuzet A., Perrier A., and Leuning R. (July 2003). A Coupled Model of Stomatal Conductance, Photosynthesis and Transpiration. en. *Plant, Cell and Environment*, 26, 1097–1116.
- Tyree M. T. and Sperry J. S. (1988). Do Woody Plants Operate near the Point of Catastrophic Xylem Dysfunction Caused by Dynamic Water Stress? Answers from a Model. *Plant physiology*, 88, 574–580.
- Urban J., Ingwers M. W., McGuire M. A., and Teskey R. O. (Mar. 2017a). Increase in Leaf Temperature Opens Stomata and Decouples Net Photosynthesis from Stomatal Conductance in *Pinus Taeda* and *Populus Deltoides x Nigra*. en. *Journal of Experimental Botany*, 68, 1757–1767.
- Urban J., Ingwers M., McGuire M. A., and Teskey R. O. (Aug. 2017b). Stomatal Conductance Increases with Rising Temperature. en. *Plant Signaling & Behavior*, 12, e1356534.
- Villalobos F., Perez-Priego O., Testi L., Morales A., and Orgaz F. (July 2012). Effects of Water Supply on Carbon and Water Exchange of Olive Trees. en. *European Journal of Agronomy*, 40, 1–7.
- Wada Y., Bierkens M. F. P., de Roo A., Dirmeyer P. A., Famiglietti J. S., Hanasaki N., Konar M., Liu J., Müller Schmied H., Oki T., Pokhrel Y., Sivapalan M., Troy T. J., van Dijk A. I. J. M., van Emmerik T., Van Huijgevoort M. H. J., Van Lanen H. A. J., Vörösmarty C. J., Wanders N., and Wheeler H. (Aug. 2017). HumanWater Interface in Hydrological Modelling: Current Status and Future Directions. en. *Hydrol. Earth Syst. Sci.*, 21, 4169–4193.
- Wang K., Dickinson R. E., and Liang S. (May 2008). Observational Evidence on the Effects of Clouds and Aerosols on Net Ecosystem Exchange and Evapotranspiration: EFFECTS OF CLOUDS AND AEROSOLS ON *NEE* AND *ET*. en. *Geophys. Res. Lett.*, 35.
- Wang L., Good S. P., and Caylor K. K. (Oct. 2014). Global Synthesis of Vegetation Control on Evapotranspiration Partitioning: VEGETATION AND ET PARTITIONING. en. *Geophysical Research Letters*, 41, 6753–6757.

- Wang L., Good S. P., Caylor K. K., and Cernusak L. A. (2012). Direct Quantification of Leaf Transpiration Isotopic Composition. *Agricultural and Forest Meteorology*, 154, 127–135.
- Wehr R., Commane R., Munger J. W., McManus J. B., Nelson D. D., Zahniser M. S., Saleska S. R., and Wofsy S. C. (Jan. 2017). Dynamics of Canopy Stomatal Conductance, Transpiration, and Evaporation in a Temperate Deciduous Forest, Validated by Carbonyl Sulfide Uptake. en. *Biogeosciences*, 14, 389–401.
- Wei Z., Yoshimura K., Wang L., Miralles D. G., Jasechko S., and Lee X. (Mar. 2017). Revisiting the Contribution of Transpiration to Global Terrestrial Evapotranspiration: Revisiting Global ET Partitioning. en. *Geophysical Research Letters*, 44, 2792–2801.
- Whelan M. E., Lennartz S. T., Gimeno T. E., Wehr R., Wohlfahrt G., Wang Y., Kooijmans L. M. J., Hilton T. W., Belviso S., Peylin P., Commane R., Sun W., Chen H., Kuai L., Mammarella I., Maseyk K., Berkelhammer M., Li K.-F., Yakir D., Zumkehr A., Katayama Y., Ogée J., Spielmann F. M., Kitz F., Rastogi B., Kesselmeier J., Marshall J., Erkkilä K.-M., Wingate L., Meredith L. K., He W., Bunk R., Launois T., Vesala T., Schmidt J. A., Fichot C. G., Seibt U., Saleska S., Saltzman E. S., Montzka S. A., Berry J. A., and Campbell J. E. (Oct. 2017). Reviews and Syntheses: Carbonyl Sulfide as a Multi-Scale Tracer for Carbon and Water Cycles. en. *Biogeosciences Discussions*, 1–97.
- Whelan M. E., Lennartz S. T., Gimeno T. E., Wehr R., Wohlfahrt G., Wang Y., Kooijmans L. M. J., Hilton T. W., Belviso S., Peylin P., Commane R., Sun W., Chen H., Kuai L., Mammarella I., Maseyk K., Berkelhammer M., Li K.-F., Yakir D., Zumkehr A., Katayama Y., Ogée J., Spielmann F. M., Kitz F., Rastogi B., Kesselmeier J., Marshall J., Erkkilä K.-M., Wingate L., Meredith L. K., He W., Bunk R., Launois T., Vesala T., Schmidt J. A., Fichot C. G., Seibt U., Saleska S., Saltzman E. S., Montzka S. A., Berry J. A., and Campbell J. E. (June 2018). Reviews and Syntheses: Carbonyl Sulfide as a Multi-Scale Tracer for Carbon and Water Cycles. en. *Biogeosciences*, 15, 3625–3657.
- Wilkinson S. and Davies W. J. (Feb. 2002). ABA-Based Chemical Signalling: The Co-Ordination of Responses to Stress in Plants. en. *Plant, Cell and Environment*, 25, 195–210.
- Wilkinson S., Ogee J., Domec J.-C., Rayment M., and Wingate L. (Mar. 2015). Biophysical Modelling of Intra-Ring Variations in Tracheid Features and Wood

- Density of *Pinus Pinaster* Trees Exposed to Seasonal Droughts. en. *Tree Physiology*, 35, 305–318.
- Wilm H. G., Thornthwaite C. W., Colman E. A., Cummings N. W., Croft A. R., Gisborne H. T., Harding S. T., Hendrickson A. H., Hoover M. D., Houk I. E., Kittredge J., Lee C. H., Rossby C.-G., Saville T., and Taylor C. A. (1944). Report of the Committee on Transpiration and Evaporation, 194344. en. *Trans. AGU*, 25, 683.
- Wilson K. B., Baldocchi D., Falge E., Aubinet M., Berbigier P., Bernhofer C., Dolman H., Field C., Goldstein A., Granier A., Hollinger D., Katul G., Law B. E., Meyers T., Moncrieff J., Monson R., Tenhunen J., Valentini R., Verma S., and Wofsy S. (Nov. 2003). Diurnal Centroid of Ecosystem Energy and Carbon Fluxes at FLUXNET Sites: DIURNAL ENERGY FLUXES AT FLUXNET SITES. en. *Journal of Geophysical Research: Atmospheres*, 108.
- Wilson K. B., Hanson P. J., Mulholland P. J., Baldocchi D. D., and Wullschleger S. D. (Jan. 2001). A Comparison of Methods for Determining Forest Evapotranspiration and Its Components: Sap-Flow, Soil Water Budget, Eddy Covariance and Catchment Water Balance. en. *Agricultural and Forest Meteorology*, 106, 153–168.
- Wilson K., Goldstein A., Falge E., Aubinet M., Baldocchi D., Berbigier P., Bernhofer C., Ceulemans R., Dolman H., Field C., Grelle A., Ibrom A., Law B., Kowalski A., Meyers T., Moncrieff J., Monson R., Oechel W., Tenhunen J., Valentini R., and Verma S. (2002). Energy Balance Closure at FLUXNET Sites. *Agricultural and Forest Meteorology*, 113, 223–243.
- Wohlfahrt G. (2017). Bi-Directional COS Exchange in Bryophytes Challenges Its Use as a Tracer for Gross Primary Productivity. *New Phytologist*, 215, 923–925.
- Wullschleger S. D., Gundersen C. A., Hanson P. J., Wilson K. B., and Norby R. J. (Mar. 2002). Sensitivity of Stomatal and Canopy Conductance to Elevated CO₂ Concentration - Interacting Variables and Perspectives of Scale. en. *New Phytol*, 153, 485–496.
- Zhou S., Yu B., Huang Y., and Wang G. (July 2014). The Effect of Vapor Pressure Deficit on Water Use Efficiency at the Subdaily Time Scale: Underlying Water Use Efficiency. en. *Geophysical Research Letters*, 41, 5005–5013.
- Zhou S., Yu B., Huang Y., and Wang G. (May 2015). Daily Underlying Water Use Efficiency for AmeriFlux Sites: DAILY UNDERLYING WUE. en. *Journal of Geophysical Research: Biogeosciences*, 120, 887–902.

- Zhou S., Yu B., Zhang Y., Huang Y., and Wang G. (Feb. 2016a). Partitioning Evapotranspiration Based on the Concept of Underlying Water Use Efficiency: ET PARTITIONING. en. *Water Resources Research*, 52, 1160–1175.
- Zhou S., Yu B., Zhang Y., Huang Y., and Wang G. (May 2018). Water Use Efficiency and Evapotranspiration Partitioning for Three Typical Ecosystems in the Heihe River Basin, Northwestern China. en. *Agricultural and Forest Meteorology*, 253-254, 261–273.
- Zhou S., Zhang Y., Park Williams A., and Gentine P. (Jan. 2019). Projected Increases in Intensity, Frequency, and Terrestrial Carbon Costs of Compound Drought and Aridity Events. en. *Science Advances*, 5, eaau5740.
- Zhou S.-X., Medlyn B. E., and Prentice I. C. (Jan. 2016b). Long-Term Water Stress Leads to Acclimation of Drought Sensitivity of Photosynthetic Capacity in Xeric but Not Riparian *Eucalyptus* Species. en. *Annals of Botany*, 117, 133–144.
- Zhou S., Duursma R. A., Medlyn B. E., Kelly J. W., and Prentice I. C. (Dec. 2013). How Should We Model Plant Responses to Drought? An Analysis of Stomatal and Non-Stomatal Responses to Water Stress. en. *Agricultural and Forest Meteorology*, 182-183, 204–214.
- Zhu Z., Wang S., and Woodcock C. E. (2015). Improvement and Expansion of the Fmask Algorithm: Cloud, Cloud Shadow, and Snow Detection for Landsats 47, 8, and Sentinel 2 Images. *Remote Sensing of Environment*, 159, 269–277.
- Zhu Z. and Woodcock C. E. (Mar. 2012). Object-Based Cloud and Cloud Shadow Detection in Landsat Imagery. en. *Remote Sensing of Environment*, 118, 83–94.

Acknowledgments

There once was a boy born to a wonderful family in Utah. He grew up happy, being encouraged to learn and work hard by his loving parents Kaylynn and Kendall, to whom he is tremendously grateful. His best friend in the world was his older sister Brittany, at least until they were joined by Peter, Zach, and Josie. They grew, played, and learned together and he misses them terribly when they are apart, but they are always there for him and he is tremendously grateful. He continued on his journey through life, being mentored along the way by teachers, friends, and his grandparents who taught him to work hard and do his best, for which he is tremendously grateful. All of these people were there to help through difficulties and celebrate success, and he wouldn't have the opportunities he did without them, and he is tremendously grateful. Eventually he left his home to find his own way, ending up at Utah State University to study Biology. Upon arrival he met a girl who would join him on this journey to this day. She would give him immeasurable support and encouragement through the years, for which he is tremendously grateful. Lennie and Lola soon joined them on their journey, and the pack of strays would face the world together.

He had many friends and mentors at USU, both academic and not who helped him figure out who he was, and he is tremendously grateful. Eventually he was given a job fixing fans in a greenhouse, where he met a professor who was willing to mentor him and give him a chance, and to Bruce he is tremendously grateful. The success he found riding atop the support from his family, the girl, his mentors, and his friends allowed him to continue his journey all the way to another continent.

He joined Markus, Martin, Mirco and Nuno to complete this thesis. Nuno gave him the hours of discussion, both about science and not, that he needed to get his thoughts straight. Mirco gave him the support and encouragement to convince him that his work was good enough, sometimes even just the needed line in an email. Markus gave him the opportunities and vision to succeed, always finding the exact question that needed to be asked. Martin gave him the constant road map, always being there to figure out the right direction, while also reminding him that he needed to be advised and not supervised. He and the four of them started talking one day and never really stopped. Thought they met in the context of completing the thesis, he would consider all of them fiends and that he is tremendously grateful.

When the pack of strays landed in Germany with two suitcases and no clue, they found tons of support from new friends such as Uli, Steffi, Sujan, and Bernhard, with whom he would be fiends with for years to come and he is tremendously grateful. He met more fiends along the way who taught him many things. Sujan and Milie taught him how to cook rice and how to be a foreigner away from your homeland. Uli taught him how to really live in Germany. He and Simon learned how to navigate academia together, for better or for worse, and he never would have survived otherwise. Oscar, Jürgen, and Sven taught him how to have a heated discussion and still stay friends. Jasper and Tina taught him how to be young again, whether on the dance floor or on the slopes. Sebastian and Julia taught him proper sauna etiquette, and along with Uli and Steffi how to hike in the Alps. Bernhard taught him how to travel with pumpkins, how to always be ready for someone to drop in and, more importantly, how to be himself. Çalar taught him what cherries are for. Basil taught him how to be a mountain person. Shane taught him how to stay up late. Yunpeng taught him how to order whiskey in Chinese. Richard taught him how to be a nerd. Nora taught him how to always be nice and to never forget to say you're sorry. Silvia taught him how to stand up for what is right. Amber taught him to draw without looking at the page. Sophia, Fabian, Uli, Martin, and Basil taught him how to work as a team. The city of Jena taught him how to feel both far away from home and right at home at the same time. The DEI team taught him how many people there are willing to make themselves and the world a better place. If there is such a thing as a Doktorvater or Doktormutter, these people and more would be his Doktorfamilie, his home away from home, and to them he is tremendously grateful.

Through the entire journey, the girl was there. Through late nights and broken bones. Through highs and through lows. Through quarantines and travel delays. Through everything, she was always there and to her he will always be tremendously grateful.

Appendices

Appendix A

Supplement to Chapter 2

A.1 File S1

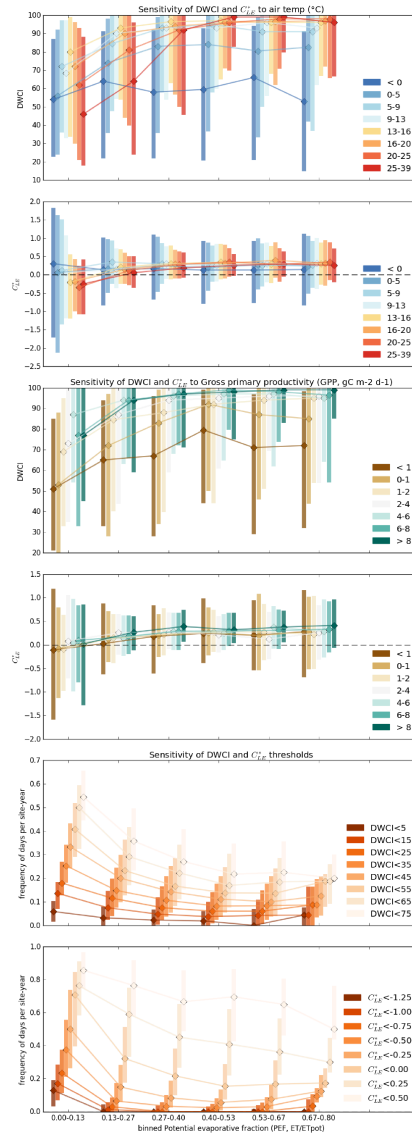


Figure A.1 Figure S1. Sensitivity analysis of DWCI and C_{ET}^* to evaporative fraction ($EF=ET/potential\ ET$) under different GPP and air temperature (T_{air}) values, as well as the sensitivity of frequency of decoupling ($DWCI < threshold$) and morning ($C_{ET}^* < threshold$) using various thresholds. Note DWCI of 0-100 indicate lowest-highest probability of diurnal carbon:water coupling and C_{ET}^* of -1-1 indicate one hour morning shifted-one hour afternoon shifted ET. Bins for GPP and T_{air} based on percentiles to give an equal number of points per bin, with the exception of $GPP < 1$ and $T_{air} < 0$, which are approximately double the size of the other bins and represent periods of low plant activity such as winter. Vertical bars represent interquartile range in all cases.

A.2 Figure S2

Figure S2 is an interactive file which can be accessed at: <https://doi.org/10.5194/bg-15-2433-2018-supplement>

A.3 File S3

```
"""
Created on Fri Aug 26 17:32:13 2016

@author: Jacob A. Nelson and Martin Jung
"""

# Uses the numpy package for matrix operations
import numpy as np

def LEtoET(LE):
    # convert LE in Wm-2 to mm per half hour
    # 2300000 J per L, latent heat of vaporization
    # 1800 seconds per half hour
    ET=np.ma.getdata(LE)*((1800)/2300000)
    return(ET)

def CSWI(precip,LE,s0=5,ConvertET=True):
    '''CSWI(precip,LE,s0=5,ConvertET=True)

    Conservative surface water index (CSWI)

    CSWI forces a positive water water storage for any time-
    ↪ step with precipitation, yet has a maximum storage of
    ↪ s0.

    Parameters
    -----
    precip : list or list like
            precipitation in mm
    LE : list or list like
        Latent energy in Wm-2 or ET in mm per half hour (must
        ↪ set ConvertET=False).
```

s0 : value, float or int
The maximum storage of the water balance
ConvertET : bool
Flag telling wheter to convert LE to ET.

Returns

```
-----  
array  
    The modified water balance  
    ,,,  
# insure that datasets are one dimensional  
precip=precip.reshape(-1)  
LE=LE.reshape(-1)  
# extract the data in case that precip has an associated  
    ↪ mask  
precipcalc=np.ma.getdata(precip)  
  
# in case of an associated mask, fill all gap values with  
    ↪ the maximum water storage  
if np.ma.is_masked(precip):  
    precipcalc[np.ma.getmask(precip)]=s0  
else:  
# in case of any negative values in precipitation fill with  
    ↪ the maximum water storage  
    precipcalc[(precip<0)]=s0  
# fill any other missing values with the maximum water  
    ↪ storage  
precipcalc[np.isnan(precip)]=s0  
precipcalc[np.isinf(precip)]=s0  
  
# create an array of zeros the same shape as the  
    ↪ precipitation data to hold the CSWI  
CSWI=np.zeros(precip.shape)  
# set the initial value of CSWI to the max storage capacity  
CSWI[0]=s0  
# if needed, convert the latent energy to mm per half hour  
if ConvertET:  
    LEmm=LEtoET(LE)  
else:  
    LEmm=LE  
  
# set any missing values in LE data to a number  
LEmm[np.isnan(LEmm)]=-9999  
LEmm[np.isinf(LEmm)]=-9999
```



```

# loop through each timestep, skipping the initial condition
for j in range(precip.shape[0]-1):
    k=j+1
    # stepVal give either the current water balance or s0,
    #   ↪ causing s0 to be a ceiling
    stepVal=min(CSWI[j]+precipcalc[k]-LEmm[k],s0)
    # in case of a positive precip value, the current CSWI
    #   ↪ is the max between the previous
    # CSWI and either the value of the precip or the s0
    #   ↪ depending on which is smaller
    if precipcalc[k]>0:
        CSWI[k]=max(stepVal, min(precipcalc[j],s0))
    # if there is no precip, the CSWI is according to the
    #   ↪ stepVal,
    # causing simple water balance behaviour
    else:
        CSWI[k]=stepVal
return(CSWI)

```

A.4 File S4

```
"""
@author: Jacob A. Nelson
"""

# Uses the numpy package for matrix operations
import numpy as np

def DiurnalCentroid(flux, UnitsPerDay=48):
    '''DiurnalCentroid(flux)

    Diurnal centroid of sub-daily fluxes

    Calculates the daily flux weighted time of a sub-daily flux
    ↪ .

    Parameters
    -----
    flux : list or list like
        sub-daily flux that must be continuous and regular
    UnitsPerDay : integer
        frequency of the sub-daily measurements, 48 for half
        ↪ hourly measurements

    Returns
    -----
    array
        The diurnal centroid, in the same units as UnitsPerDay,
        ↪ at a daily frequency
    '''

    # calculate the total number of days
    days, UPD=flux.reshape(-1, UnitsPerDay).shape
    # create a 2D matrix providing a UPD time series for each
    ↪ day, used in the matrix operations.
    hours=np.tile(np.arange(UPD), days).reshape(days, UPD)
    # calculate the diurnal centroid
    C=np.sum(hours*flux.reshape(-1, 48), axis=1)/np.sum(flux.
    ↪ reshape(-1, 48), axis=1)
    C=C*(24/UnitsPerDay)
    return(C)
```

```
def NormDiurnalCentroid(LE,Rg,UnitsPerDay=48):
```

```
    '''NormDiurnalCentroid(LE,Rg)
```

```
    Normalized diurnal centroid of latent energy (LE)
```

```
    Calculates the diurnal centroid of LE relative to the  
    ↪ diurnal centroid of incoming radiation (Rg).
```

```
    Parameters
```

```
    -----  
    LE : list or list like
```

```
        Latend energy, can be any unit
```

```
    Rg : list or list like
```

```
        Incoming radiation, can be any unit
```

```
    UnitsPerDay : integer
```

```
        frequency of the sub-daily measurements, 48 for half  
        ↪ hourly measurements
```

```
    Returns
```

```
    -----  
    array
```

```
        The normalized diurnal centroid, in the same units as  
        ↪ UnitsPerDay, at a daily frequency
```

```
    ,,,
```

```
    C_LE=DiurnalCentroid(LE,UnitsPerDay=UnitsPerDay)
```

```
    C_Rg=DiurnalCentroid(Rg,UnitsPerDay=UnitsPerDay)
```

```
    return(C_LE-C_Rg)
```

A.5 File S5

```
# -*- coding: utf-8 -*-
"""
Created on Tue Mar 28 13:24:22 2017

@author: jnelson
"""

import numpy as np
from scipy.stats import ss

def daily_corr(x, y, Rg_pot):
    '''daily_corr(x, y)

    Daily correlation coefficient

    Calculates a daily correlation coefficient between two sub-
    ↪ daily timeseries

    Parameters
    -----
    x : list or list like
        x variable
    y : list or list like
        y variable
    Rg_pot : list or list like
        potential radiation
    Returns
    -----
    array
    ..., correlation coefficents at daily timescale
    '''
    x=x.reshape(-1,48)
    y=y.reshape(-1,48)
    Rg_pot=Rg_pot.reshape(-1,48)
    mask=Rg_pot<=0
    x=np.ma.MaskedArray(x,mask=mask)
    y=np.ma.MaskedArray(y,mask=mask)
    x=x/x.max(axis=1)[: ,None]
    y=y/y.max(axis=1)[: ,None]
    mx = x.mean(axis=1)
    my = y.mean(axis=1)
```

```

xm, ym = x - mx[... , None], y - my[... , None]
r_num = np.ma.add.reduce(xm * ym, axis=1)
r_den = np.ma.sqrt(np.ma.sum(xm**2, axis=1) * np.ma.sum(ym
    ↪ **2, axis=1))
r = r_num / r_den
return(r**2)

```

```

def DWCIcalc(Rg_pot ,LE ,GPP ,VPD ,NEE ,LE_sd ,GPP_sd ,NEE_fall ,
    ↪ LE_fall):
    '''DWCIcalc(Rg_pot ,LE ,GPP ,LE_sd ,GPP_sd ,NEE_fall , LE_fall)

```

Diurnal water:carbon index (DWCI)

DWCI measures the probability that the carbon and water are

- ↪ *coupled within a given day. Method takes the*
- ↪ *correlation between evapotranspiration (LE) and gross*
- ↪ *primary productivity (GPP) and calculated the*
- ↪ *correlation within each day. This correlation is then*
- ↪ *compare to a distribution of correlations between*
- ↪ *artificial datasets built from the signal of*
- ↪ *potential radiation and the uncertainty in the LE and*
- ↪ *GPP.*

Parameters

Rg_pot : list or list like

Sub-daily timeseries of potential radiation

LE : list or list like

Sub-daily timeseries of evapotranspiration or latent
 ↪ *energy*

GPP : list or list like

Sub-daily timeseries of gross primary productivity

VPD : list or list like

Sub-daily timeseries of vapor pressure deficit

NEE : list or list like

Sub-daily timeseries of net ecosystem exchange

LE_sd : list or list like

Sub-daily estimation of the uncertainty of LE

GPP_sd : list or list like

Sub-daily estimation of the uncertainty of GPP

NEE_fall : list or list like

Modeled sub-daily timeseries of net ecosystem exchange
 ↪ *i.e. no noise*

LE_fall : list or list like

*Modeled sub-daily timeseries of evapotranspiration or
↳ latent energy i.e. no noise*

Returns

```
-----  
array  
    The diurnal water:carbon index (DWCI)  
    ,,,  
  
# reshape all variables as number of days by number of half  
    ↳ hours  
varList=[Rg_pot,LE,GPP,VPD,NEE,LE_sd,GPP_sd,NEE_fall,  
    ↳ LE_fall]  
for j in range(len(varList)):  
    varList[j]=varList[j].reshape(-1,48)  
Rg_pot,LE,GPP,VPD,NEE,LE_sd,GPP_sd,NEE_fall,LE_fall=varList  
# the number of artificial datasets to construct  
repeats=100  
# the number of days in the timeseries. Assumes data is  
    ↳ half hourly  
days=int(LE.shape[0])  
# creates an empty 2D dataset to hold the artificial  
    ↳ distributions  
StN=np.zeros([repeats,days])*np.nan  
corrDev=np.zeros([days,2,2])  
  
# create the daily cycle by dividing Rg_pot by the daily  
    ↳ mean  
daily_cycle=Rg_pot/Rg_pot.mean(axis=1)[: ,None]  
mean_GPP=GPP.mean(axis=1)  
mean_LE=LE.mean(axis=1)  
  
# Isolate the error of the carbon and water fluxes.  
NEE_err=NEE_fall-NEE  
LE_err=LE_fall-LE  
  
# loops through each day to generate an artificial dataset  
    ↳ and calculate the associate correlation  
for d in range(days):#days  
    if np.isnan(mean_GPP[d]) or np.isnan(mean_LE[d]):  
        continue  
    if np.isnan(NEE_err[d]).sum()>0 or np.isnan(LE_err[d]).  
        ↳ sum()>0 or np.isnan(GPP_sd[d]).sum()>0 or np.  
        ↳ isnan(LE_sd[d]).sum()>0:  
        continue
```

```

# find the correlation structure of the uncertainties to
    ↪ pass onto the artificial datasets

if np.all(LE_err[d]==0) or np.all(NEE_err[d]==0):
    corrDev[d]=np.identity(2)
else:
    corrDev[d] = np.corrcoef(-(NEE_err[d]), LE_err[d])

# create our synthetic GPP and LE values for the
    ↪ current day
synGPP = np.zeros((repeats,48))*np.nan
synLE   = np.zeros((repeats,48))*np.nan

# this loop builds the artificial dataset using the
    ↪ covariance matrix between NEE and LE
for i in range(48):
    # compute the covariance matrix (s) for this half
        ↪ hour
    m = [GPP_sd[d, i], LE_sd[d, i]]
    s = np.zeros((2,2))*np.nan
    for j in range(2):
        for k in range(2):
            s[j, k] = corrDev[d, j, k]*m[j]*m[k]

    Noise = np.random.multivariate_normal([0,0], s
        ↪ ,100) # generate random 100 values with the
        ↪ std of this half hour and the correlation
        ↪ between LE and GPP
    synGPP[:, i] = daily_cycle[d, i]*mean_GPP[d]+Noise
        ↪[:,0] # synthetic gpp
    synLE[:, i] = daily_cycle[d, i]*mean_LE[d]+Noise
        ↪[:,1] # synthetic le

# calculate the 100 artificial correlation coefficients
    ↪ for the day
StN[:, d]=daily_corr(synGPP, synLE, np.tile(daily_cycle[
    ↪ d],100).reshape(-1,48))

# calculate the real correlation array
pwc=daily_corr(LE, GPP*np.sqrt(VPD), Rg_pot)

# calculate the rank of the real array within the
    ↪ artificial dataset giving DWCI
DWCI=(StN<np.tile(pwc, repeats).reshape(repeats, -1)).sum(
    ↪ axis=0)

```

```
DWCI[np.isnan(StN).prod(axis=0).astype(bool)]=-9999
```

```
return (DWCI)
```


Appendix B

Supplement to Chapter 3

B.1 Figure S1

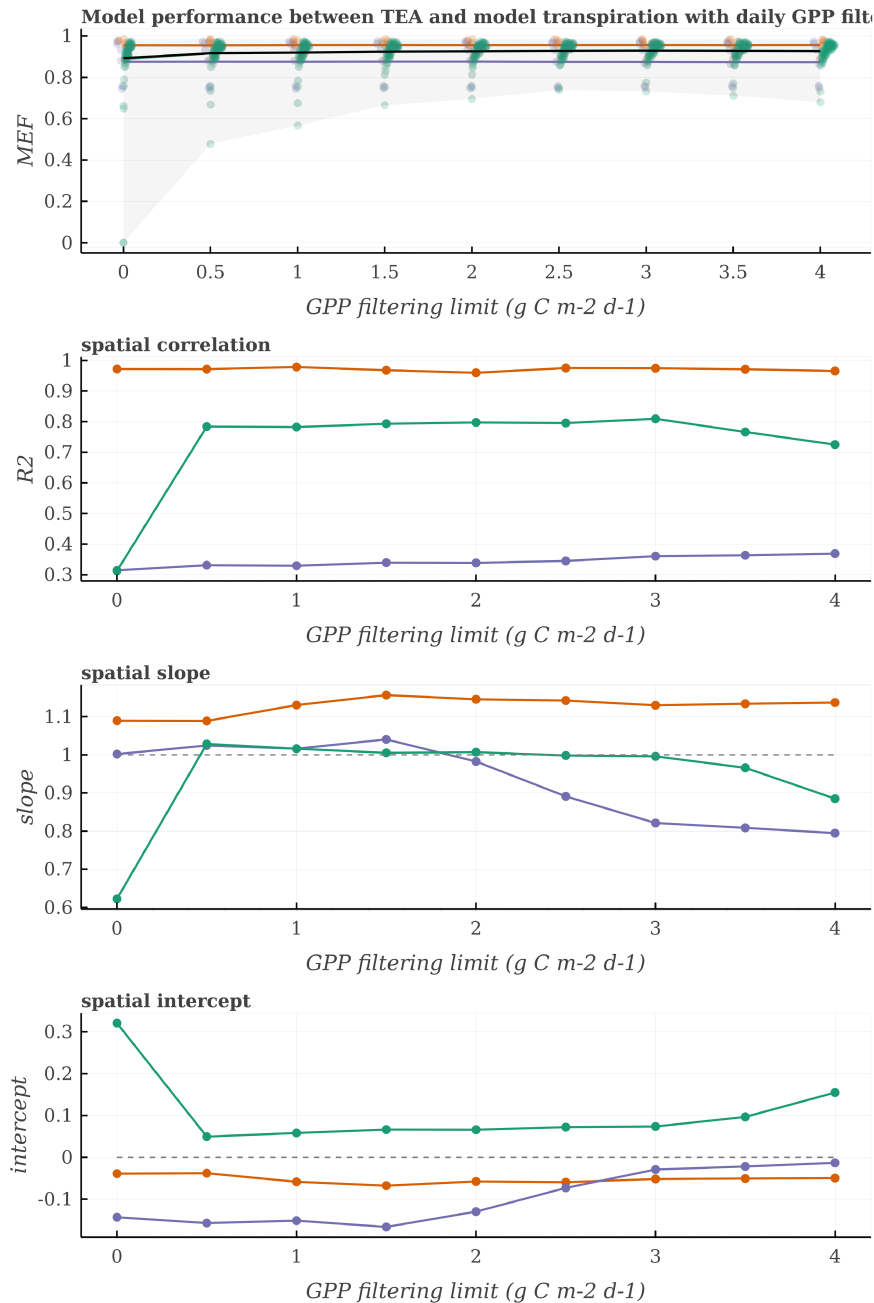


Figure B.1 Sensitivity of daily GPP threshold filter to modeling efficiency (MEF) and spatial correlation, slope, and intercept. Filter limits above 0 show significant improvements, particularly with JSBACH spatial performance. Higher limits show degraded performance with MuSICA spatial performance, likely due to decreased training set data in dry sites under high GPP limits.

B.2 Figure S2

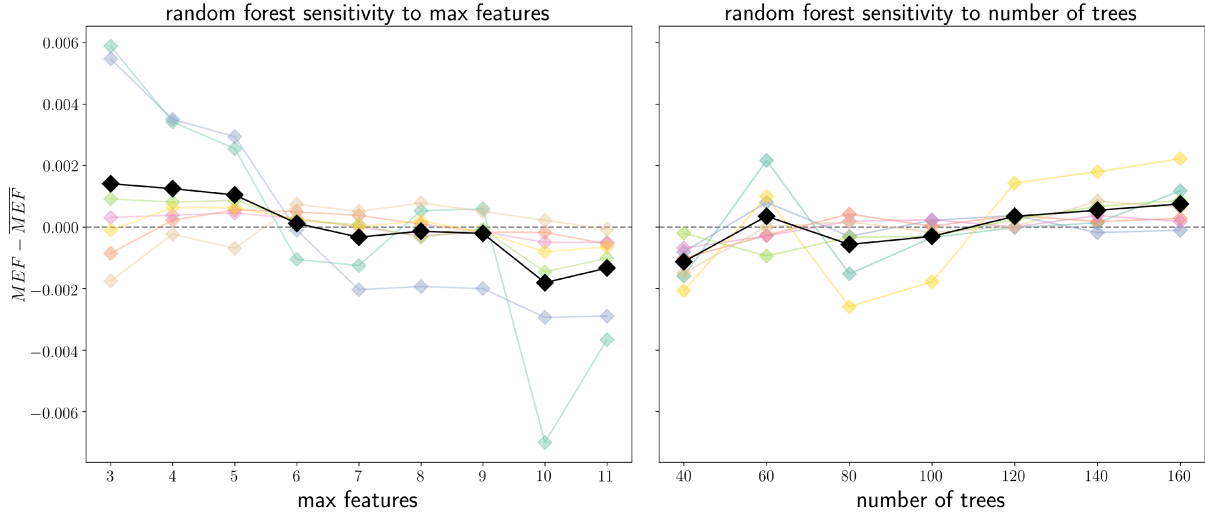


Figure B.2 A sensitivity analysis of the number of trees and max number of feature parameters on modeling efficiency (MEF) for seven site from MuSICA model output. The mean MEF across all max feature experiments for each site was subtracted to make sites comparable. Colored lines represent different sites, while the black line represents the mean from the seven sites. Though the number of max features used had little effect, a value of four showed the lowest variability and corresponds to the standard practice of using one third of the number of features. MEF decreased when the number of trees went below 100.

B.3 Figure S3

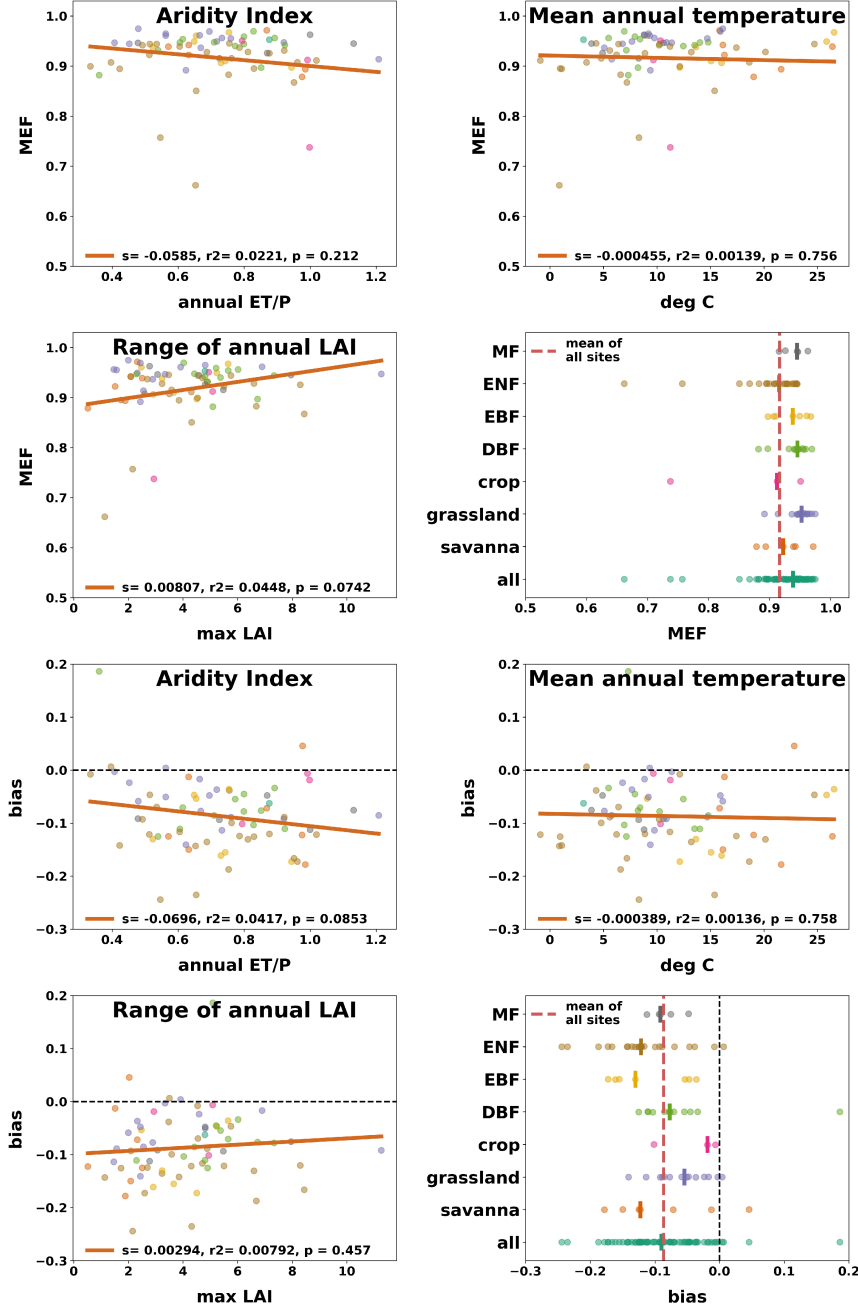


Figure B.3 Modeling efficiency (MEF) and relative bias response to plant function and climate across 72 site-runs from JSBACH. Climate variables (aridity index and mean annual temperature) showed no significant effect on MEF. Vegetation parameters show a slight effect, but is primarily driven by three sites.

B.4 Figure S4

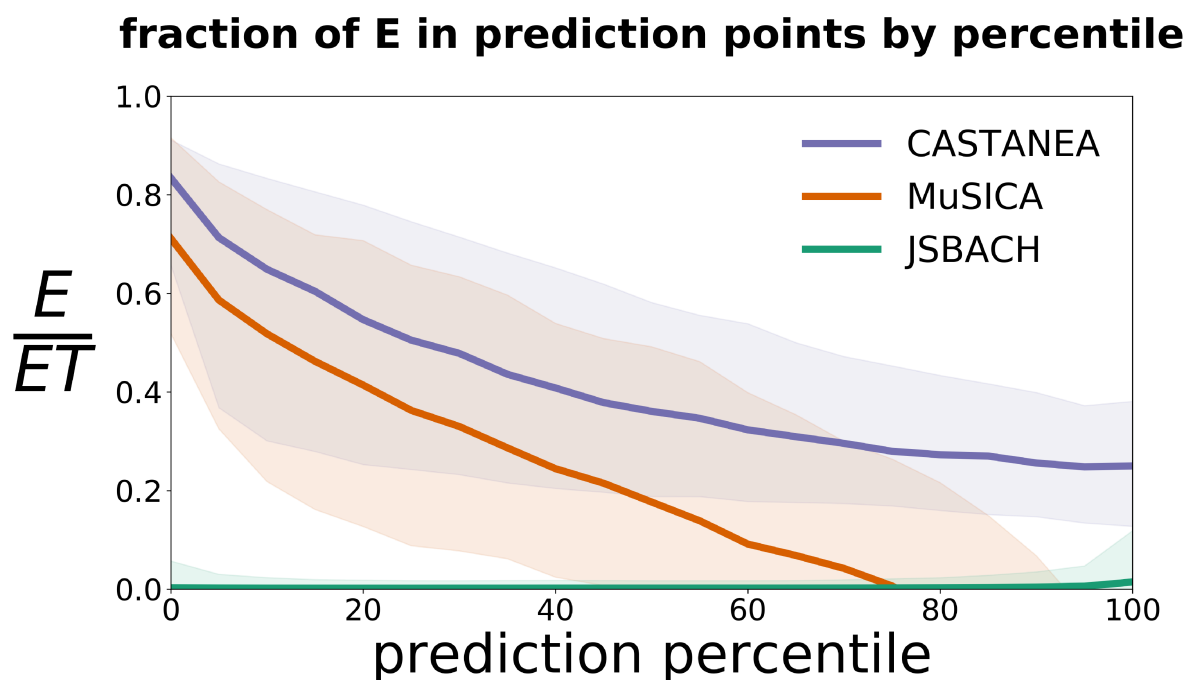


Figure B.4 Relationship between the fraction of evaporation (directly from the models) the prediction percentiles used. E/ET is calculated by retrieving the specific half hours corresponding to the predicted WUE as output from the Random Forest from the training dataset. The E/ET is then calculated in these corresponding half hours, giving the actual contamination from the predictive points. Note that this process is done for each half hour of the dataset, giving a distribution of E/ET values which is dependent on the percentile used in prediction (each percentile gives a different corresponding half hour from the training dataset). Lines represent the median across all model runs, with shading representing the interquartile range.

B.5 Figure S5

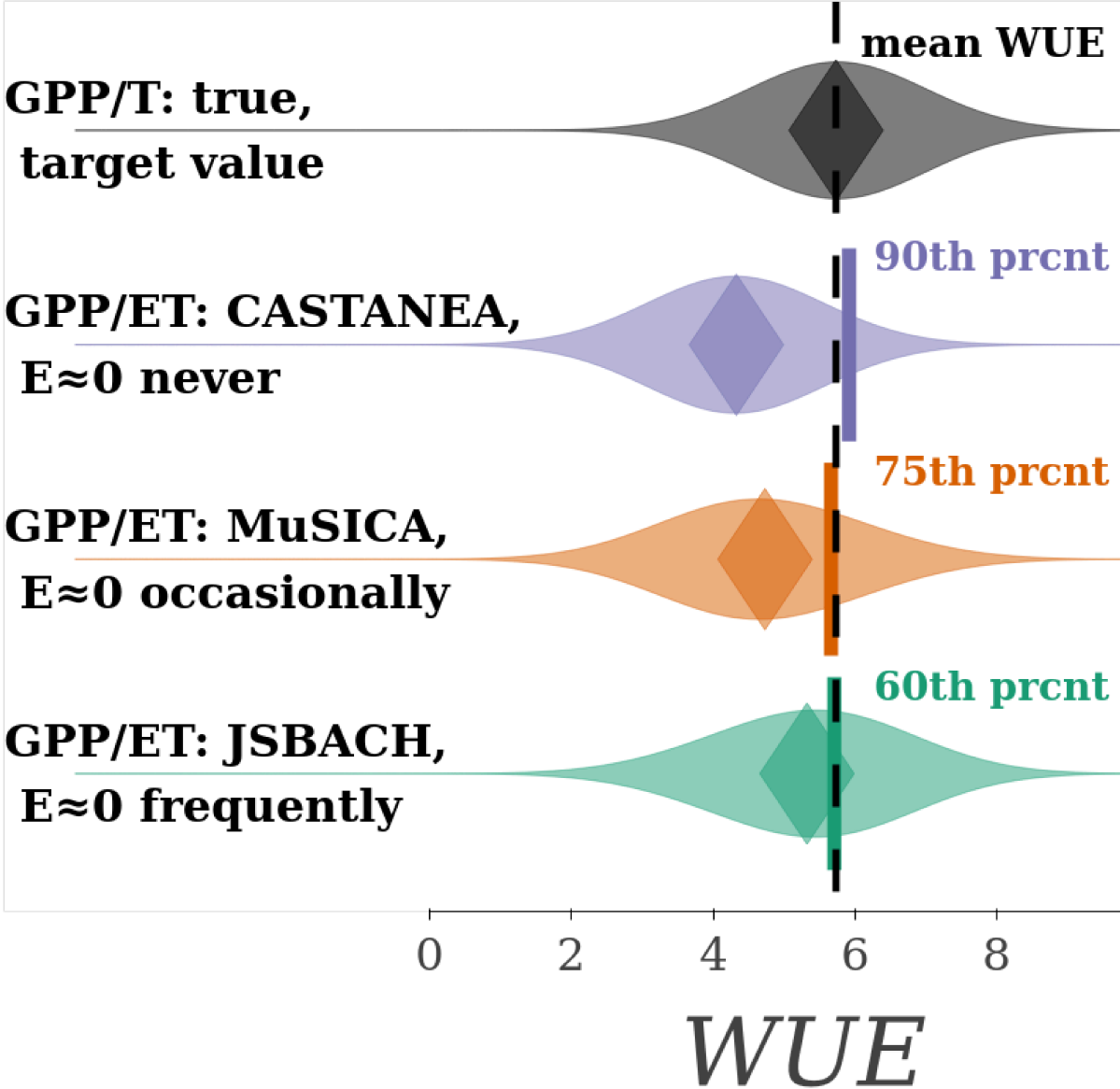


Figure B.5 Theoretical diagram showing how the average true WUE (GPP/T, gray lines) can be estimated using the prediction percentile of eWUE (GPP/ET) under three scenarios: "CASTANEA" where evaporation is always 30% of ET, "MuSICA" where evaporation is high but does reach 0 at some points, and "JSBACH" where evaporation is usually 0. In all three scenarios, including when evaporation is never 0, the mean WUE can be approximated using different percentiles, with the caveat that highest percentiles of WUE cannot be estimated in the "CASTANEA" scenario and would then be truncated.

B.6 File S6: List of 73 sites used from 3 models

B.6.1 MuSICA

| | Site ID | Site Name | Start Year | End Year |
|--|---------|--------------------------------------|------------|----------|
| | DE-Tha | Anchor Station Tharandt - old spruce | 1998 | 2010 |
| | FI-Hyy | Hyytiala | 1998 | 2011 |
| | FR-Gri | Grignon (after 6/5/2005) | 2006 | 2012 |
| | FR-Hes | Hesse Forest- Sarrebourg | 1998 | 2011 |
| | FR-LBr | Le Bray (after 6/28/1998) | 1998 | 1999 |
| | IL-Yat | Yatir | 2001 | 2002 |
| | US-Ha1 | MA - Harvard Forest EMS Tower (HFR1) | 2013 | 2013 |

B.6.2 CASTANEA

| | Site ID | Site Name | Start Year | End Year |
|--|---------|--------------------------------------|------------|----------|
| | DE-Hai | Hainich | 2000 | 2007 |
| | DE-Tha | Anchor Station Tharandt - old spruce | 1997 | 2007 |
| | FI-Hyy | Hyytiala | 1997 | 2007 |
| | FR-Fon | Fontainebleau | 2005 | 2013 |
| | FR-Hes | Hesse Forest- Sarrebourg | 1997 | 2007 |
| | FR-Pue | Puechabon | 2000 | 2007 |

B.6.3 JSBACH

| | Site ID | Site Name | Start Year | End Year |
|--|---------|-------------------------------|------------|----------|
| | AT-Neu | Neustift/Stubai Valley | 2002 | 2005 |
| | AU-How | Howard Springs | 2002 | 2005 |
| | AU-Tum | Tumbarumba | 2002 | 2005 |
| | AU-Wac | Wallaby Creek | 2006 | 2006 |
| | BE-Bra | Brasschaat (De Inslag Forest) | 2000 | 2002 |

| | Site ID | Site Name | Start Year | End Year |
|--|---------|--------------------------------------|------------|----------|
| | BE-Vie | Vielsalm | 2000 | 2006 |
| | BR-Ma2 | Manaus - ZF2 K34 | 2003 | 2005 |
| | BW-Ma1 | Maun- Mopane Woodland | 1999 | 2001 |
| | CA-Man | BOREAS NSA - Old Black Spruce | 1999 | 2003 |
| | CA-Qfo | Quebec Mature Boreal Forest Site | 2004 | 2006 |
| | CA-SF3 | Sask.- Fire 1998 | 2003 | 2005 |
| | CH-Oe1 | Oensingen1 grass | 2002 | 2006 |
| | DE-Bay | Bayreuth-Waldstein/WeidenBrunnen | 1997 | 1998 |
| | DE-Geb | Gebesee | 2004 | 2006 |
| | DE-Hai | Hainich | 2000 | 2006 |
| | DE-Meh | Mehrstedt 1 | 2004 | 2006 |
| | DE-Tha | Anchor Station Tharandt - old spruce | 1998 | 2003 |
| | DE-Wet | Wetzstein | 2002 | 2006 |
| | DK-Lva | Lille Valby (Rimi) | 2005 | 2006 |
| | DK-Sor | Soroee- LilleBogeskov | 1997 | 2006 |
| | ES-ES1 | El Saler | 1999 | 2004 |
| | ES-LMa | Las Majadas del Tietar | 2004 | 2006 |
| | FI-Hyy | Hyytiala | 2001 | 2006 |
| | FI-Sod | Sodankyla | 2003 | 2006 |
| | FR-Gri | Grignon (after 6/5/2005) | 2005 | 2006 |
| | FR-Hes | Hesse Forest- Sarrebourg | 2001 | 2006 |
| | FR-LBr | Le Bray (after 6/28/1998) | 2003 | 2006 |
| | FR-Lq2 | Laqueuille extensive | 2004 | 2006 |
| | FR-Pue | Puechabon | 2001 | 2006 |
| | HU-Bug | Bugacpuszta | 2003 | 2006 |
| | ID-Pag | Palangkaraya | 2002 | 2003 |
| | IE-Ca1 | Carlow1 | 2004 | 2006 |
| | IL-Yat | Yatir | 2001 | 2002 |
| | IT-Amp | Amplero | 2003 | 2006 |
| | IT-Cpz | Castelporziano | 2001 | 2006 |
| | IT-Lav | Lavarone (after 3/2002) | 2006 | 2006 |
| | IT-MBo | Monte Bondone | 2003 | 2006 |
| | IT-PT1 | Zerbolo-Parco Ticino- Canarazzo | 2003 | 2004 |

| | Site ID | Site Name | Start Year | End Year |
|--|---------|---|------------|----------|
| | IT-Ro2 | Roccarespampani 2 | 2002 | 2006 |
| | IT-SRo | San Rossore | 2003 | 2006 |
| | NL-Ca1 | Cabauw | 2003 | 2006 |
| | NL-Hor | Horstermeer | 2006 | 2006 |
| | NL-Loo | Loobos | 1997 | 2006 |
| | PT-Esp | Espirra | 2002 | 2006 |
| | PT-Mi1 | Mitra (Evora) | 2003 | 2005 |
| | PT-Mi2 | Mitra IV Tojal | 2005 | 2005 |
| | RU-Fyo | Fyodorovskoye wet spruce stand | 2002 | 2006 |
| | SE-Fla | Flakaliden | 2000 | 2002 |
| | SE-Nor | Norunda | 1996 | 1997 |
| | UK-EBu | Easter Bush- Scotland | 2006 | 2006 |
| | US-Bar | NH - Bartlett Experimental Forest | 2004 | 2005 |
| | US-Blo | CA - Blodgett Forest | 2000 | 2006 |
| | US-FPe | MT - Fort Peck | 2000 | 2003 |
| | US-Goo | MS - Goodwin Creek | 2004 | 2004 |
| | US-Ha1 | MA - Harvard Forest EMS Tower (HFR1) | 1995 | 1999 |
| | US-Ha2 | MA - Harvard Forest Hemlock Site | 2004 | 2004 |
| | US-Ho1 | ME - Howland Forest (main tower) | 1996 | 2004 |
| | US-LPH | MA - Little Prospect Hill | 2003 | 2004 |
| | US-Los | WI - Lost Creek | 2003 | 2005 |
| | US-MMS | IN - Morgan Monroe State Forest | 2000 | 2005 |
| | US-MOz | MO - Missouri Ozark Site | 2005 | 2006 |
| | US-Me4 | OR - Metolius-old aged ponderosa pine | 1996 | 2000 |
| | US-PFa | WI - Park Falls/WLEF | 1998 | 2000 |
| | US-SP3 | FL - Slashpine-Donaldson-mid-rot- 12yrs | 2001 | 2004 |
| | US-SRM | AZ - Santa Rita Mesquite | 2004 | 2006 |
| | US-Syv | MI - Sylvania Wilderness Area | 2002 | 2004 |
| | US-Ton | CA - Tonzi Ranch | 2002 | 2006 |
| | US-UMB | MI - Univ. of Mich. Biological Station | 2000 | 2003 |
| | US-Var | CA - Vaira Ranch- Ione | 2001 | 2006 |
| | US-WCr | WI - Willow Creek | 2000 | 2005 |
| | VU-Coc | CocoFlux | 2002 | 2003 |

| Site ID | Site Name | Start Year | End Year |
|---------|-------------------------------|------------|----------|
| ZA-Kru | Skukuza- Kruger National Park | 2001 | 2003 |

Appendix C

Supplement to Chapter 4

C.1 Supplementary Table S1

Eddy co-variance variables used in this analysis.

| variable | description | units |
|---------------|--|--|
| G | Soil heat flux, | W m ⁻² |
| GPP_NT | Gross Primary Production - from Nighttime partitioning method - based on NEE_VUT_USTAR50, | umolCO ₂ m ⁻² s ⁻¹ |
| G_QC | Quality flag of G_F_MDS, 0 = measured-,1 = good quality gapfill-,2 = medium-,3 = poor | dimensionless |
| H | Sensible heat flux - gapfilled using MDS method, | W m ⁻² |
| H_QC | Quality flag for H_F_MDS - H_CORR - H_CORR25 - and H_CORR75, 0 = measured-,1 = good quality gapfill-,2 = medium-,3 = poor | dimensionless |
| H_RANDOMUNC | Random uncertainty of H - from measured only data, uses only data point where H_F_MDS_QC is 0 and two hierarchical methods (see header and H_RANDOMUNC_METHOD) | W m ⁻² |
| H_RANDOMUNC_N | Number of half-hour data points used to estimate the random uncertainty of H, | dimensionless |
| LE | Latent heat flux - gapfilled using MDS method, | W m ⁻² |
| LE_QC | Quality flag for LE_F_MDS - LE_CORR - LE_CORR25 - and LE_CORR75, 0 = measured-,1 = good quality gapfill-,2 = medium-,3 = poor | dimensionless |

| variable | description | units |
|-----------------|--|---|
| LE_RANDOMUNC | Random uncertainty of LE - from measured only data, uses only data point where LE_F_MDS_QC is 0 and two hierarchical methods (see header and LE_RANDOMUNC_METHOD) | W m ⁻² |
| LE_RANDOMUNC_N | Number of half-hour data points used to estimate the random uncertainty of LE, | dimensionless |
| NEE | Net Ecosystem Exchange - using Variable Ustar Threshold (VUT) for each year - from 50 percentile of USTAR threshold, | umolCO ₂ m ⁻² s ⁻¹ |
| NEE_QC | Quality flag for NEE_VUT_USTAR50, 0 = measured-, 1 = good quality gapfill-, 2 = medium-, 3 = poor | dimensionless |
| NEE_RANDOMUNC | Random uncertainty for NEE_VUT_USTAR50 - from measured only data, uses only data points where NEE_VUT_USTAR50_QC is 0 and two hierarchical methods see header and NEE_VUT_USTAR50_RANDOMUNC_METHOD | umolCO ₂ m ⁻² s ⁻¹ |
| NEE_RANDOMUNC_N | Number of half-hour data points used to estimate the random uncertainty of NEE_VUT_USTAR50, | dimensionless |
| NETRAD | Net radiation, | W m ⁻² |
| P | Precipitation, | mm |
| PA | Atmospheric pressure, | kPa |
| SW_IN | Shortwave radiation - incoming - gapfilled using MDS (negative values set to zero - e.g. - negative values from instrumentation noise), | W m ⁻² |
| SW_IN_POT | Shortwave radiation - incoming - potential (top of atmosphere), | W m ⁻² |

| variable | description | units |
|----------|--|---------------|
| SW_IN_QC | Quality flag for SW_IN_F_MDS, 0 = measured-,1 = good quality gapfill-,2 = medium-,3 = poor | dimensionless |
| TA | Air temperature - gapfilled using MDS method, | deg C |
| TA_QC | Quality flag for TA_F_MDS, 0 = measured-,1 = good quality gapfill-,2 = medium-,3 = poor | dimensionless |
| VPD | Vapor Pressure Deficit - gapfilled using MDS, | hPa |
| VPD_QC | Quality flag for VPD_F_MDS, 0 = measured-,1 = good quality gapfill-,2 = medium-,3 = poor | dimensionless |
| WS | Wind speed, | m s-1 |

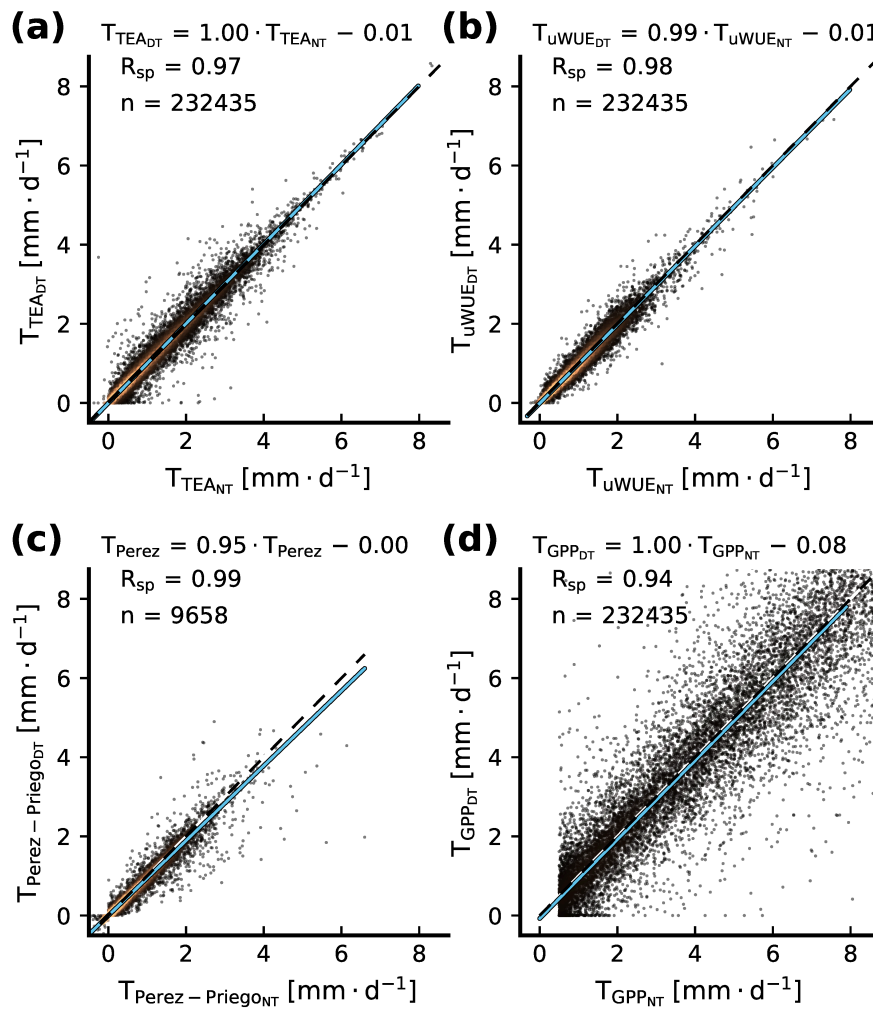
C.2 Supplementary Table S2

| site | total # trees | species | method | species calibration | radial integration ² | azimuthal integration ³ | BAI |
|------------|---------------------|--|--------------------------|---------------------|--|--|-----|
| AU- Cum | 10 | Eucalyptus tereticornis (100%,10) | HP- Tmax ¹ | no | No radial correction ² | No az- imuthal correction ³ | 2 |
| FR- Fon | 8 | Quercus petraea (79%, 5), Carpinus betulus (15%, 3) | TD ⁴ | yes | Corrected, species coefficients ⁵ | No az- imuthal correction ³ | 6 |
| FR- Pue | 12 | Quercus ilex (95%, 12) | TD ⁴ | no | No radial correction ² | No az- imuthal correction ³ | 2.4 |
| NL- Loo | 6 | Pinus sylvestris (100%, 6) | TD ⁴ | yes | Measured ⁷ | No az- imuthal correction ³ | 2.2 |
| RU- Fyo | 17 | Picea abies (86%,13), Betula sp. (13%, 2), Pinus sylvestris (1%, 2) | TD ⁴ | no | Corrected, measured radial variation ⁶ | No az- imuthal correction ³ | 3.5 |
| US- UMB | 57 | Populus grandidentata (12, 52%), Quercus rubra (14,12%), Acer rubrum (12, 20%), Pinus strobus (11, 8%), Betula papyrifera (10, 8%) | TD ⁴ | yes | No radial correction ² | No az- imuthal correction ³ | 3.5 |

Description of sites from SAPFLUXNET used in this study, including the total number of measured trees per site. The number measured tree per species and the percent basal area of each species is reported as (basal area%, # measured). ¹Heat pulse T-max method. ²Radial variation of sap flux not considered. ³Azimuthal variation of sap flux not considered. ⁴Thermal dissipation method. ⁵Species-specific corrections of radial variation of sap flux density. ⁶Site- and species-specific corrections of radial variation of

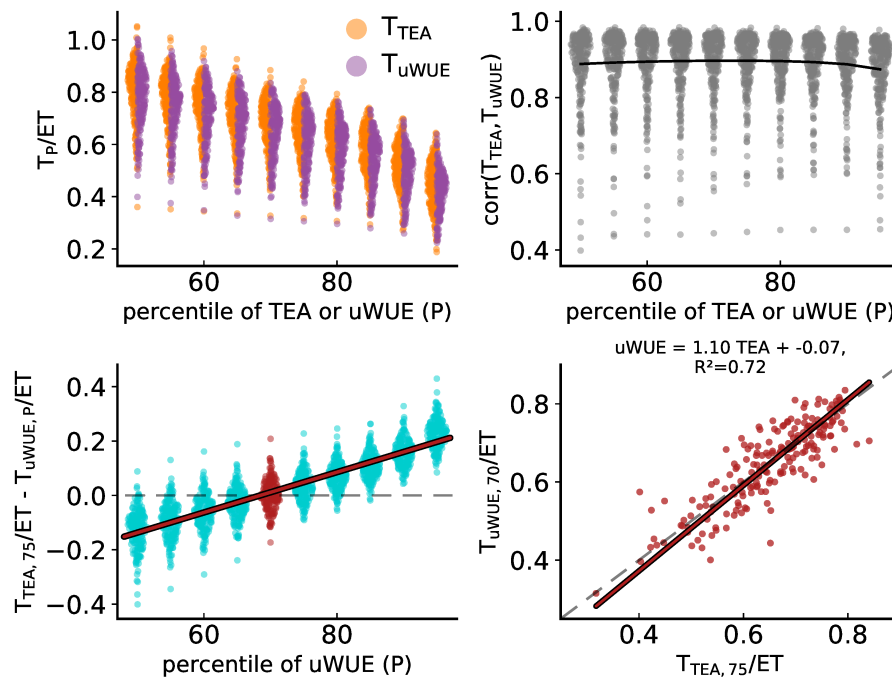
sap flux density. ⁷Tree-specific measurements of radial variation of sap flux density.

C.3 Supplementary Figure S1



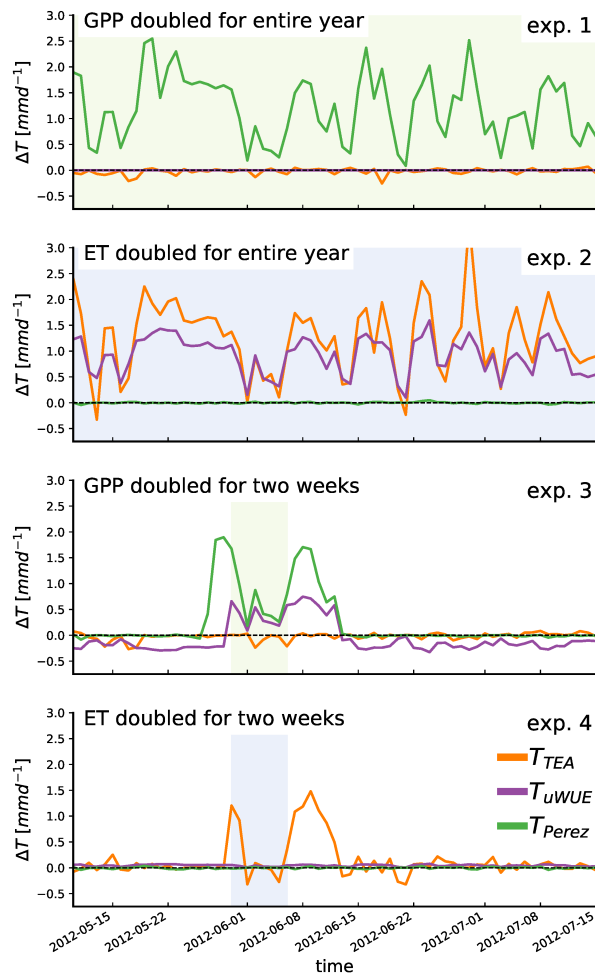
Comparison daily T estimates using both the day-time (DT) and night-time (NT) GPP estimation methods. Results show that GPP product used has a minimal effect on the resulting T. Note that the Pérez-Priego used a random sub-sample of ~100 days from each site to reduce processing time.

C.4 Supplementary Figure S2



Comparison of yearly T/ET across all sites based on different prediction percentiles from the TEA and uWUE methods. Methods scale almost linearly across percentiles with little change in temporal correlation. Using the 70th percentile with the uWUE method is most comparable to the 75th percentile from TEA method.

C.5 Supplementary Figure S3



The response of T estimates from three methods in four data manipulation experiments, compared to a control with no manipulation. The vertical axis show the difference between the T estimated from a manipulated dataset to the original T (control). Data is from the Tharandt (DE-Tha) site during 2012. Shading corresponds to the period where data was manipulated, with blue indicating ET was doubled and green indicating GPP was doubled. Experiment 1 doubles all the values of GPP, which has a minimal effect on the TEA and uWUE methods, but causes the T estimates from the Pérez-Priego method to nearly double as the Pérez-Priego method is directly tied to GPP. Experiment 2 doubles all values of ET, which causes T from the TEA and uWUE methods to double but has no effect on Pérez-Priego (small variations are due to stochastic processes in the partitioning). Experiment 3 doubles GPP for two weeks, which causes local errors in the uWUE and Pérez-Priego methods (due to each using a moving window) and an overall error in uWUE due to the estimation of $uWUE_p$. Experiment 4 doubles ET for two weeks, which has no effect on the uWUE and Pérez-Priego methods but causes errors in TEA which are strongest around the error, but smaller errors are seen in periods which have similar conditions.

Appendix D

List of tables and figures

List of Figures

| | | |
|-----|--|----|
| 1.1 | Global transpiration as a fraction of terrestrial ET. Shading represents the probability density functions based on either model variability (CMIP5 and remote sensing) or reported uncertainty (global isotopes and up-scaled site estimates). CMIP5 data from Berg and Sheffield (2019), remote sensing data from Miralles et al. (2016), global isotopes from Good et al. (2015) and up-scaled site estimates from Wei et al. (2017) and Schlesinger and Jasechko (2014). | 12 |
| 1.2 | Transpiration from eddy covariance data provides the missing step between physiological measurements at the leaf/plant scale and global to regional modeling. The data driven approach presented in Chapter 3 (the Transpiration Estimation Algorithm, TEA) provides an alternate view of ecohydrological function compared to the process based approaches which rely on scaling stomatal conductance processes to global scales. Leaf photo from Peggy Greb (CC BY 2.0), Plant and Ecosystem photos from Mirco Miglivacca. | 15 |
| 1.3 | Locations and time-spans of eddy covariance data used in this dissertation, colored by plant functional type (PFT). | 16 |
| 2.1 | One month average cycle (solid lines) and accompanying diurnal centroid (vertical dashed lines) of incoming shortwave radiation (R_g), evapotranspiration (ET), and gross primary productivity (GPP) at the Peuchabon, France ('FR-Pue') site during 2003. May is relatively wet (32 mm rainfall, left) and July is relatively dry (0 mm rainfall, right). While ET and R_g correspond well in the wet month, the dry month shows a distinct phase shift in both GPP and ET fluxes towards the morning, as well as a midday depression in GPP. | 31 |

- 2.2 Theoretical overview of diurnal water carbon index upper panels: One month average diurnal cycle of incoming shortwave radiation (R_g), evapotranspiration (ET), vapor pressure deficit (VPD), gross primary productivity (GPP), and $GPP * VPD^{-0.5}$ at the Peuchabon Forest, France ('FR-Pue') site during 2003. Discrepancies between $GPP * VPD^{-0.5}$ and ET increase from the relatively wet May (32 mm rainfall, left) to the relatively dry July (0 mm rainfall, right). lower panels: These discrepancies are reflected in the daily correlation values between $GPP * VPD^{-0.5}$ and ET, giving an indication of the appropriateness of the uWUE model for each day, as well as the degree of coupling between water and carbon signals. 33
- 2.3 Monthly median diurnal water carbon index (DWCI, lower panels) and diurnal centroids (C_{ET}^* , upper panels) for 6 sites in Europe. Data from all years available (black) is compared to 2003 (red) during which a drought event resulted in high temperatures and low precipitation throughout the summer. Note DWCI of 0-100 indicate lowest-highest probability of diurnal carbon:water coupling and C_{ET}^* of -1 to 1 indicate one hour morning shifted to one hour afternoon shifted ET. Vertical bars represent interquartile range. Sites from 4 plant functional types: evergreen broadleaf (EBF), deciduous broadleaf (DBF) and evergreen needleleaf (ENF) forests, as well as grasslands (GRA). Ecosystems show tendencies of morning shifts (e.g. DK-Sor and NL-Loo) and carbon:water decoupling (e.g. ES-ES1 and HU-Bug) during the drought year. 35
- 2.4 The frequency of morning-shifted Diurnal Centroids ($C_{ET}^* < -0.25$ hours, upper panels a,b) and low diurnal water carbon index (DWCI < 25, lower panels c,d) for 690 fluxnet site-years/192 sites, grouped by climate group (left panels a,c) and plant functional type (right panels b,d). Group labels on x-axis indicate the number of site-years/sites ($n = \text{site-years/sites}$) for each category. Dashed line is the median for all site-years. Color shade indicates level of significance, with light colors and dark colors having p-values < 0.10 and < 0.05 respectively (Wilcoxon–Mann–Whitney two-sample rank-sum test), red and blue colors indicate distributions higher and lower respectively compared to data from all sites excluding the group. Only sites-years with at least 20 data points and groups with more than 5 site-years were included. 37

- 2.5 Median diurnal water carbon index (DWCI, upper panel) and diurnal centroid (C_{ET}^* , lower panel) of plant functional types binned by evaporative Fraction (EF, low values indicate dry conditions). Note DWCI of 0-100 indicate lowest-highest probability of diurnal carbon:water coupling and C_{ET}^* of -1 to 1 indicate one hour morning shifted to one hour afternoon shifted ET. Evergreen needleleaf (ENF), deciduous broadleaf (DBF), and evergreen broadleaf (EBF) forests show increased morning shifts (low C_{ET}^*) with decreasing EF when compared to grassland (GRA) sites which tended to have decreased carbon:water decoupling (low DWCI) with decreasing EF. Savanna ecosystems (SAV) show a high degree of decoupling and intermediate levels of morning shifts. Vertical bars represent interquartile range. 39
- 2.6 Mean DWCI (upper panels) and C_{ET}^* (lower panels) with respect to evaporative fraction (EF) by vapor pressure deficit VPD (a,d), latent energy (LE) by Rn (b,e) and LE by GPP (c,g). Note DWCI of 0-100 indicate lowest-highest probability of diurnal carbon:water coupling and C_{ET}^* of -1 to 1 indicate one hour morning shifted to one hour afternoon shifted ET. Points with high Rn and low LE are associated with both low DWCI and C_{ET}^* , indicating that both metrics are related to water limitations. Though both metrics are associated with low EF, DWCI shows a much higher response to atmospheric demand as measured by VPD, with C_{ET}^* showing very limited response. Both metrics, and DWCI in particular, show low values with high ET and low Rn, though these points are also associated with over closed energy balances ($LE+H>Rn$). Both metrics are associated with low GPP, but the C_{ET}^* is restricted to both low GPP and ET, indicating water and carbon can decouple over a wider range of water stress. This also holds when points with energy balance over-closer are excluded (data not shown). 41

- 2.7 Difference in modeled and measured WUE for Katul-Zhou (a), Boese (b), and random forest (c) models. The random forest model was fit using Rg, VPD, T_{air} , GPP, and year. Thresholds designating dry, morning shifted, and C:W uncoupled days were $EF < 0.2$, $C_{ET}^* < -0.25$, and $DWCI < 25$ respectively for each day. The distributions span from the 5th to 95th percentiles, and the width of each gives an indication of the variance, which is larger in the sub groups compared to all points. Furthermore, the mean difference in WUE (black lines) tends to be shifted in dry and morning shifted days indicating a mean underestimation of WUE by the models mostly due to the long tails. Decoupled days show higher variance, but no clear pattern in under- or over-estimation. The percentage of days in each category are designated next to y-axis label in parenthesis. 42
- 3.1 Theoretical outline of both the TEA algorithm (lower section) and validation steps (upper section). TEA consists of a filtration step to isolate dry periods when vegetation is active using the conservative surface water index (CSWI), then a Random Forest Regressor is trained on the filtered dataset to characterize WUE dynamics, which are then predicted for the entire time-series. The validation scheme involves using model output as a synthetic flux dataset, to evaluate if TEA is able to replicate the WUE dynamics encoded in the models. 59
- 3.2 Average seasonal cycle of 4 output variables from JSBACH, CASTANEA, and MuSICA, all driven with the same meteorological forcing from three forest sites. Modeled years were 1997-2011 for FI-Hyy and FR-Hes, and 1997-2010 for DE-Tha. Data presented corresponds to daily data averaged across all years, and are intended to show seasonal trends. 64
- 3.3 Conceptual diagram showing persistent evaporation in the training dataset (E_{train}). In the case without persistent evaporation, many periods of the training dataset contain little E_{train} , meaning the algorithm can likely find periods where $eWUE = WUE$, $(GPP/ET) = (GPP/T)$, and $ET = T$. In the case with high E_{train} , every period contains significant E, which is likely to cause a bias in WUE estimates and ultimately an overestimation of T. 67

-
- 3.4 Average seasonal cycle of T/ET both from model output and the TEA estimate from model output, as well as total T/ET from the entire time-series. TEA algorithm was run on each individual site and model independently. Modeled years were 1997-2011 for FI-Hyy and FR-Hes, and 1997-2010 for DE-Tha. Data presented corresponds to daily data averaged across all years, and are intended to show seasonal trends. 69
- 3.5 The TEA algorithm captures mean seasonal and daily cycles of WUE from MuSICA output forced with data from Yatir Forest from 2001. Mean daily cycles are based on half hourly data for each month, whereas the seasonal cycles are an average from 5 days. 70
- 3.6 Overall model performance in space (right) and time (left). All models show high correlation across timescales, with some degradation at annual scale. In space (i.e. across sites), the TEA algorithm shows the highest agreement with the MuSICA model runs ($r^2 \approx 0.97$), and RMSE for JSBACH, CASTANEA, and MuSICA were 8.4%, 15.3%, and 3.2% respectively. 71
- 3.7 Sensitivity of TEA performance to CSWI limit hyperparameter. Though low CSWI limits help reduce the impact of E_{train} , strict filters also decrease the number of points available in the training dataset, which can exclude some wet sites entirely. A filter of -0.5 shows good MEF between T_{TEA} and T_{model} across sites (a), with little improvement using stricter filtering. The negative effect of strict filtering can be seen in the spatial correlation (b) of the JSBACH models, which significantly decreases at limits less than -2. 72

- 3.8 Sensitivity analysis of prediction percentile (P) used in TEA. Modeling efficiency (a), while generally stable, shows the highest values at relatively high percentiles ($P \approx 80 - 90$), whereas bias (b) is minimized at around P_{70} for MuSICA and JSBACH. Similarly, percentiles near the maximum (P_{100}) shows the lowest sensitivity to evaporation content in the training dataset (d), yet these high percentiles are also very sensitive to noise in the training dataset (c). Given that residual evaporation will likely be present in the training dataset, causing predictions to be overestimated, percentiles below the median (P_{50}) can be discounted. As such, by treating each percentile above the median ($P \geq 50$) as an equally likely estimate we can calculate the mean of $T_{P_{50}}, \dots, T_{P_{100}}$, the results of which are seen as the far right points in each plot, or the median which corresponds to P_{75} 74
- 3.9 Comparison of mean seasonal cycle of T/ET (5 day aggregation) results from model simulations (JSBACH, CASTANEA, and MuSCIA) and TEA algorithm partitioning of original EC data (ET, GPP, and meteorological variables). Modeled years were 2001-2006 for FI-Hyy and FR-Hes, and 1998-2003 for DE-Tha. Seasonal cycles are an average of 5 days. 76
- 4.1 Inter-comparison of the three T estimation methods presented here at daily resolution. Points ($n = 53390$ from 127 sites) come from the intersection of all methods where T could be estimated. R_{sp} values correspond to Spearman rank correlations to reduce the influence of outliers. Linear equation was estimated using orthogonal-least-squares regression which assumes observational errors exist in both x and y. Dark to light point coloration corresponds to low to high relative point density, respectively. 95
- 4.2 Comparison of sap flow based estimates of transpiration (T_{SF}) against estimated transpiration (T) and measured evapotranspiration (ET) from eddy covariance (EC). Note the three different sizes of markers in the correlation plots ($\text{corr}(\text{EC}, \text{SF})$, Pearson correlation), where the largest markers represents the mean correlation, the smallest markers represent the correlations from each available year, and the medium sized markers represent the selected year shown (time series in the left column of sub-figures). 96

- 4.3 Daily T/ET from each EC based method as a function of MODIS LAI. For each PFT, the associated relationship derived from Wei et al. (2017) is shown in black, which was derived from site level T/ET estimates. Points show the distribution within the given LAI bin, truncated to the 25th and 75th percentiles. PFTs were grouped to match those found in Wei et al. (2017) and are slightly different compared to subsequent figures. 97
- 4.4 Mean monthly seasonal cycles of T/ET grouped by PFT from the TEA and uWUE methods. Mean seasonal cycles for each site are grouped by PFT, with lines indicating the median across sites and shading indicating the interquartile range. Note that data from sites in the Southern Hemisphere have been shifted by six months, e.g. January in the figure would correspond to July in a Southern Hemisphere site. 98
- 4.5 Relationship of both WUE (top row) and T/ET (bottom row) to day-time mean VPD at daily scale across 124 sites. Lines indicate the median value from one hPa wide bins. Only days with a mean temperature above 5ř C, at least 1 *mm day*⁻¹ of ET, and where all three partitioning methods could be applied were included. 99
- 4.6 Percentage of evaporation (*E/ET*) estimated using the TEA, uWUE, and Pérez-Priego methods for progressive days after rain (rainy days defined as receiving > 0.1 mm in one day). Upper and lower panels show daily aggregated and diurnal cycles of *E/ET*, respectively. Diurnal cycles are estimated as the median for each half hour, with the interquartile range shown as shading. Only days with a mean temperature above 5ř C, at least 1 *mm day*⁻¹ of ET, and where all partitioning methods could be applied for all half hours in a day were included. 100
- 4.7 Comparison of variability of T/ET across years and across sites. Variability across years was calculated as the T/ET for each year of one site minus the mean across years from that site (only sites with at least 2 years of data). Each point refers to a site and the vertical spread indicates the distribution of points (the uWUE method is mirrored for better comparability). Variability across sites was calculated as the mean T/ET for each site minus the mean across all 140 sites. Overall, the standard deviations across sites was 1.6 and 1.5 times the standard deviations across years (for the uWUE and TEA methods, respectively). 101

- 4.8 Evaluation of the performance of the Random Forest model according to the amount of spatial variability explained across sites. Predicted values are from the out of bag estimates of T/ET, i.e. estimates from the Random Forest model that do not use the corresponding point being predicted. Features used in this model were: mean LANDSAT NDMI, crop designation, grassland designation, min. MODIS LAI, mean MODIS EVI, coarse fragment vol., soil pH, % sand. 102
- 4.9 Selection frequency, or how often each variable was selected during feature selection, gives an indication of variable importance. Points represent the median selection frequency from ten iterations of feature selection, with the interquartile range shown as error bars. Remote sensing derived variables come from either LANDSAT, TIP, or MODIS (see Methods for a full description). PFT designations are site reported. Climate data comes from site measurements. Soil data was derived from the SOILGRIDS dataset (Hengl et al., 2017). 103
- 5.1 Relationship with Diurnal Water Carbon Index (DWCI) and max daily temperature. Diamond markers indicate median DWCI within the temperature bin. Reduction in DWCI is seen at high temperatures when transpiration as estimated by TEA (T_{TEA} , $mm\ d^{-1}$) is low, indicating water limitations. Data was filtered for high quality and a minimum daily mean GPP of $1\ \mu mol\ CO_2\ m^{-2}\ s^{-1}$ 116
- 5.2 Diurnal Water Carbon Index (DWCI), transpiration (from TEA) and ET during the growing season at a seasonally dry savanna (Majadas de Tiétar), a mixed temperate forest (Harvard), and an irrigated maize field (Shangqui). 119
- 5.3 Summary of results from a nutrient manipulation experiment in a savanna ecosystem (Majadas de Tiétar). Results are shown as a difference of the nutrient treatment data compared to an untreated control (as a percent of the control). Each treatment was measured from an individual eddy covariance tower, with transpiration and evaporations estimates from TEA. Analysis ran from 2014 to 2020, with fertilization applied in 2014, 2015, and 2016. Values are from Table 4 in El-Madany et al. (2021). 123

5.4 The relationship between T/ET from FLUXNET (via TEA) and mean LAI derived from MODIS. Colors indicate the patterns of grassland (fractions of sites within a bin designated as grassland), normalized difference moisture index (NDMI, from LANDSAT), and soil coarse fragment volume (from SOILGRIDS). See Section 4.2.5 for complete data description. . . . 125

5.5 Comparison between T/ET estimates from literature used in Lian et al. (2018) and T/ET from FLUXNET using transpiration estimates from TEA. FLUXNET values were estimated as the mean of T/ET across available years. **(a)** Compares the distribution of T/ET from 33 Lian values compared to 204 values from FLUXNET. **(b)** Comparison of spatially coincident points. As values are not always coincident in time, all available FLUXNET years are shown as points, with distributions showing temporal variability. Distributions from Lian values represent reported measurement uncertainty. **(c)** As Lian et al. (2018) used site estimates to constrain models run on 1°x1° spatial resolution, FLUXNET estimates are dense enough to compare the variability among sites less than 0.5° away, demonstrating that within grid cell variability is as large as global variability. 127

5.6 Initial attempts at transpiration upscaling using the FLUXCOM methodology. 129

A.1 Figure S1. Sensitivity analysis of DWCI and C_{ET}^* to evaporative fraction (EF=ET/potential ET) under different GPP and air temperature (Tair) values, as well as the sensitivity of frequency of decoupling (DWCI < threshold) and morning ($C_{ET}^* < \text{threshold}$) using various thresholds. Note DWCI of 0-100 indicate lowest-highest probability of diurnal carbon:water coupling and C_{ET}^* of -1-1 indicate one hour morning shifted-one hour afternoon shifted ET. Bins for GPP and Tair based on percentiles to give an equal number of points per bin, with the exception of GPP<1 and Tair<0, which are approximately double the size of the other bins and represent periods of low plant activity such as winter. Vertical bars represent interquartile range in all cases. 162

- B.1 Sensitivity of daily GPP threshold filter to modeling efficiency (MEF) and spatial correlation, slope, and intercept. Filter limits above 0 show significant improvements, particularly with JSBACH spatial performance. Higher limits show degraded performance with MuSICA spatial performance, likely due to decreased training set data in dry sites under high GPP limits. 174
- B.2 A sensitivity analysis of the number of trees and max number of feature parameters on modeling efficiency (MEF) for seven site from MuSICA model output. The mean MEF across all max feature experiments for each site was subtracted to make sites comparable. Colored lines represent different sites, while the black line represents the mean from the seven sites. Though the number of max features used had little effect, a value of four showed the lowest variability and corresponds to the standard practice of using one third of the number of features. MEF decreased when the number of trees went below 100. 175
- B.3 Modeling efficiency (MEF) and relative bias response to plant function and climate across 72 site-runs from JSBACH. Climate variables (aridity index and mean annual temperature) showed no significant effect on MEF. Vegetation parameters show a slight effect, but is primarily driven by three sites. 176
- B.4 Relationship between the fraction of evaporation (directly from the models) the prediction percentiles used. E/ET is calculated by retrieving the specific half hours corresponding to the predicted WUE as output from the Random Forest from the training dataset. The E/ET is then calculated in these corresponding half hours, giving the actual contamination from the predictive points. Note that this process is done for each half hour of the dataset, giving a distribution of E/ET values which is dependent on the percentile used in prediction (each percentile gives a different corresponding half hour from the training dataset). Lines represent the median across all model runs, with shading representing the interquartile range. 177

- B.5 Theoretical diagram showing how the average true WUE (GPP/T, gray lines) can be estimated using the prediction percentile of eWUE (GPP/ET) under three scenarios: "CASTANEA" where evaporation is always 30% of ET, "MuSICA" where evaporation is high but does reach 0 at some points, and "JSBACH" where evaporation is usually 0. In all three scenarios, including when evaporation is never 0, the mean WUE can be approximated using different percentiles, with the caveat that highest percentiles of WUE cannot be estimated in the "CASTANEA" scenario and would then be truncated. 178
- figno Comparison daily T estimates using both the day-time (DT) and night-time (NT) GPP estimation methods. Results show that GPP product used has a minimal effect on the resulting T. Note that the Pérez-Priego used a random sub-sample of ~100 days from each site to reduce processing time. 189
- figno Comparison of yearly T/ET across all sites based on different prediction percentiles from the TEA and uWUE methods. Methods scale almost linearly across percentiles with little change in temporal correlation. Using the 70th percentile with the uWUE method is most comparable to the 75th percentile from TEA method. 190

- figno:3 The response of T estimates from three methods in four data manipulation experiments, compared to a control with no manipulation. The vertical axis show the difference between the T estimated from a manipulated dataset to the original T (control). Data is from the Tharandt (DE-Tha) site during 2012. Shading corresponds to the period where data was manipulated, with blue indicating ET was doubled and green indicating GPP was doubled. Experiment 1 doubles all the values of GPP, which has a minimal effect on the TEA and uWUE methods, but causes the T estimates from the Pérez-Priego method to nearly double as the Pérez-Priego method is directly tied to GPP. Experiment 2 doubles all values of ET, which causes T from the TEA and uWUE methods to double but has no effect on Pérez-Priego (small variations are due to stochastic processes in the partitioning). Experiment 3 doubles GPP for two weeks, which causes local errors in the uWUE and Pérez-Priego methods (due to each using a moving window) and an overall error in uWUE due to the estimation of $uWUE_p$. Experiment 4 doubles ET for two weeks, which has no effect on the uWUE and Pérez-Priego methods but causes errors in TEA which are strongest around the error, but smaller errors are seen in periods which have similar conditions. 192

List of Tables

- 1.1 A brief overview of methods for estimating ecosystem scale transpiration. Methods are reviewed in detail in Stoy et al. (2019) and Section 3.1. 17
- 3.1 Overview of filters used to isolate conditions where the signal of ET is dominated by T. *GPP* and *T_{air}* filters were designed to ensure plants are active, while *Rg* filters remove nighttime values. The *CSWI* filter attempts to remove periods where the surface is likely to be wet, a sensitivity analysis of which can be found in section 3.2. 61
- 3.2 Overview of key processes in the 3 models used for validation. 65

List of Publications

Papers included in this thesis

- **Nelson, J.A.**, Carvalhais, N., Cuntz, M., Delpierre, N., Knauer, J., Ogée, J., Migliavacca, M., Reichstein, M., & Jung, M. (2018). Coupling Water and Carbon Fluxes to Constrain Estimates of Transpiration: The TEA Algorithm. *Journal of Geophysical Research: Biogeosciences* DOI: [10.1029/2018JG004727](https://doi.org/10.1029/2018JG004727)
- **Nelson, J.A.**, Carvalhais, N., Migliavacca, M., Reichstein, M., & Jung, M. (2018). PWater-stress-induced breakdown of carbon–water relations: indicators from diurnal FLUXNET patterns. *Biogeosciences* 15 (8): 2433–47. DOI: [10.5194/bg-15-2433-2018](https://doi.org/10.5194/bg-15-2433-2018)
- **Nelson, J. A.**, Pérez-Priego, O., Zhou, S., Poyatos, R., Zhang, Y., Blanken, P. D., Gimeno, T. E., Wohlfahrt, G., Desai, A. R., Gioli, B., Limousin, J., Bonal, D., Paul-Limoges, E., Scott, R. L., Varlagin, A., Fuchs, K., Montagnani, L., Wolf, S., Delpierre, N., Berveiller, D., Gharun, M., Belelli Marchesini, L., Gianelle, D., Šigut, L., Mammarella, I., Siebicke, L., Andrew Black, T., Knohl, A., Hörtnagl, L., Magliulo, V., Besnard, S., Weber, U., Carvalhais, N., Migliavacca, M., Reichstein, M., & Jung, M. (2020). Ecosystem Transpiration and Evaporation: Insights from Three Water Flux Partitioning Methods across FLUXNET Sites. *Global Change Biology* 2020. DOI: [10.1111/gcb.15314](https://doi.org/10.1111/gcb.15314)

Papers related to this thesis

- El-Madany, T.S., Reichstein, M., Carrara, A., Martín, M.P., Moreno, G., Gonzalez-Cascon, R., Peñuelas, J., Ellsworth, D.S., Burchard-Levine, V., Hammer, T.W., Knauer, J., Kolle, O., Luo, Y., Pacheco-Labrador, J., **Nelson, J.A.**, Perez-Priego, O., Rolo, V., Wutzler, T., & Migliavacca, M. (2021) How Nitrogen and Phosphorus Availability Change Water Use Efficiency in a Mediterranean Savanna Ecosystem. *J Geophys Res Biogeosci.* DOI: [10.1029/2020JG006005](https://doi.org/10.1029/2020JG006005)
- Scott, R. L., Knowles, J. F., **Nelson, J. A.**, Gentine, P., Li, X., Barron-Gafford, G., Bryant, R., & Biederman, J. A. (2020). Water Availability Impacts on Evapotranspiration Partitioning. *Agricultural and Forest Meteorology*, 108251. DOI: [10.1016/j.agrformet.2020.108251](https://doi.org/10.1016/j.agrformet.2020.108251)
- Shan, N., Zhang, Y., Chen, J. M., Ju, W., Migliavacca, M., Peñuelas, J., Yang, X., Zhang, Z., **Nelson, J. A.**, & Goulas, Y. (2021). A Model for Estimating Transpiration from Remotely Sensed Solar-Induced Chlorophyll Fluorescence. *Remote Sensing of Environment* 2021, 252, 112134. DOI: [10.1016/j.rse.2020.112134](https://doi.org/10.1016/j.rse.2020.112134)
- Jung, M., Schwalm, C., Migliavacca, M., Walther, S., Camps-Valls, G., Koirala, S., Anthoni, P., Besnard, S., Bodesheim, P., Carvalhais, N., Chevallier, F., Gans, F., Goll, D. S., Haverd, V., Köhler, P., Ichii, K., Jain, A. K., Liu, J., Lombardozzi, D., Nabel, J. E. M. S., **Nelson, J. A.**, O’Sullivan, M., Pallandt, M., Papale, D., Peters, W., Pongratz, J., Rödenbeck, C., Sitch, S., Tramontana, G., Walker, A., Weber, U., & Reichstein, M. (2018). Scaling Carbon Fluxes from Eddy Covariance Sites to Globe: Synthesis and Evaluation of the FLUXCOM Approach. *Biogeosciences* 2020, 17 (5), 1343–1365. DOI: [10.5194/bg-17-1343-2020](https://doi.org/10.5194/bg-17-1343-2020)

Presentations

- **Nelson, J.A.**, Carvalhais, N., Migliavacca, M., Reichstein, M., & Jung, M. (2018). Sub-Daily Water and Carbon Flux Changes during Dry-down Events. In *EGU General Assembly Conference Abstracts*, 18:17549.
- **Nelson, J.A.**, Carvalhais, N., Cuntz, M., Delpierre, N., Knauer, J., Migliavacca, M., Ogee, J., Reichstein, M., & Jung, M. (2017). Data Driven Estimation of Transpiration from Net Water Fluxes: The TEA Algorithm. In *AGU Fall Meeting Abstracts*.

Manuscript declarations

The co-authors of the manuscripts used in the present cumulative doctoral thesis have been informed about the use of the manuscripts and about the declared individual contributions; they have given their consent.

Jacob A. Nelson

Ort, Datum, Unterschrift

I give my consent to the submission of a cumulative doctoral thesis and confirm the correctness of the information provided above.

Anke Hildebrandt

Ort, Datum, Unterschrift

Publication #1 :Water-stress-induced breakdown of carbonwater relations: indicators from diurnal FLUXNET patterns
status: *published*

| Author | Conceptual research design | Planning of research activities | Data collection | Data analyses and interpretation | Manuscript writing | Suggested publication equivalence value |
|-------------------|----------------------------|---------------------------------|-----------------|----------------------------------|--------------------|---|
| Jacob A. Nelson | ✗ | ✗ | ✗ | ✗ | ✗ | 1.0 |
| Nuno Carvalhais | ✗ | ✗ | | ✗ | | |
| Mirco Migliavacca | ✗ | ✗ | | ✗ | | |
| Markus Reichstein | ✗ | ✗ | | ✗ | | |
| Martin Jung | ✗ | ✗ | | ✗ | | |

Publication #2 :Coupling water and carbon fluxes to constrain estimates of transpiration: the TEA algorithm
status: *published*

| Author | Conceptual research design | Planning of research activities | Data collection | Data analyses and interpretation | Manuscript writing | Suggested publication equivalence value |
|--------------------|----------------------------|---------------------------------|-----------------|----------------------------------|--------------------|---|
| Jacob A. Nelson | ✗ | ✗ | ✗ | ✗ | ✗ | 1.0 |
| Nuno Carvalhais | ✗ | ✗ | | ✗ | | |
| Matthias Cuntz | ✗ | ✗ | ✗ | | | |
| Nicolas Delapierre | ✗ | ✗ | ✗ | | | |
| Jürgen Knauer | ✗ | ✗ | ✗ | | | |
| Jérôme Ogée | ✗ | ✗ | ✗ | | | |
| Mirco Migliavacca | ✗ | ✗ | ✗ | | | |
| Markus Reichstein | ✗ | ✗ | | ✗ | | |
| Martin Jung | ✗ | ✗ | | ✗ | | |

Publication #3 :Ecosystem transpiration and evaporation: Insights from three water flux partitioning methods across FLUXNET sites
status: *published*

| Author | Conceptual research design | Planning of research activities | Data collection | Data analyses and interpretation | Manuscript writing | Suggested publication equivalence value |
|-------------------------|----------------------------|---------------------------------|-----------------|----------------------------------|--------------------|---|
| Jacob A. Nelson | ✗ | ✗ | ✗ | ✗ | ✗ | 1.0 |
| Oscar Pérez-Priego | | | ✗ | ✗ | | |
| Sha Zhou | | | ✗ | ✗ | | |
| Rafael Poyatos | | | ✗ | ✗ | | |
| Yao Zhang | | | ✗ | ✗ | | |
| Peter D. Blanken | | | ✗ | ✗ | | |
| Teresa E. Gimeno | | | ✗ | ✗ | | |
| Georg Wohlfahrt | | | ✗ | ✗ | | |
| Ankur R. Desai | | | ✗ | ✗ | | |
| Beniamino Gioli | | | ✗ | ✗ | | |
| Jean-Marc Limousin | | | ✗ | ✗ | | |
| Damien Bonal | | | ✗ | ✗ | | |
| Eugénie Paul-Limoges | | | ✗ | ✗ | | |
| Russell L. Scott | | | ✗ | ✗ | | |
| Andrej Varlagin | | | ✗ | ✗ | | |
| Kathrin Fuchs | | | ✗ | ✗ | | |
| Leonardo Montagnani | | | ✗ | ✗ | | |
| Sebastian Wolf | | | ✗ | ✗ | | |
| Nicolas Delpierre | | | ✗ | ✗ | | |
| Daniel Berveiller | | | ✗ | ✗ | | |
| Mana Gharun | | | ✗ | ✗ | | |
| Luca Beletti Marchesini | | | ✗ | ✗ | | |
| Damiano Gianelle | | | ✗ | ✗ | | |
| Ladislav igut | | | ✗ | ✗ | | |
| Ivan Mammarella | | | ✗ | ✗ | | |
| Lukas Siebicke | | | ✗ | ✗ | | |
| T. Andrew Black | | | ✗ | ✗ | | |
| Alexander Knohl | | | ✗ | ✗ | | |
| Lukas Hörtnagl | | | ✗ | ✗ | | |
| Vincenzo Magliulo | | | ✗ | ✗ | | |
| Simon Besnard | | | ✗ | ✗ | | |
| Ulrich Weber | | | ✗ | ✗ | | |
| Nuno Carvalhais | ✗ | ✗ | | ✗ | | |
| Mirco Migliavacca | ✗ | ✗ | | ✗ | | |
| Markus Reichstein | ✗ | ✗ | | ✗ | | |
| Martin Jung | ✗ | ✗ | | ✗ | | |